Heterogeneous Fog Chemistry and S(IV) Oxidation in the San Joaquin Valley

Katherine J. Hoag
Jeffrey L. Collett, Jr.

Research Supported by San Joaquin Valleywide Air Pollution Study Agency and the National Science Foundation (ATM-9509596).

Colorado State University

DEPARTMENT OF ATMOSPHERIC SCIENCE

PAPER NO. 639

Heterogeneous Fog Chemistry and S(IV) Oxidation in the San Joaquin Valley

by

Katherine J. Hoag
Jeffrey L. Collett, Jr.

Department of Atmospheric Science
Colorado State University
Ft. Collins, Colorado 80523

Research Supported by

San Joaquin Valleywide Air Pollution Study Agency and
the National Science Foundation (ATM-9509596)

December, 1997

ABSTRACT

HETEROGENEOUS FOG CHEMISTRY AND S(IV) OXIDATION
IN THE SAN JOAQUIN VALLEY

Chemical and microphysical properties of winter radiation fogs present in the San Joaquin Valley (SJV) of California were measured during December 1995 and January 1996 as a part of the 1995 Integrated Monitoring Study (IMS95). The purpose of the study was to characterize winter particulate air quality problems often observed in this area. Stagnant conditions in the winter often lead to the formation of persistent and dense radiation fogs. These fogs act as processors of particulate matter through particle scavenging and removal in sedimenting fog drops and through particle production via chemical reactions that occur in the aqueous phase. The goal of the fog study portion of IMS95 was to gain more information about the fog drop chemistry as a function of drop size in an effort to more accurately determine the role of fogs in aerosol processing in this region.

The major species measured in fogwater during this project were ammonium, nitrate, sulfate, acetate, formate and formaldehyde. The fogwater was also alkaline (median pH = 6.5) compared to a pH of 5.6 expected for atmospheric water in equilibrium with carbon dioxide. Droplet pH affects the amount of SO_2 that is absorbed by the droplets and influences the relative importance of different S(IV) oxidation pathways. S(IV) oxidation

by ozone was determined to be of primary importance (dominating 88 percent of the time in the southern SJV) because at the high pH values observed it becomes faster than S(IV) oxidation by hydrogen peroxide, which is more commonly investigated, and trace metal catalyzed autooxidation. High fog pH and abundant formaldehyde also led to significant formation of the S(IV) aldehyde complex hydroxymethanesulfonate (HMS).

Size resolved fog drop collection revealed differences in fogwater chemical composition as a function of droplet size. In general, smaller drops were more acidic and more concentrated in ionic species than large drops. Calculations have been performed to determine the effect this chemical heterogeneity has on the roles fogs have in aerosol processing. Due to the nonlinearity of the ozone S(IV) oxidation rate, the acidity variations with drop size tend to enhance the oxidation. The observed S(IV) oxidation rates were 1.0 to 7.8 times faster than rates calculated using average fogwater acidity. Variations in other solute concentrations with drop size could affect the removal rates of these species from the air by deposition. Calculations assuming settling as the dominant deposition process estimate that using average fogwater composition of ionic species overestimates their removal rates by as much as a factor of 3.5.

ACKNOWLEDGMENTS

We are grateful to Aaron Bator, D. Eli Sherman, Oliver Graf, Xin Rao, and Teresa Campos for their assistance during the field campaign. L. Willard Richards, Paul Solomon and Karen Magliano were also instrumental in the planning and management of various portions of the IMS95 field campaign. Mark Cox and Elisabeth Andrews are acknowledged for assisting with sample analysis. Prof. Sonia M. Kreidenweis and Prof. Gary E. Maciel are acknowledged for providing constructive recommendations for this work.

Funding for this work was provided by the San Joaquin Valleywide Air Pollution Study Agency and the National Science Foundation (ATM-9509596).

DISCLAIMER

TABLE OF CONTENTS

LIST OF FIGURES

LIST OF TABLES

Chapter 1: Introduction

The importance of characterizing atmospheric particulate matter as a large contributor to air quality problems is widely recognized. Aerosols are important due to their potential for harmful health effects through inhalation, the damage they cause to natural and man-made structures through deposition of harmful substances, their effect on visibility degradation, and their radiative effect on climate. Since these effects depend on the particle's size and chemical composition, the aerosol population must be characterized not only by number and size distribution, but also chemical composition as a function of particle size.

In addition to directly affecting air quality in the same ways as aerosols, fogs can interact with aerosols, producing additional possibilities for affecting air quality under certain conditions. Fogs scavenge preexisting gases and particles and can increase the amount of particulate matter through chemical reactions that occur readily in the aqueous phase. One such reaction is the oxidation of aqueous free S(IV) into sulfuric acid. Gaseous sulfur dioxide is absorbed into fog droplets where it can be oxidized by oxidants also absorbed from the gas phase or produced in situ. Ozone, hydrogen peroxide and oxygen in the presence of certain transition metals from the particulate phase, can be effective S(IV) oxidants. S(IV) oxidation occurs much faster in the aqueous phase than

in the gas phase. This chemistry contributes to the acidity of the fogwater and produces nonvolatile solute (sulfate) that is added to the aerosol mass burden when droplets evaporate. When the fogs evaporate, they leave behind processed aerosols that may have much different chemical and physical characteristics than the aerosol present before the fog. Several S(IV) oxidation pathways have rates that are very dependent on droplet acidity and oxidant and catalyst concentrations. Droplet populations whose chemical characteristics vary as a function of drop size can have varying amounts of sulfate production occurring in different sized drops. This effect would change the overall contribution of the fog to particle production. Fogs can also remove scavenged particulate matter and pollutants from the air by deposition processes such as sedimentation, which are more efficient for the relatively large fog drops than for small aerosol particles. Since both aerosol production and removal capabilities of a fog are dependent on drop size and chemical composition, size resolved chemical measurements are needed to understand the chemical and physical processes occurring in fogs in order to determine the role they have in affecting overall air quality.

Extended periods of stagnation and strong inversions often occur in the San Joaquin Valley (SJV) of California during the winter. Figure 1.1 is a map of California showing the SJV and the surrounding mountains that contribute to these meteorological conditions. This meteorology, coupled with pollution sources such as oil recovery activities, large cities, highways, agriculture and animal husbandry operations, leads to frequent high particulate matter (PM) episodes during the winter. Widespread heavy radiation fogs also occur during the winter in conjunction with these stagnation episodes.

Studies of the fog in the SJV have been performed mostly during the 1980's (Munger et al., 1993, Jacob et al., 1984, Jacob et al., 1986). Table 1.1 shows the median fog composition at Bakersfield, California, for two of these studies. The major species

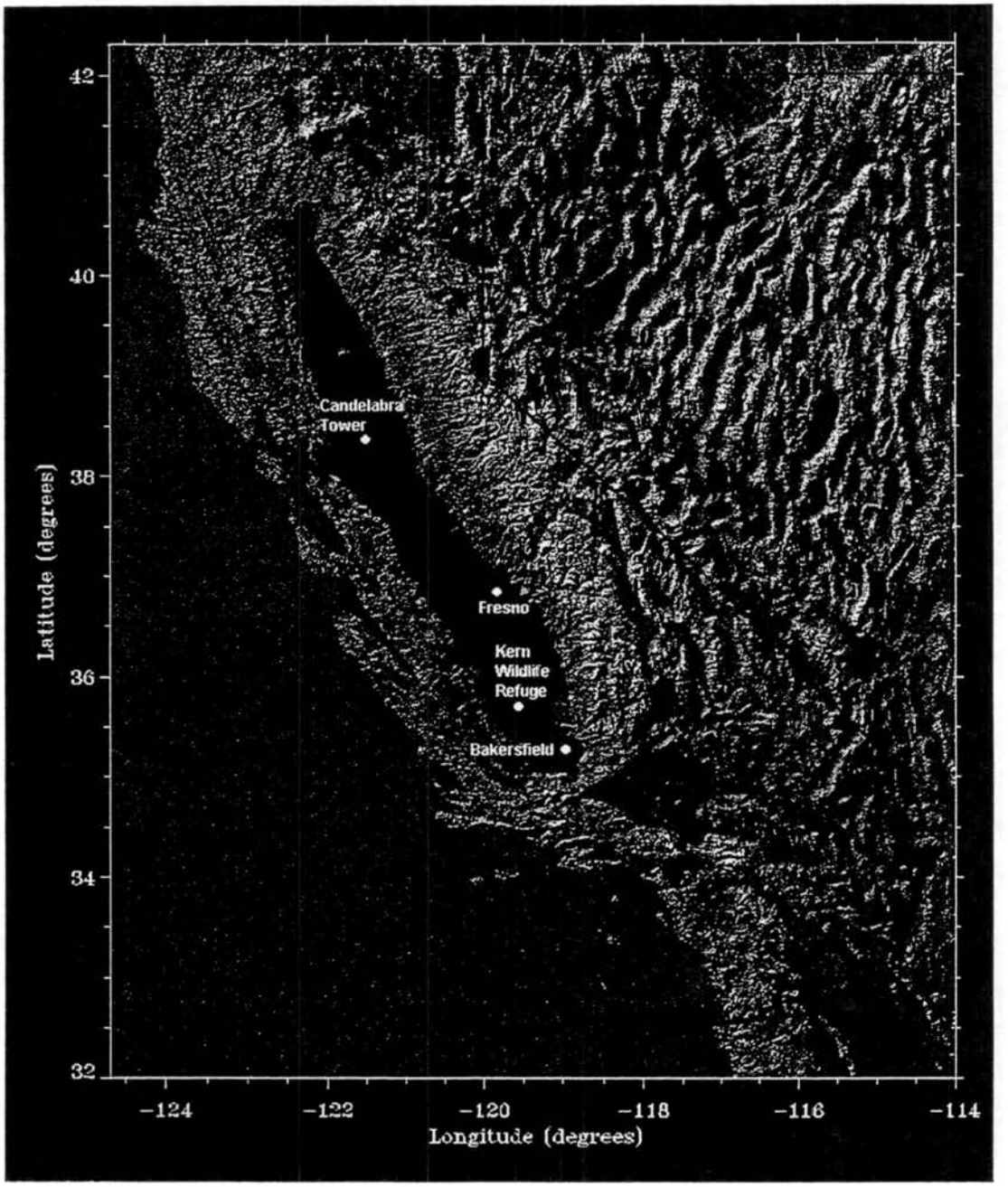

Figure 1.1: Map of California showing the San Joaquin Valley and the IMS95 fog sampling sites. Courtesy of Ray Sterner at Johns Hopkins University Applied Physics Laboratory. (http://fermi.jhuapl.edu/states/maps1/ca.gif)

Table 1.1: Average concentrations in fogwater collected at Bakersfield, California; Jacob et al., 1984 and Jacob et al., 1986. (All concentrations given in microequivalents per liter of water except pH and S(IV).)

Date	pH	Na^+	NH_4^+	Ca^{2+}	Mg^{2+}	Cl^-	NO_3^-	SO_4^{2-}	S(IV) μM
1982-83	4.2	19.5	1,440	47	6.3	47	850	1,160	515
1983-84	5.7	11	3,270	169	33	122	819	2,070	384

measured were ammonium, sulfate and nitrate, and the pH was usually rather alkaline. More SJV fog chemistry measurements have been performed during the 1990's by Professor Collett's group (Collett et al., 1994a, b, Rao and Collett, 1995, Bator and Collett, 1997). These measurements found compositions similar to those of previous studies, with dominant ionic species being ammonium, nitrate and sulfate, and the average pH being 6.0. Jacob et al. (1984) found that solute concentrations in the fogs typically decreased throughout the course of an event, presumably due to removal of aerosols by deposition of the fog droplets. The presence of the fogs was also observed to limit particle buildup during these stagnation episodes. No measurements have been made to characterize vertical variations in fogwater chemistry in this area.

Chemical and microphysical properties of winter radiation fogs present in the SJV were measured during December 1995 and January 1996 as a part of the 1995 Integrated Monitoring Study (IMS95). This study was part of the Phase 1 planning effort for the California Regional PM10 Air Quality Study (CRPAQS). An overview of the overall

field study is presented by Solomon et al. (1996). One goal of the fog study portion of IMS95 was to gain more information about the fog drop chemistry as a function of drop size in an effort to more accurately determine the role of fogs in the processing of aerosols and therefore in the air quality of this region. Other goals of the fog study included characterizing the spatial and temporal variability of the fog characteristics and determining the oxidant availability to better predict what chemical reactions were important during fog episodes.

Bulk fogwater was collected at the ground at three main sites in the southern SJV, (Bakersfield, Fresno, and Kern Wildlife Refuge), and at various elevations on a 430 m television tower located in Walnut Grove, California, just south and west of Sacramento (see Figure 1.1). Fogwater separated into two drop size fractions was also collected at the three southern SJV sites. Chemical analyses were performed on preserved quantities of the fogwater to characterize certain important species such as pH, major inorganic ions, total S(IV), peroxides and total iron and manganese. This thesis will look at the chemical characteristics, including temporal and spatial variations, of the fogs measured during this experiment. A series of calculations and data analyses have been performed to ascertain the relative importance of various S(IV) oxidation processes in the drops and to estimate their potential contribution to particulate matter concentrations in this area. An initial investigation was also performed to estimate the role the observed fogs had on species removal through wet deposition by sedimentation. A portion of this work is also dedicated to investigating the possible effect that variations in fog drop chemistry as a function of size could have on these processes. The following chapters of this thesis

describe the methods and results of these measurements and analyses as well as explore their implications for topics such as future air quality sampling and characterization efforts in regimes like the SJV.

Chapter 2: Field sampling methods and chemical analyses

During winter 1995/96 Colorado State University conducted measurements of fog chemistry at four locations in California's San Joaquin Valley as part of the 1995 Integrated Monitoring Study (IMS95). Ground-based measurements were made at three of the four study core sites (Bakersfield, Kern Wildlife Refuge (KWR), and Fresno) during the IMS95 winter study in December and January. In early January, sampling equipment was moved north to the Candelabra Tower, near Walnut Grove, California, where measurements were made of vertical variations in fog chemistry. The following chapter provides documentation concerning the methods for fog sampling and analysis, and data processing and validation procedures.

Cloud/fog samplers used in IMS95

Four different cloud/fog sampler types were used in IMS95. One type collected "bulk" samples representative of the entire fog drop size distribution, while two other types collected multiple independent cloud drop size fractions. These collectors are described below. Sample times for bulk fog samples were typically one hour, but ranged from 20 minutes to several hours. Size-fractionated fog sample periods ranged from one hour to several hours, with typical times of approximately two hours.

The Caltech Active Strand Cloudwater Collector Version 2 (CASCC2)

The Caltech Active Strand Cloudwater Collector Version 2 (CASCC2) (Hoffmann et al., 1989; Collett et al., 1994b; Demoz et al., 1996) was used to collect bulk fog samples at the three IMS95 winter core sites and from the Candelabra Tower. This instrument (see Figure 2.1) collects fog droplets by inertial impaction on a bank of Teflon cylinders. The cylinders are comprised of 508 μm diameter Teflon strand, wrapped around three Teflon-coated frames, for a total of six collector rows. The frames are enclosed in a Plexiglas housing and supported above a Teflon sample trough. Air is drawn through the CASCC2 at 5.8 m^3/min by a fan located at the rear of the collector. The theoretical 50% size cut for the CASCC2 corresponds to a drop diameter of 3.5 μm. As droplets impact on the Teflon collection strands, they coalesce and are pulled by gravity and aerodynamic drag down into the sample trough. Collected fogwater flows from the sample trough, through a Teflon sample tube, into a polyethylene sample bottle. During IMS95 the sample was retrieved manually at the end of each sample period.

Aliquots of CASCC2 samples were prepared for analysis of pH, major ions, S(IV), organic acids, trace metals, formaldehyde, and hydroperoxides at all sites. In some cases not all species were analyzed, especially when insufficient sample was available or insufficient time was available to preserve unstable species. Some samples collected at KWR and the Candelabra tower were also analyzed for hydroxymethanesulfonate (HMS), total organic carbon (TOC), and dissolved organic carbon (DOC).

The Size-fractionating Caltech Active Strand Cloudwater Collector (sf-CASCC)

The size-fractionating Caltech Active Strand Cloudwater Collector (sf-CASCC) (Munger et al., 1989; Demoz et al., 1996), is a larger version of the CASCC2 with an additional inlet designed to collect large fog drops. This collector, depicted in Figure 2.1, was deployed at the core site near the Kern Wildlife Refuge. Air is drawn through the sf-CASCC at 19 m^3/min. The inlet of the sf-CASCC contains four rows of 12.7 mm diameter Teflon rods. The theoretical 50% size cut for this stage is 23 μm. The second

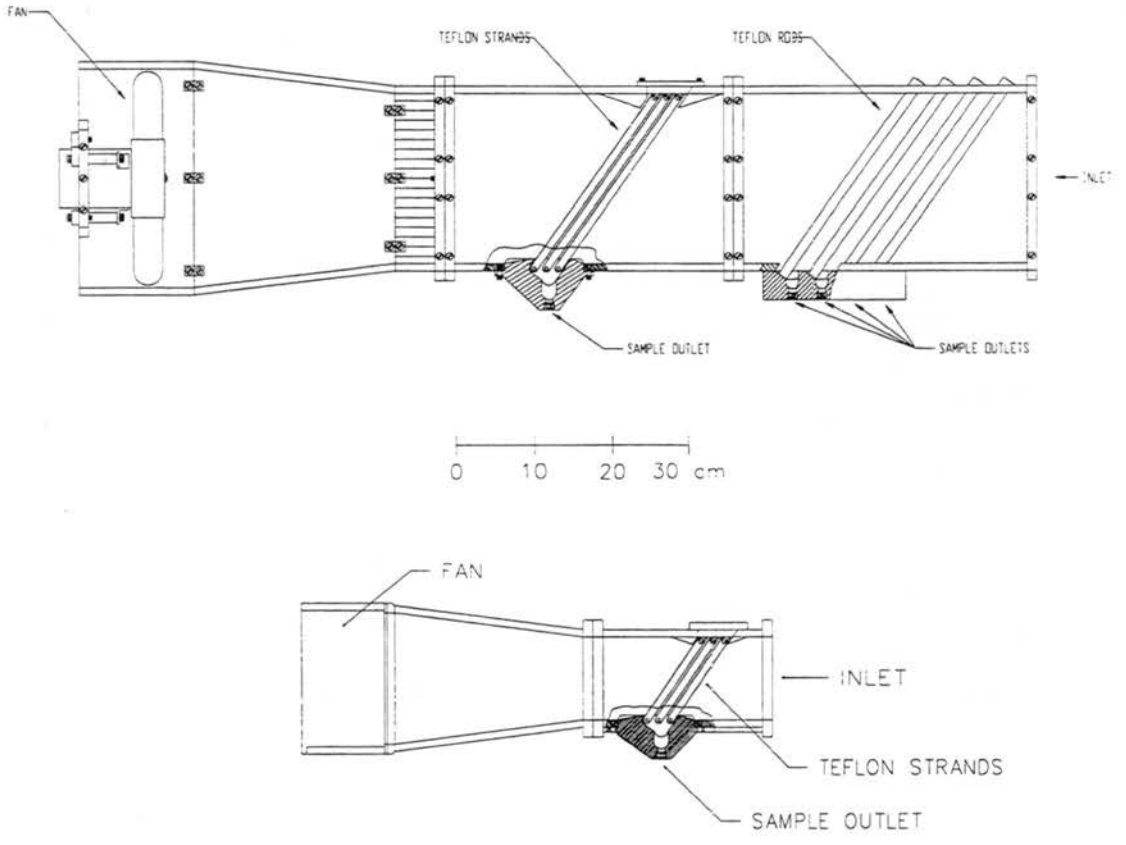

Figure 2.1: The CASCC2 (bottom) and the sf-CASCC (top)

stage of the collector contains six rows of 508 μm diameter Teflon strand and provides a 50% size cut of 4 μm. Both collector stages are contained in a Plexiglas housing. Sample from each collection stage drains through a collection trough into a polyethylene sample bottle via a Teflon sample tube. Samples are retrieved manually at the end of each sampling period.

Aliquots of sf-CASCC samples were prepared for analysis of pH, major ions, S(IV), organic acids, trace metals, formaldehyde, HMS, hydroperoxides and TOC as sample volume and time permitted. Some samples collected at KWR were also analyzed for DOC.

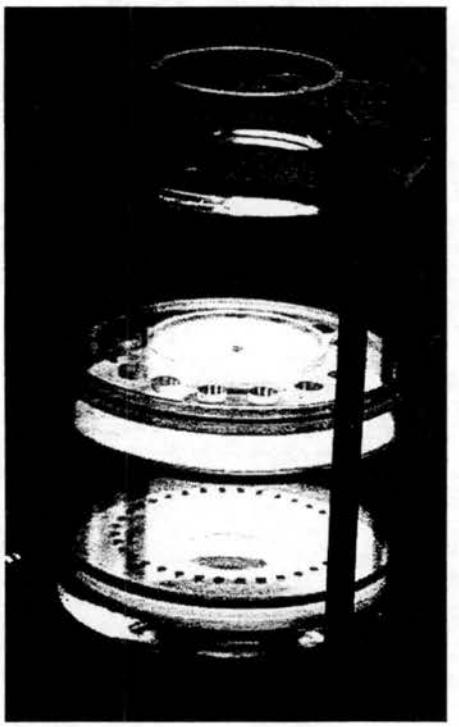

Figure 2.2: The 2-stage ETH fog impactor.

The ETH impactor

Two-stage jet impactors were used at Bakersfield and Fresno to collect separate samples of large and small fog drops. The ETH impactor (Collett et al., 1993, 1995), shown in Figure 2.2, contains two impaction stages in series. Air is drawn through the impactor by a regenerative blower. The flow rate is set by adjustment of a gate valve downstream of the impactor. The flow is checked by measuring the time to inflate a bag of known

volume or by readout from an in-line volumetric flow meter. The ETH impactor is typically operated at flow rates between 300 and 400 lpm. The size cut of each stage is a weak function of flow rate in this range. Drops larger than 10 μm (depending on flow rate) are collected on the first stage, while drops with diameters between 3 and 10 μm (depending on flow rate) are collected on the second stage. Each stage consists of a Plexiglas jet plate and a Teflon impaction plate. Shallow troughs in the impaction plates help confine the collected sample to facilitate sample retrieval. Samples are manually retrieved at the end of each sampling period by disassembling the impactor and transferring the sample collected on each stage to a polyethylene sample vial using a pipette. Samples from the ETH impactors were analyzed for pH and major ions as sample volume permitted.

Fog drop size distribution measurements

In addition to collecting fog samples, CSU ran a Particle Measurement Systems Classical Scattering Aerosol Spectrometer Probe (CSASP-100-HV) to measure the droplet size distribution during several fog events at KWR during the IMS95 study. The CSASP uses a helium-neon laser to illuminate the sampling zone where the air flow is flowing perpendicular to the laser beam. If no particles are within the sample air flow then the laser terminates on a dump spot and no particles are counted. Particles which pass through the sampling zone scatter light in proportion to their size around the dump spot of the laser and into the collecting optics where it is condensed onto a photo-detector.

The CSASP is capable of measuring the size distribution of fog droplets between 0.5 and 47 microns with four ranges. Each range contains 15 evenly spaced channels between each range maximum and minimum. Range 0 measures the distribution between 3 and 47 microns, Range 1 measures the distribution between 2 and 32 microns, Range 2 measures the distribution between 1 and 16 microns, and Range 3 measures the distribution between 0.5 and 8 microns. Range 1 provided the best coverage of drop size distributions measured during IMS95.

Field operations of the CSASP included field calibration checks with glass microspheres (Duke Scientific Corp., 15.7 ± 1.1 μm) before collecting data. The CSASP was operated to count particles in each range for 10 seconds, cycling through each range continuously until the CSASP was shut off. Post-processing of the data included selecting out only range 1 and then converting the particle counts/10 seconds to particle counts/cc of air sampled. The manufacturer's specified flow rate of 12.5 cc/sec was used to make the conversion. In some cases the number of droplets counted in a particular channel exceeded the maximum permitted.

Gas phase species measured during IMS95

CSU in cooperation with NCAR scientists operated two continuous gas phase hydrogen peroxide monitors during IMS95. Since there were only two of these instruments, one operated continuously at Kern while the other was used at Bakersfield or Fresno at

different times of the study. These monitors detect hydroperoxides by fluorescence; more detail about the operation of the monitors can be found in Lazrus, et al. (1986) and Richards et al. (1997). A detection limit of 50 pptv was determined for these instruments.

Sonoma Technology, Inc. (STI) and the California Air Resources Board (CARB) operated continuous SO_2 and O_3 monitors at each of the sites during IMS95. A lowest quantifiable level (LQL) of 1 ppbv was determined for all of these measurements. More information about gas phase measurements performed by STI can be found in Wright et al. (1996) and Richards et al. (1997).

Chemical species analyzed in IMS95 fog samples

Several chemical species were analyzed in fog samples collected during IMS95. Some of these were analyzed in the field, while others were analyzed in the laboratory at Colorado State University. Several of the more unstable species were stabilized for later analysis immediately after samples were collected in the field. All stored samples were refrigerated prior to analysis. Figure 2.3 illustrates how collected samples were split, preserved, and analyzed for the various chemical species. Descriptions of these procedures follow below. Quality control measures and data validation procedures are described in Appendix A.

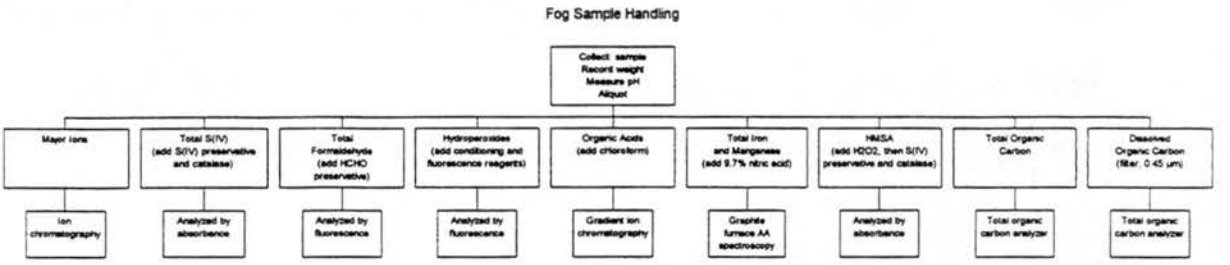

Figure 2.3: Fog sample handling procedures. Sample pH was measured on-site, while other species were aliquotted and preserved (as indicated) for later analysis in the laboratory.

Fogwater pH

Fog sample pH was measured on-site using an Orion electronic pH meter (Model 250 or 290) equipped with a combination microelectrode (Microelectrodes, Inc. Model MI-710). Prior to sample measurement, the electrode was calibrated with pH 4 and 7 buffers.

Inorganic Ions and Low Molecular Weight Organic Acids

A Dionex DX-500 dual channel ion chromatograph was used for analysis of inorganic ions and low molecular weight organic acids. One channel is dedicated to analysis of cations (sodium, ammonium, potassium, magnesium, and calcium). The other channel switches between analysis for anions (chloride, nitrate, and sulfate) and selected organic acids (acetic, formic, oxalic, pyruvic, and propionic). Each channel of the DX-500 ion chromatograph (IC) is attached to an AS3500 autosampler which allows random access to the sampling vials. This permits analysis of the same set of calibration standards at the beginning and end of each run of samples. In addition, the autosampler can be

programmed to automatically run duplicate samples. To make sure that the IC is running properly while unattended during a long run, periodic duplicates are run as check standards. At the beginning of each run of samples, regardless of whether they are run for anions, cations or organic acids, a DI water blank is loaded. Then ten standards are run, followed by two commercial calibration check standards, and another blank sample. Ten samples are then run, the last of which is injected twice. After this duplicate, one of the standards is run. Samples are run in groups of ten, ending with a duplicate injection followed by a standard injection, until the sample set to be analyzed is complete. At the end of the samples, standards are run again before turning off the instrument. This procedure provides a check on whether the response of the instrument changes during the course of a run, as well as information on the reproducibility of the injections. Separate calibration curves are prepared for each analytical run. When appropriate, two calibration curves are determined from the ten calibration standards run, one representing a lower concentration range and the other a higher concentration range.

Operating Conditions for Cation Analysis

Cations are analyzed with a Dionex CS-12 Column preceded by a CG-12 guard column, with a Dionex Cation Self Regenerating Supressor (CSRS-1) operating in Auto Suppression Recycle Mode. Detection is with a Dionex conductivity detector. Injections are made by the AS3500 autosampler with a 50 µl sample loop.

The eluent used is 20 mM Methanesulfonic Acid, prepared from concentrated methanesulfonic acid (Kodak; Product Number CAT 116 5570) and water prepared from a Nanopure reverse osmosis - deionization system (hereafter referred to as DI water). The pump is primed for one minute at 9 ml/minute with the waste bypass valve open. The valve is then closed, and the system is started with a flow rate of 1 ml/minute and left to equilibrate for one hour before starting analyses. The time, pressure and total conductivity are recorded in a logbook at this point and hourly while the instrument is running. Expected background conductivity for the cation analysis is between 1 and 2 μS.

Previously prepared sample vials are then loaded into racks of forty for the AS3500 autosampler. If samples have not been previously prepared, 500 μl of each sample is pipetted into a sample vial and the top is securely screwed on. Sample vials are polypropylene 500 μL with screw-type polyethylene caps with Teflon septa.

Ten calibration standards are prepared from a stock solution prepared by dissolving appropriate amounts of reagent grade salts in DI water. Two calibration curves are used to determine the concentrations of the samples. The lower range is from 2 to 100 μN (microequivalents/liter) for each cation. If the sample concentration is above this range, a higher curve, extending up to 1600 μN is used.

Operating Conditions for Anion Analysis

Anions are analyzed with a Dionex AS4A-SC Column and AG4A-SC guard column. Suppression of background conductivity is achieved using a Dionex Anion Self Regenerating Suppressor (ASRS-1), and detection is by a Dionex conductivity detector. An AS3500 autosampler is used to introduce the samples into the column. Sample loop volume is 25 µl. The anion eluent is 1.8 mM Na_2CO_3/1.7 mM $NaHCO_3$. The eluent is prepared from a stock solution of 180 mM Na_2CO_3/170 mM $NaHCO_3$ prepared from reagent grade salts and DI water.

The pump is primed for one minute at 9 ml/minute with the waste bypass valve open. The valve is then closed and the system is started with a flow rate of 2 ml/minute and left to equilibrate for one hour before starting analyses. The time, pressure and total conductivity are recorded in a logbook at this point and hourly while the instrument is running. The expected background conductivity for the anion analysis is 2.8 µS.

Previously prepared sample vials are then loaded into racks of forty for the AS3500 autosampler. If samples have not been previously prepared, 500 µl of each sample is pipetted into a 500 µl polypropylene sample vial and the top is securely screwed on. Sample vials are polypropylene 500 µL with screw-type polyethylene caps, with Teflon septa.

Ten calibration standards are prepared from a stock solution prepared by dissolving appropriate amounts of reagent grade salts in DI water. Two calibration curves are used to determine the concentrations of the samples. The lower is from 2 to 100 μN for each anion, except chloride which is from 1 to 50 μN. If the sample concentration is above this range, a higher curve extending up to 1600 μN (800 μN for chloride) is used.

Operating Conditions for Organic Acid Analysis

Organic acids (acetate, propionate, formate, pyruvate and oxalate) are analyzed on the same system as the anions, but with a different column and eluent combination. The organic acid column is a Dionex AS-11 column with an AG-11 guard column. Species are eluted from the column using a NaOH gradient (Figure 2.4).

500 μl of previously stabilized organic acid sample is pipetted into a glass autosampler vial and the top is securely screwed on. Sample vials are then loaded into racks of forty in the AS3500 autosampler.

Calibration standards are prepared by diluting a standard stock solution made by dissolving reagent grade salts in DI water. Two calibration curves are used to determine the concentrations of the samples. The lower range is from 2 to 100 μN for each organic acid. If the sample concentration is above this range, a higher curve up to 1600 μN is used.

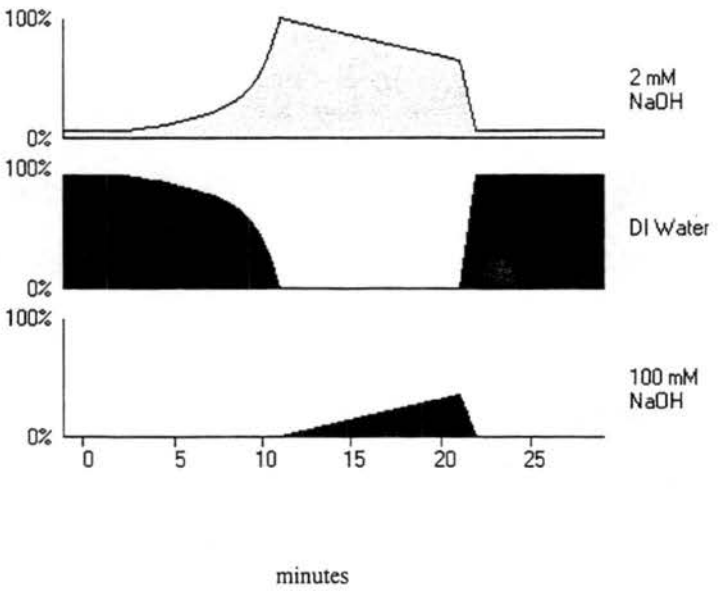

Figure 2.4: Time profiles for the three components of the gradient eluent used in the organic acids determination.

Total S(IV) and hydroxymethanesulfonate (HMS)

Since free S(IV) in cloudwater can be readily oxidized by H_2O_2, O_3 and O_2 in the presence of transition metals, samples are preserved as soon as possible after collection. Preservation is accomplished by adding a preserving solution containing formaldehyde, CDTA (trans-1,2-Cylohexylenedinitrilo-tetraacetic acid) and sodium hydroxide. The ratio of preservation solution to cloudwater is 1:15. More information about this measurement technique is found in Dasgupta et al. (1980).

The principle of preservation is that S(IV) reacts rapidly with formaldehyde to form HMS (hydroxymethanesulfonate). HMS is stable in the preserved cloudwater samples since it is not easily oxidized. HMS formed in the preserved cloudwater can then be easily decomposed to free S(IV) before analysis. CDTA in the preservative solution prevents interference of trace metals in the S(IV) analysis. A catalase solution is also added to the samples to destroy any H_2O_2 in cloudwater, since aqueous oxidation of S(IV) by H_2O_2 is a very fast reaction and could interfere with the measurements. Preserved samples are kept at 4 ^{0}C until analysis for total S(IV) content.

It is also possible to analyze HMS contained in fog samples in a similar way. Before adding the preservative solution, however, hydrogen peroxide is added to rapidly oxidize any free S(IV) present in the sample. The sample is then preserved as described in the preceding paragraphs until it is analyzed for HMS content.

To analyze preserved S(IV) samples, HMS is first decomposed to HCHO and free S(IV) by adding strong base, and then free S(IV) and HCHO react with acidic pararosaniline to form a purple compound, which is measured spectrophotometrically using a Hitachi U-2000 UV/VIS spectrophotometer. A calibration curve relating absorbance to S(IV) concentration was prepared daily by analyzing calibration solutions prepared by diluting a stock solution of Na_2SO_3. Free S(IV) concentrations can be obtained by subtracting the HMS concentration from the total S(IV) concentration.

Due to limited available sample volumes, duplicate analyses could not be completed for S(IV) or HMS. Estimates of precision were made using duplicate analyses of calibration standards.

Formaldehyde

Formaldehyde in fog samples can be preserved by adding bisulfite to form HMS. HMS can later be decomposed to formaldehyde to be analyzed (Dong et al., 1987). A formaldehyde preservation solution containing bisulfite is added on site. The volume ratio of preservative to sample is 1:10. This technique measures total formaldehyde ("free" formaldehyde plus HMS). The concentration of free formaldehyde (HCHO plus the hydrated form, $CH_2(OH)_2$) can be obtained by subtracting the HMS concentration (measured according to the procedure described in the preceding section) from the measured total formaldehyde concentration.

In the presence of small amounts of formaldehyde, 2,4-pentanedione and ammonia react with formaldehyde quantitatively to form a yellow product, diacetyldihydrolutidine (DDL). DDL can be measured by fluorescence. Since the amount of DDL produced equals the amount of formaldehyde present in solution (provided 2,4-pentanedione and ammonia are in excess) the formaldehyde concentration can be determined from the amount of DDL. Analysis was completed using a Shimadzu RF-1501 fluorescence spectrophotometer and calibration standards prepared by diluting a stock solution of

NaHMS. A new calibration was determined for each set of analyses. Approximately 20% of the samples were run in duplicate.

Hydroperoxides

The measurement of hydroperoxides using a fluorescence spectrophotometer measures both hydrogen peroxide and soluble organic hydroperoxides. For simplicity, hydrogen peroxide will be used here to denote hydroperoxides.

Hydrogen peroxide can be reduced by a hydrogen donor molecule, such as *p*-hydroxyphenylacetic acid (POPHA), in the presence of peroxidase. A dimeric product is formed which can be measured quantitatively by fluorescence. One molecular dimer is produced from one molecule of hydrogen peroxide. The hydrogen peroxide concentration in cloudwater can therefore be determined by measuring the dimer concentration. Hydrogen peroxide is very active chemically, however, requiring immediate analysis or preservation on site as soon as possible after cloudwater is taken from the collectors.

Hydrogen peroxide in fog samples was preserved on site by addition of *p*-hydroxyphenylacetic acid (POPHA) to form a stable dimer. The sample preservation is accomplished by adding 200 µl conditioning reagent and 200 µl fluorescent reagent to 1.0

ml cloudwater (or add conditioning and fluorescent reagents to cloud sample in a 1:5 ratio for smaller sample volumes). The conditioning reagent contains potassium hydrogen phthalate (KHP), which acts as a buffer (pH = 5.5), and EDTA, which can also act as a buffer (pH = 5.5) and prevents interference by metal ions.

Calibration standards were made from a reagent grade commercial 30% H_2O_2 solution (standardized by titration with potassium iodide) and DI water. A Shimadzu RF-1501 spectrofluorophotometer was used to measure the fluorescent intensity. Approximately 10% of the samples were analyzed in duplicate. More about this technique of peroxide preservation and analysis can be found in Lazrus et al. (1985) and Lodge (1985).

Total Fe and Mn

Total iron and manganese in fog samples were analyzed using a Varian SpectrAA Zeeman-corrected Graphite Furnace Atomic Absorption Spectrophotometer (GFAAS). These metals are of importance due to their influence on aqueous phase S(IV) oxidation.

Trace metal aliquots of fog samples were stabilized in the field by acidification with 9.73% nitric acid (1 part acid added to ten parts fogwater). Standard methods for Zeeman corrected GFAAS of aqueous iron and manganese were used for the analysis. The method contains an auto-dilution program that can perform a calibration by injecting incremented amounts of a stock standard. Stock standards of 50 $\mu g\ L^{-1}$ Fe and 80 $\mu g\ L^{-1}$

Mn were prepared by dilution of commercial standard Fe and Mn solutions. The following calibration standard concentrations were used:

Std.	Fe ($\mu g\ l^{-1}$)	Mn ($\mu g\ l^{-1}$)
1	5	8
2	10	16
3	20	24
4	30	48
5	40	64
6	50	80

Another low Mn concentration method was used for samples below the initial method's calibration range. The concentrations of additional standards for this method were 2, 4, 8, 10, and 20 $\mu g\ L^{-1}$.

All the samples were analyzed in duplicate; quality control parameters contained in the method regulate the amount the duplicates are allowed to differ before the run is stopped. After every 10 samples, a zero and a standard were run again. The run proceeds past this point only if the new values are within 10 percent of the previous responses. This prevents error due to the instrument drifting during measurements on a long series of samples.

Total Organic Carbon (TOC) and Dissolved Organic Carbon (DOC)

At the collection sites, the water available for organic carbon analysis was divided into two samples of approximately 2-3 ml each. The first sample was pipetted directly into a glass vial. This sample provided water for total carbon and total inorganic carbon

analysis (with the difference between the two representing total organic carbon). The second sample was filtered through a 10 ml syringe with a 0.45 μm nylon twist-on filter (Gelman) into the glass vial. This sample provided water for analysis of dissolved carbon and dissolved inorganic carbon (with the difference representing dissolved organic carbon).

The collected organic carbon samples were analyzed using a Shimadzu TOC 5000a total organic carbon analyzer. The technique used to determine the total carbon (TC) content of a sample involves vaporization and decomposition of the sample in a 680° C furnace and measurement of the evolved CO_2. Inorganic carbon (IC) is determined by measurement of the CO_2 produced by reaction of the sample with 25% phosphoric acid. The instrument does not respond to elemental carbon, since it is not oxidized at the furnace temperature used.

The 2-3 ml sample volumes did not provide enough water for direct measurement of both TC and IC in the original sample vials. Thus it was necessary to dilute the samples. A dilution of 1:3 (sample:DI water) was chosen. The original sample provided two 400 μl volumes, each of which was diluted with 1200 μl of DI water, thus providing samples for both TC and IC analysis.

Standards were prepared using 1000 ppm stock solutions of potassium hydrogen phthalate for TC and of sodium bicarbonate and sodium carbonate for IC. These stock

solutions were prepared using reagent grade salts and DI water. Two sets of four point calibration curves were run for both TC and IC, spanning the ranges 0-20 ppm and 0-100 ppm. After calibration a deionized water sample was run to remove any residual material from the standards remaining in the sample lines.

At the beginning of a new batch of analyses, a check of the calibration curves was made using 5 and 10 ppm standards. If the standard check was within 10%, a DI water sample was run and then an analysis run was initiated. If the calibration check failed, a new calibration curve was generated before starting an analysis run.

All samples were analyzed in duplicate or triplicate. After each set of ten samples (TC and IC) a standard check was made using 10 ppm standards. If the standard check was within 10 percent, the analysis run was continued, otherwise a new calibration curve was generated.

During analysis it was discovered that one batch of glass vials was contaminated. These vials were used for storing TOC and DOC aliquots made early in the study at the KWR site. Due to the contamination problems no TOC or DOC values are reported for these samples.

Chapter 3: General SJV Conditions

In most cases, the radiation fogs we sampled became dense enough to sample at the ground during the late night or early morning hours and would continue throughout the morning, lifting by noon. There were several occasions when the fog was very patchy and not thick enough to sample at one or more of the sites. This was particularly true of the urban sites, as fog was typically less dense in the cities than directly outside. There were six fog events sampled at Kern, six at Fresno and three at Bakersfield. Two events were sampled at all three sites concurrently, and one additional event was sampled simultaneously at both Kern and Fresno. Two events were sampled at the Candelabra Tower on January 12 and 14. Figure 3.1 shows a timeline of pH values for the southern portion of the study (Bakersfield, Fresno and Kern). Similar plots for all measured aqueous species are found in Appendix A. This also is a helpful overview of the events sampled, their duration and the locality of the fog.

The fog collected during IMS95 was relatively basic (compared to a pH of 5.6 which is expected for atmospheric water in equilibrium with carbon dioxide). The range of pH in the samples from all sites was 4.97 to 7.43, with a median value of 6.49. The distribution of pH values at the three southern sites, as depicted in Figure 3.2, shows that the fogwater at Kern was slightly more basic than that sampled at Fresno or Bakersfield. Also, the

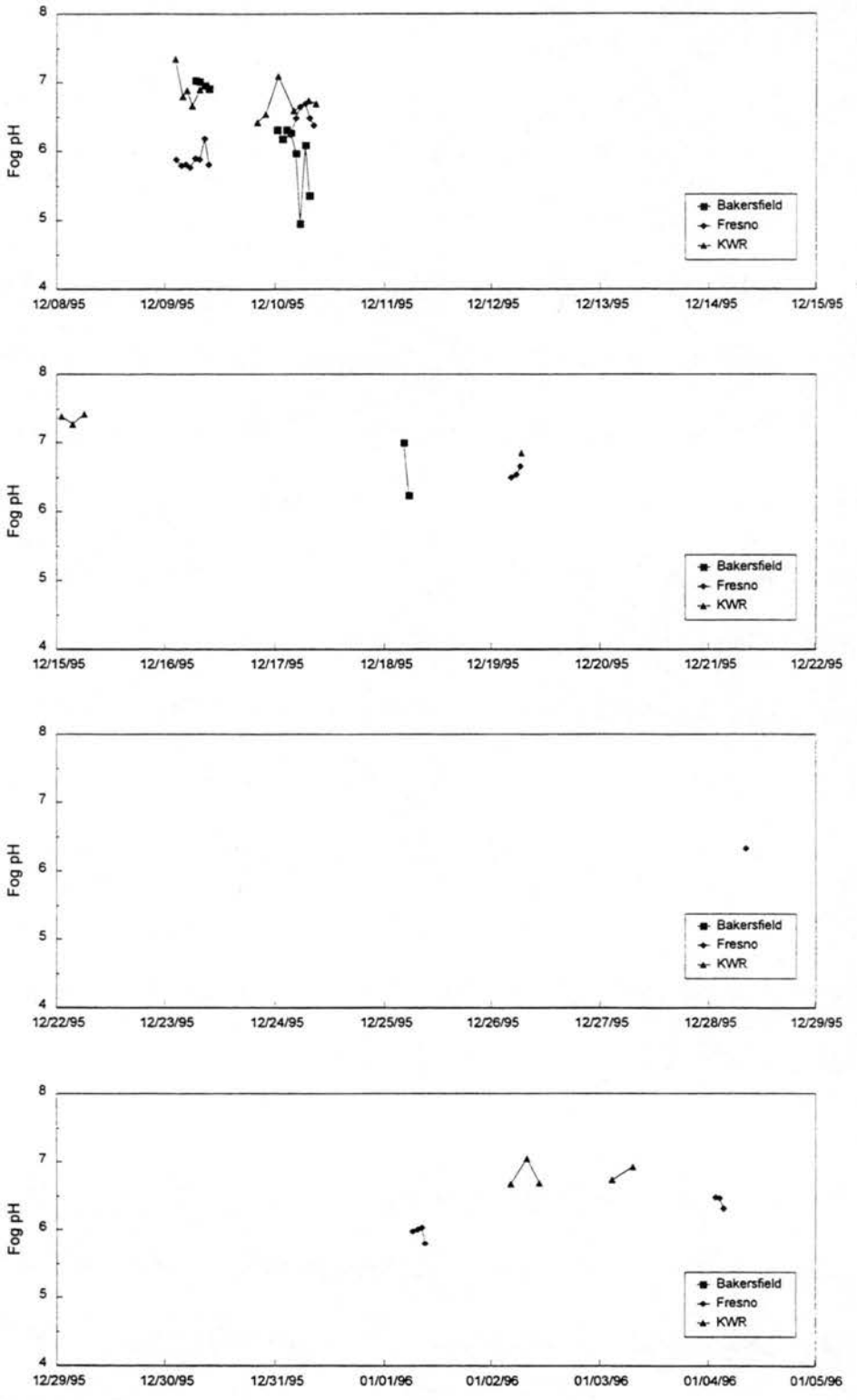

Figure 3.1: Fog pH values measured in bulk fog samples collected with the CASCC2 collectors at the three southern IMS95 sites.

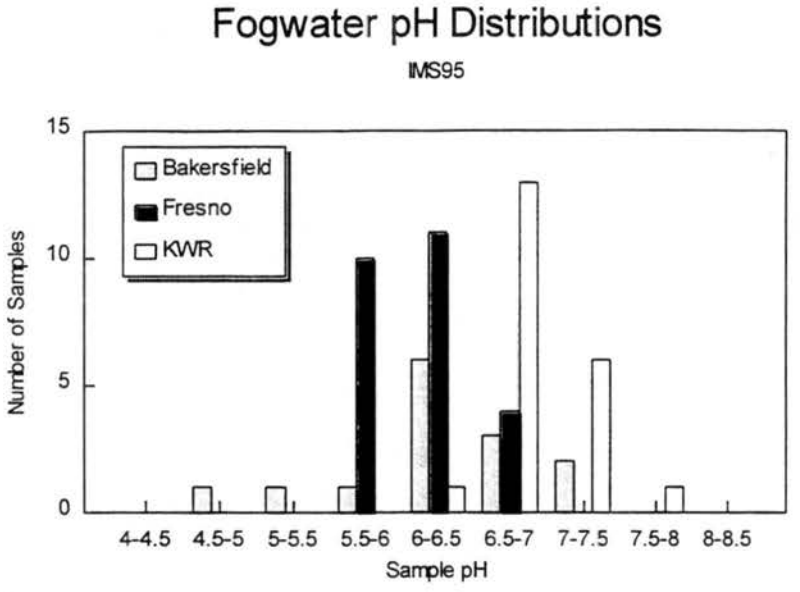

Figure 3.2: Frequency distributions of pH values observed in CASCC2 bulk fog samples from the three IMS95 core sites.

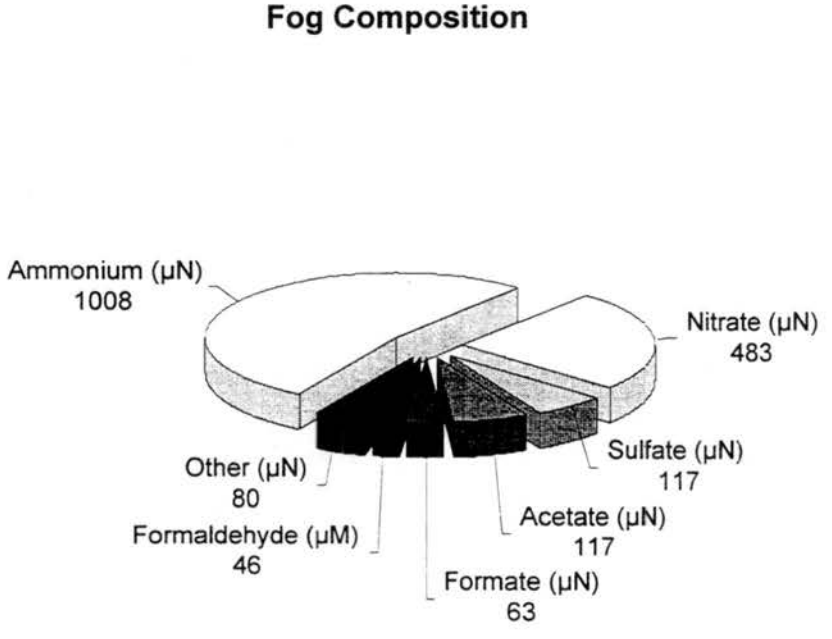

Figure 3.3: Median fog composition for southern SJV fog samples. The other slice represents additional species measured (Ca^{2+}, K^{+}, Na^{+}, Mg^{2+}, Cl^{-}, propionate, pyruvate and oxalate) were present at lower concentrations (in μN).

range of observed pH was greater at Bakersfield due to several high acidity spikes (discussed later) which were observed on short time scales during the first two fog events. Figure 3.3 shows the median sample composition for the southern SJV sites. The dominant species measured were ammonium, sulfate, nitrate, acetate, formate and formaldehyde. Inorganic species were typically present in similar concentrations at the three sites, except for very large sulfate spikes in certain Bakersfield samples. Organic species, however, were often more concentrated in the urban fog samples (Bakersfield and Fresno) than in samples from the rural site (Kern). A charge balance was performed by comparing the sum of the anionic species concentrations (chloride, nitrate, sulfate and organic acids) to the sum of the cationic species concentrations (H^+, sodium, ammonium, potassium, magnesium and calcium). A deficiency was usually seen on the anionic side, presumably due to unmeasured species (other organic acids, nitrite, bicarbonate, carbonate), yielding typical charge ratios of 0.7 to 0.9. Repeat IC analysis of species flagged for low charge balance gave results close to the original analyses.

Significant chemical differences were seen between large and small drop fractions (see Figure 3.4). Plots of large drop versus small drop concentrations of all chemical species measured are presented in Appendix A. Small drops usually had a lower pH, and greater amounts of all measured inorganic ionic species. This size dependence is different from patterns observed previously in the SJV and elsewhere, where the mechanically generated crustal and sea salt ions such as calcium, magnesium, sodium and chloride were often more concentrated in the larger drops (Bator and Collett, 1997). The larger drops had higher concentrations of acetate and propionate, but the small drops were enhanced in the

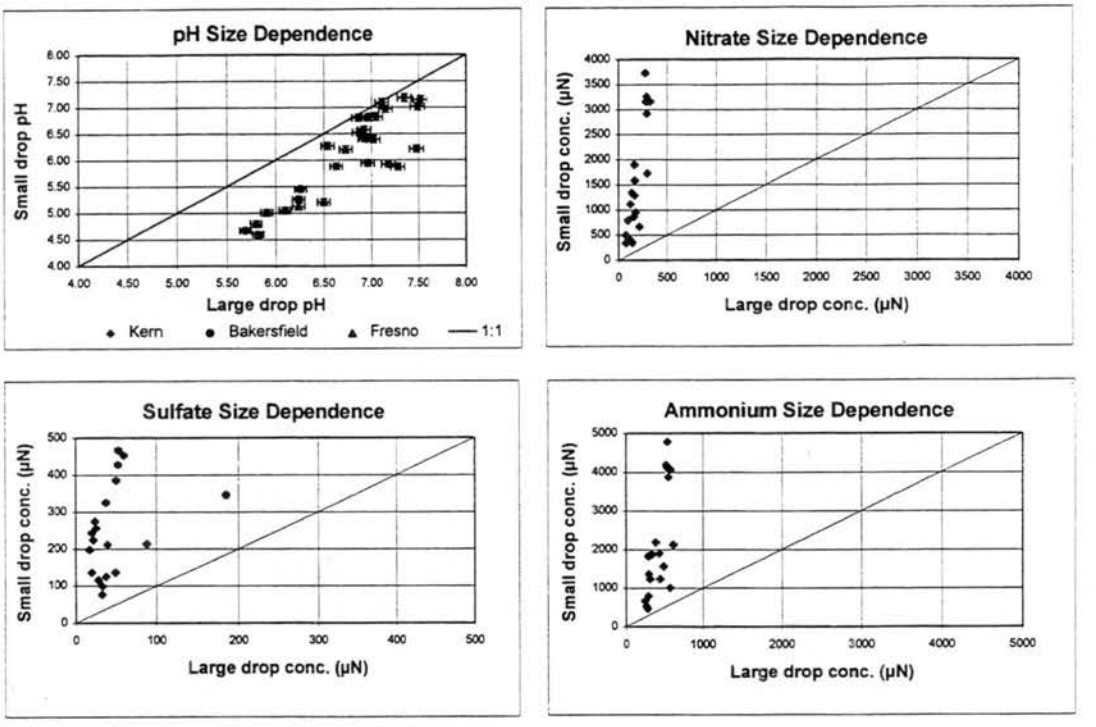

Figure 3.4: Size dependence of pH in SJV samples and major ionic species concentrations in Kern fogwater. Bakersfield and Fresno samples were collected with ETH impactors and Kern samples were collected with a sf-CASCC. Error bars represent analytical uncertainties expressed as σ (see Table A-1).

other three organic acids measured. The smaller drops were also more enhanced in total free S(IV), total formaldehyde, HMS and total organic carbon. There was no consistent size dependence to the concentrations of peroxide, iron and manganese.

Figure 3.5 shows ammonium, nitrate and sulfate concentrations in fogwater from each site sampled during the first two fog events. Concentrations of all species were comparable between sites except for high values of ammonium and nitrate in evaporating fog at the end of the December 9 event at Fresno and high concentrations of ammonium and sulfate during the December 10 event at Bakersfield.

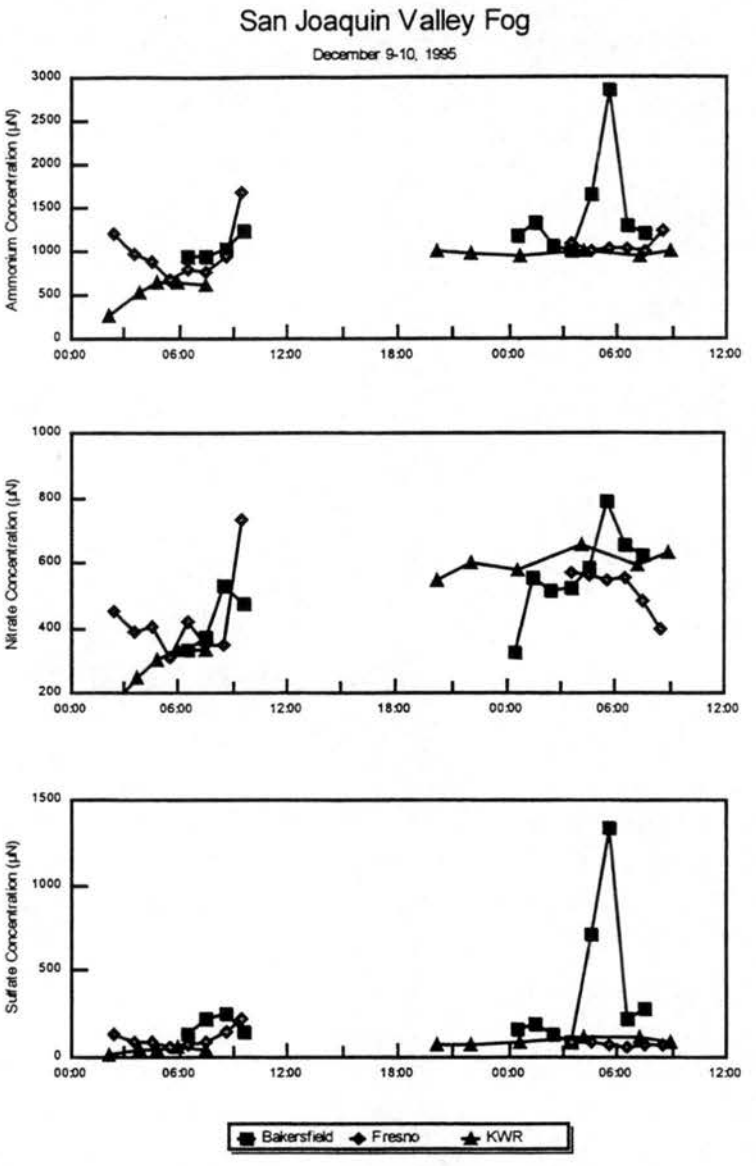

Figure 3.5: Concentrations of ammonium, nitrate, and sulfate measured in fog samples collected with the CASCC2 collectors at the three IMS95 core sites on the mornings of December 9 and 10, 1995. Points are plotted at the midpoint of the sampling intervals.

Figure 3.6 shows timelines of the concentrations of some of the major species in the fog samples collected at Bakersfield on December 10, 1995. A large pH drop was observed for the sample collected between 5:00 and 6:00 AM. This pH drop is accompanied by large increases in sulfate, S(IV) and, to a lesser extent, nitrate. There is also a large

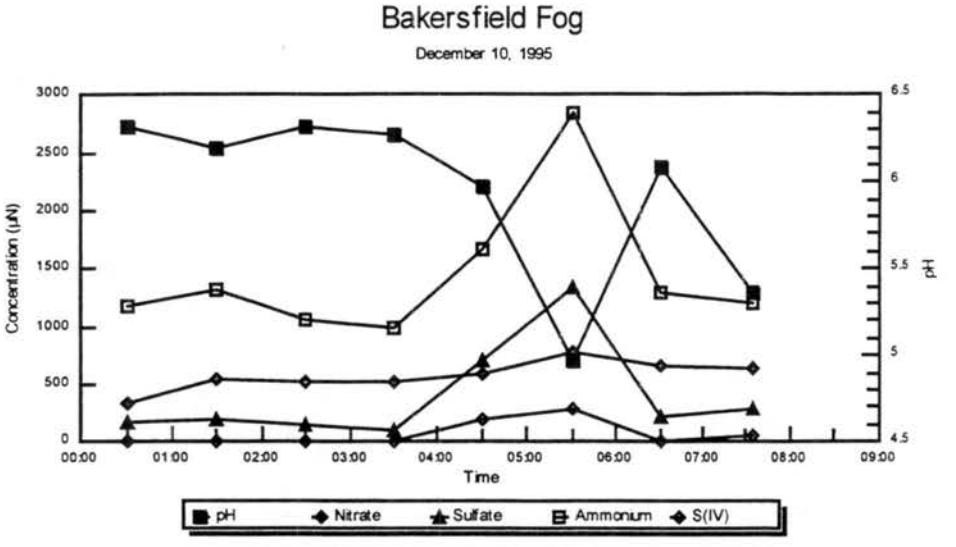

Figure 3.6: Temporal changes in fog composition at Bakersfield on the morning of December 10, 1995. Samples were collected with the CASCC2 and are plotted at the midpoint of each sampling interval.

increase in ammonium in the fogwater, but it is not enough to neutralize the increased acidic species. Other such spikes can be seen on December 9th and 18th. We have postulated that there are localized sources or plumes that were affecting the Bakersfield site during these times, since during most other times, the concentrations of inorganic species at Bakersfield were relatively close to those measured at the other two sites.

Liquid water content (LWC) was calculated using CASCC2 collection rates and efficiencies as described by Demoz et al (1996). Figure 3.7 shows a timeline plot of LWC at each of the three sites throughout the southern SJV study. LWC was comparable at each of the three southern SJV sites during events for which simultaneous sampling was possible. The distribution of liquid water between the large and small drop fractions as measured by the sf-CASCC at Kern is shown in Figure 3.8.

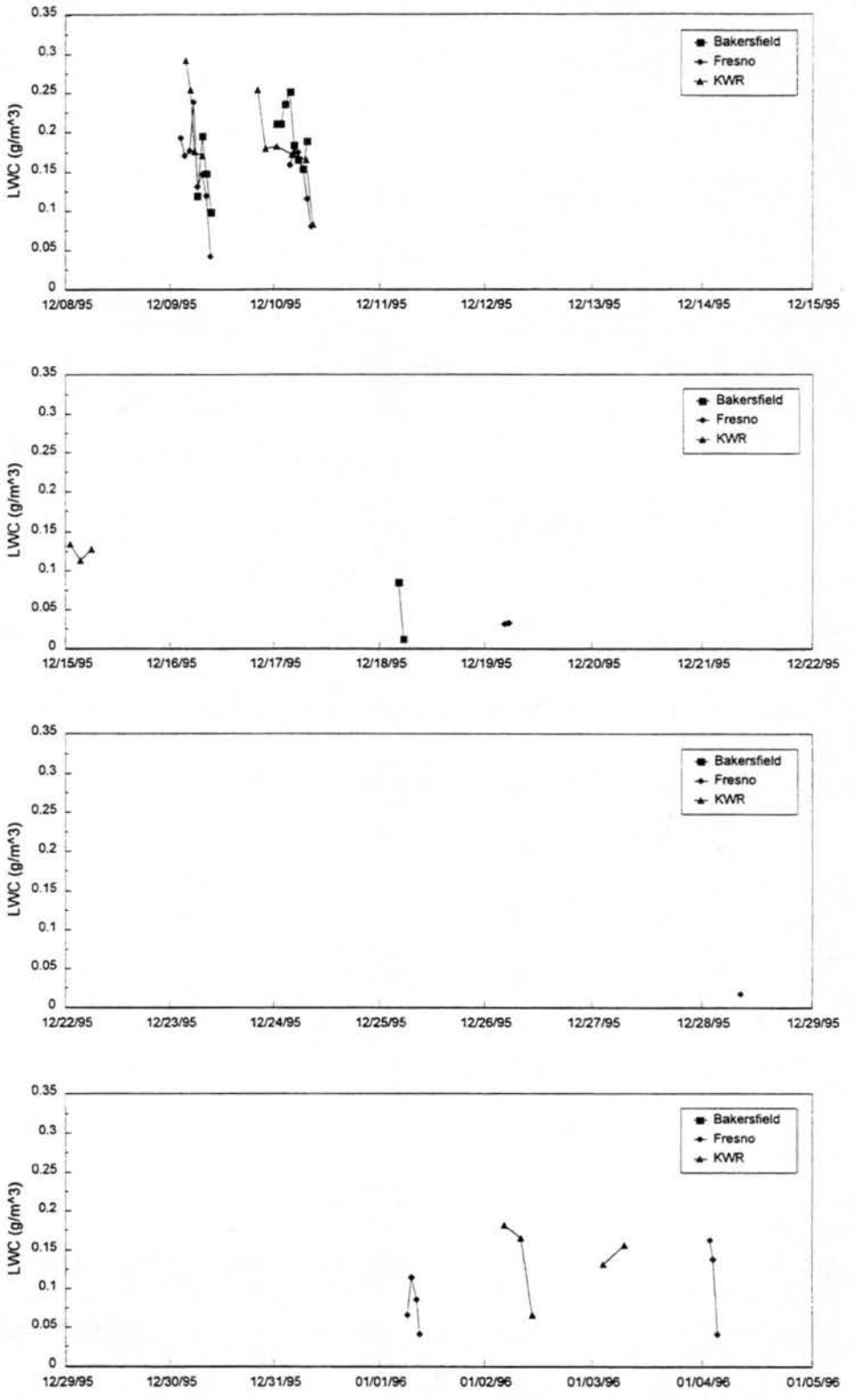

Figure 3.7: Liquid water content (LWC) timelines of the southern SJV fog events.

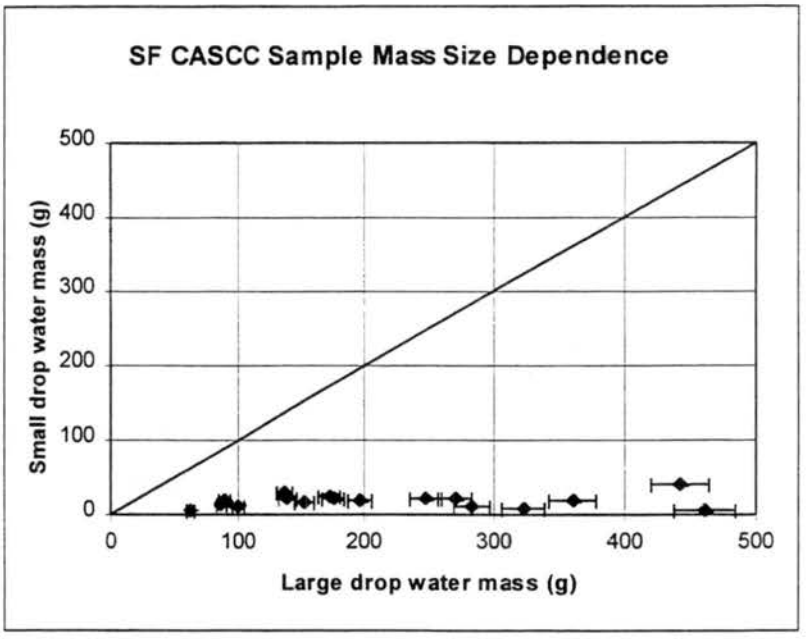

Figure 3.8: The size distribution of liquid water mass. Each point represents the mass of the large and small drop masses from samples collected with the sf-CASCC at Kern. The error bars depict a 5 percent uncertainty in the mass measurements.

The concentration loading of a species in the fog water is defined as its concentration per m^3 of air. This quantity is calculated by multiplying the aqueous concentration of the species by the liquid water content of the fog. Figure 3.9 shows the sulfate, nitrate and ammonium loadings for December 9-10 at the three southern sites. The decrease toward the end of the events at Fresno and Kern suggests that significant removal of these species to the ground was taking place. This is consistent with a significant water flux to the ground observed during those fog events.

Continuous gas phase measurements of SO_2 and O_3 were also made at Bakersfield, Fresno and Kern by the California Air Resources Board and Sonoma Technology, Inc.. Figure 3.10 shows the SO_2 concentrations for the entire study at these three sites. The

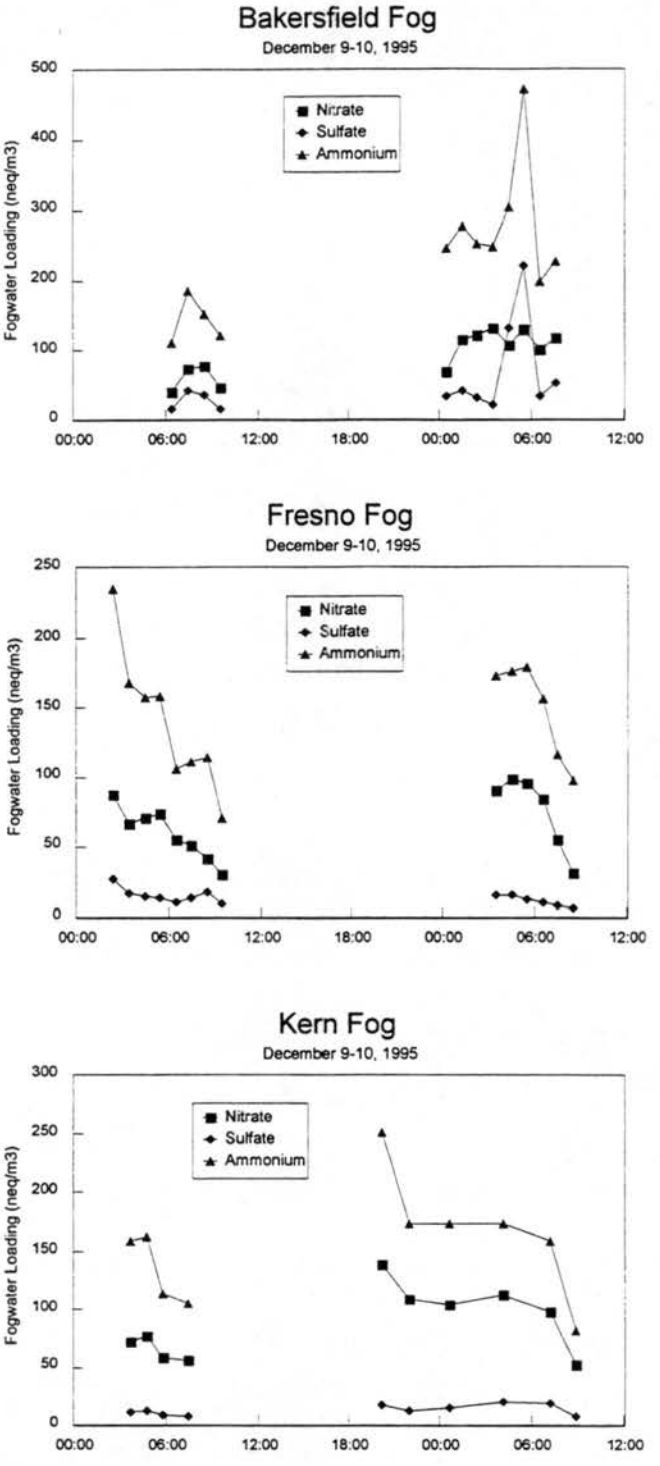

Figure 3.9: Fogwater loadings of ammonium, nitrate and sulfate at Bakersfield, Fresno and Kern on the mornings of December 9 and 10, 1995. The fogwater loading of a species is its aqueous phase concentration multiplied by the fog liquid water content, and represents the total amount of that species in the aqueous phase per unit volume of air.

lowest quantifiable level (LQL) was 1 ppb for these instruments and is indicated on each plot with a heavy black line. SO_2 levels were comparable at Bakersfield and Fresno, ranging from 0 to 10 ppb, whereas at Kern SO_2 concentrations were usually below 1 ppb.

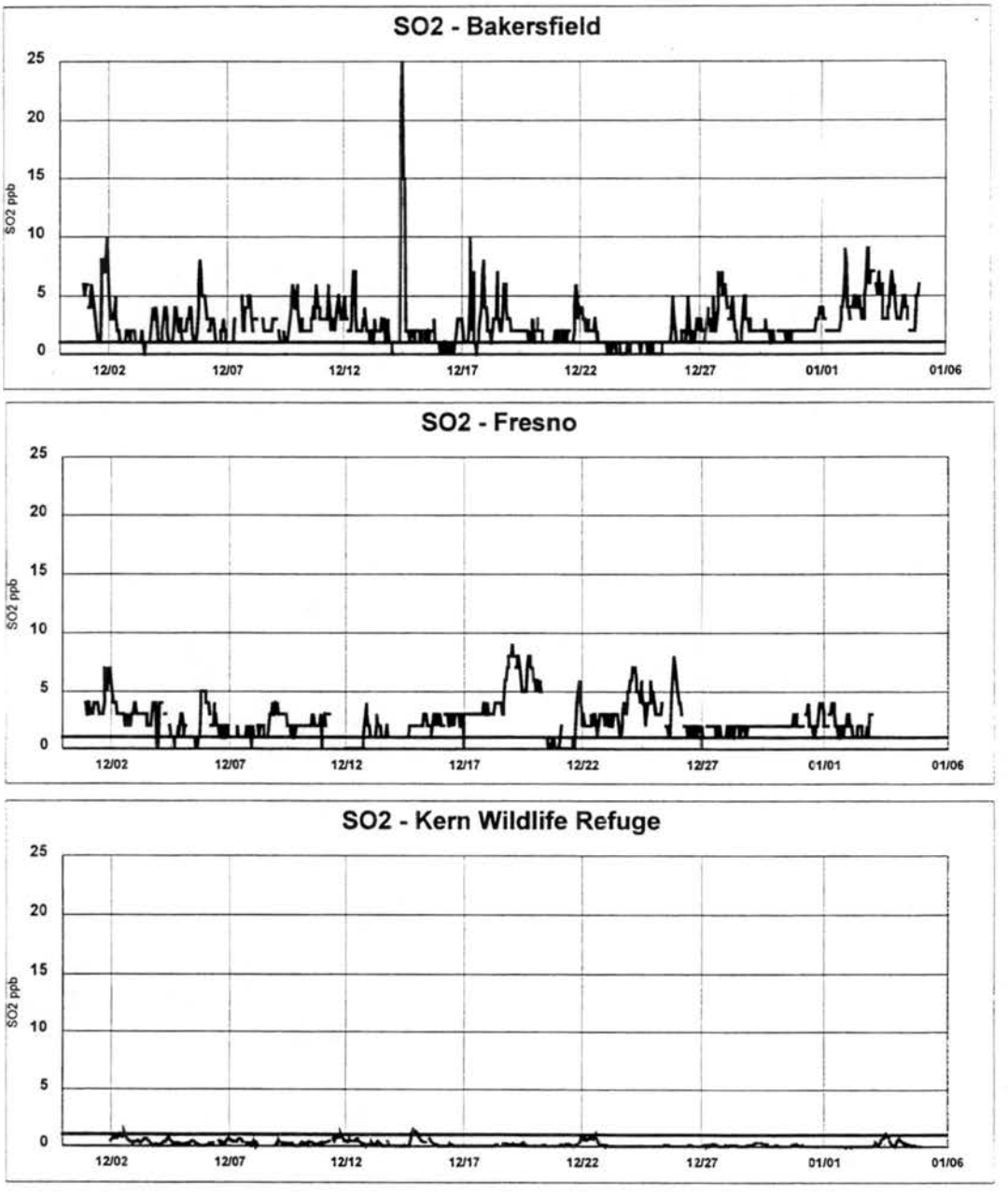

Figure 3.10: SO_2 concentrations measured at the fog sampling sites during IMS95. (LQL = 1 ppb)

Figure 3.11 shows the ozone concentrations for the three fog sites. A strong diurnal pattern is seen with peak values occurring in the afternoon for each site, most often after the fog had evaporated. Peak concentrations are usually between 10 and 40 ppb and

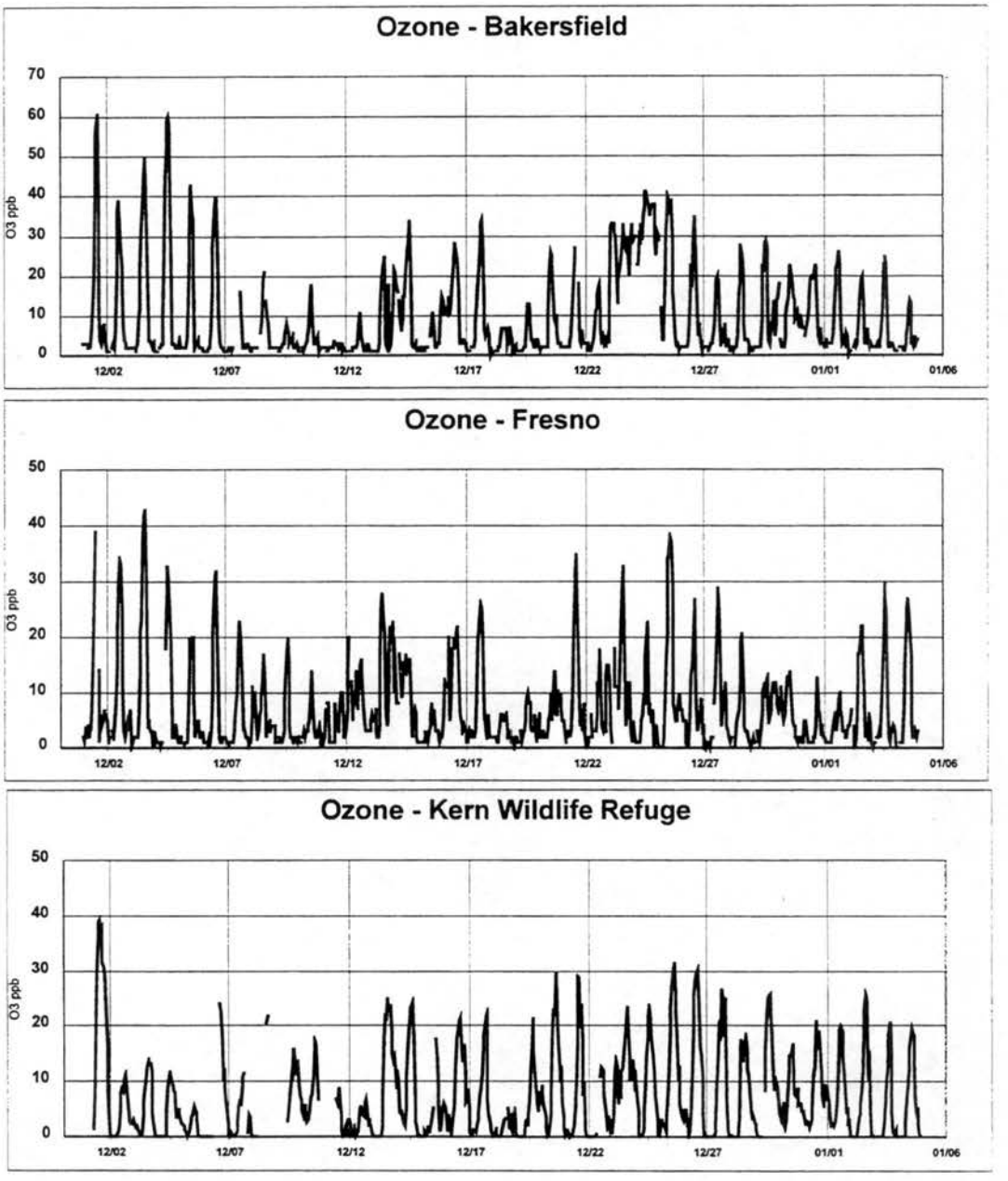

Figure 3.11: O_3 concentrations measured at the fog sampling sites during IMS95. (LQL = 1 ppb)

occurred usually between 1:00 and 3:00 PM. This diurnal profile can be explained by the basic photochemical cycle of O_3 with NO and NO_2 given by the following reactions:

$$NO_2 + h\nu \rightarrow NO + O \qquad (1)$$

$$O + O_2 + M \rightarrow O_3 + M \qquad (2)$$

$$O_3 + NO \rightarrow NO_2 + O_2 \qquad (3)$$

Low nighttime values of O_3 are due to the fact that reaction (1) is not active, so that no ozone is being made but O_3 is still consumed in (3) by fresh NO emissions. Higher daytime O_3 is due to photochemical production and perhaps also transport from ozone rich air aloft. Figure 3.12 shows a typical daily profile of ozone for the three southern SJV sites.

Gas phase peroxide concentrations were measured by CSU and NCAR using two fluorometric analyzers. These two instruments were moved among the three sampling sites. Gas phase peroxide data for each site are shown in Figure 3.13. Data are more sporadic and noisy at the low concentrations observed, but a diurnal pattern can be seen at Bakersfield and Fresno with a daily peak occurring between 12:00 and 1:00 PM. Peak values range from 0.2 to 0.6 ppb at Fresno and Bakersfield and as high as 1.2 ppb at Kern.

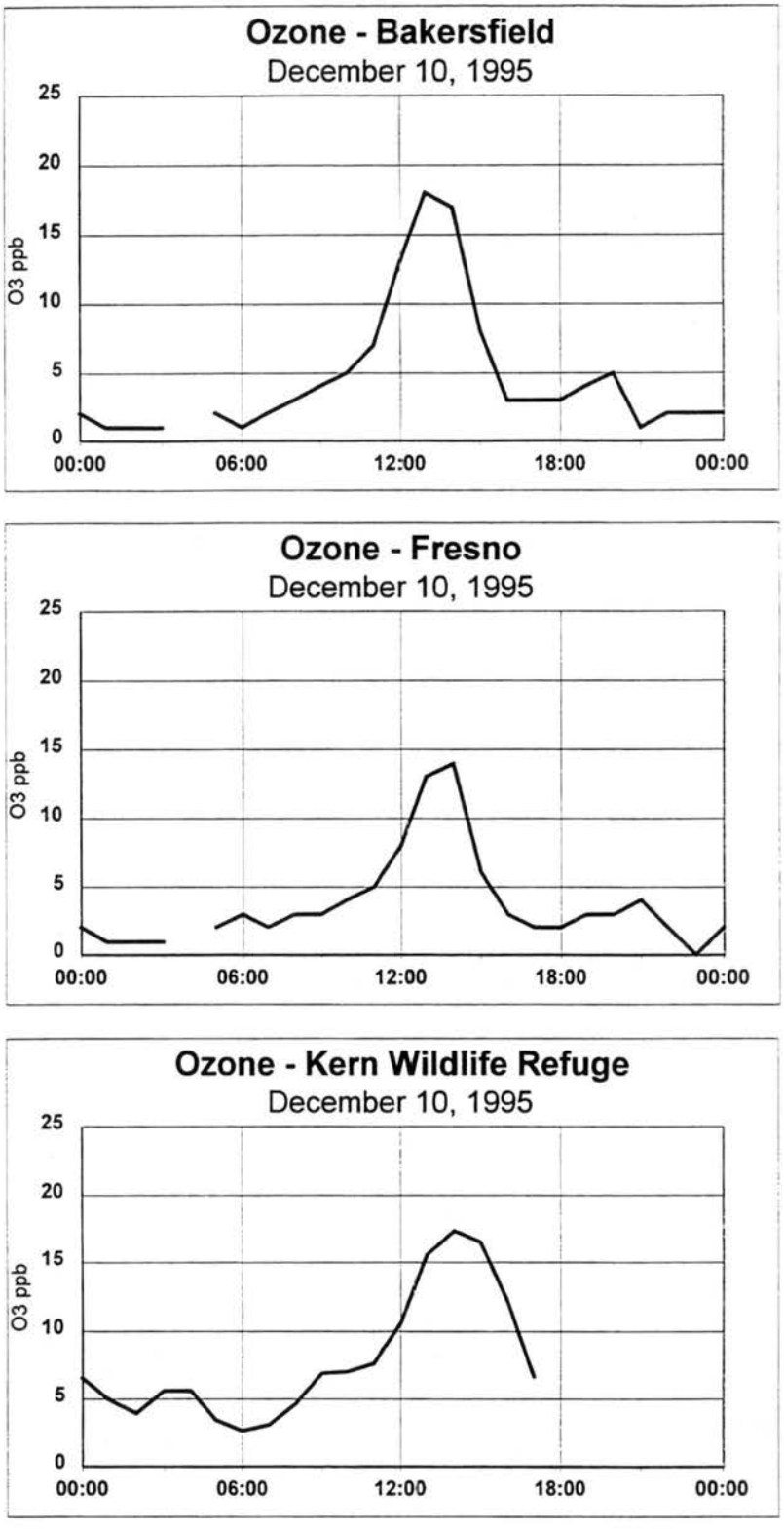

Figure 3.12: Daily profile of ozone at each of the southern SJV fog sampling sites.

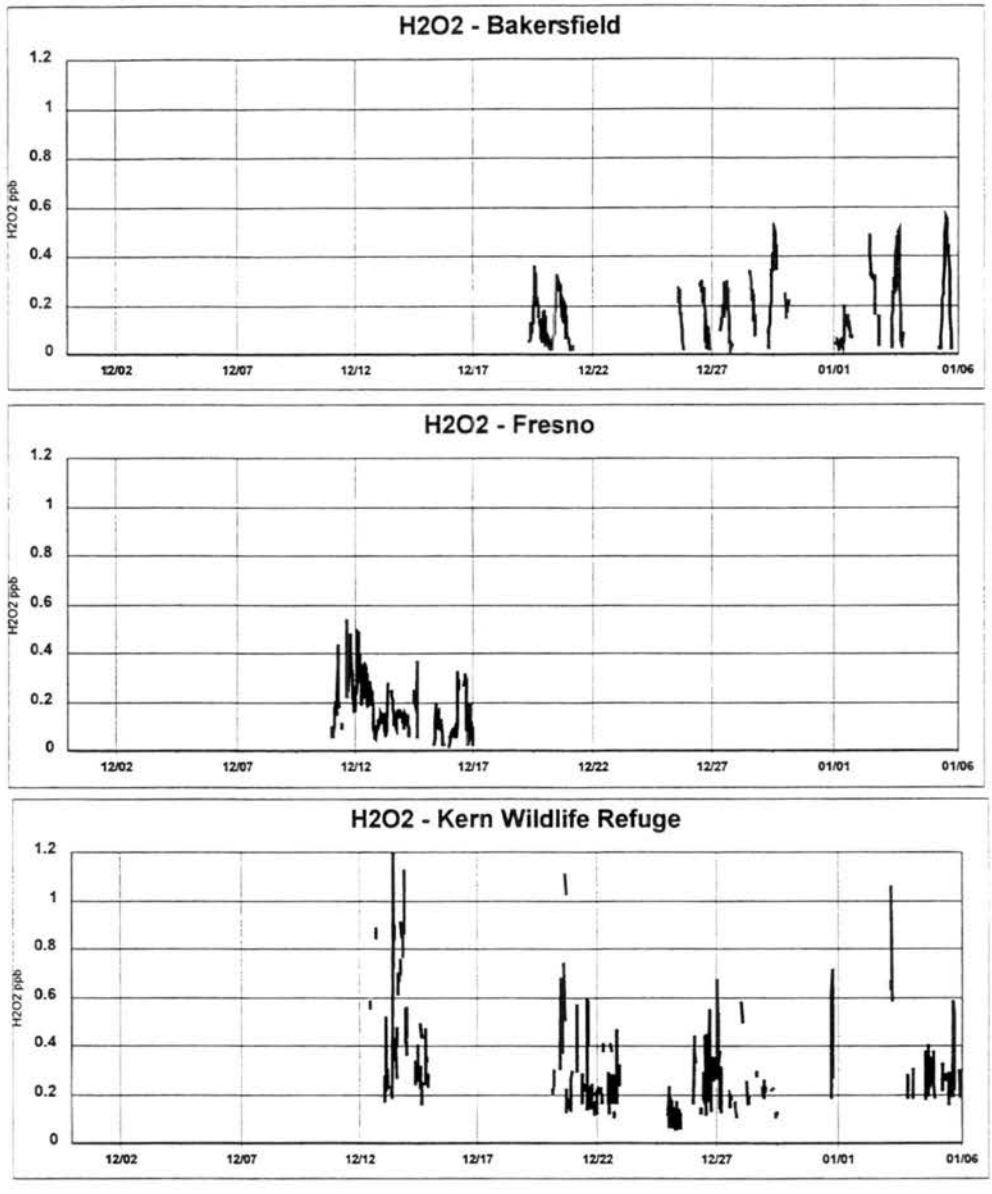

Figure 3.13: H_2O_2 concentrations measured at the fog sampling sites during IMS95.

Aerosol total mass and some chemical speciation measurements were performed by the University of Nevada Desert Research Institute (DRI). Aerosol total mass, ammonium, nitrate, sulfate, organic and elemental carbon mass averages and ranges for the three hour averages are shown in Tables 3.1 (PM_{10}) and 3.2 ($PM_{2.5}$). Silicon, iron, aluminum, elemental sulfur, non-volatilized nitrate, chloride and potassium were also usually present

Table 3.1: PM_{10} total mass and major species contributions at each of the southern SJV sites. All concentrations are given in $\mu g/m^3$. Total mass was obtained from about 200 samples in each case, and chemical information was obtained from about 64 samples.

Site	Total Mass	NH_4^+	NO_3^-	SO_4^{2-}	OC	EC
Bakersfield	49.7 (2.1-145.6)	6.0 (0.8-10.8)	16.9 (1.0-32.5)	2.9 (0.9-6.2)	15.2 (4.3-39.1)	6.8 (0.9-16.4)
Fresno	60.5 (8.6-269.5)	5.4 (1.0-10.9)	15.5 (1.8-29.4)	2.5 (0.9-5.0)	22.5 (3.7-101.3)	8.1 (1.1-30.0)
Kern	32.1 (6.3-86.8)	5.3 (2.1-10.3)	15.6 (5.5-34.3)	2.1 (0.6-4.3)	4.6 (1.9-8.9)	1.9 (1.0-3.5)

Table 3.2: $PM_{2.5}$ total mass and some major species contributions at each of the southern SJV sites. All concentrations are given in $\mu g/m^3$. Total mass was obtained from about 200 samples in each case, and chemical information was obtained from about 64 samples.

Site	Total Mass	NH_4^+	NO_3^-	SO_4^{2-}	OC	EC
Bakersfield	37.0 (1.8-120.0)	4.9 (0.8-9.6)	14.5 (0.9-29.1)	2.5 (0.6-5.1)	13.3 (4.5-38.7)	5.3 (0.9-12.7)
Fresno	49.1 (6.7-240.8)	4.4 (0.9-10.5)	15.4 (1.4-37.9)	2.1 (0.4-4.6)	20.4 (2.5-98.3)	7.3 (1.1-28.0)
Kern	24.6 (1.2-77.3)	4.1 (0.0-8.9)	14.9 (3.6-32.3)	1.6 (0.3-5.5)	3.4 (1.8-6.6)	1.6 (0.6-3.2)

in concentrations above 0.5 $\mu g/m^3$ in PM_{10} measurements. Nitric acid, ammonia, OC from backup filters and elemental sulfur were also present in concentrations above 0.5 $\mu g/m^3$ in $PM_{2.5}$ measurements. Concentrations of chemical species are similar at each site for both the PM_{10} and $PM_{2.5}$ fractions except total mass and organic and elemental carbon which are significantly lower at Kern. Additional information concerning these measurements and their results can be found in Chow and Egami (1997).

Vertical variations in gas concentrations and fogwater composition and liquid water content were investigated during the sampling events at the Candelabra Tower. Figure

3.14 shows typical SO_2, H_2O_2 and O_3 vertical profiles and Figure 3.15 shows timelines of concentrations of each gas at the ground and at 430 m (the top of the tower). H_2O_2 and especially O_3 were higher at the top of the tower, while SO_2 was much higher at the ground.

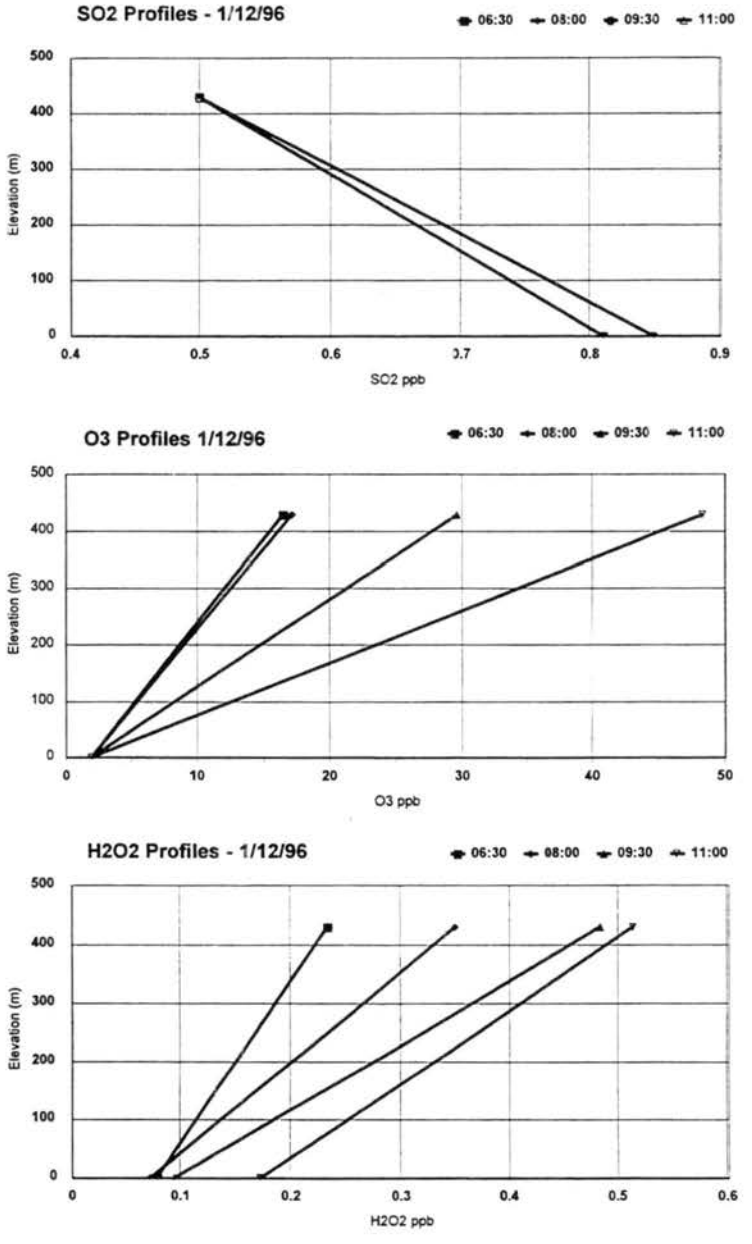

Figure 3.14: Profiles of gas concentrations measured at the ground and 430 m on January 12, 1996.

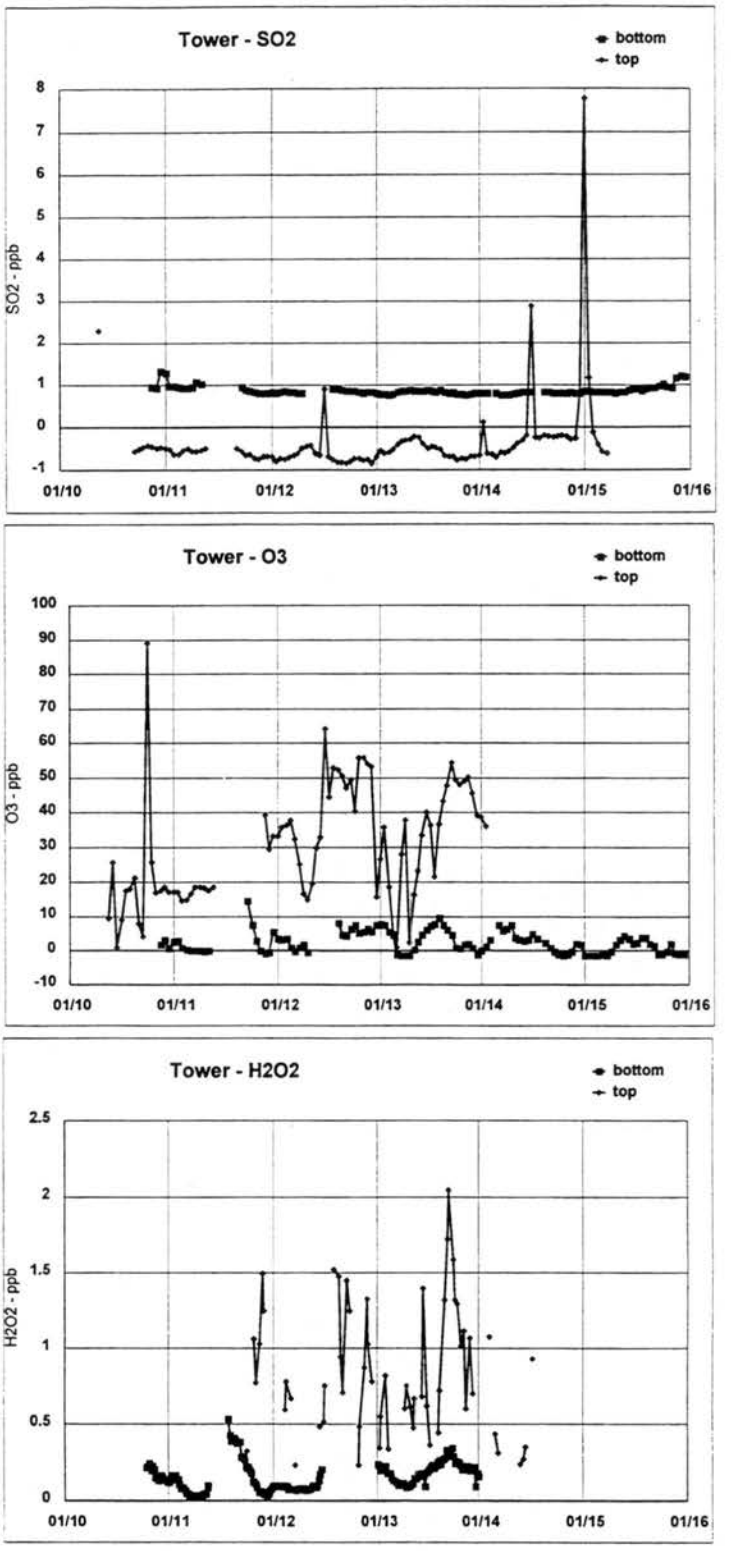

Figure 3.15: Timelines of gas concentrations at the ground and the top of the Candelabra Tower (430 m) during the northern IMS95 study.

Figure 3.16 shows the LWC content profiles for the January 12 event. LWC was higher at higher elevations and decreased at each level over the course of the event.

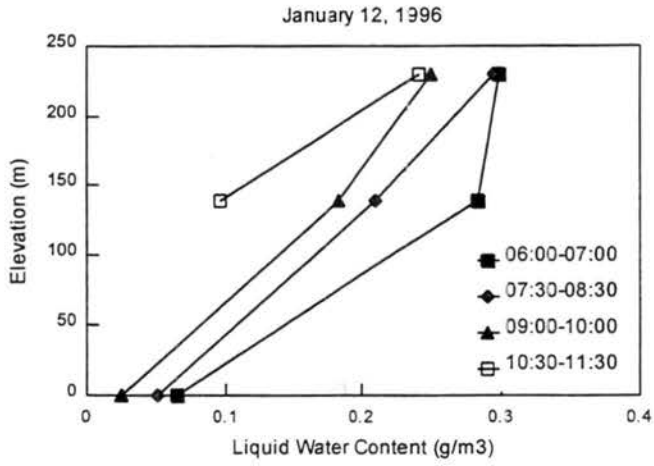

Figure 3.16: Vertical profiles of liquid water content measured at the Candelabra Tower on January 12, 1996.

Figures 3.17 and 3.18 show the aqueous concentrations of major ionic species in fogwater collected on January 12 as a function of height and time. Ionic species were most concentrated near the ground, but the concentrations at each level remained rather constant during the fog event. Fogwater acidity varied less than 0.5 pH units throughout the fog layer, but the shape of the profile changed more throughout the evolution of the fog with higher pH at the ground at the beginning of the event and higher pH aloft as the fog evaporated (see Figure 3.19). Figure 3.20 shows the fogwater ion loadings (in nanoeq/m^3) for ground and 230 m samples on January 12. The loadings of these at both elevations appear to decrease with time. This suggests that material was being removed from the cloud with time, either by transport out of the column we were sampling (by

advection or surface deposition) or by complete evaporation of some drops, since LWC decreased with time over the period of these measurements.

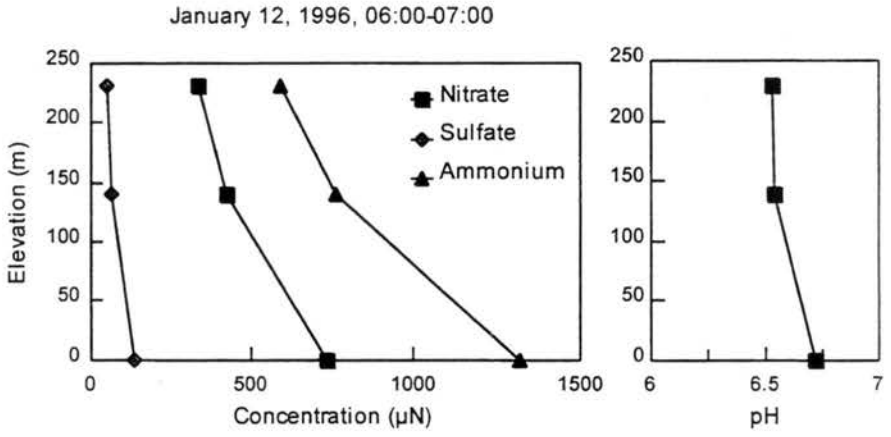

Figure 3.17: Vertical profiles of major ions and pH on January 12, 1996.

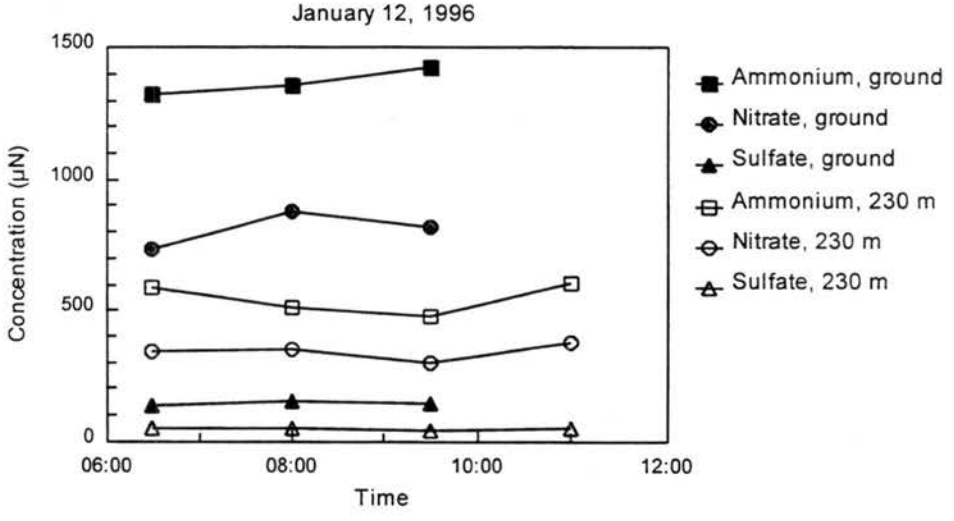

Figure 3.18: Timelines of major ionic species measured at the ground and at 230 m on January 12, 1996.

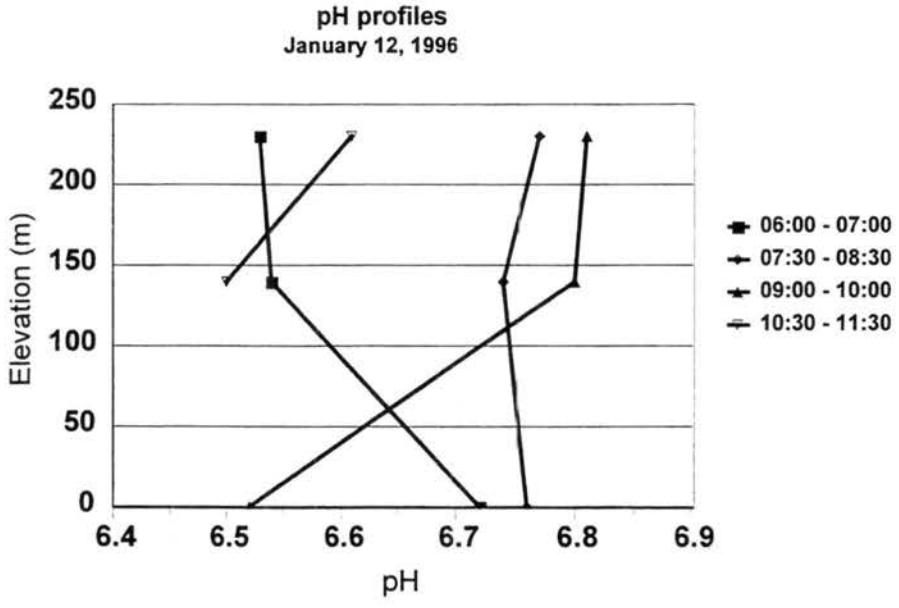

Figure 3.19: A time series of the measured vertical pH profile on January 12, 1996 at the Candelabra Tower. Each line represents simultaneous fog samples collected at the indicated heights during the listed time periods.

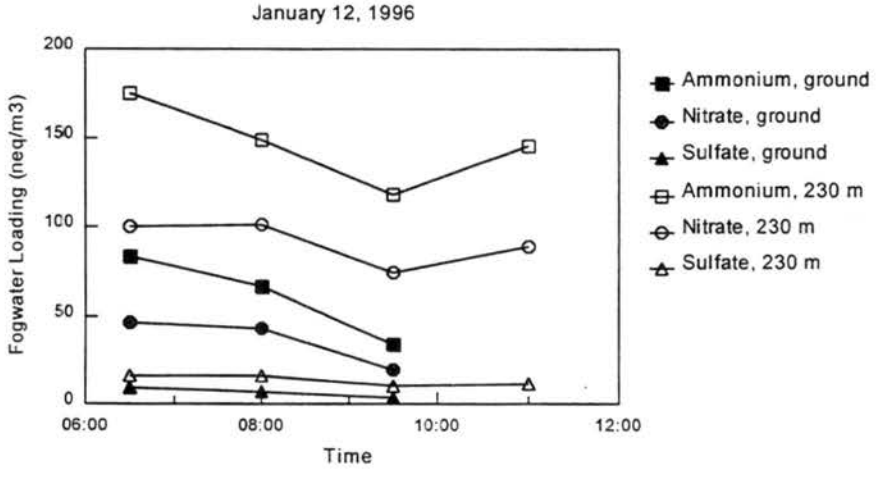

Figure 3.20: Fogwater loadings of major ions at the ground and 230 m on January 12, 1996.

Chapter 4: Bulk S(IV) Oxidation

SO_2, a major gaseous primary pollutant, is absorbed by fog drops and is one of the major contributors to aqueous phase atmospheric chemistry. In its aqueous form, SO_2 is partitioned into H_2SO_3, HSO_3^- and SO_3^{2-}. This partitioning tends toward sulfite (SO_3^{2-}) at high pH, allowing more SO_2 into the droplet. Conversely, if the drop pH falls, the equilibrium tends toward H_2SO_3, limiting further absorption of $SO_{2(g)}$.

Once in aqueous form SO_2 (S(IV)) oxidizes readily to H_2SO_4 (S(VI)). There are three main oxidation pathways corresponding to different oxidants: hydrogen peroxide, ozone and oxygen. The oxygen pathway is catalyzed by Fe(III) and Mn(II), metals commonly found in atmospheric particles upon which fog drops form. Previous studies usually focused on S(IV) oxidation by the hydrogen peroxide pathway, since with ample amounts of all oxidants and catalysts, this pathway would be dominant at the lower pH range usually seen in atmospheric water. However, the H_2O_2 pathway is pH independent over a pH range from 2 to 8, while the other two oxidation pathways are very pH dependent, their rates increasing dramatically with increasing pH (see Fig 4.1). Therefore, in more alkaline fogs, the oxidation process must be examined more carefully to determine dominant mechanisms.

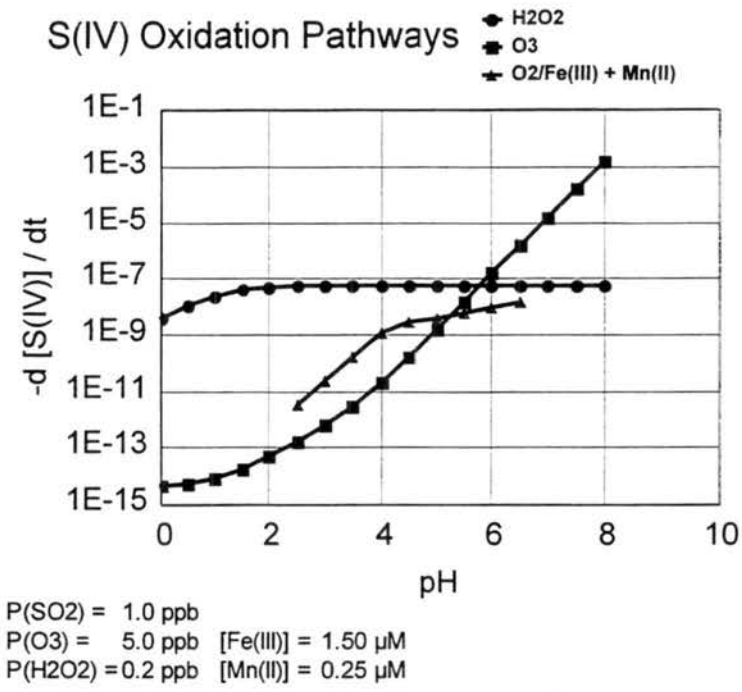

Figure 4.1: S(IV) oxidation rates as a function of pH for typical San Joaquin Valley conditions. Increases of SO_2 would shift all curves together, whereas increases in individual oxidant or catalyst concentrations would shift only the pertaining rate curve. (H_2O_2: Seinfeld, 1986; O_3: Hoffmann, 1986; O_2/Fe(III)+Mn(II): Ibusuki and Takeuchi, 1987) Rates are given in M s^{-1}.

The following equations are used for S(IV) oxidation rate calculations in this thesis (all concentrations are in units of **M** and rate constants are given for 10°C, representative of the general conditions during the fog events):

H_2O_2:

$$-d[S(IV)]/dt = k\,[H^+]\,[H_2O_2]\,[HSO_3^-] / (1+13[H^+])$$

where k = 3.20 E+7 $M^{-1}s^{-1}$, (Seinfeld, 1986).

O_3:

$-d[S(IV)]/dt = [O_3](k_1[H_2SO_3] + k_2[HSO_3^-] + k_3[SO_3^{2-}])$

where k_1 = 2.4 E+4 $M^{-1}s^{-1}$, k_2 = 1.4 E+5 $M^{-1}s^{-1}$, and k_3 = 5.9 E+8 $M^{-1}s^{-1}$, (Hoffmann, 1986).

O_2/Fe(III)+Mn(II) (4.2 < pH < 6.5):

$-d[S(IV)]/dt = k\,[Fe(III)]\,[Mn(II)]\,[S(IV)]\,[H^+]^{0.67}$

where k = 6.3 E+12 $M^{-1}s^{-1}$, (Ibusuki and Takeuchi 1987). This rate expression was also applied to samples whose pH was above 6.5 due to the lack of other experimental rate results for relevant concentrations including the synergistic effect between iron and manganese.

Measured fog pH values and measured metals concentrations were used in the calculations. Dissolved Fe(III) was assumed to comprise one quarter of the total aqueous iron concentration. Henry's Law (constants at 10°C) was used to obtain aqueous O_3, H_2O_2, and SO_2 concentrations from measured gas concentrations averaged over relevant sampling times. The speciation of $SO_{2(aq)}$ was calculated at 10°C. When gas concentrations were below the lowest quantifiable level (LQL) of the instrument the concentration of the gas was assumed to be the LQL. When data were unavailable for SO_2 or O_3, concentrations at the corresponding time period on preceding or subsequent days were used. In cases when H_2O_2 data were missing, concentrations were taken from an average diurnal pattern calculated as an average for each hour of the day for all study

days. This was done because large variability in the data made it difficult to determine a representative daily pattern from one day of data alone. Figure 4.2 shows histograms of

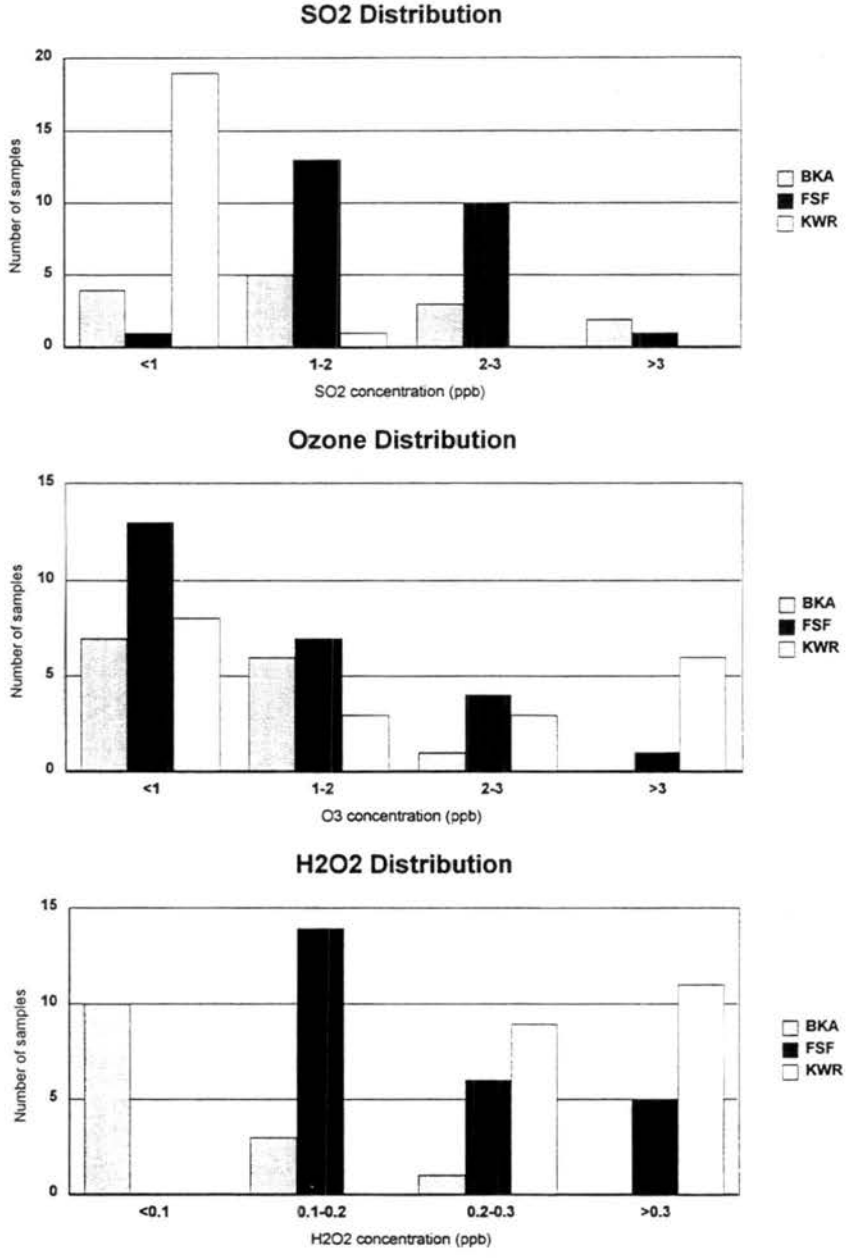

Figure 4.2: Gas phase concentrations of sulfur dioxide, ozone and hydrogen peroxide used in the S(IV) oxidation calculations.

the sulfur dioxide, ozone, and hydrogen peroxide gas phase concentrations (including actual measurements and estimated values) used in the S(IV) oxidation calculations.

At the tower, gases were measured at the ground and at the top of the tower (430 m), while two of the samplers were located in between these elevations. Gas concentrations

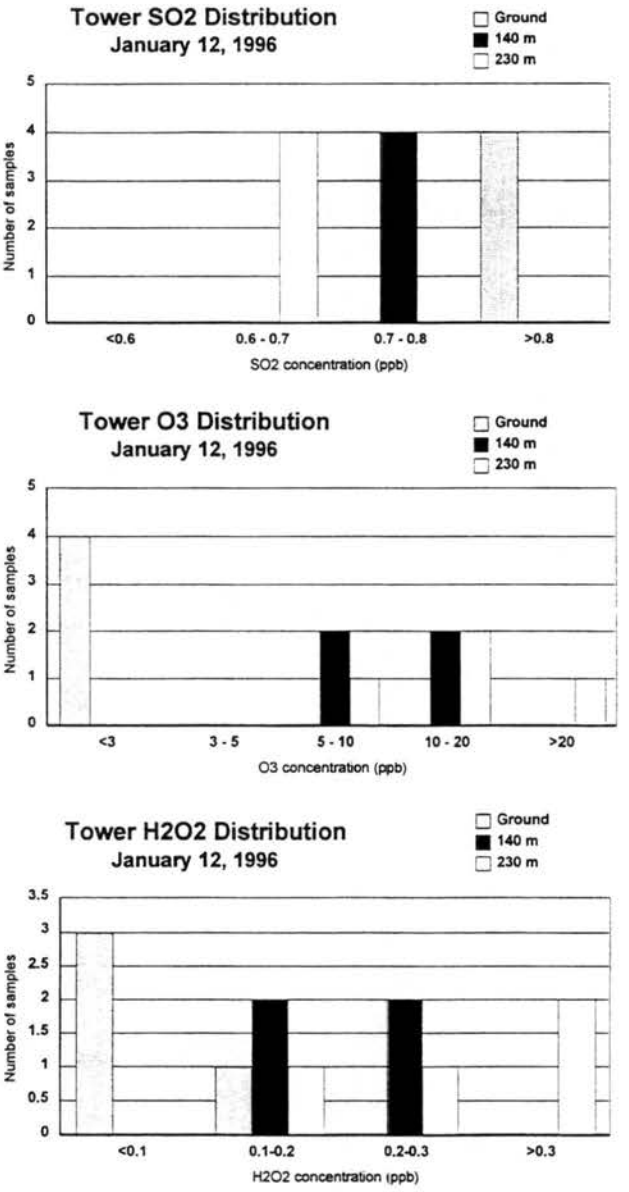

Figure 4.3: Gas concentrations used for January 12 oxidation calculations at the Candelabra Tower. Gases were collected at the ground and 430 m, and linear vertical profiles were assumed.

for intermediate elevations on the tower were estimated by assuming a linear profile of each gas between the ground and top of the tower. Figure 4.3 shows the histograms of the gas concentrations used for the S(IV) oxidation calculations for the samples collected at the tower. It is clear that SO_2 levels are fairly low, but O_3 and H_2O_2 levels are fairly high compared to the southern SJV urban sites.

The results of the S(IV) oxidation rate calculations for the first two southern SJV events and for one tower event are shown in Figures 4.4-4.7 (plots of the rates for all IMS95 events, in addition to a table listing the values used in all the calculations, are found in Appendix C). It is clear that in most cases the ozone pathway is dominant; it is often faster by an order of magnitude or more.

At Bakersfield S(IV) oxidation rates were dominated by ozone, with some samples having hydrogen peroxide as the primary oxidant. The cases where the peroxide pathway was faster (samples #6 and #8 on 12/10/95) also exhibited lower than average pH values. S(IV) and sulfate concentrations were also very elevated in these samples. The significantly lower pH allows the H_2O_2 oxidation pathway to dominate over the O_3 pathway, which slows at lower pH.

At Fresno, the fog events on December 10, 19, 28 and January 4 were all alkaline enough so that ozone is the primary S(IV) oxidant. On December 9, different oxidants dominated in different samples. At the beginning and end of the event, high iron and manganese values along with a pH below 6 allowed metal catalyzed autooxidation to be fastest.

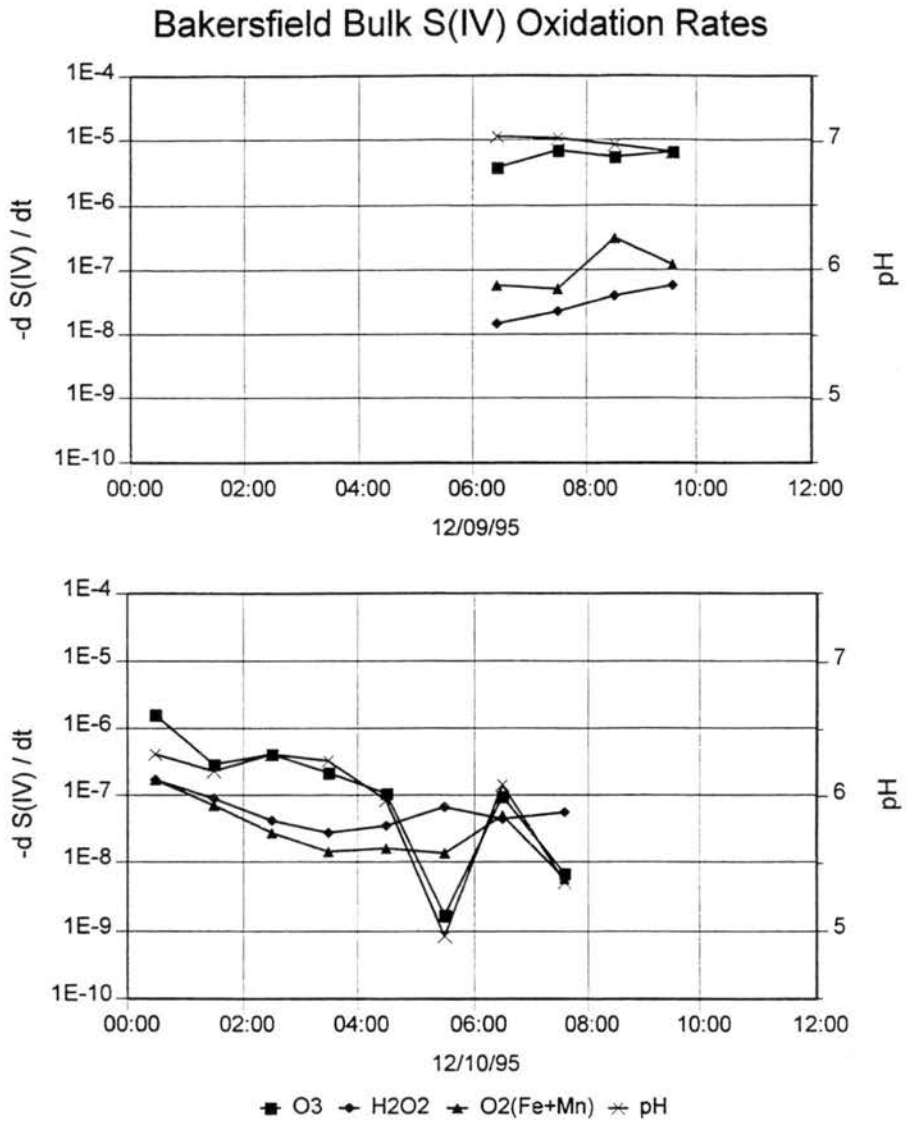

Figure 4.4: S(IV) oxidation rates calculated for bulk samples collected at Bakersfield as functions of time. Field pH values are also plotted for each sample. Rates are given in M s^{-1}.

During the middle of the event, the metals concentrations are lower and the peroxide pathway dominates except for one sample with a pH above 6, for which the ozone pathway is fastest. During the January 1 event, metals concentrations are very low and the pH of the fog remains around 6 so that at different times ozone or hydrogen peroxide

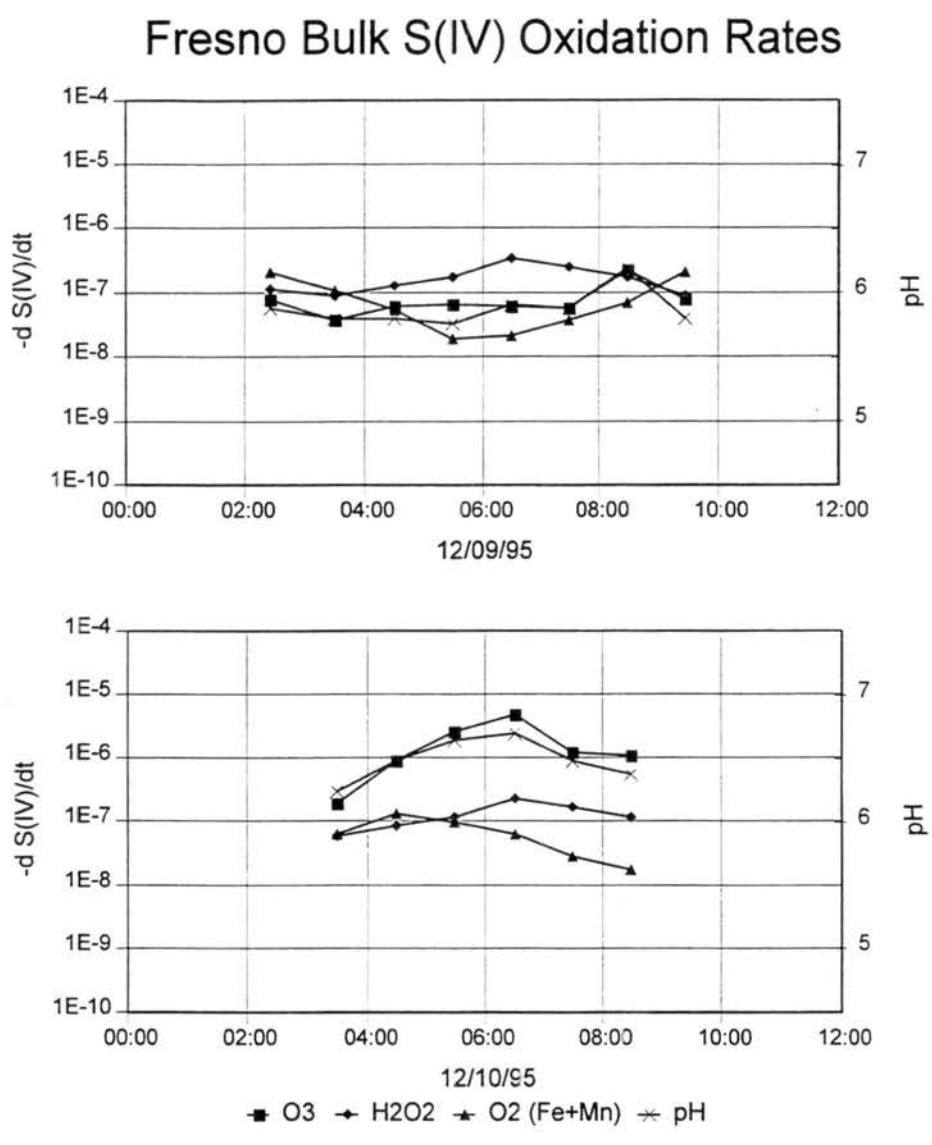

Figure 4.5: S(IV) oxidation rates calculated for bulk samples collected at Fresno as functions of time. Field pH values are also plotted for each sample. Rates are given in M s^{-1}.

are the primary oxidant. For the first and last samples of this event, the peroxide and ozone rates are within 10 percent of each other so both are important. Since gas concentrations are fairly constant over the events at Fresno, it seems that high metals concentrations and low pH values are necessary for the metal catalyzed autooxidation pathway to dominate, and that the peroxide pathway is usually dominant for pH $\leq$ 6.

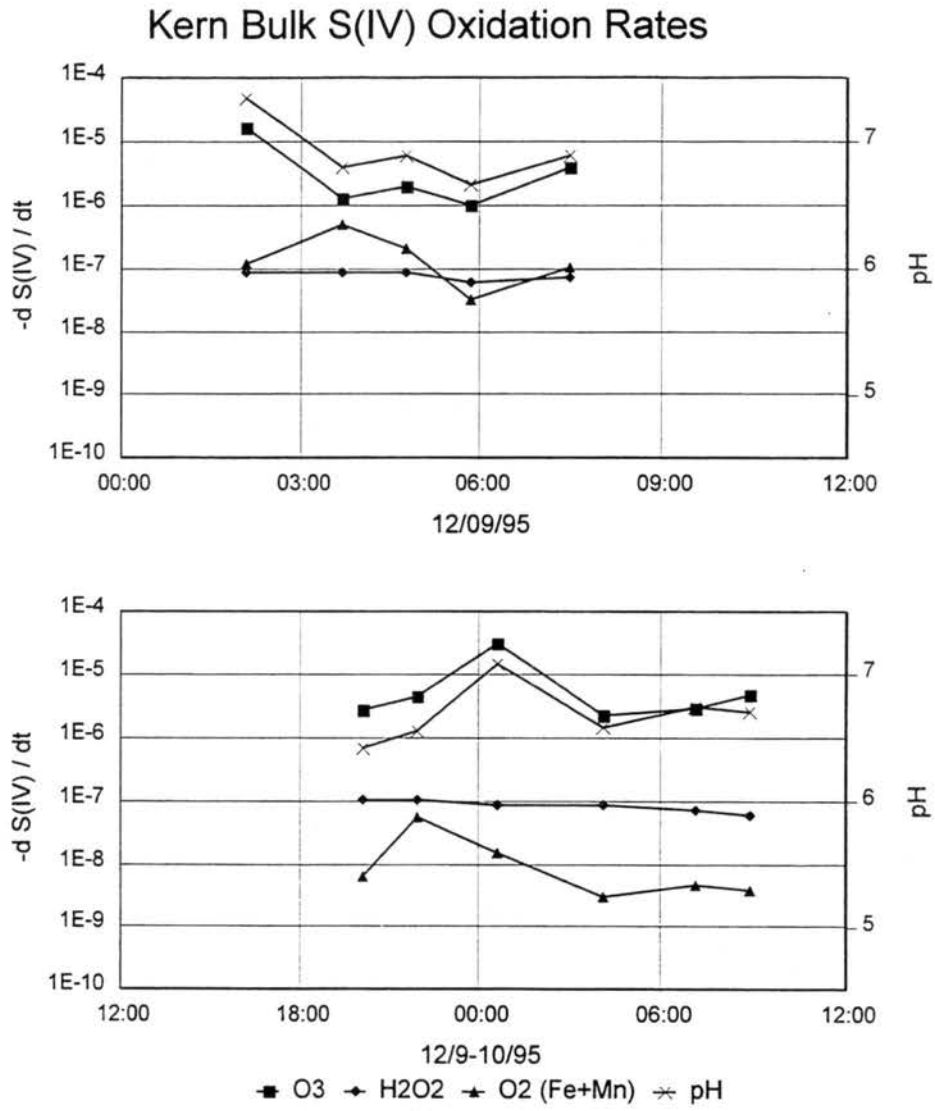

Figure 4.6: S(IV) oxidation rates calculated for bulk samples collected at Kern Wildlife Refuge as functions of time. Field pH values are also plotted for each sample. Rates are given in M s^{-1}.

Fogs sampled at Kern Wildlife Refuge tended to be more alkaline than the other two southern sites and the ozone pathway was always fastest. This was also true at Candelabra Tower, where high pH values provide conditions in which the ozone pathway

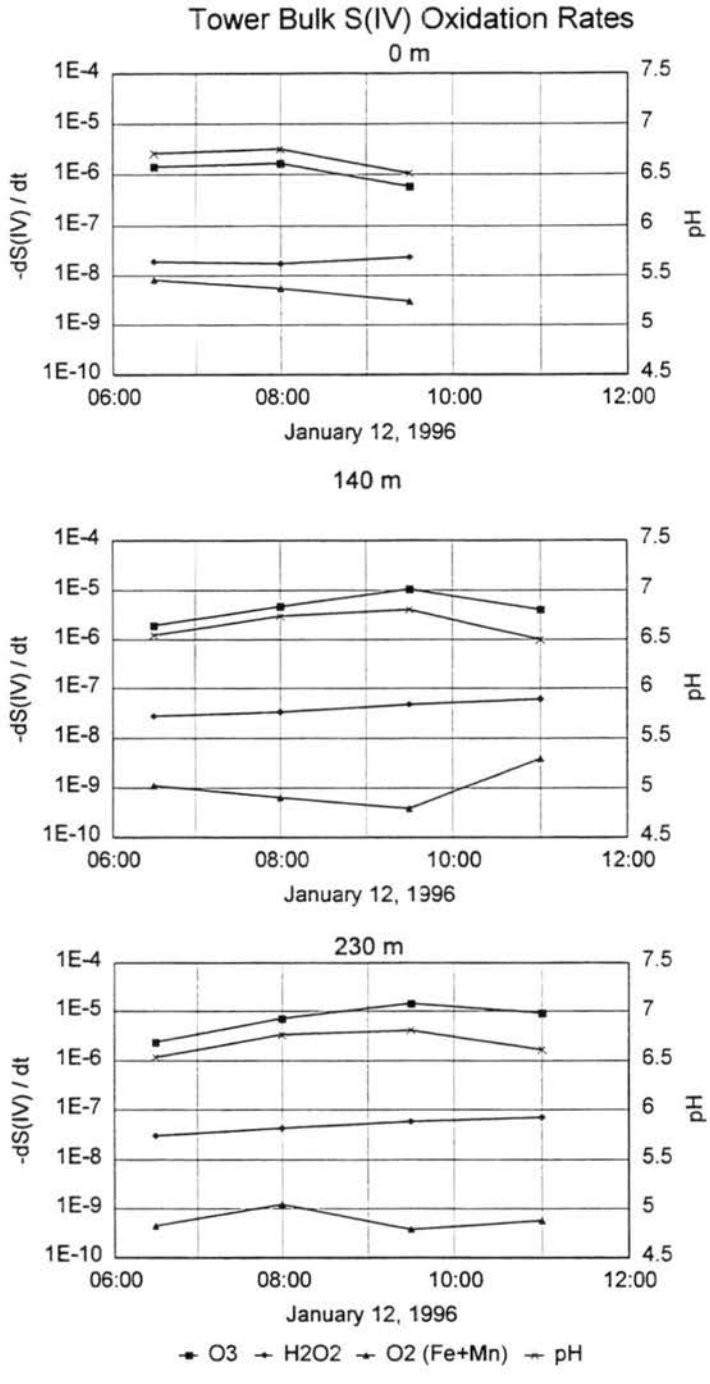

Figure 4.7: S(IV) oxidation rates calculated for bulk samples collected at the ground and two elevations on the Candelabra Tower as functions of time. Field pH values are also plotted for each sample. Rates are given in M s^{-1}.

was always at least an order of magnitude faster than the peroxide pathway and metal catalyzed autooxidation is much slower still.

Generally, oxidation rates are comparable between the three southern sites, only slightly higher at Kern and the tower due to the higher fog pH observed there. In most cases, oxidation rates were also fairly constant with time throughout the fog event, suggesting that oxidation did not cease over time due to the acidification of the drops. In fact, even when significant pH decreases occurred (Bakersfield, December 10), the peroxide pathway becomes important and the overall S(IV) oxidation rate remains fairly constant.

Figure 4.8 shows the percentage of time that each of the S(IV) oxidation pathways is dominant (at least 10 percent faster than competing pathways) for each of the IMS95 fog sites for all of the events sampled. The ozone S(IV) oxidation pathway is dominant 85 percent of the time at Bakersfield, 60 percent at Fresno and during every event sampled at Kern. (The ozone pathway is also dominant at each elevation during every event sampled at the Candelabra Tower.) Overall, in the fogs sampled during IMS95, ozone was the primary oxidant of aqueous S(IV) 88 percent of the time, peroxide 8 percent of the time and oxygen 3 percent of the time. During 1 percent of the time, both ozone and hydrogen peroxide were important oxidants. It is even more apparent that ozone is dominating these chemical processes when the low oxidant concentrations are considered. The observed concentrations of ozone, particularly during the fog episodes are lower than those expected for background tropospheric values. The low ozone could be due to the time of day the fogs were sampled (ozone is consumed at night by reaction with NO), a

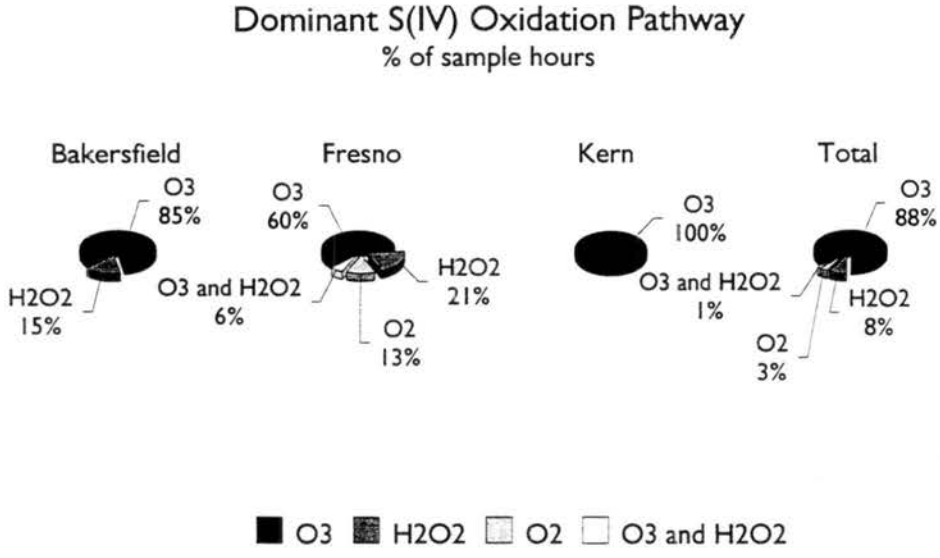

Figure 4.8: Dominant S(IV) oxidation pathways for each southern SJV site and all three sites combined (total). The percentages represent the fraction of sampling hours that the designated pathway was at least 10% faster than the other pathways. The 'O_3 and H_2O_2' fraction represents periods of the fog when both the ozone and peroxide S(IV) oxidation path were dominant (within 10% of each other).

lack of photochemical production during these overcast periods, or consumption by the aqueous phase processes.

A clear pattern is seen if the dominant pathway is considered in light of the sample pH. Table 4.1 breaks down the dominant pathway for three pH ranges. Above a sample pH of 6.0, S(IV) oxidation by ozone is fastest for 98 percent of the samples collected. Samples with pH values between 5.5 and 6.0 exhibit more of a range of various dominant S(IV) oxidation pathways. In these cases, a higher oxidant or catalyst concentration is likely to determine the fastest pathway. There are only two samples with pH below 5.5, and S(IV)

Table 4.1: The percent of samples in three pH ranges dominated by each S(IV) oxidation pathway.

pH	# of samples	% O_3	% H_2O_2	% O_2 / Fe(III)+Mn(II)	% O_3 and H_2O_2 *
> 6.0	47	98	2	0	0
5.5 - 6.0	10	10	40	30	20
< 5.5	2	0	100	0	0

* rates within 10 % of each other

oxidation by H_2O_2 is fastest for both. Since the ozone pathway depends on $[H^+]$ nonlinearly and the peroxide pathway is relatively independent of $[H^+]$, the chemistry occurring with ozone as the primary oxidant will differ significantly from peroxide dominated environments. Therefore, as will be shown in the next section, observed differences in the fog acidity as a function of drop size will greatly affect the total in-fog sulfate production since it is governed by a nonlinear reaction with respect to $[H^+]$.

Calculations were performed to determine the sensitivity of the S(IV) oxidation calculations to oxidant and catalyst concentrations. Rates were determined with half the O_3, twice the H_2O_2, four times the Fe(III) and two times the Mn(II) concentrations used in the original calculations. These factors represent upper bounds on the gas concentration and metals speciation uncertainties that would tend toward making O_3 a less important pathway. Calculations were also made taking each of these conditions into account separately. Figure 4.9 shows the results of applying all these uncertainties at once. It is clear that these conditions decrease the dominance of the ozone oxidation pathway at Fresno and Bakersfield primarily through an increase of the importance of the autooxidation pathway. Kern oxidation rates were affected only slightly by all the

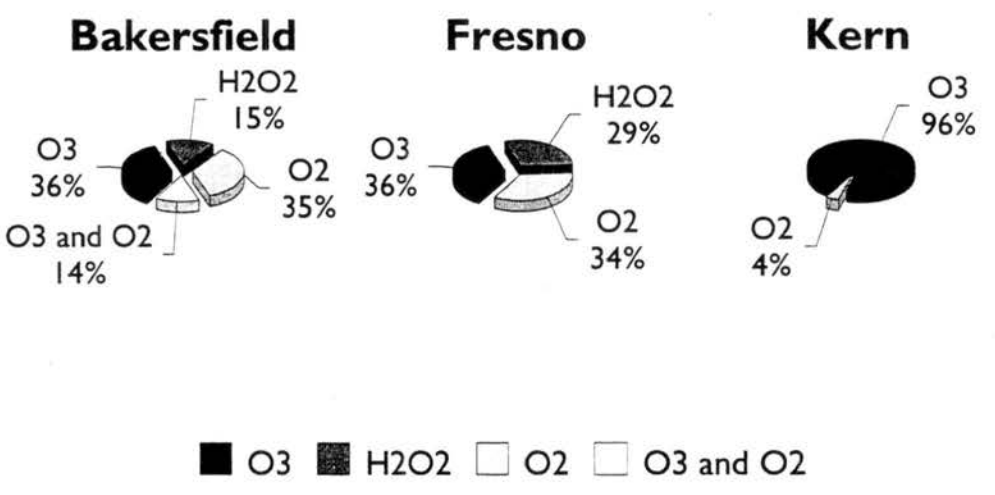

Figure 4.9: Sensitivity tests showing dominant S(IV) oxidation pathways for each southern SJV site and all three sites for conditions tending to minimize the importance of S(IV) oxidation by ozone.

changes. Figure 4.10 shows the dominant pathways when oxidation calculations are performed taking into account changes in ozone, hydrogen peroxide or the metals concentrations separately, in addition to the case in which ozone concentrations are doubled. In each case, particularly when metals concentrations are altered, samples collected at Bakersfield and Fresno exhibit major changes in the percent of time that each pathway is fastest (decreasing the amount of time ozone is the primary oxidant). Conversely, at Kern, the ozone pathway remains dominant regardless of altering O_3 or H_2O_2 alone, and decreases negligibly when the metals concentrations are raised. When

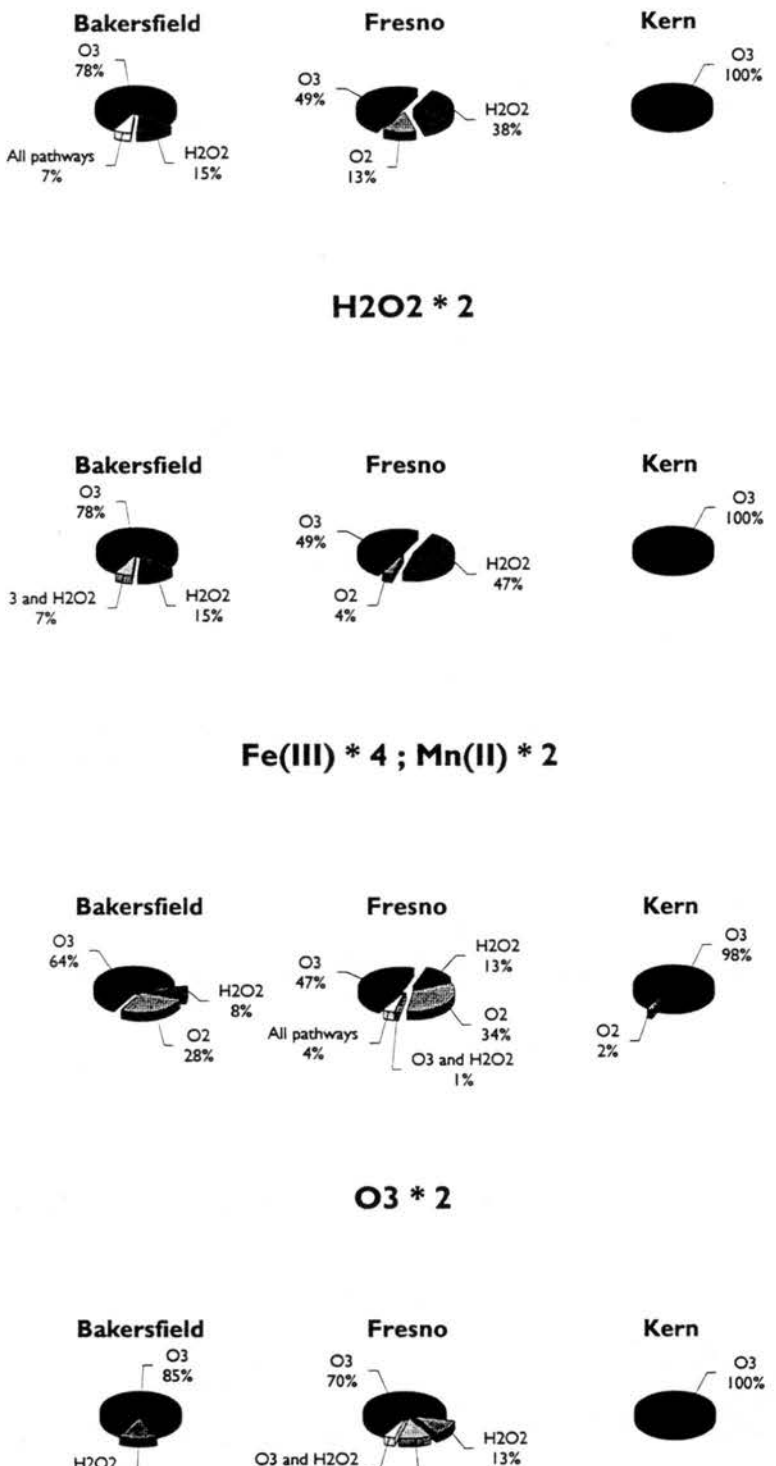

Figure 4.10: Dominant pathways calculated for each of the sensitivity conditions (and doubling ozone) separately.

ozone concentrations are doubled the dominant rates at Bakersfield and Kern remain the same as when calculated with initial concentrations and the ozone mechanism increases in dominance by 10 percent at Fresno at the expense of the peroxide pathway. These calculations show that oxidant concentrations and particularly the metals concentrations

Table 4.2: Comparison of dominant S(IV) oxidation pathways at Bakersfield, considering ozone to be absent when below the LQL and throughout the entire event.

Sensitivity Conditions	% O_3	% H_2O_2	% O_2 / Fe(III)+Mn(II)	% O_3 and H_2O_2 *	% H_2O_2 and O_2 *
Original	85	15	0	0	0
O3 = 0 below LQL	78	15	7	0	0
No O3	0	50	36	0	14

Table 4.3: Comparison of dominant S(IV) oxidation pathways at Fresno, considering ozone to be absent when below the LQL and throughout the entire event.

Sensitivity Conditions	% O_3	% H_2O_2	% O_2 / Fe(III)+Mn(II)	% O_3 and H_2O_2 *	% H_2O_2 and O_2 *
Original	60	21	13	6	0
O3 = 0 below LQL	49	32	13	6	0
No O3	0	78	17	0	4

Table 4.4: Comparison of dominant S(IV) oxidation pathways at Kern, considering ozone to be absent when below the LQL and throughout the entire event.

Sensitivity Conditions	% O_3	% H_2O_2	% O_2 / Fe(III)+Mn(II)	% O_3 and H_2O_2 *	% H_2O_2 and O_2 *
Original	100	0	0	0	0
O3 = 0 below LQL	68	32	0	0	0
No O3	0	83	17	0	0

Table 4.5: Comparison of dominant S(IV) oxidation pathways at the Candelabra Tower, considering ozone to be absent when below the LQL and throughout the entire event.

Sensitivity Conditions	% O_3	% H_2O_2	% O_2 / Fe(III)+Mn(II)	% O_3 and H_2O_2 *	% H_2O_2 and O_2 *
Original	100	0	0	0	0
O3 = 0 below LQL	100	0	0	0	0
No O3	0	100	0	0	0

are important to know accurately for precise determinations of the in-fog sulfate production.

Model simulations of these fog episodes by Spyros Pandis have suggested that sufficient NO is present to titrate the ozone to zero. S(IV) oxidation rates were recalculated for two cases. Case one assumed ozone to be zero when the data were below the lower quantitation limit (LQL), and case two assumed there was no ozone throughout the entire study. Tables 4.2-5 show the results of these calculations for each site. For case one, the dominance of S(IV) oxidation by ozone decreases at Bakersfield leading to an increase of importance of the metal catalyzed autooxidation pathway. At Fresno and Kern a decrease in the importance of ozone led to an increase in the importance of the peroxide pathway. The tower S(IV) oxidation rates exhibited no change since all ozone values there were above the LQL. At the three southern sites, the dominance of both the peroxide and autooxidation pathways were increased significantly in the absence of ozone (case two), whereas at the tower the peroxide pathway was always dominant. In the absence of ozone, the total S(IV) oxidation rates are often an order of magnitude slower than when it is present. This would lower the amount of sulfate the fog was capable of producing.

Aqueous oxidation rates can also be multiplied by fog liquid water content (derived from the fogwater collection rate of the CASCC2 fog collectors as described by Demoz et al. (1996)) to obtain a rate of sulfate production per m^3 of air. The ranges and median values for sulfate production for each southern SJV site are listed in Table 4.6. (Timelines of

these production rates can be found in Appendix C). It is clear that the S(IV) oxidation rates are fast enough to produce large amounts of sulfate in the absence of restrictions due to SO_2 or oxidant depletion or other reactions competing for S(IV). Assuming that SO_2 is the limiting quantity, and that all SO_2 is converted into sulfate, then for SO_2 concentrations of 1 and 10 ppb, 4 and 41 $\mu g\ m^{-3}$ of air of sulfate are produced respectively. This corresponds to the lower and upper bounds of observed SO_2 concentrations during fog events. It is clear from these calculations that aqueous phase sulfate production is capable of contributing a large amount to the overall aerosol mass and could be significant to the PM 10 and PM 2.5 standards which are 150 $\mu g/m^3$ and 65 $\mu g/m^3$ respectively for 24 hour samples (U.S. EPA, 1997). On December 10 at Bakersfield measured SO_2 concentrations may indicate that SO_2 is being depleted as the fog evolves, but this is not seen in any of the other events.

Table 4.6: Ranges and median values for possible sulfate production calculated from S(IV) oxidation rates. (Units are $\mu g/m^3$ hr of air)

Site	Number of Samples	Range of Production	Median
Bakersfield	14	3-277	20
Fresno	25	1-488	38
Kern	20	45-1967	195

A process that can compete with the oxidation of S(IV) to S(VI) is the complexation of S(IV) with formaldehyde (Boyce and Hoffmann, 1984, Olson and Hoffmann, 1986, 1989, and Kok et al., 1986) . This reaction occurs with SO_3^{2-} or HSO_3^- to give hydroxymethanesulfonate (HMS). This has been shown to be important in some fog regimes (Rao and Collett, 1995). For a typical value of $[HCHO]_{aq}$ - $[HMS]_{aq}$ of about 33

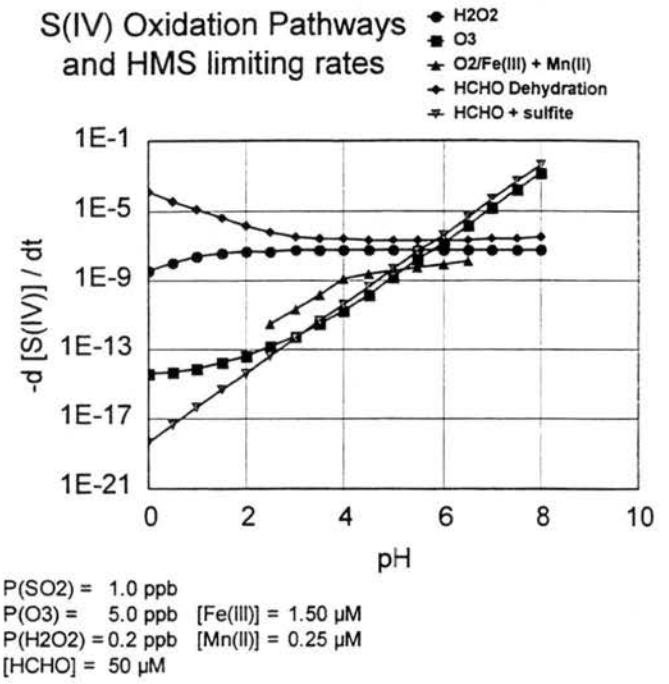

Figure 4:11: HMS formation limiting rates plotted with S(IV) oxidation rates as a function of pH. Rates are given in M s^{-1}. Rates are plotted for typical IMS95 fog conditions.

µM, predicted gas phase concentrations of HCHO are about 1.7 ppb. This is comparable or higher than the SO_2 concentrations measured at the same time. Therefore, since HCHO is more soluble than SO_2, it is possible that aldehyde complexation could be a significant limiting factor to S(IV) oxidation. Two possible limiting steps of the reaction are the dehydration of the gem-diol of formaldehyde (methylene glycol) and the bimolecular addition of sulfite and formaldehyde (Olson and Hoffmann, 1986). The bimolecular addition of bisulfite and formaldehyde is much slower than the reaction with sulfite and therefore is not considered in this approach. The pH dependence of these rates for typical SJV conditions are shown in Figure 4.11 along with the three S(IV) oxidation rates. Since most formaldehyde in the aqueous phase exists as its gem-diol, the rate of the dehydration of formaldehyde could limit HMS formation if HCHO is not absorbed

from the gas phase fast enough. At lower pH, dehydration is much faster than the bimolecular addition of SO_3^{2-} and HCHO. Figures 4.12-14 show the rates of S(IV) depletion for each of these steps, along with previously shown S(IV) oxidation rates for the first two fog events at Bakersfield, Fresno and Kern calculated for measured aqueous

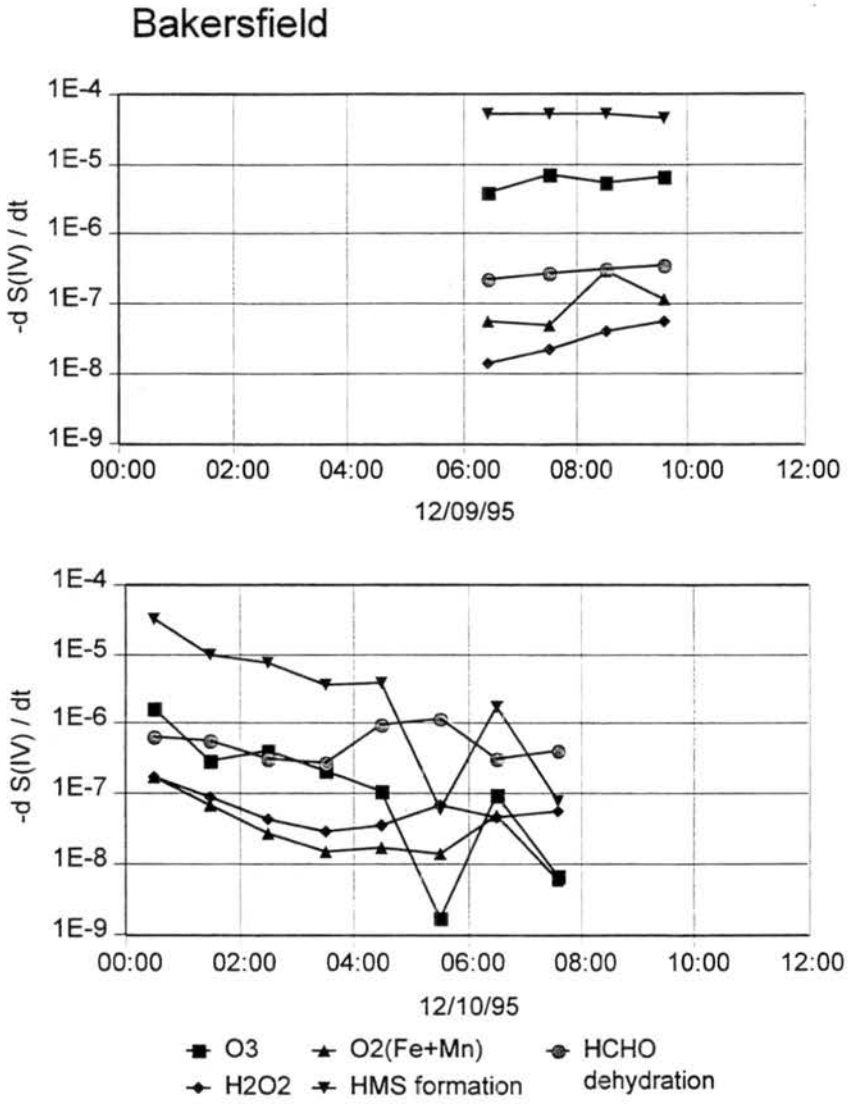

Figure 4.12: Rates for the bimolecular addition of HCHO and SO_3^{2-} (HMS formation) and the dehydration of hydrated HCHO plotted with S(IV) oxidation rates as functions of time for the first two fog events at Bakersfield. Rates are given in M s^{-1}.

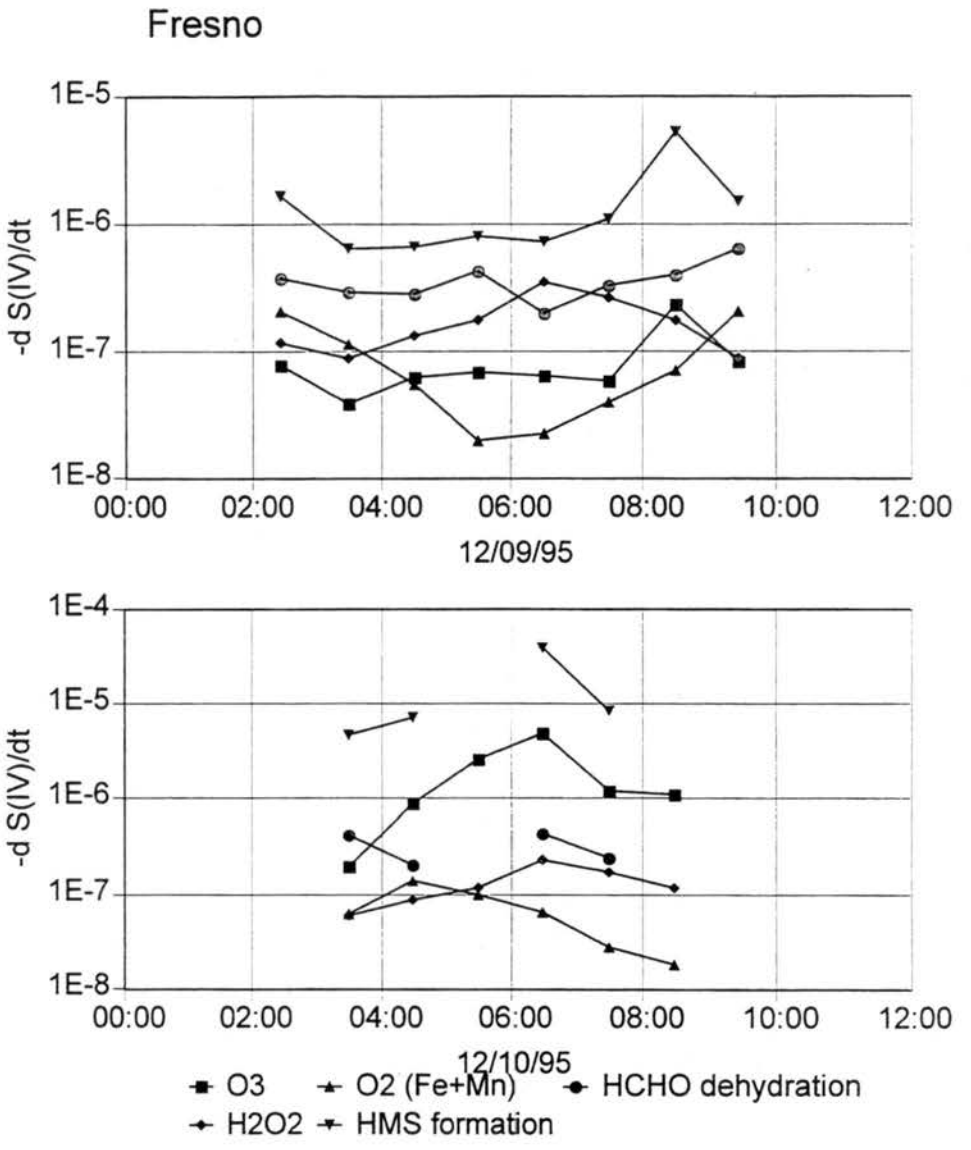

Figure 4.13: Rates for the bimolecular addition of HCHO and SO_3^{2-} (HMS formation) and the dehydration of hydrated HCHO plotted with S(IV) oxidation rates as functions of time for the first two fog events at Fresno. Rates are given in M s^{-1}.

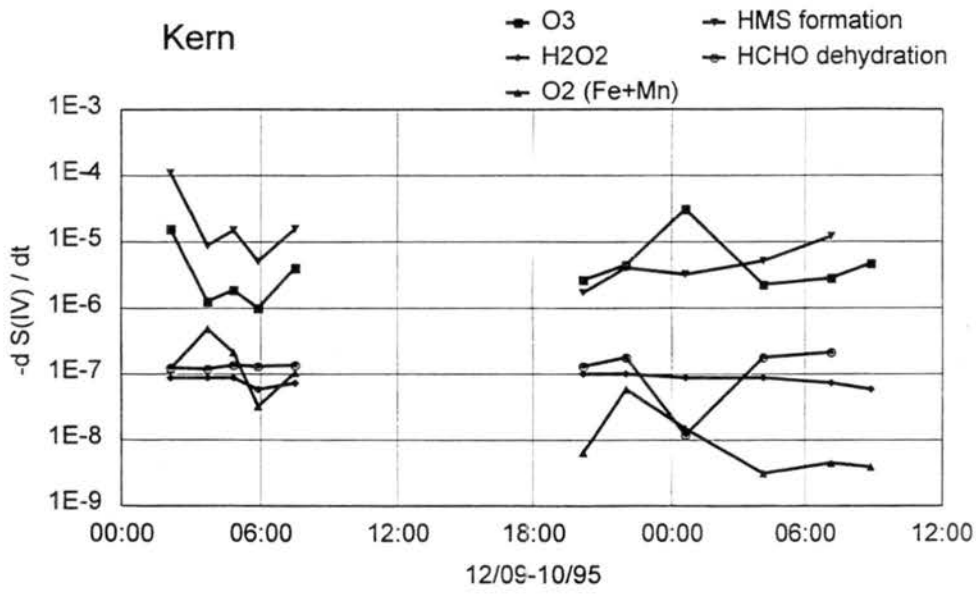

Figure 4.14: Rates for the bimolecular addition of HCHO and SO_3^{2-} (HMS formation) and the dehydration of hydrated HCHO plotted with S(IV) oxidation rates as functions of time for the first two fog events at Kern wildlife Refuge. Rates are given in M s^{-1}.

HCHO concentrations. In most cases, the HMS formation reaction is faster than S(IV) oxidation. When insufficient HCHO is available in the gas phase, or if its absorption into the droplets is mass transfer limited, then the dehydration reaction would limit the rate of HMS formation in most cases. If this is the case, then oxidation of S(IV) is still the dominant process during the first event at Bakersfield and during all the events at Kern. The second event at Bakersfield and both events at Fresno exhibit a mixture of S(IV) oxidation and complexation. It is clear that S(IV) complexation with formaldehyde therefore could be an important competitor for available S(IV) in the fog drops, but more information is needed about gas and aqueous phase formaldehyde concentrations to be able to determine how this complexation is limited. Measured HMS concentrations for IMS95 fog samples account for most of the measured S(IV) in many cases, indicating

that HMS formation is an important process occurring in the fog. However, this complexation could compete with oxidation for S(IV) only if dissolved SO_2 concentrations cannot be kept at equilibrium levels due to slow mass transport, most likely for large drops, or if SO_2 is depleted from the gas phase.

Limited rates of SO_2 mass transport into drops could also directly limit rates of sulfate production. It has been shown (Schwartz, 1988) that gas phase and interfacial mass transport could limit the uptake rate for SO_2 with respect to oxidation by ozone for large fog drops ($d > 30$ μm) with pH levels above 6. With respect to S(IV) oxidation by H_2O_2, the temperature and droplet size affect mass transfer processes limiting SO_2 uptake more than pH, but it is estimated from the graphical representations given by Schwartz that no reduction is expected for 20 μm drops at 10 °C. However, specific calculations of mass transfer rates for lower concentrations of O_3 and H_2O_2, as well as for droplet sizes characteristic of fogs observed during IMS95, would be needed to determine the magnitude of such a possible effect on sulfate production.

Chapter 5: Effects of heterogeneous drop chemistry on S(IV) oxidation

As seen previously, fog drop composition varies with drop size. Since this includes pH, average fog drop acidity (measured in bulk fog samples) is not usually a good predictor of the average sulfate production rate for pH dependent pathways since the oxidation rates in IMS95 fogs are generally not linear functions of $[H^+]$. This means that calculations based on bulk measurements could yield results much different than what actually occurs in the fog, where the chemically distinct drops are separate. Chemical heterogeneity as a function of drop size would not alter S(IV) oxidation rates by hydrogen peroxide, since the rate is pH independent over a wide range, and H_2O_2 concentrations do not exhibit a strong drop size dependence. For the ozone pathway, however, variations in acidity as a function of drop size tend to enhance sulfate production. The effect these variations have on the metal-catalyzed oxidation pathway is more difficult to predict since variations in both the acidity and metals concentrations in the drops change the sulfate production rate. Size dependent oxidation rate calculations are imperative to accurately determining sulfate production when the peroxide pathway is not dominant. Since the observed pH difference is often large and the ozone pathway is usually dominant for observed IMS95 conditions, size dependent treatment of the oxidation processes is essential.

Size fractionated samples were collected with a sf-CASCC at Kern Wildlife Refuge and with ETH impactors at Fresno and Bakersfield. Both samplers collect a large and a small drop fraction over a given sampling period.

Calculations of oxidation rates by ozone as a function of drop size were performed in the same manner as for the bulk samples using the pH of large and small drop samples collected at each of the southern SJV sites. Then the masses of these small and large drop fractions were used to calculate a weighted average H^+ concentration. This $[H^+]_{avg}$ was then used to calculate an oxidation rate that simulates the rate calculated from a bulk sample. This simulated bulk rate is analogous to the situation where the fog drop composition is independent of drop size. A weighted average of the small and large drop oxidation rates gives a more accurate picture of the actual oxidation occurring in the fog, since oxidation is occurring in distinct droplets. However, this depiction is still rather artificial since many more than two compositions are likely present within the fog. The simulated bulk rate and the weighted average rate can be compared to show the extent of oxidation enhancement that occurs due to chemical heterogeneity. This enhancement factor is calculated as the ratio of the weighted average rate to the calculated bulk rate.

Figures 5.1-3 show the ozone pathway S(IV) oxidation rates for large and small drop fractions, for a weighted average pH (simulated bulk sample), and the liquid water weighted average of the large and small drop oxidation rates for fog samples collected at Bakersfield, Fresno and Kern. Since the pH of the small drops is much lower than the

large drops, the ozone oxidation rate is much slower in the small drops. Since the ozone pathway is nonlinear in [H^+] and most of the water is found in the large drop fraction, this average rate is much different than the 'bulk' rate. In fact, the weighted average rates, which are a better depiction of the actual fog characteristics, are very close to the rates for

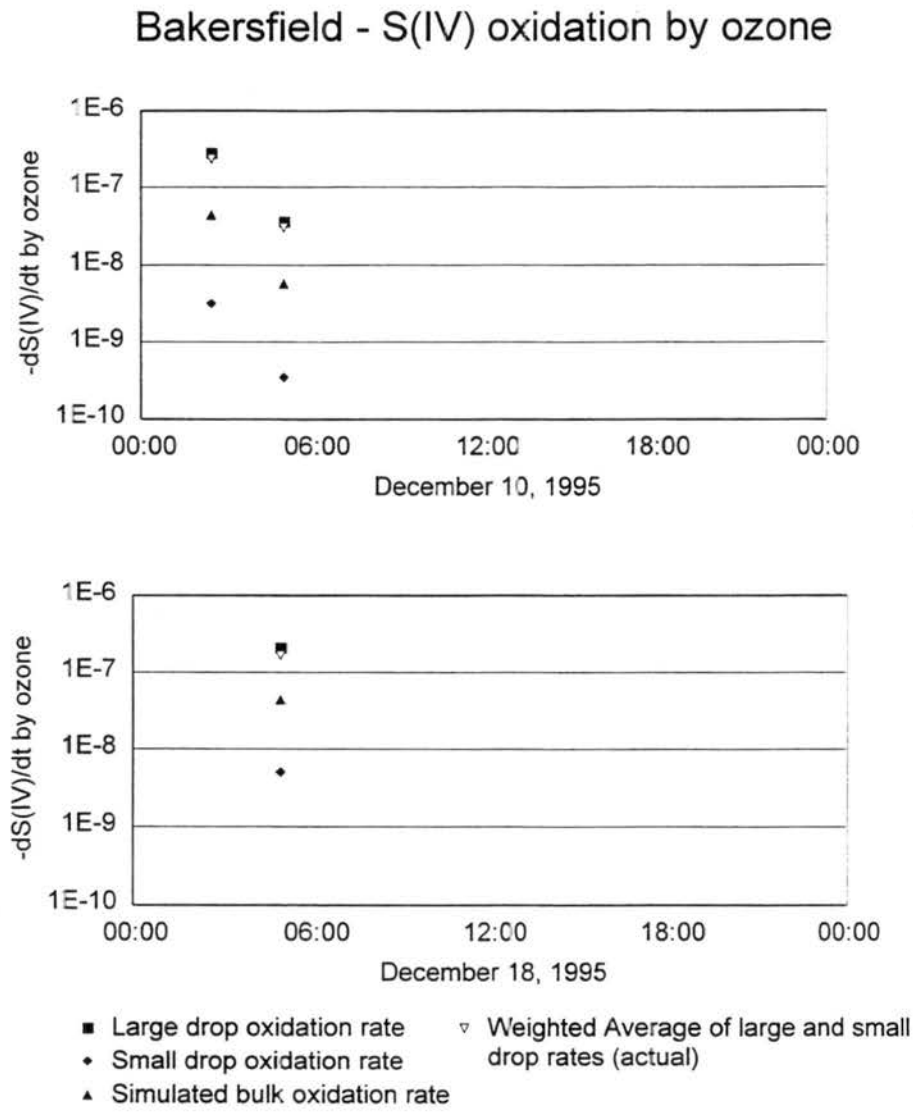

Figure 5.1: The effects of size dependent fog drop acidity on S(IV) oxidation by ozone as functions of time. Large and small drop pH values are from size fractionated samples collected at Bakersfield with an ETH impactor. Simulated bulk rates are calculated from LWC weighted [H+]. Rates are given in M s^{-1}.

the large drop fraction. Enhancement ratios, calculated as the weighted average rate divided by the bulk rate, determine the magnitude of the effect chemical variations have on sulfate production. Figure 5.4 shows the distribution of ozone pathway enhancement factors calculated for events sampled at all three sites. The enhancement ratios are

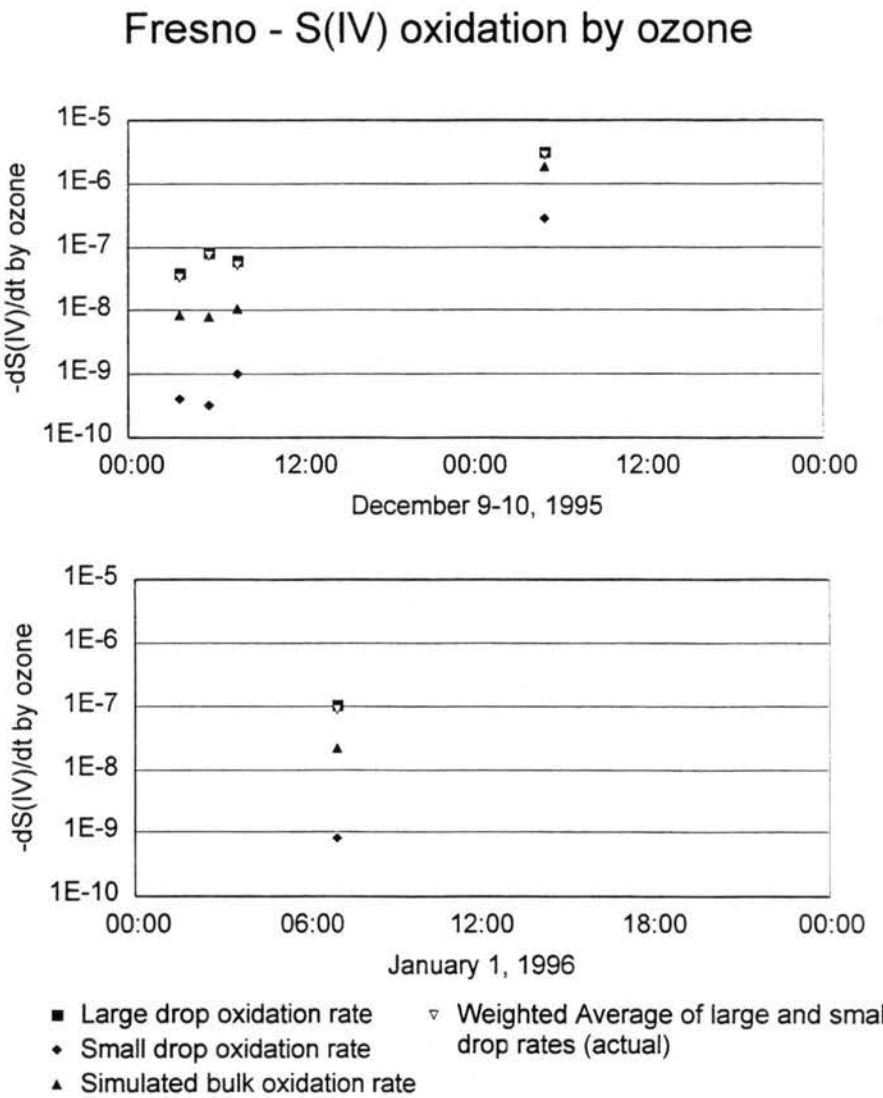

Figure 5.2: The effects of size dependent fog drop acidity on S(IV) oxidation by ozone as functions of time. Large and small drop pH values are from size fractionated samples collected at Fresno with an ETH impactor. Simulated bulk rates are calculated from LWC weighted [H+]. Rates are given in M s^{-1}.

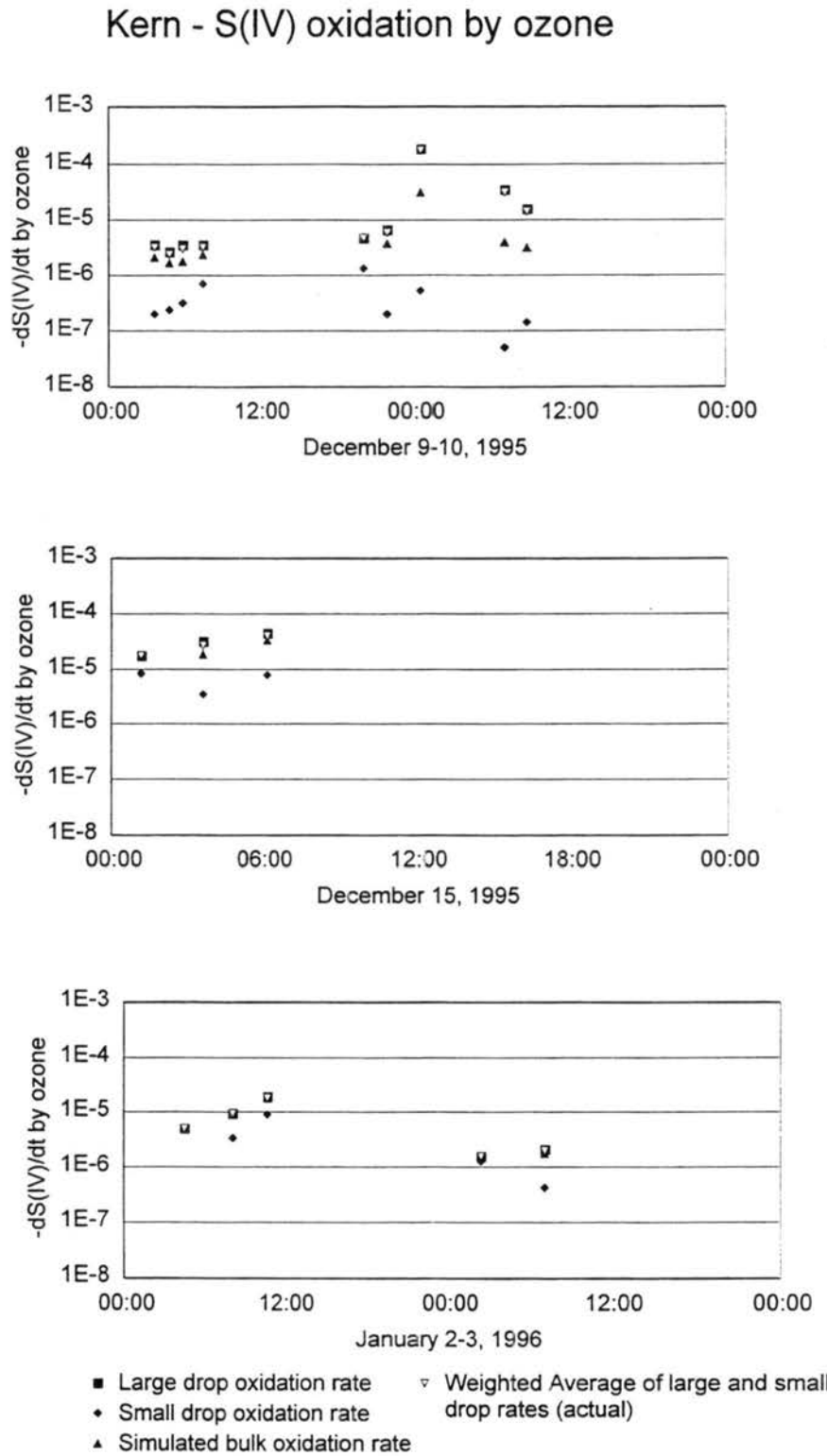

Figure 5.3: The effects of size dependent fog drop acidity on S(IV) oxidation by ozone as functions of time. Large and small drop pH values are from size fractionated samples collected at Kern Wildlife Refuge with the sf-CASCC. Simulated bulk rates are calculated from LWC weighted [H+]. Rates are given in M s^{-1}.

highest at Bakersfield and lowest at Kern, but of significant magnitude at all sites. Table 5.1 lists the ranges and median values for the enhancement ratios for the ozone pathway for the three southern SJV sites. Although the median enhancement factors are much higher at Bakersfield and Fresno, it is not possible to say whether these differences are due to the different locations or due to the different size cuts employed by the ETH impactor and the sf-CASCC. The form of the [H^+] nonlinearity in the ozone S(IV) oxidation rate expression causes the enhancement factor for this pathway due to the

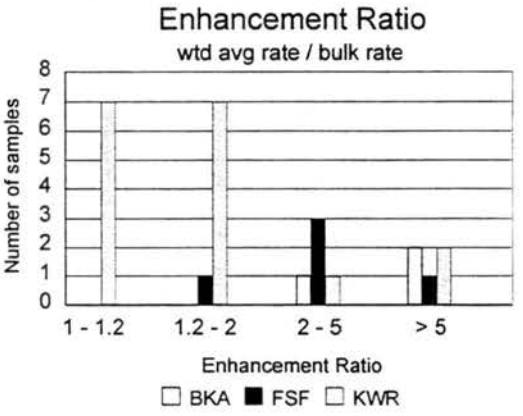

Figure 5.4: Enhancement ratios (ratio of the weighted average of large and small drop S(IV) oxidation rates to the simulated bulk rate) for southern SJV samples. Calculated using S(IV) oxidation by ozone only.

Table 5.1: The lowest, highest and median enhancement ratios for oxidation by ozone due to variations in fogwater acidity with drop size.

site	# of samples	lowest	highest	median
Bakersfield	3	3.7	5.3	5.2
Fresno	5	1.5	8.9	4.1
Kern	17	1.0	7.9	1.3

observed pH size dependence to always be greater than one. For the metals catalyzed autooxidation pathway both the pH and the metals concentrations affect the S(IV) oxidation rate, so that even though the pH size dependence enhances S(IV) oxidation rates, the size dependence of the metals could act in the opposite direction, making enhancement factors of less than one possible (Rao and Collett, 1996).

Total oxidation rates for both size fractions and a simulated bulk composition were calculated as the sum of all three pathways. These rates could be calculated only for Kern samples due to the lack of size fractionated metals measurements at Fresno and Bakersfield. Figure 5.5 shows the timelines of the total oxidation rates for the same calculations depicted in Figure 5.3. Figure 5.6 shows the corresponding total enhancement ratio for the events sampled at Kern. The enhancement ratio ranges from 1.0 to 7.8. The fact that these results are similar to the results for the ozone pathway suggests that the ozone pathway is sufficient to characterize the S(IV) oxidation occurring during these times, since it is significantly faster than the other oxidation rates. Total oxidation rates were calculated for the Fresno and Bakersfield samples for which either the ozone or peroxide path was dominant. When the ozone pathway was dominant, the total enhancement ratio was similar to the enhancement ratio considering the ozone rate alone. However, for samples dominated by the peroxide pathway the enhancement ratios considering both ozone and peroxide pathways were significantly lower than for just ozone.

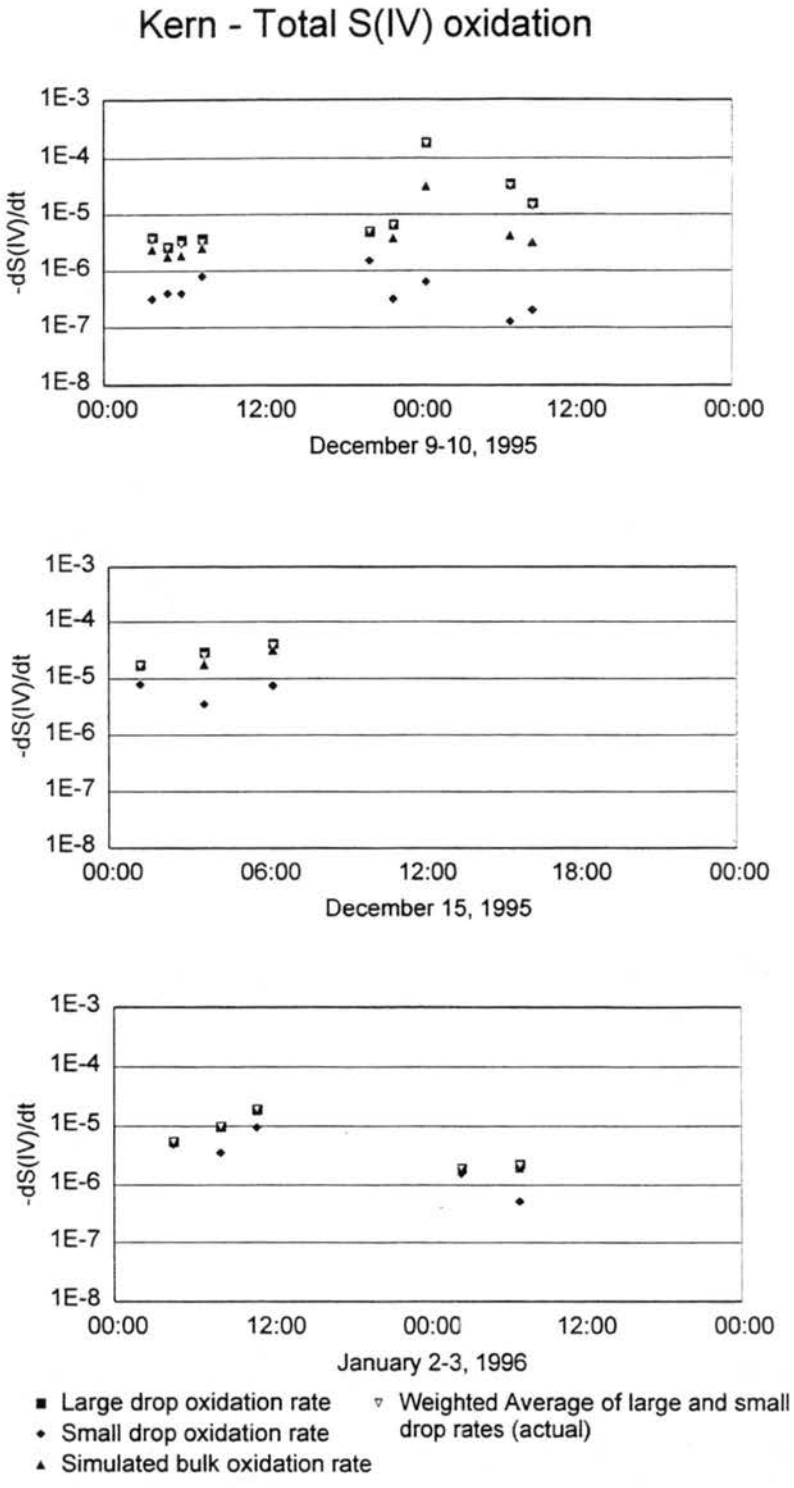

Figure 5.5: The effects of size dependent fog drop acidity on S(IV) oxidation by ozone and metal catalyzed oxygen as functions of time. Large and small drop pH values are from size fractionated samples collected at Kern Wildlife Refuge with the sf-CASCC. Simulated bulk rates are calculated from LWC weighted [H+]. Rates are given in M s^{-1}.

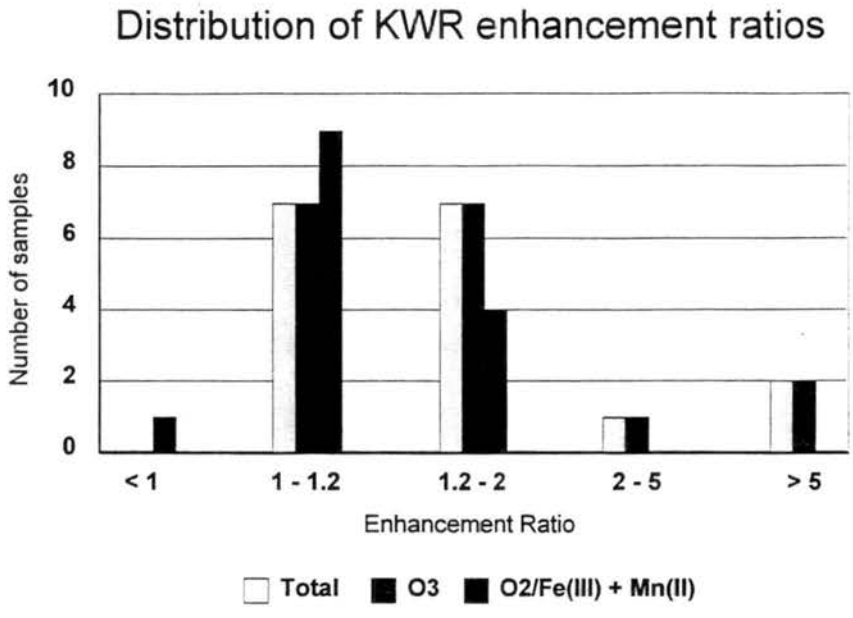

Figure 5.6: Enhancement ratios (ratio of the weighted average of large and small drop S(IV) oxidation rates to the simulated bulk rate) for Kern samples. Total enhancement ratio is calculated using S(IV) oxidation by all three pathways.

The calculated enhancement ratios for the IMS95 fog events show that the effect chemical heterogeneity is having on the sulfate production is not negligible and the assumption that the fog drops have a uniform composition spectrum with size is not valid in most cases. Therefore, in these conditions, determining the chemistry using values from bulk collections of fogwater would significantly underestimate the amount of sulfate produced. In fact, these calculations using only two independent compositions still represent a simplified approach to the actual oxidation occurring in the cloud. Resolving the fog drop chemical variations further would be desired, since greater heterogeneity supports even faster S(IV) oxidation rates for the ozone pathway.

Chapter 6: Heterogeneous Chemistry Effects on Deposition

Wet deposition to surfaces and the ground is a significant removal process for pollutants and nutrients found in fog drops (Waldman and Hoffmann, 1987). During IMS95 significant deposition of water to the ground was observed. Water from 14.5 cm deposition plates set out at the Fresno site was analyzed for inorganic ions. Table 6.1 shows the plate exposure times, water mass and ion concentrations for water collected on these plates. Fluxes of these species to the surface were estimated using the equation:

$$Ion\ Flux = Flux_{water} \times Ion\ Conc.$$

where the water flux was calculated from the mass of the deposited water. Fluxes for major ions (nitrate, sulfate and ammonium) ranged from 0.08 to 5.41 nanomoles m^{-2} s^{-1}, showing there was significant removal of these species (see Table 6.2).

Table 6.1: Collection times, water mass (g), and aqueous phase ion concentrations (μN) for the two deposition plate samples collected at Fresno.

Date	Start	End	Mass	Cl^-	NO_3^-	SO_4^{2-}	Na^+	NH_4^+	K^+	Mg^{2+}	Ca^{2+}
12/9	02:17	09:00	3.4	9.8	165	60	10.2	635	10.3	10.4	36.1
12/10	03:00	09:00	1.0	9.3	271	57	6.2	1,185	11.9	5.5	14.0

Table 6.2: Ion fluxes for the two deposition plate samples collected at Fresno. Units are nanomoles/m^2 sec.

Date	Cl^-	NO_3^-	SO_4^{2-}	Na^+	NH_4^+	K^+	Mg^{2+}	Ca^{2+}
12/9	0.08	1.41	0.26	0.09	5.41	0.09	0.04	0.15
12/10	0.03	0.76	0.08	0.02	3.32	0.03	0.01	0.02

Since deposition in a stagnant environment is highly dependent on drop size, knowledge of the drop size-dependent composition of the suspended fog drops is needed to accurately predict the flux of various constituents to the ground. Assuming that sedimentation was the dominant deposition mechanism, calculations were made from size-fractionated fog chemistry observations (sf-CASCC) and measured drop size spectra (PMS-CSASP) to give a calculated flux of each species to the surface. Characteristic drop sizes were obtained from drop size distributions by converting the distributions into deposition velocities. Then the average deposition velocity was converted back to a characteristic drop size (one for the whole distribution for a 'bulk' size and one for each part of the distribution sampled by the two stages of the sf-CASCC to give representative small and large drop sizes). Water fluxes for large and small drop fractions were calculated by the equation:

$$Flux = LWC \times X_m \times v_s$$

where LWC is the liquid water content in g m^{-3} (calculated from drop size distributions), X_m is the mass fraction of the water in the small or large size fraction (both of which were

calculated from PMS-CSASP size distributions), and v_s is the droplet terminal fall speed given by:

$$v_s = \left[\frac{\varrho_w \, g \, D_o^2}{18 \, \mu} \right]$$

where ρ_w is the density of water, g is the gravitational acceleration, D_o is the characteristic diameter of the large or small fraction derived from the CSASP distributions, and μ is the dynamic viscosity. Ion fluxes were then calculated using the fogwater concentrations from size fractionated samples (C_{lg} and C_{sm}):

$$Ion\ Flux_{\lg\ drops} = Lg\ Drop\ Water\ Flux \times C_{\lg}$$

$$Ion\ Flux_{sm\ drops} = Sm\ Drop\ Water\ Flux \times C_{sm}$$

Estimated errors for these fluxes were calculated assuming the following uncertainties: 20 percent in LWC, 5 percent in mass measurements, 3 μm in characteristic drop size estimates and the previously stated analytical uncertainties for the ion concentrations. Figure 6.1 shows the distribution of liquid water between the large and small size drop fractions, derived from measured drop size distributions. Figure 6.2 shows the small drop fluxes compared to the large drop fluxes for several major ionic species. This figure shows that the large drop ion fluxes are usually smaller than the small drop ion fluxes, with some scatter. This occurs because the concentrations of the ionic species are much larger in the small drops than in the large drops, but the faster settling velocity of the

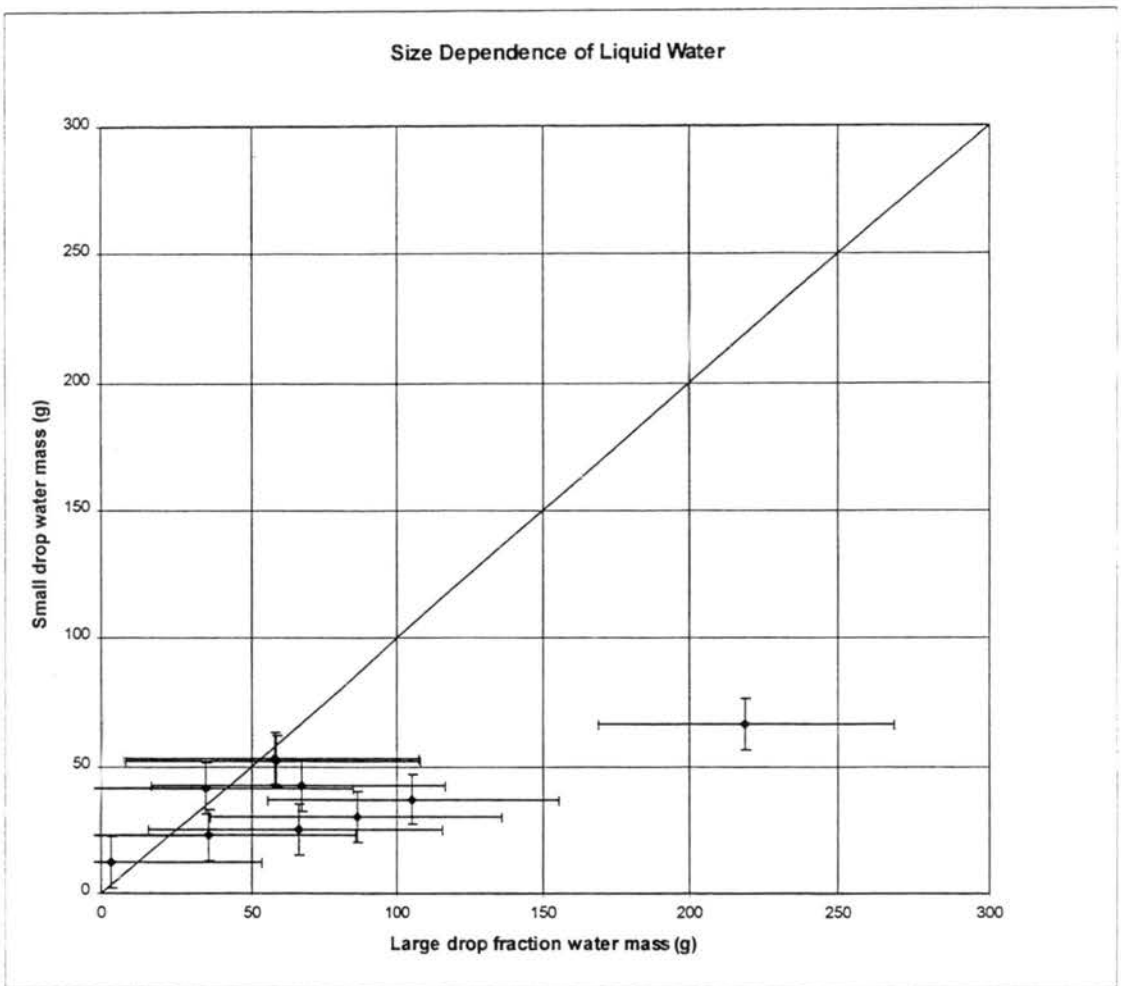

Figure 6.1: Distribution of liquid water in two size fractions corresponding to the size fractionated fog collector size ranges. Calculated from PMS-CSASP data. Error bars represent a 20 percent uncertainty in the liquid water calculations.

large drops can occasionally compensate for the concentration difference. The results were compared to similar calculations for a characteristic bulk drop size and a liquid water weighted average of the large and small drop ion concentrations to estimate the magnitude of the effect drop size-dependent chemistry has on prediction of the removal rates of atmospheric species present in the fogwater. Figure 6.3 shows the comparison of the sum of the large and small drop fluxes to the simulated bulk flux for several major

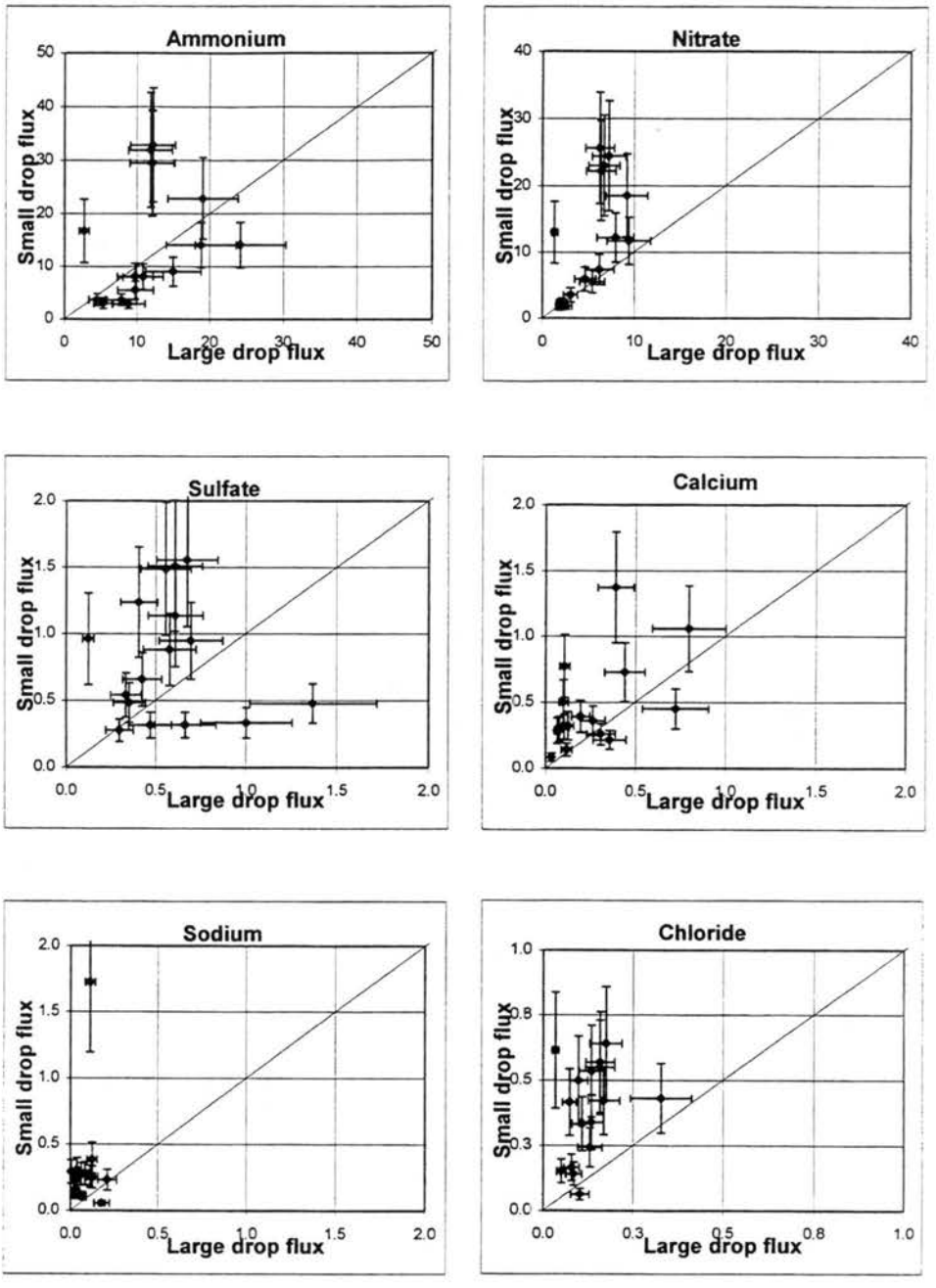

Figure 6.2: A comparison of the large and small drop fluxes of major ionic species. All values are in nanomoles m^{-2} s^{-1}. Error bars represent uncertainties in concentrations, drop sizes and liquid water content, propagated through the flux calculations.

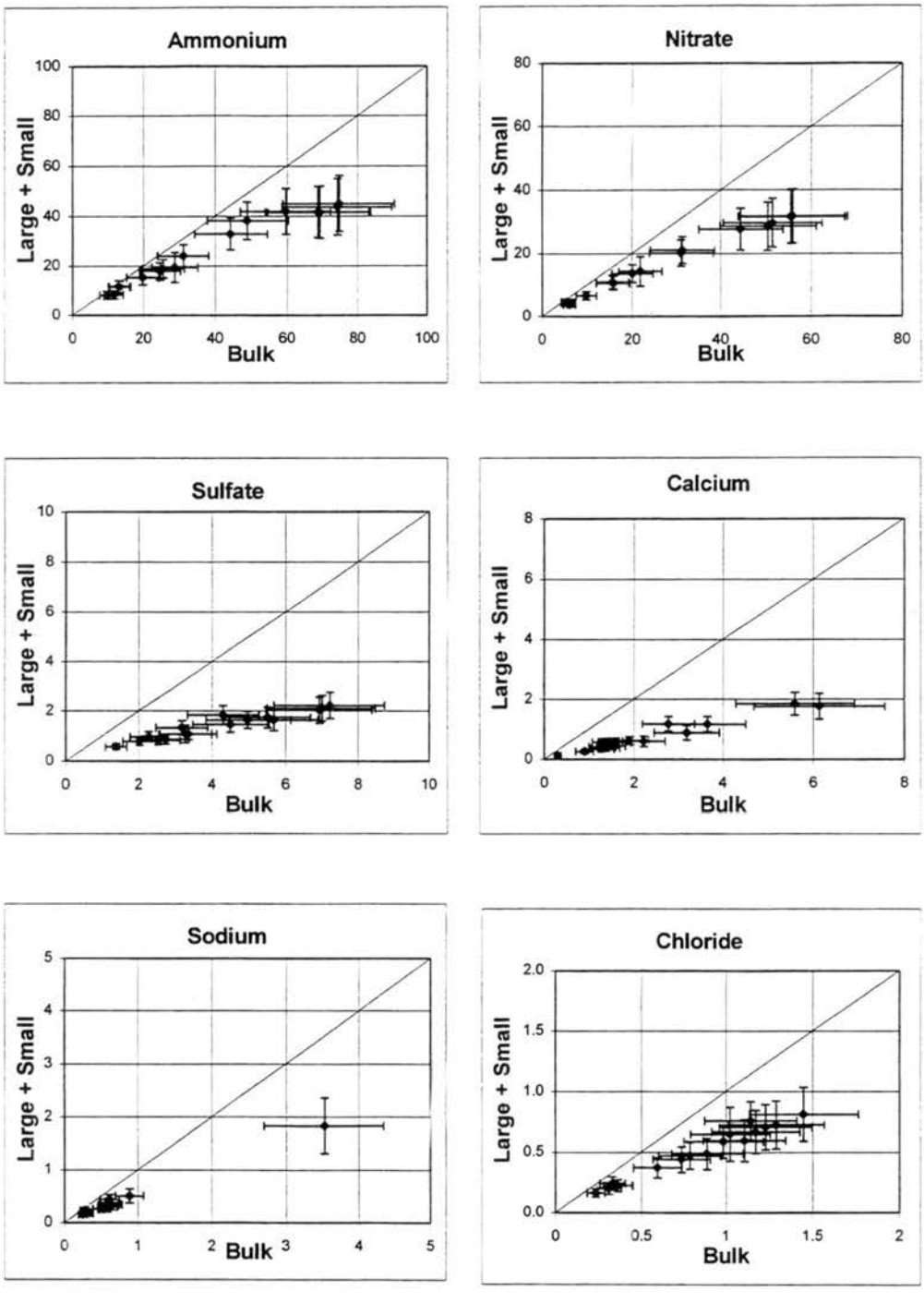

Figure 6.3: A comparison of the sum of the large and small drop fluxes to a flux calculated using simulated bulk fog chemistry. All values are in nanomoles m^{-2} s^{-1}. Error bars represent uncertainties in concentrations, drop sizes and liquid water content, propagated through the flux calculations.

ions. Since the concentrations of the ionic species are significantly more concentrated in small drops that are more slowly removed by settling ($v_s \sim d^2$), the majority of the water being removed is less concentrated than the average fog composition. The initial findings of this study have shown that estimating the removal of species, during the event studied, using bulk fog chemistry and microphysics tends to overpredict the removal rates of these ionic species by factors as large as 3.5.

In other fog events, some species have been more concentrated in the large drop fraction (Bator and Collett, 1997). Considering only bulk chemistry in such cases would lead to underpredicting the removal rates of these species, since the large drops are settling out faster than average. More concurrent observations of fog microphysics and size-fractionated drop chemistry are needed to accurately characterize the magnitude of the removal of fogwater constituents through wet deposition. These measurements should also be accompanied by deposition plate measurements to more accurately determine the water fluxes to the surface during the fog event being characterized.

Drop size distributions can vary in the mean size of the droplets in different locations and with cloud or fog type. Also, Ogren et al. (1992) and Pandis et al. (1990) have measured and modeled drop size distributions that suggest that the solute distribution as a function of size may be U-shaped. This shape occurs due to smaller equilibrium growth droplets, whose solute concentrations increase with decreasing size and a larger condensational growth droplet regime in which solute concentrations increase with increasing size.

While sampling with size fractionating collectors gives more size information than bulk type samplers such as the CASCC2, the fixed cut sizes of the stages can lead to sampling different portions of the drop spectrum in different fogs. For example, the 4-23 μm "small" drop fraction in the sf-CASCC may capture most of the droplets in a fog with a small mass mean diameter but may sample only the lower tail of the drop distribution in another fog containing predominantly large drops. Since this would lead to sampling different portions of the solute size distribution, influencing which collected drop fraction contains the highest concentration of a given species, it is important to consider where this division of the drop spectrum is made since. This becomes less important with increasing number of drop size fractions sampled, since a more resolved size distribution gives a more accurate picture of the drop chemistry as a function of drop size.

Chapter 7: The Effects of Internal Buffering Capacity on Sulfate Production

Acid buffering capacity is the ability of a compound or substance to resist changes in pH as small amounts of a strong acid are added. Internal buffering refers to buffering caused by protonating a weak acid present in the solution. External buffering occurs when a gas (e.g. ammonia) is absorbed into the droplet and neutralizes the acid being produced.

Buffering in cloud and fog water has been investigated previously with the predominant focus on external buffering and internal contributions from NH_3, HCO_3^-, $HCOO^-$, and CH_3COO^- (Liljestrand, 1985, Jacob et al., 1986, and Facchini et al., 1992). However, it has also been seen that there could be times when these mechanisms alone cannot account for all the buffering capacity that was measured. Calculations have been made to deduce the amount of buffering present due to carbonate/bicarbonate and ammonia/ammonium in the system for the conditions found in the titrated fog samples. When this theoretical buffering capacity was calculated for pH values measured concurrently with later titrations, it was found that in many cases more buffering is observed than is predicted. Therefore we hypothesize that there are one or more conjugate bases of other weak acids present in the fog water, buffering the addition of acid into the system.

Determining the presence of any such additional internal buffering agents is a very important part in understanding the overall chemistry of the fog. As sulfur dioxide is absorbed by fog drops and oxidized to sulfuric acid, the droplets get more acidic, effectively slowing down or stopping further sulfate production by inhibiting the further absorption of SO_2, and by slowing the pH dependent S(IV) oxidation pathways. The presence of a buffer in the droplet could keep the pH elevated, even as acidic sulfate was being formed, long enough to significantly increase the amount of H_2SO_4 produced.

Fogwater collected at Bakersfield in January 1994 has been titrated numerous times between one and four years after collection. All the IMS95 samples that still had sufficient sample volume were titrated in August 1997. A few IMS95 samples were titrated at the time of collection; some were also titrated in June 1996. The following section describes the methods and results of these titrations.

Previous to 1997 all the titrations performed on the fog samples were done manually. Several kinds of electrodes were used, including an Orion semi-micro combination pH electrode and a Microelectrodes, Inc. MI-710 combination pH electrode. Orion 250 or 290 pH meters were used and the electrode response was calibrated using pH 4.01 and 7.00 buffers. Occasionally a calibration point at 10.01 was also used. A sample volume of 1.0 μL of fog was used in a 2.0 ml cryovial. An initial pH of the sample was taken and then 1, 2 or 10 mN H_2SO_4 was added in 10 μL increments, mixing and measuring the pH after each addition. Duplicates using this method were performed and the results were very repeatable (see Figure 7.1).

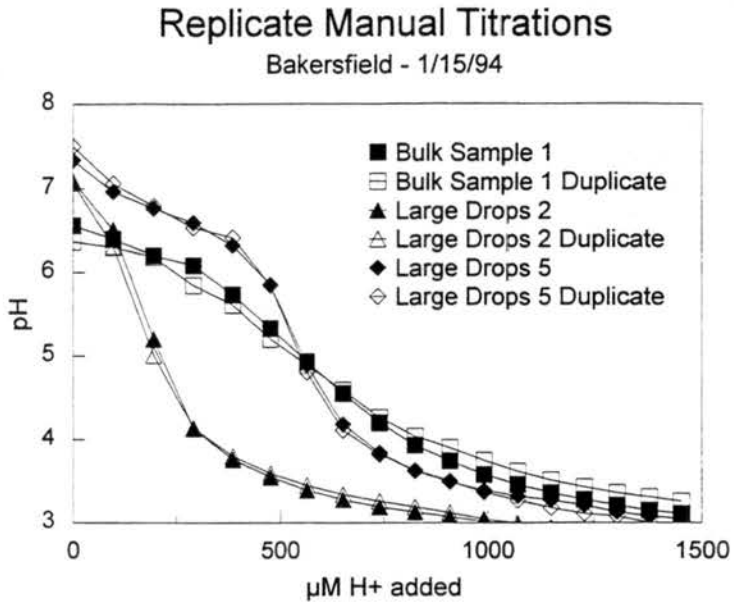

Figure 7.1: Replicate manual titrations of 1994 Bakersfield fog samples

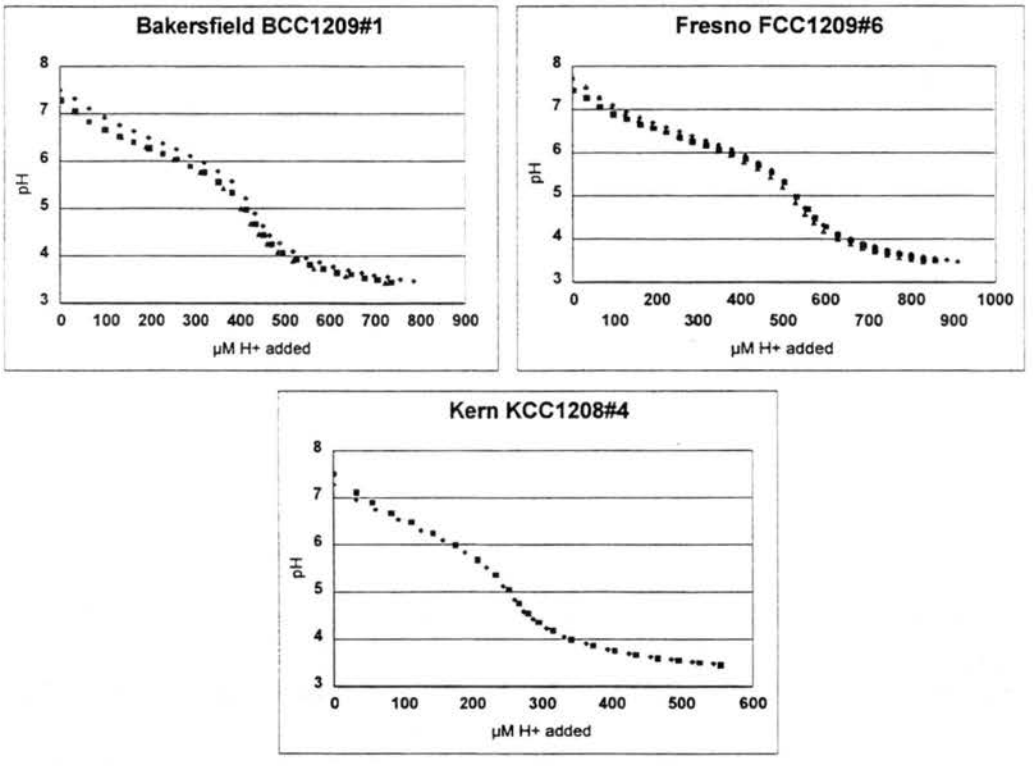

Figure 7.2: Replicate automatic titrations of IMS95 samples.

In 1997 a QC-Titrate automatic titration system from Man-Tech Associates, Inc. was used with a Microelectrodes, Inc. MI-410 combination pH electrode. A three point calibration (pH 4.01, 7.00, and 10.01) was always used. A sample volume of 1.5 ml was used when possible and a 1.0 ml sample when there was less than 1.5 ml of sample remaining. The instrument was set for a potentiometric titration using 10 mN sulfuric acid. The added amount of the acid was controlled by setting a maximum allowable pH change of 0.25 pH units between injections. The software calculates this pH change and can adjust the injections (in μL increments) to measure the endpoint of the titration more accurately. The smallest volume of titrant possible to add is one microliter, giving very good resolution of the shape of the titration curve. Duplicates were performed and were found to be very repeatable (see Figure 7.2).

Base titrations were also performed on selected samples. For these titrations, 20 μL of 0.1 N H_2SO_4 were added to 2 ml of sample to acidify the sample before pipetting 1.5 ml into the titration vial. Then automatic base titrations were performed in a manner similar to the acid titrations using 10 mN KOH.

As a control check for each method, a daily titration of nanopure water was performed in the same manner as for the samples. These checks revealed that the method was working properly before the titrations were started each time and that interaction of the titrated sample with air in the laboratory did not contribute significant buffering capacity to the sample during the titration.

Table E-1 in Appendix E shows when each sample was titrated for each of the investigations described below. Automatic titrations are denoted with an (A).

A comparison of the manual and automatic titration methods was performed to permit comparison of the recent results to data collected in previous years. Eight samples were selected for this intercomparison study from 1994 Bakersfield samples and IMS95 samples from Bakersfield, Fresno, and Kern Wildlife Refuge. In most cases, manual and automatic titrations performed within a week of each other were very close with minor deviations in some cases (see Figure 7.3). In one case (FCC0103#2), when two sets of manual and automatic titrations were performed, only one of the manually performed titrations deviated from the other three. One case (FCC1231#1) had significant differences between the curves but there was not enough sample to retitrate by either method.

Sample pH changes with time, usually increasing from the time of collection. A comparison of sample pH over sample storage time was made using data from titrations before acid additions. These results can be seen in Figure 7.4. One can see that there is a general trend that sample pH usually increases. However there are also times when sample pH decreases with time, or increases then decreases.

One interest was to examine whether the buffering capacity changed as the samples were stored, since most of the titrations have been performed a considerable amount of time after collection. Titrations of samples taken at the time of sample collection (same day and 12 days after), were compared to titrations performed between 6 months and over 1.5 years after collection. In each case the results of titrations done at the time of sampling are radically different, less apparent buffering, than those of the later titrations. In cases such as the 1994 Bakersfield samples, where

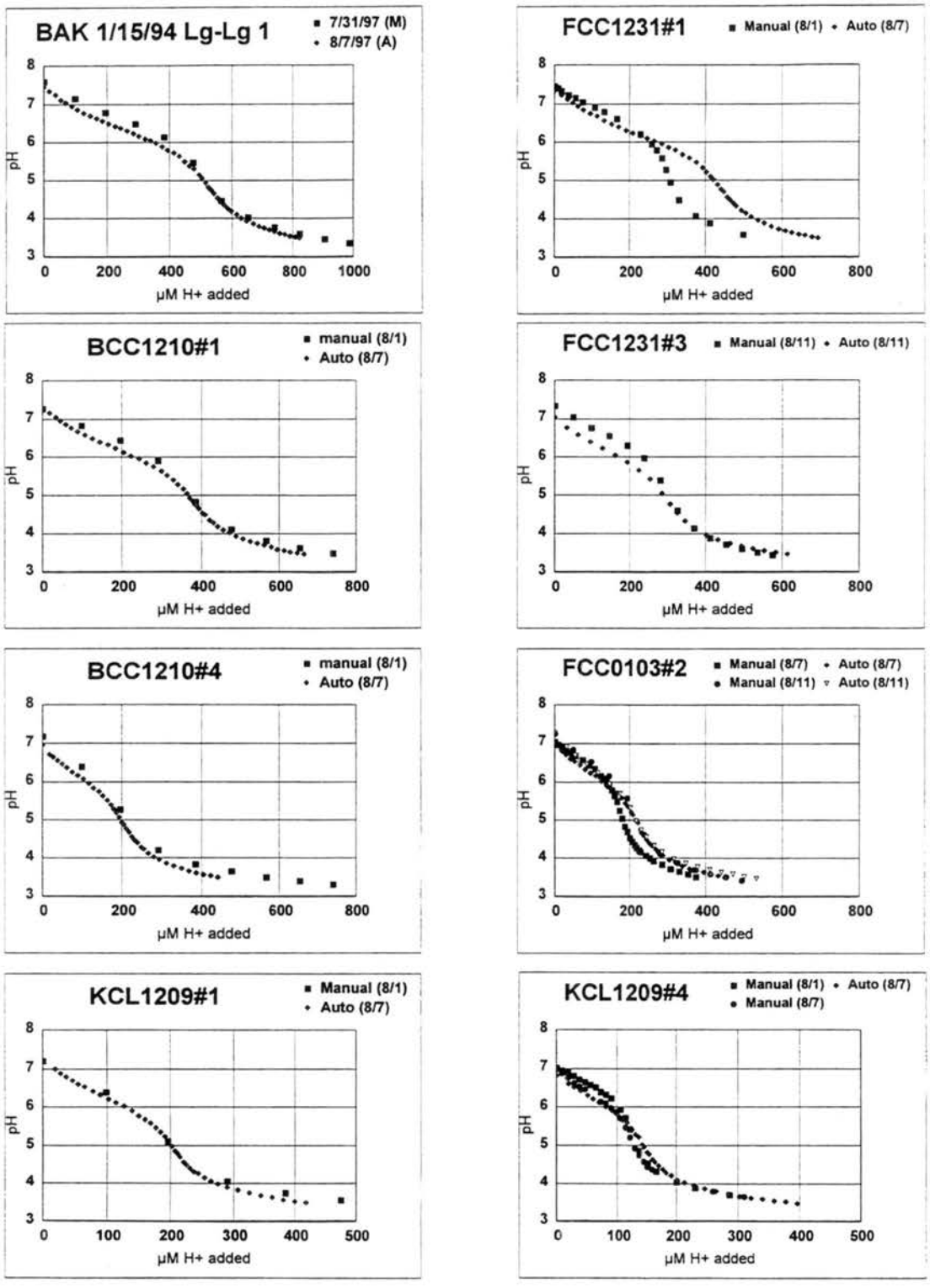

Figure 7.3: Comparisons of manual and automatic titration methods.

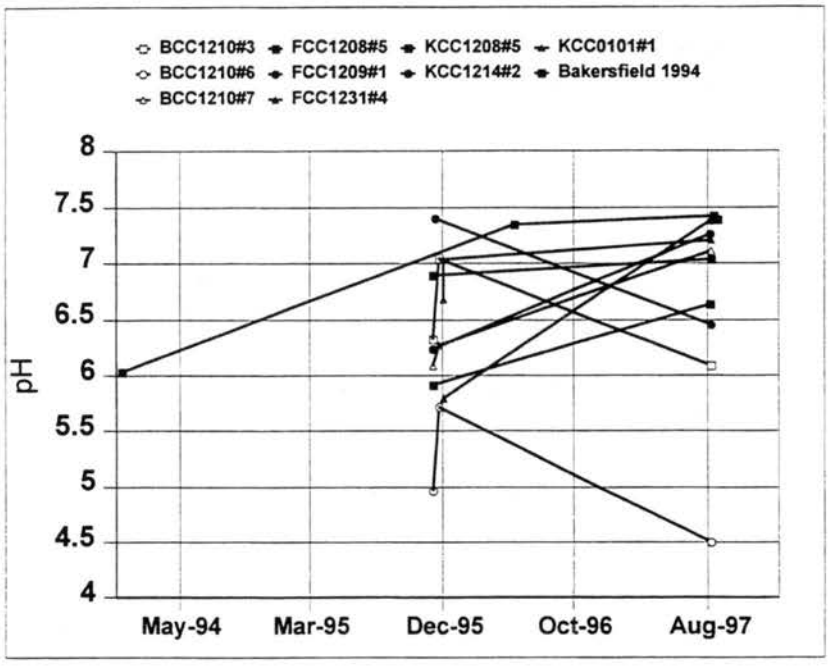

Figure 7.4: Storage effects on fogwater sample pH.

no titrations were performed at collection, the titrations performed between less than 1.5 years to over 3.5 years after collection showed the same amount of buffering capacity. This would suggest that a change goes on in the amount or effectiveness of the internal buffering agent during the first six months of storage. Data suggest that the increase in buffering during storage may come from increased amounts of carbonate and bicarbonate that result from carbon dioxide absorbed as the pH increases. More work is needed to resolve this issue.

Without measurements of known buffering species (carbonate/bicarbonate and ammonium) trends in the buffering capacity due to the unknown agents are not possible. However, there tends to be more overall internal buffering (more acid needed to reach a pH of 5 due to all buffering species present) ocurring in samples collected at Fresno and Bakersfield than at Kern.

Samples taken at the ground and top levels at the Candelabra Tower near Walnut Grove were also titrated in August 1997. In the two cases studied, the overall buffering in the ground sample was much greater than the elevated samples and the lower of the two elevated samples exhibited slightly more buffering than the top sample. Titrations of size fractionated samples from Kern showed that overall buffering could be greater in either the large or small drop fractions (Figure 7.5).

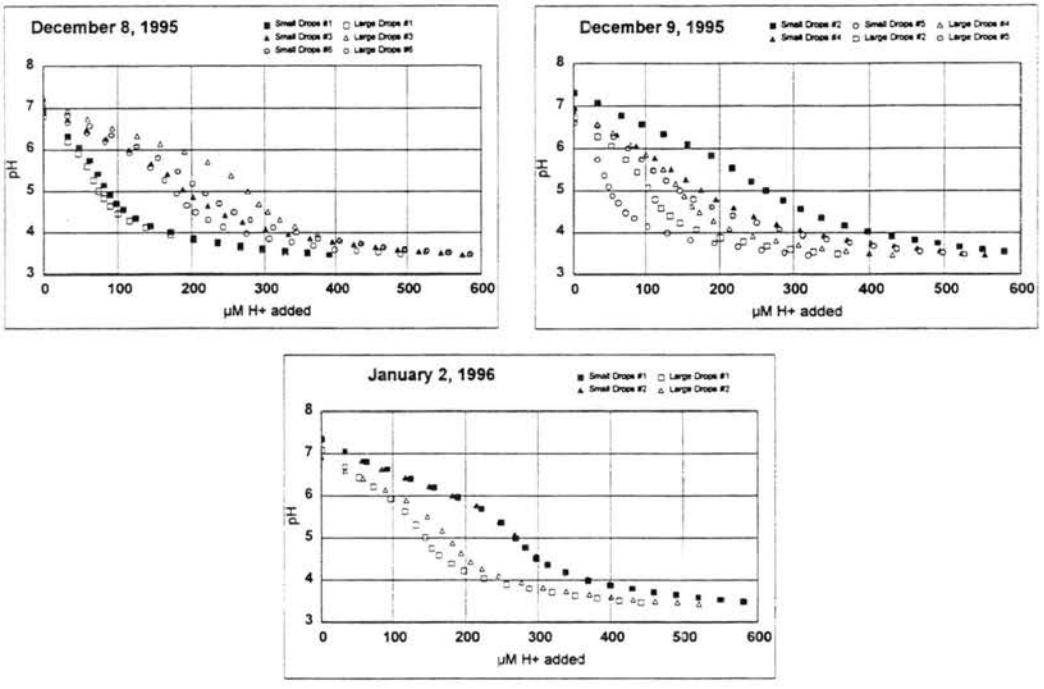

Figure 7.5: Titrations of small and large drop fractions of fogwater collected by the size-fractionating CASCC at Kern Wildlife Refuge.

To determine whether particulate matter in the samples was causing the buffering, a set of samples, both filtered and non-filtered, were titrated concurrently. A 0.2 µm (10 mm) Anotop10 IC inorganic membrane filter was used with a 3 cc syringe to filter 2 ml of sample into a cryovial before pipetting 1.5 ml of filtered sample into the titration vial. Unfiltered samples were titrated

as described above. Filtered and unfiltered titrations of deionized water showed that the filtering process did not add anything to the buffering capacity of the liquid. Eleven samples were titrated with no significant difference observed between filtered and unfiltered samples (see Figure 7.6).

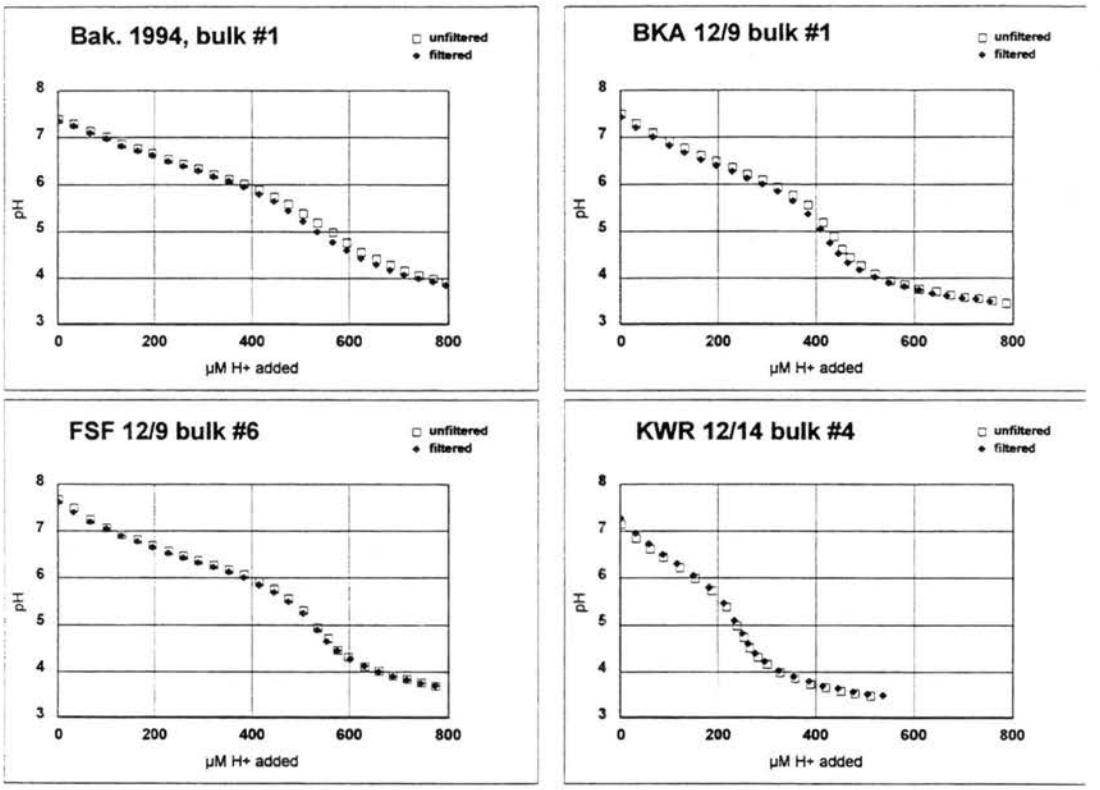

Figure 7.6: Titrations of filtered and unfiltered samples characteristic of each site.

The amount of buffering can be expressed in terms of buffering intensity β, given by the equation:

$$\beta = -\frac{dC}{dpH}$$

for an acid titration of a basic sample and

$$\beta = \frac{dC}{dpH}$$

for a base titration of an acidified sample, where C is the amount of added titrant.

Analyzing a curve of buffering intensity, β, as a function of pH, one should see relative maxima when the pH value is equal to the pKa's of the responsible buffering agents. This occurs because the change in pH is expected to be small for a given acid addition when the solution pH is equal to the buffer's pKa. In order to capture information about the pKa of a sample being titrated, it must be started at a pH sufficiently above or below the pKa value. Eleven samples were made more basic through the addition of small amounts of 0.5 M KOH and titrated. The results from these titrations show that the samples from Bakersfield in 1994 and the IMS95 core fog sites exhibited an apparent pKa between 5.8 and 6.6 (see Figure 7.7). These values agreed well with the routine titrations performed on the same samples. Base titrations on acidified samples were performed as described above. These were performed to ensure that the pKa value obtained from the acid titrations of the raised pH samples was not caused by the high pH sample absorbing

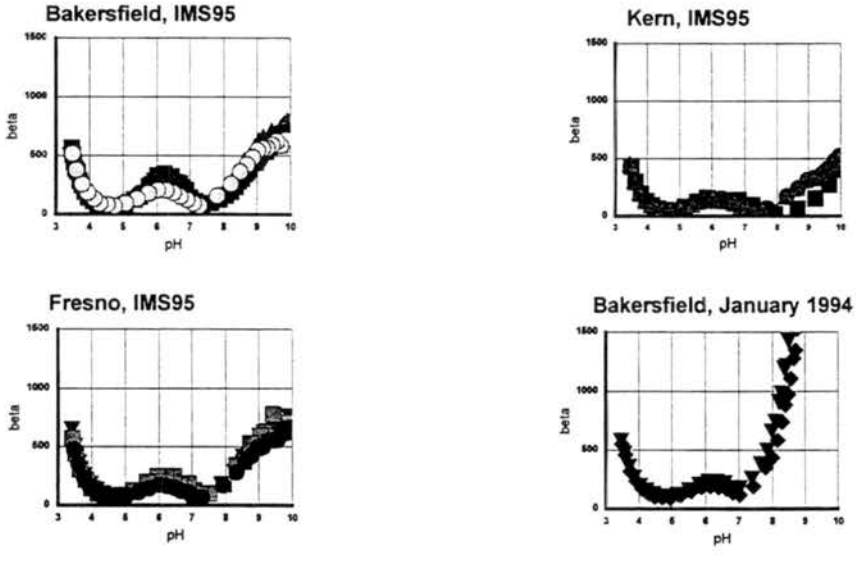

Figure 7.7: Buffering intensity, β, calculated for several base titrated fog samples collected at each of the SJV valley sites during IMS95 and at Bakersfield in 1994.

more CO_2 from the room air. The β was calculated as described above and examined for a local maximum (see Figure 7.8). In two of the samples pKa values between 6 and 6.5 are apparent. However, the peak value of β is much smaller in thebase titrations of acidified samples than the

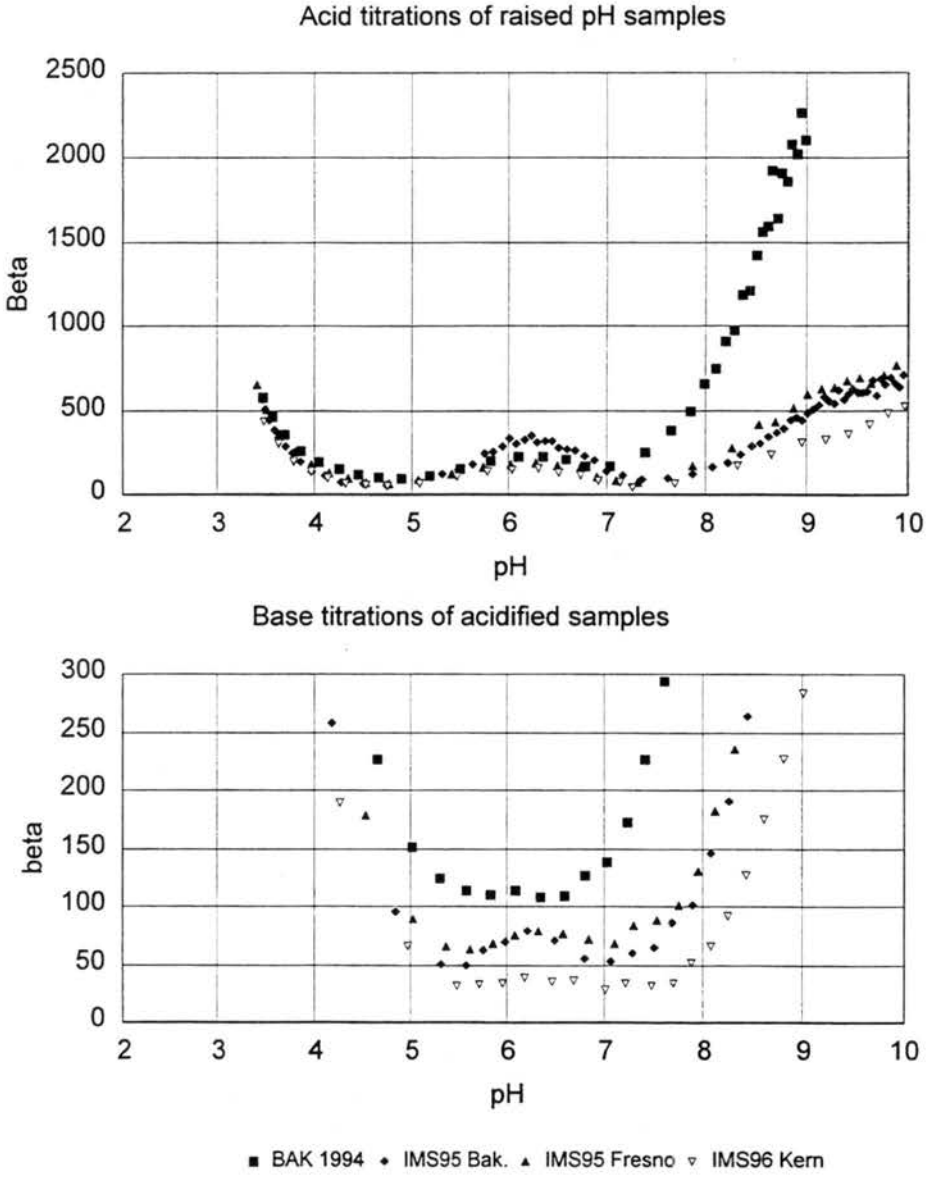

Figure 7.8: Buffering capacity calculations for bulk samples during IMS95 (one from each site) and one bulk sample collected in Bakersfield in January 1994. In the upper panel, samples were raised to a pH > 9 with KOH and titrated with H2SO4. In the lower panel, samples were acidified to a pH < 3 and then titrated with KOH.

acid titrations of the same samples. In the other two samples, a local maximum in β is not discernible. This could mean that the responsible species (including bicarbonate) is volatile and is being outgassed at low pH and not reequilibrating on the time scale of the titrations.

Bicarbonate was measured in selected fog samples by ion chromatography. A Dionex DX-500 system was used with a Dionex AS-11 column and an AG-11 guard column. A gradient elution method was used to vary the concentration of NaOH in order to separate the desired components and maintain a reasonable assay length. Bicarbonate standards were always prepared immediately before the start of the analysis run due to the potential for CO_2 gas exchange during storage. The measured values of fogwater bicarbonate ranged from about 40 μN to about 450 μN (see Table 7.1).

Spectroscopic scans were also performed on three filtered and unfiltered samples from 270 nm to 1100 nm. The scans showed no significant peaks or absorption features except a gradual

Table 7.1: Bicarbonate levels in fogwater measured in August 1997 by ion chromatography.

Sample Name	Bicarbonate (μM)
BCC1209#1	358
BCC1209#2	284
BCC1209#4	353
BCC1210#1	254
FCC1208#1	259
FCC1209#6	464
FCC1231#2	196
KCC1208#4	237
KCC1214#4	240
Bak 94 bulk #1	264
Bak 94 bulk #2	204
Bak 94 Lg-Lg #1	429
Bak 94 Lg-Lg #2	337
Bak 94 Lg-Sm #2	43

increase in absorption of wavelengths below about 400 nm. Further research may include looking at absorption at specific wavelengths in order to identify or eliminate possible species responsible for the buffering. For example, the aromaticity of humic substances can be determined by comparing the absorption at 400 and 600 nm (Aiken et al., 1985).

Other chemical analyses are being investigated to be further probes to add information to our knowledge of this system, including GC-MS and HPLC. We expect the species to have a pKa(s) between 4 and 7 from calculations comparing observed buffering to that explained by contributions of measured ammonium and carbonate/bicarbonate. Possibilities include nitrated phenols or possibly a humic substance. Changes in buffering during sample storage indicate a need for more titrations to be performed concurrently with sample collection. The understanding of the contribution of dissolved CO_2 to the buffering would benefit from simultaneous measurements of gaseous CO_2 or aqueous phase carbonate (H_2CO_3, HCO_3^- and CO_3^{2-}) in addition to field titrations.

Measured buffering capacities can be incorporated into a fog chemistry model in order to investigate the effects internal buffering could have on fog pH and acid production rates throughout the evolution of the fog event. A cooperative effort with Spyros Pandis at Carnegie Mellon University is currently incorporating profiles of internal acid buffering capacity measured and calculated for IMS95 fog samples as discussed above, and measured fog chemistry in a preexisting fog chemistry model, to investigate these effects more thoroughly.

Chapter 8: Conclusions

There are several significant findings from this work concerning the general characterization of fogs in the San Joaquin Valley, chemical reactions occurring in the aqueous phase, the effects size varying drop chemistry has on sulfate production and aerosol removal and a possible effect on the fog chemistry due to internal buffering.

The dominant species measured in the fog collected during IMS95 were ammonium, nitrate, sulfate, acetate, formate and formaldehyde. There tended to be significantly lower sulfate concentrations than were previously measured in this area (Jacob et al., 1984,1986, and Collett et al., 1994, 1997). The concentrations of formaldehyde and the organic acids measured were higher at the two urban sites than at Kern. The fogwater was relatively alkaline for atmospheric water, having a pH range of 4.97 to 7.43 for the three southern SJV sites, with a median value of 6.49.

The high pH of the fogwater causes the oxidation of S(IV) by ozone to be much faster than the oxidation by other oxidants in most cases. In the fogwater collected at the southern San Joaquin Valley sites, the oxidation rate was always dominated by the ozone pathway when the pH of the water was above 6. The dominant oxidant was much less predictable when the pH was between 5 and 6, with all three pathways having an

important contribution for the sample set in this study. It appears that the oxidation rate would be dominated by the hydrogen peroxide pathway below a pH of 5, but there is an insufficient number of samples to be certain. Temporal variations in total S(IV) oxidation rates seem to suggest that oxidation remains an important chemical process occurring in the fog throughout the duration of the fog lifetime. Initial results from calculating amounts of sulfate that the fog may be capable of producing show that the amounts are significant compared to measured PM_{10} concentrations and also the EPA standard.

However, other reactions such as S(IV) complexation with formaldehyde to form HMS can compete with oxidation for S(IV) if ample quantities of formaldehyde are available as observed during IMS95. Mass transfer of S(IV) into the droplets also may be a limiting factor in sulfate production at least in large drops.

Sensitivity studies, in addition to the discovery that each of the S(IV) oxidation and complexation reactions discussed in this thesis could dominate sulfur chemistry in fogs in this area, suggest that measurements of ozone, metals, formaldehyde and HMS are particularly important in efforts to characterize the role of SJV fog in aerosol formation through S(IV) oxidation. Observed vertical variations in fogwater composition, liquid water content and various oxidants imply that S(IV) oxidation rates may vary throughout the fog layer. This would lead to varied aerosol formation rates as a function of elevation which could affect vertical PM_{10} profiles.

Variations in fogwater chemistry with drop size were observed. Small drops were more acidic than large drops and were also more concentrated in all the inorganic ions measured. The observed chemical heterogeneities in the composition of the droplet spectrum have a potential to significantly change the aerosol production and removal processes in the fog. The variations of fog drop acidity coupled with the nonlinearity of the S(IV) oxidation rate by ozone lead to an enhancement of sulfate production in the observed fogs. The observed enhancement of S(IV) oxidation due to this heterogeneity ranges from a factor of 1.0 to a factor of 7.8 for the southern SJV sites. These numbers should be considered as lower bounds on the true enhancement due to chemical heterogeneity, since more than two independent compositions are certainly present in the fog. Removal of fog drops by wet deposition is also size dependent. Therefore, calculating removal of ionic species in the fogwater by sedimentation of the fog drops suggests that estimating removal using bulk chemistry could overestimate solute removal rates by as much as a factor of 3.5. This effect probably depends strongly on where the experimental division is made between large and small drops in the drop size spectrum. Greater resolution in composition versus drop size would help evaluate this effect more precisely.

Internal acid buffering has been observed in IMS95 fog water. Other initial findings suggest that additional buffering is present beyond that from dissolved carbonate/bicarbonate and ammonia/ammonium in the water (Collett et al., 1997). This would imply that more sulfate could be produced before the increasing acidity of the drop shut down the absorption of more SO_2 and the ozone oxidation reaction. Initial findings

from this work suggest that the responsible species are dissolved and that concentrations of at least one of the internal buffering agents change significantly during the first year of sample storage.

In conclusion, the chemical characteristics of the fogs collected in the SJV during IMS95 stem from a complex combination of industrial, transportation and agricultural sources. These characteristics, including the variation of fogwater chemistry as a function of drop size, have great impacts on the resulting aqueous chemistry and other aerosol processing mechanisms. IMS95 provided a sampling platform by which it was possible to characterize several aspects of the chemical and physical fog processes in addition to fog-aerosol interactions. However, the shortcomings of these results in resolving several questions have led to determining the importance of specific measurements to such characterizations.

Chapter 9: Future Work and Recommendations

The following discussion contains several suggestions for future sampling studies seeking to characterize the processes examined in this thesis. It is clear that different overall objectives and economic constraints could alter the approach to such sampling experiments.

Sensitivity studies showed that oxidant and catalyst concentrations, particularly trace metals concentrations, can have significant effects on the dominating oxidation pathways. The particular sensitivity to the metals concentrations suggests that characterizing the speciation of the total iron and manganese present may also be an important factor. Since sulfate production in ambient conditions observed during IMS95 is affected greatly by chemistry variations as a function of drop size, it would also be beneficial to characterize the fogwater chemistry as a function of drop size. The resolution of the size fractionated fog collection could also be important to the results of a sampling effort. Continuous gas phase measurements of the oxidant concentrations as a function of elevation are needed for better characterization of this variability in addition to calculations to determine whether these gases are in equilibrium with the droplets.

More measurements of contributing species along with titrations performed on recently collected samples are needed to better evaluate the possible effects of internal buffering on sulfate production. Modeling efforts by Spyros Pandis at Carnegie Mellon University are presently addressing effects of the observed internal buffering on aqueous phase aerosol formation rates in IMS95 fogs.

Bibliography:

Aiken G.R., McKnight D.M., Wershaw R.L., and MacCarthy P. (1985) *Humic Substances in Soil, Sediment, and Water: Geochemistry, Isolation, and Characterization.* John Wiley and Sons, New York.

Bator A. and Collett J.L. Jr. (1997) Cloud chemistry varies with drop size. *J. Geophys Rev.* In press.

Boyce S.D., and Hoffmann M.R. (1984) Kinetics and mechanism of the formation of hydroxymethanesulfonic acid at low pH. *J. Phys. Chem.* **88**, 4740-4746.

Chow J.C. and Egami R.T., (1997) San Joaquin Valley 1995 Integrated Monitoring Study: Documentation, evaluation and descriptive data analysis of PM_{10}, $PM_{2.5}$, and precursor gas measurements. Technical Support Studies 4 and 8. Prepared for the California Regional Particulate Air Quality Study, California Air Resources Board, Sacremento, CA.

Collett J.L. Jr., Oberholzer B. and Staehelin J. (1993) Cloud chemistry at Mt. Rigi Switzerland: Dependence on drop size and relationship to precipitation chemistry. *Atmos. Environ.* **27A**, 33-42.

Collett J.L. Jr., Bator A., Demoz B. and Rao X. (1994a) Cloud chemistry varies with drop size. In *Transactions from the Air & Waste Management Association 87th Annual Meeting, Cincinnati, OH*, Air & Waste Management Association, Pittsburgh, PA.

Collett J.L. Jr., Bator A., Rao X. and Demoz B. (1994b) Acidity variations across the cloud drop size spectrum and their influence on rates of atmospheric sulfate production. *Geophys. Rev. Lett.* **21**, 2393-2396.

Collett J.L. Jr., Iovinelli R. and Demoz B. (1995) A three-stage cloud impactor for size-resolved measurements of cloud drop chemistry. *Atmos. Environ.* **29**, 1145-1154.

Collett J.L. Jr., Rao X. and Hoag K. (1997) Enhanced aerosol formation rates in fogs from internal acid buffering. Presented at the 1997 Conference of the American Association for Aerosol Research (AAAR), October 13-17, 1997, Denver.

Dasgupta P. K., DeCesare K. and Ullrey J. C. (1980) Determination of atmospheric sulfur dioxide without tetrachloromercurate(II) and the mechanism of the Schiff reaction. *Anal. Chem.* **52**, 1912-1922.

Demoz B., Collett J.L. Jr. and Daube B.C. Jr., (1996) On the Caltech Active Strand Cloudwater Collectors. *Atmos. Res.* **41**, 47-62.

Dong S. and Dasgupta P. K. (1987) Fast fluorometric flow injection analysis of formaldehyde in atmospheric water. *Environ. Sci. Technol.* **21**, 581-588.

Facchini M.C., Fuzzi S., Wobrock W., Jaeschke W., Arends B.G., Mols J.J., Solly I., Kruisz C., Reischl G., Pahl S., Hallberg A., Ogren J.A., Fierlinger H., Marzorati A. and Schell D. (1992) The chemistry of sulfur and nitrogen species in a fog system. A multiphase approach. *Tellus* **44B**, 505-521.

Jacob D.J., Waldman J.M., Munger J.W. and Hoffmann, M.R. (1984) A field investigation of physical and chemical mechanisms affecting pollutant concentrations in fog droplets. *Tellus* **36B**, 272-285.

Jacob D.J., Munger J.W., Waldman J.M. and Hoffmann, M.R. (1986) The H_2SO_4-HNO_3-NH_3 system at high humidities and in fogs. 1. Spatial and temporal patterns in the San Joaquin Valley of California. *J. Geophys. Rev.* **97**, 1073-1088.

Hoffmann M. R. (1986) On the kinetics and mechanism of oxidation of aquated sulfur dioxide by ozone. *Atmos. Environ.* **20**, 1145-1154.

Hoffmann M.R., Collett J.L. Jr. and Daube B.C. Jr. (1989) Characterization of cloud chemistry and frequency of canopy exposure to clouds in the Sierra Nevada. Final report prepared for the California Air Resources Board, Sacremento, CA.

Ibusuki T. and Takeuchi K. (1987) Sulfur dioxide oxidation by oxygen catalyzed by mixtures of manganese (II) and iron (III) in aqueous solutions at environmental reaction conditions. *Atmos. Environ.* **21**, 1555-1560.

Kok G.L., Gitlin S.N. and Lazrus A.L. (1986) Kinetics of the formation and decomposition of hydroxymethanesulfonate. *J. Geophys. Res.* **91**, 2801-2804.

Lazrus A.L., Kok G. L., Gitlin S. N. and Lind J. A. (1985) Automated fluorometric method for hydrogen peroxide in atmospheric precipitation. *Anal. Chem.* **57**, 917-922.

Lazrus A.L., Kok G.L., Lind J.A., Gitlin, S.N., Heikes B.G. and Shetter R.E. (1986) Automated fluorometric method for hydrogen peroxide in air. *Anal. Chem.* **58**, 594-597.

Liljestrand H.M. (1985) Average rainwater pH, concepts of atmospheric acidity, and buffering in open systems. *Atmos. Environ.* **19**, 487-499.

Lodge J.P. Jr. *Methods of air sampling and analysis*, 3rd ed.; Lewis Publishers, inc.: Chelsea, MI, 1989.

Munger J.W., Jacob D.J., Waldman J.M. and Hoffmann, M.R. (1983) Fogwater chemistry in an urban atmosphere. *J. Geophys. Rev.* **88**, 5109-5121.

Munger J.W., Collett J.L. Jr., Daube B. Jr. and Hoffmann M.R. (1989) Chemical composition of coastal stratus clouds: dependence on droplet size and distance from the coast. *Atmos. Environ.* **23**, 2305-2320.

Ogren J.A., Noone K.J., Hallberg A., Heintzenberg J., Schell D., Berner A., Solly I., Kruisz C., Reischl G., Arends B.G. and Wobrock W. (1992) Measurements of the size dependence of the concentration of non-volatile material in fog droplets. *Tellus* **44B**, 570-580.

Olson T.M. and Hoffmann M.R. (1986) On the kinetics of formaldehyde-S(IV) adduct formation in slightly acidic solution. *Atmos. Environ.* **20**, 2277-2278.

Olson T.M. and Hoffmann M.R. (1989) Hydroxymethanesulfonate formation: Its role as a S(IV) reservoir in atmospheric water droplets. *Atmos. Environ.* **23**, 985-997.

Pandis S.N., Seinfeld J.H. and Pilinis C. (1990) Chemical composition differences in fog and cloud droplets of different sizes. *Atmos. Environ.* **24A**, 1957-1969.

Rao X. and Collett J.L. Jr. (1995) The behavior of S(IV) and formaldehyde in a chemically heterogeneous cloud. *Environ. Sci. Tech.* 29, 1023-1031.

Rao X. and Collett J.L. Jr. (1996) The drop size-dependence of iron and manganese concentrations in clouds and fogs: implications for sulfate production. *J. Atmos. Chem.* Submitted December 9, 1996, in review.

Richards L.W., Pandis S.N. and Campos T. (1997) Technical Support Study 11: Investigating the Dynamics and Chemistry of Fog Formation and Dissipation. Phase II Report: Measurement at the Candelabra Tower (STI-95090-1727). Prepared for the California Air Resources Board, Sacremento, CA.

Seinfeld J.H. (1986) *Atmospheric Chemistry and Physics of Air Pollution.* Wiley, New York.

Solomon P.A., Thuillier, R.H. Magliano, K., et al. (1996) 1995 Integrated Monitoring Study: Study objectives and design. In *Proceedings of the 1996 A&WMA/U.S. EPA Symposium on measurement of Toxic and Related Air Pollutants,* Air & Waste Management Association, Pittsburgh, PA.

Schwartz S.E. (1988) Mass-transport limitation to the rate of in-cloud oxidation of SO_2: Re-examination in the light of new data. *Atmos. Environ.* **22**, 2491-2499.

U.S. EPA (1997) Current and Revised Standards for Ozone and Particulate Matter, (http://www.epa.gov/airprogm/oar/oaqps/ozpmbro/current.htm)

Waldman, J. M. and Hoffmann, M. R. (1987) Sources and Fates of Aquatic Pollutants, in ACS Advances in Chemistry Series No. 216, R. A. Hites and S. J. Eisenreich Eds.; American Chemical Society, New York, pp. 79-129.

Wright D.B. and Roberts P.T. (1996) Collection of Continuous Gas-Phase Data at Two Sites During IMS95. Final Report (STI-95173-1625-FR). Prepared for the San Joaquin Valleywide Air Pollution Study Agency, California Air Resources Board, Sacremento, CA.

Appendix A: Quality Control, Quality Assurance and Data Validation

A variety of procedures were undertaken to minimize problems with information collected as part of this study and to quantify uncertainties in the data reported. Some of these procedures have been outlined in the preceding discussion of measurement methods and analytical techniques. Here we provided a brief summary of additional measures taken and report our findings of analytical precision, detection limits, and laboratory intercomparability.

Instrument Blanks

Following our standard operating procedures, the fog samplers used in the study were cleaned with DI water prior to each event. When possible, and in most cases, collector blanks were taken to test the adequacy of the cleaning procedures. Blanks were collected by spraying water onto the collection surfaces and allowing it to flow through the same path followed by actual samples. One limitation to this approach is that soluble gases are efficiently captured by the sprayed water and contribute to the chemical loading in the collected blank. Some aerosol particles may also contribute in this way, although their collection should be less efficient. A second point worth noting is that the collector is

"cleaned" by collected fogwater during the course of an event. Consequently, a high blank may contribute much more to the first sample collected than to subsequent samples. Further, material rinsed off collection surfaces during blank collection is no longer present to contribute to the chemical loading of collected samples.

Due to these limitations, our standard procedures do not call for blank correcting sample concentrations. Instead we have chosen to flag samples for which corresponding blanks indicate potential contamination. This has been done on a species by species basis. Due to the absorption of gaseous compounds by the sprayed DI water, we have excluded species coming predominantly from the gas phase from this flagging procedure.

Determination of Uncertainties and Detection Limits

As part of the analytical procedure of the study, values were determined for the uncertainty and detection limit of each species measured. Procedures and results are outlined below for the chemical species measured in fog and for the aerosol and gas measurements made at the Candelabra Tower.

Uncertainties and Detection Limits for the Fog Chemistry Measurements

As mentioned previously, no blank corrections were made to the fog chemistry measurements. Therefore the uncertainty and detection limits for the fog composition measurements are given by the uncertainties and detection limits for the analytical

methods employed. Methods for calculating these quantities are outlined below and results of the calculations are presented in Table A-1.

Table A-1. Calculated analytical uncertainties and detection limits for all chemical

Species	**Analytical Uncertainty relative standard deviation % (# replicates, replicate conc. range, avg. replicate conc.)**	**Instrument Detection Limit (# replicates)**
Chloride	5.1 (21, 1.9-33.2 μN, 10.2 μN)	1.36 μN (15)
Nitrate	0.34 (21, 49.4-875.9 μN, 265.7 μN)	0.78 μN (15)
Sulfate	1.1 (21, 17.0-2408.5 μN, 168.6 μN)	1.27 μN (15)
Sodium	1.2 (21, 0 - 49.0 μN, 7.6 μN)	0.91 μN (19)
Ammonium	0.62 (21, 7.6 - 3129.7 μN, 603.2 μN)	1.15 μN (19)
Potassium	3.1 (21, 1.4 - 49.9 μN, 11.8 μN)	0.97 μN (19)
Magnesium	5.3 (21, 1.7 - 50.1 μN, 7.8 μN)	0.84 μN (19)
Calcium	4.2 (21, 2.5 - 143.6 μN, 30.4 μN)	0.90 μN (19)
Acetate	2.6 (19, 0 - 325.9 μN, 63.8 μN)	1.05 μN (7)
Propionate	7.9 (19, 0 - 54.3 μN, 17.9 μN)	2.02 μN (7)
Formate	0.74 (19, 0 - 124.3 μN, 44.7 μN)	1.97 μN (7)
Pyruvate	0.22 (19, 0 - 50.7 μN, 16.9 μN)	0.79 μN (7)
Oxalate	0.66 (19, 0 - 108.8 μN, 42.6 μN)	5.45 μN (7)
S(IV)	14.4 (36, 0.9-55.2 μM, 14.4 μM)	0.89 μM (18)
HMS	14.4 (36, 0.9-55.2 μM, 14.4 μM)	0.89 μM (18)
Formaldehyde	5.3 (45, 0.9 - 196.3 μM, 28.8 μM)	0.15 μM (13)
Hydrogen Peroxide	5.6 (18, 0.1 - 16.3 μM, 5.4 μM)	0.45 μM (8)
TOC	10.8 (81, 0 - 5.4 ppm, 2.0 ppm)	1.27 ppm (31)
TDOC	10.8 (81, 0 - 5.4 ppm, 2.0 ppm)	1.27 ppm (31)
Iron	5.0 (20, 0 - 1886.0 μg/l, 409.0 μg/l)	1.82 μg/L (17)
Manganese	8.6 (20, 7.3 - 57.6 μg/l, 22.1 μg/l)	0.22 μg/L (20)

Analytical uncertainties are calculated and reported as relative standard deviations (RSD), in percent. The RSD (σ^*_s) for each species was calculated from large (>10 and usually >20) numbers of replicate sample analyses x_1 and x_2, except for S(IV) and HMS where replicate analyses of calibration standards were used due to insufficient available sample volumes. Equation A-1 shows the formula used for calculating the RSD, where x_{bar} is the average value of all the replicates.

$$\sigma_s^* = \frac{\left[\left(\frac{1}{M}\right)\cdot\sum_{j=1}^{M}\left(\sigma_j'\right)^2\right]^{1/2}}{x_{bar}}\cdot 100 \qquad \text{(A-1)}$$

σ'_j is calculated as shown in Equation A-2.

$$\sigma_j' = \frac{|x_1 - x_2|}{\sqrt{2}} \qquad \text{(A-2)}$$

The absolute uncertainties reported are the products of the calculated relative standard deviations and the reported concentrations.

Equation A-3 was used for estimating instrument detection limits. As many blanks as possible were used for each calculation. In some cases no analyte was detected in the blanks and the detection limits had to be calculated by examining variability in analysis of a low concentration standard.

$$\Delta x_{\min} \geq t \cdot s_b \cdot \sqrt{\frac{N_b + N_s}{N_b \times N_s}} \qquad \text{(A-3)}$$

where t is the student t value at the 95% confidence level for the appropriate number of degrees of freedom, s_b is the standard deviation of the blanks, N_b is the number of blanks and N_s is the number of sample measurements. Detection limits were all calculated

assuming a single sample analysis; lower detection limits are possible if replicate analyses are used.

Checks on Laboratory Performance

Ion concentrations measured by CSU were checked by two methods. Internally, standard solutions containing known concentrations of the measured ions were purchased to use as spot checks on analytical performance. CSU also participated in a sample intercomparison with the CARB analytical laboratory in Sacramento. Results of these tests, provided below, indicate that CSU reported accurate values for ion concentrations measured in this study.

Internal Calibration Checks

CSU ion chromatography calibration standards were prepared by diluting stock solutions prepared from reagent grade salts and DI water. Analyses of the calibration standards were made daily to generate current calibration curves as explained above. NIST traceable cation and anion standards were purchased from Dionex corporation to provide a check on the accuracy of ion concentrations determined by ion chromatography analysis in the CSU lab. The standards purchased were combined five anion and combined six cation standards. Dilutions (1:100) of the Dionex standards were prepared and used as check standards periodically throughout the analysis of samples collected as part of IMS95.

Figure A-1 depicts the ratios of measured ion concentrations to nominal ion concentration values for the Dionex check standards. Measured values for all ion concentrations were within 10% of the nominal concentrations, and six of the eight ions were measured within 5% of the nominal values. The greatest disagreement was for chloride (nominal value 8.3 μN, measured concentration 9.0 μN), a species which is somewhat difficult to quantify at concentrations below 10 μN. Table A-2 lists more complete information about the comparison, including the nominal and average measured ion concentrations of the check standards and the relative standard deviations (RSD) of the measurements.

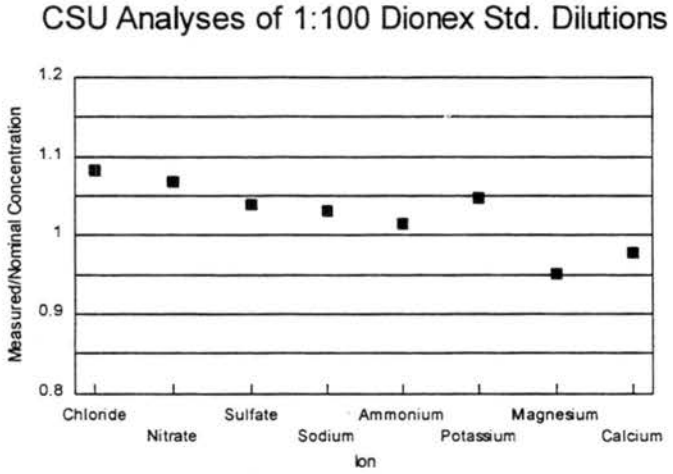

Figure A-1. CSU analyses of calibration check standards made from NIST-traceable solutions purchased from Dionex Corporation.

Laboratory Intercomparison

As part of the study, CSU and the CARB inorganics analytical laboratory (Dr. Charles Cowell) in Sacramento participated in a laboratory intercomparison where samples were

Table A-2. CSU Analyses of Dionex Check Standards

Ion	Nominal Concentration (μN)	Avg. Measured Concentration (μN)	Number of Measurements	RSD of Measurements (%)	Measured/Nominal
Chloride	8.32	9.01	5	11.5	1.08
Nitrate	16.13	17.21	5	3.6	1.07
Sulfate	31.23	32.46	5	3.2	1.04
Sodium	87.86	90.68	12	3.9	1.03
Ammonium	225.43	228.62	12	1.8	1.01
Potassium	51.15	53.59	12	4.2	1.05
Magnesium	168.72	160.40	12	2.2	0.95
Calcium	509.48	498.26	12	2.7	0.98

exchanged for ion analysis by both laboratories. CSU sent portions of six fog samples from IMS95 to the CARB lab and the CARB lab prepared six anion and six cation synthetic samples which were sent to CSU for analysis.

Table A-3 lists CSU's reported concentrations for the twelve synthetic samples prepared by CARB. Each sample was measured five times. The average concentration and standard deviation are shown for each sample and species. Also shown are the nominal concentration values reported by CARB (C. Cowell, CARB, personal communication). For most species and samples the concentrations reported by CSU show excellent agreement with the nominal concentration values. In many cases the reported concentrations are within a few percent of the nominal values. Two exceptions stand out. When nominal concentration values are very low (e.g., Anion samples B and E and Cation samples B and F where concentrations are 100 μg/l or less), the disagreement increases. There is also considerable disagreement between reported and nominal concentration values at all levels for calcium.

Table A-3. CSU Analyses of Synthetic Samples Provided by CARB

Sample		Nominal Anion Conc. (µg/l)	Chloride (µg/l)	Nitrate (µg/l)	Sulfate (µg/l)	Sample		Nominal Cation Conc. (µg/l)	Sodium (µg/l)	Ammonium (µg/l)	Potassium (µg/l)	Magnesium (µg/l)	Calcium (µg/l)
Anion A	average	1000	987.9	991.8	1024.9	Cation A	average	700	710.8	686.3	691.4	753.4	940.0
	std dev		28.9	22.3	36.4		std dev		2.6	4.9	9.6	9.6	32.7
	measured/nominal		0.99	0.99	1.02		measured/nominal		1.02	0.98	0.99	1.08	1.34
Anion B	average	100	111.8	71.1	112.7	Cation B	average	50	91.0	35.1	33.2	70.5	167.1
	std dev		8.9	9.6	15.5		std dev		3.3	4.3	2.2	1.9	2.8
	measured/nominal		1.12	0.71	1.13		measured/nominal		1.82	0.70	0.66	1.41	3.34
Anion C	average	1850	1784.9	1823.2	1855.4	Cation C	average	1000	985.1	961.6	961.8	1014.2	1252.0
	std dev		29.9	26.5	28.3		std dev		49.3	52.4	61.0	61.8	77.6
	measured/nominal		0.96	0.99	1.00		measured/nominal		0.99	0.96	0.96	1.01	1.25
Anion D	average	700	649.4	656.8	673.3	Cation D	average	400	398.8	367.3	373.0	435.7	577.1
	std dev		38.5	23.5	40.5		std dev		2.4	10.6	17.7	7.8	18.0
	measured/nominal		0.93	0.94	0.96		measured/nominal		1.00	0.92	0.93	1.09	1.44
Anion E	average	80	66.8	67.0	71.9	Cation E	average	1550	1501.7	1531.1	1483.5	1529.3	1732.0
	std dev		24.6	19.7	41.3		std dev		65.5	75.0	79.9	79.4	84.9
	measured/nominal		0.83	0.84	0.90		measured/nominal		0.97	0.99	0.96	0.99	1.12
Anion F	average	400	398.9	415.7	380.6	Cation F	average	100	94.7	87.7	86.9	127.8	235.0
	std dev		24.4	18.6	27.9		std dev		3.5	4.6	5.8	3.6	6.2
	measured/nominal		1.00	1.04	0.95		measured/nominal		0.95	0.88	0.87	1.28	2.35

The increased disagreement between nominal concentrations and values reported by CSU at low concentration levels is not surprising for a number of reasons. First, concentrations below 100 µg/l are comparable to the analytical detection limit of the ion chromatograph for these species as operated for this study and are well below the concentration range for which the calibration curves were optimized (calibration ranges were selected to match likely fogwater concentrations of the analytes). Second, at such low concentrations the likelihood of observable effects of contamination increases. Third, CARB shipped the samples unrefrigerated, increasing the likelihood that chemical and/or biological transformations might lead to changes in sample composition. CSU's standard operating procedures call for keeping all samples refrigerated until analysis. If one excludes samples in this low concentration range, one finds that reported anion values are all within 7% of the nominal concentrations, with an average disagreement just under 3%. Excluding samples with concentrations of 100 µg/l or below and excluding

calcium, one finds a maximum disagreement of 9% and an average disagreement of 3.5% for the cation samples.

The disagreement between reported and nominal calcium values is not so readily explained. Values reported by CSU are consistently higher than the nominal concentration values reported by CARB. This is somewhat surprising, since CSU's internal checks described in the preceding section found calcium to be accurately measured. Further, as described below, CARB's analysis of the calcium levels in the fog samples substantially exceeded the values reported by CSU for all six samples. One possible explanation for these findings is that calcium was inadvertently introduced as a contaminant to the synthetic samples prepared by CARB and the fog samples measured by CARB. Calcium contamination could have occurred during handling in either lab, although the fact that CSU was able to accurately measure calcium in the Dionex check standards and reported lower calcium concentrations in the fog samples suggests that significant calcium contamination is probably not occurring at CSU. One piece of information that might help clarify the situation would be the analytical results of the CARB lab for the synthetic samples they prepared, although it is not clear whether these samples were ever analyzed in their laboratory. In any case, we should keep in mind that calcium is generally a minor contributor to the fog composition and there is good evidence that the major species are accurately measured.

Table A-4 illustrates the findings from the laboratory intercomparison of fog sample ion analysis. Both laboratories report similar values for nitrate, sulfate, and ammonium (with

one exception). Reasonable agreement is also evident for sodium values. The agreement is poorer for chloride, potassium, magnesium and calcium concentrations. Values reported by CARB for chloride and calcium are consistently higher than those reported by CSU, while CARB values for potassium are consistently lower and magnesium values are lower in five of six cases. In many cases disagreement between the reported values is likely due to the low analyte levels being measured. For example, in samples where magnesium or chloride concentrations exceeded 5 μN, moderate agreement was observed between concentrations of these species reported by the two labs.There are several samples, however, where potassium or calcium concentrations exceed 10 μN, a level that should be accurately quantifiable, and large discrepancies are present between the values measured by the two laboratories. In the case of calcium, the fact that CARB reported no

Table A-4. Laboratory Intercomparison of Fog Composition. All concentrations are in μN.

Sample	Cl- CSU	CARB	Difference/Mean (%)	Sample	Na+ CSU	CARB	Difference/Mean (%)
BCC1210#2	37.5	40.3	-7.3	BCC1210#2	9.3	8.2	12.1
FCC1209#2	16.1	18.0	-11.5	FCC1209#2	3.9	4.0	-4.6
KCC0102#1	3.0	10.7	-112.0	KCC0102#1	1.2	1.6	-27.5
KCL0101#1	3.2	13.2	-121.4	KCL0101#1	2.5	2.5	0.5
KCL0101#2	2.7	10.1	-115.6	KCL0101#2	2.3	2.0	14.4
KCL1209#3	7.1	9.9	-32.0	KCL1209#3	9.6	8.0	18.2
Sample	**NO3- CSU**	**CARB**	**Difference/Mean (%)**	**Sample**	**NH4+ CSU**	**CARB**	**Difference/Mean (%)**
BCC1210#2	551.7	546.8	0.9	BCC1210#2	1320.5	1380.6	-4.4
FCC1209#2	564.8	571.0	-1.1	FCC1209#2	1014.8	1062.8	-4.6
KCC0102#1	128.6	114.5	11.6	KCC0102#1	226.3	244.4	-7.7
KCL0101#1	76.4	75.8	0.8	KCL0101#1	267.3	291.7	-8.7
KCL0101#2	97.3	100.0	-2.8	KCL0101#2	314.7	388.3	-20.9
KCL1209#3	326.0	337.1	-3.4	KCL1209#3	537.3	530.0	1.4
Sample	**SO4= CSU**	**CARB**	**Difference/Mean (%)**	**Sample**	**K+ CSU**	**CARB**	**Difference/Mean (%)**
BCC1210#2	197.2	189.0	4.3	BCC1210#2	31.1	10.8	96.8
FCC1209#2	94.0	87.0	7.8	FCC1209#2	14.5	5.0	96.6
KCC0102#1	30.4	27.3	11.0	KCC0102#1	2.2	0.5	129.7
KCL0101#1	28.4	25.8	9.5	KCL0101#1	1.3	0.6	79.8
KCL0101#2	88.2	86.2	2.3	KCL0101#2	2.8	0.4	154.1
KCL1209#3	50.4	52.0	-3.2	KCL1209#3	8.6	3.6	81.0
Sample	**Ca2+ CSU**	**CARB**	**Difference/Mean (%)**	**Sample**	**Mg2+ CSU**	**CARB**	**Difference/Mean (%)**
BCC1210#2	6.8	21.3	-103.5	BCC1210#2	3.0	1.7	52.2
FCC1209#2	9.1	23.8	-89.5	FCC1209#2	5.3	2.6	67.5
KCC0102#1	3.8	19.4	-134.9	KCC0102#1	2.2	1.6	34.7
KCL0101#1	6.4	31.6	-133.1	KCL0101#1	1.8	2.3	-23.0
KCL0101#2	5.0	21.3	-124.5	KCL0101#2	2.5	1.4	55.4
KCL1209#3	65.5	131.5	-67.0	KCL1209#3	8.9	6.8	26.1

values below 19 μN despite the existence of CSU reported values as low as 4 μN, suggests the possibility of calcium contamination during sample handling.

Data Validation

Level 0 validation included collection of collector blanks, measurement of cloud collector flows, and record keeping of sampling procedures and events likely to affect data quality. These records were reviewed as part of data validation prior to submission of the final databases. The most common problem was lack of sufficient information about sample volume (for example if some sample was spilled during collection) to permit accurate calculation of fog liquid water content. In a few cases field records indicated contamination of samples. Measurements for which level 0 data validation indicated problems were removed from the database.

It was our intent to collocate fog samplers during the study as part of a level I data validation effort. The CASCC2 samplers were all relocated for this purpose to Fresno during a break in IMS95 measurements in mid-December. Unfortunately no fog events occurred during this time and a side-by-side measurement comparison was not possible. A previous side-by-side comparison of five CASCC2 collectors constructed for a CARB fog monitoring network, however, reported excellent agreement among the collectors for sample mass and ion concentrations. A summary of these findings is presented in Table A-5.

Table A-5. Results of CASCC2 intercomparison (5 collectors) at San Pedro Hill, California in May 1989. Relative standard deviations are presented as a percentage of the mean value for each sample. Source: B. Daube, personal communication.

Species	Sample Mass (g)	H^+ (μN)	NH_4^+ (μN)	Na^+ (μN)	K^+ (μN)	Ca^{2+} (μN)	Mg^{2+} (μN)	Cl^- (μN)	NO_3^- (μN)	SO_4^{2-} (μN)
Sample 1 avg.	125.2	515.3	458.3	175.1	7.3	43.3	49.3	205.7	546.4	489.5
Sample 1 rsd (%)	2.2	1.9	0.9	3.2	9	4.7	4	2.1	1	0.6
Sample 2 avg.	243.9	468	340.7	80.2	5.1	23.4	23.6	98.5	407.2	401.6
Sample 2 rsd (%)	2.9	4.1	1.4	5.8	14.5	8.1	5.7	5.9	0.8	0.5
Sample 3 avg.	161.1	1,047.2	848.6	73.7	6.6	45.8	26.5	143.4	1,027.1	902.4
Sample 3 rsd (%)	1.2	1.6	1.1	1.7	4.3	7.9	4.1	3.1	1.5	1.7

After sample analysis, a number of tests were applied as part of level II data validation. These tests are outlined below, along with an indication of flags applied to the submitted databases. Table A-6 provides a summary for the southern San Joaquin Valley of the number of possible samples, the number of valid samples, and the number of samples above the limit of detection and the limit of quantitation (taken as three times the limit of detection). The fraction of samples not flagged for each species (% valid) ranged from a low of 54% for dissolved organic carbon (DOC) to a high of 93% for sodium, potassium and manganese. When flags due to high or low charge balances were excluded (in the SJV we have found that charge balances frequently are quite low when calculated as the sum of anions divided by the sum of cations (see below), presumably due to large concentrations of ionic species not analyzed), all species except total and dissolved organic carbon had total valid fractions of 89% or higher. In the Candelabra Tower study, 100% of the samples were determined valid except for total and dissolved organic carbon (with valid fractions of 88% each) and sodium (valid fraction of 94%). In the

southern San Joaquin Valley study the fractions of samples above the detection limit were quite high, although smaller fractions of propionate, pyruvate, oxalate, and HMS were found to be above the limit of quantitation. At the Candelabra Tower, most species were measured at concentrations above the limit of quantitation, although magnesium, pyruvate, propionate, oxalate, and HMS concentrations were below this level in more than half the samples.

Table A-6. Southern San Joaquin Valley fog sample statistics. The Limit of Quantitation (LOQ) is taken as three times the Limit of Detection (LOD).

Species	# samples	# flagged	# flagged excluding charge balance	# valid samples (#samples - #flagged)	% valid	% valid (excluding charge balance)	# above LOD	% above LOD	#above LOQ	% above LOQ
Cl-	111	20	7	91	82	94	111	100	95	86
NO3-	111	20	4	91	82	96	111	100	111	100
SO42-	111	20	5	91	82	95	111	100	111	100
Na+	113	20	6	93	82	95	107	95	92	81
NH4+	111	20	4	91	82	96	111	100	111	100
K+	113	20	5	93	82	96	110	97	103	91
Mg2+	113	20	4	93	82	96	112	99	96	85
Ca2+	113	22	8	91	81	93	113	100	111	98
Acetate	76	10	0	66	87	100	76	100	76	100
Propionate	76	10	0	66	87	100	59	78	30	39
Formate	76	10	0	66	87	100	76	100	75	99
Pyruvate	76	10	0	66	87	100	60	79	19	25
Oxalate	76	10	0	66	87	100	69	91	18	24
S(IV)	92	9	9	83	90	90	90	98	68	74
HMSA	57	6	6	51	89	89	47	82	29	51
HCHO	92	4	4	88	96	96	92	100	92	100
H2O2	87	2	2	85	98	98	84	97	68	78
TOC	18	6	6	12	67	67	18	100	18	100
DOC	13	6	6	7	54	54	13	100	13	100
Fe	88	9	9	79	90	90	88	100	88	100
Mn	85	6	6	79	93	93	83	98	83	98

Collector Blanks

As mentioned previously, there are several limitations to the information gained by taking fog collector blanks. Foremost among these is the uptake of soluble gases by the DI water sprayed onto collection surfaces. Nonetheless, there are times when collector

blanks reveal that collector cleaning procedures were inadequate. We have set flags in the submitted database to identify the following situations:

- Chloride, sulfate, sodium, potassium, or calcium concentrations in a collector blank are > 5 μN and > 50% of the ion concentration measured in the first subsequent sample collected.
- Fe blank concentration >50 μg/l and >50% of the following fog sample Fe concentration
- Mn blank concentration >5 μg/l and >50% of the following fog sample Mn concentration

Charge Balance

If all ionic species present in a sample are accurately measured, the ion charge balance should sum to zero (the electroneutrality condition). In many environments, especially highly polluted ones like the San Joaquin Valley, many charged species are present in solution which are not measured by conventional methods. This situation is exacerbated by high fog pH values, such as those present in SJV fogs, due to increases in solubility of many gaseous compounds. In general, most of the charged species not accounted for tend to be anions, so that measured species tend to show an excess of positively charged species in the ion balance.

With these limitations in mind, we established the following criteria for examining samples with large ion imbalances:

- in cases where complete inorganic ion analysis and low molecular weight organic acid analysis was completed and the sum of anion charges divided by the sum of cation charges was below 0.70 or above 1.15, the sample was reanalyzed. If the charge balance ratio still fell outside these bounds it was flagged in the database. Numerous samples fell into this category and were reanalyzed. Upon reanalysis we generally found the charge ratio little changed, suggesting that the charge imbalance was due to unmeasured species, rather than to inaccuracies in sample analysis. Some of the missing species are likely of an organic nature. Others probably include carbonate, bicarbonate, and nitrite, which were not specifically analyzed.
- samples where low molecular weight organic acid analysis was not completed, and the anion/cation charge balance ratio was below 0.35 or above 1.5, were flagged in the database.

Concentration Comparisons

Hydroxymethanesulfonate (HMS) is one species contributing to total S(IV) and dissolved organic carbon (DOC) is a subset of total organic carbon (TOC). Consequently we

expect sample analysis to show that HMS and DOC concentrations are less than or equal to S(IV) and TOC concentrations, respectively.

In order to test for cases when HMS concentrations were significantly larger than S(IV) concentrations, we applied a one-tailed test using the parameter

$$Z = \frac{[HMS - S(IV)]}{\sigma_{HMS-S(IV)}} \tag{A-13}$$

where

$$\sigma_{HMS-S(IV)} = \sqrt{\sigma^2_{HMS} + \sigma^2_{(S(IV)}} \tag{A-14}$$

and σ_{HMS} and $\sigma_{S(IV)}$ represent the absolute uncertainties of the HMS and S(IV) measurements. A 5% significance level was used for the test, corresponding to a critical Z value of 1.645. When Z was computed to exceed this critical value, a flag was applied to the sample in the database. The same approach was used to flag samples when DOC was found to significantly exceed TOC concentrations.

Size-fractionated Sample Comparisons

If the fog drop size spectrum is sampled in multiple fractions, the concentrations of a conserved chemical species contained in the sampled size fractions should average

together (weighted by the liquid water content in each size fraction) to give the bulk fog concentration of that species. In other words, the concentration of a conserved chemical species in a bulk fog sample should fall between its concentrations in large and small drop fractions. If it does not, it suggests that the species is not truly conserved upon mixing, or that some sampling or analysis artifact was encountered (e.g., evaporation of one or more sample fractions).

We compared bulk fog concentrations of sulfate (collected by CASCC2 samplers) with large and small drop fraction (collected by the size-fractionating CASCC) sulfate concentrations for corresponding sample periods. Size-fractionated samples for which the bulk sulfate concentration did not fall between the small and large drop sulfate fractions were flagged in the database.

S(IV) over range

A flag was applied when the measured sample concentration of a species exceeded the highest calibration standard concentration. This flag needed to be applied for only a few S(IV) concentrations measured in Bakersfield fog samples.

Appendix B:

Size dependence plots for other species from fogwater collected with the sf-CASCC. Each point represents a size fractionated sample collected at Kern. Error bars represent analytical uncertainties expressed as the absolute standard deviation (see Table A-1).

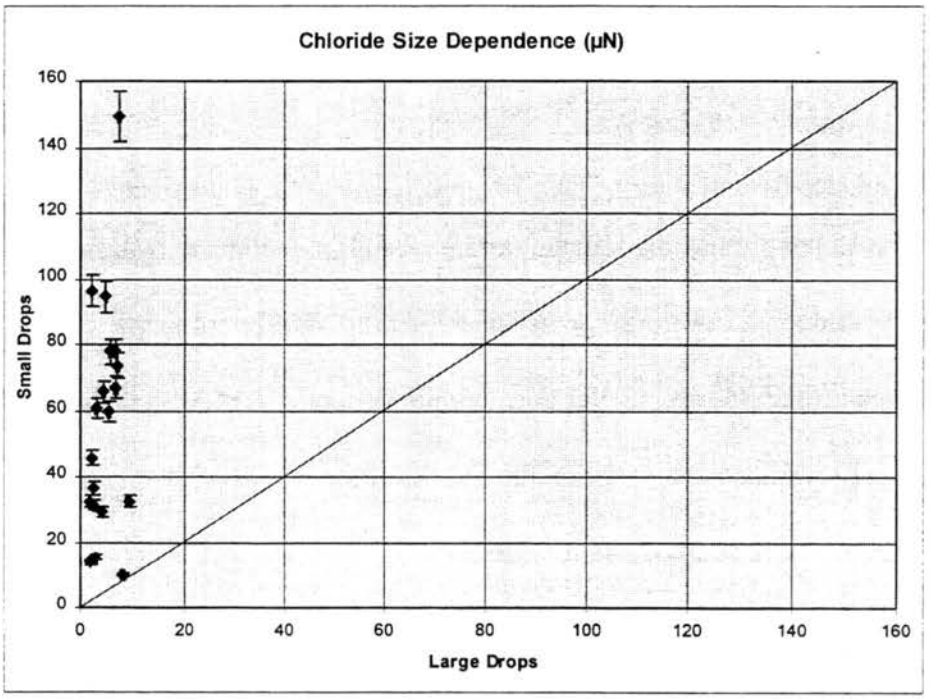

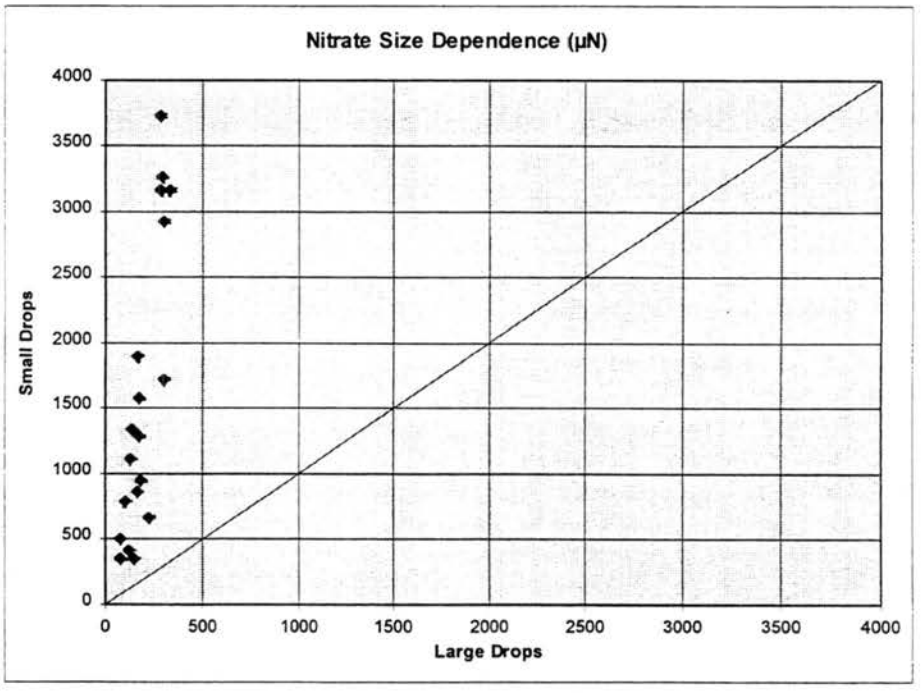

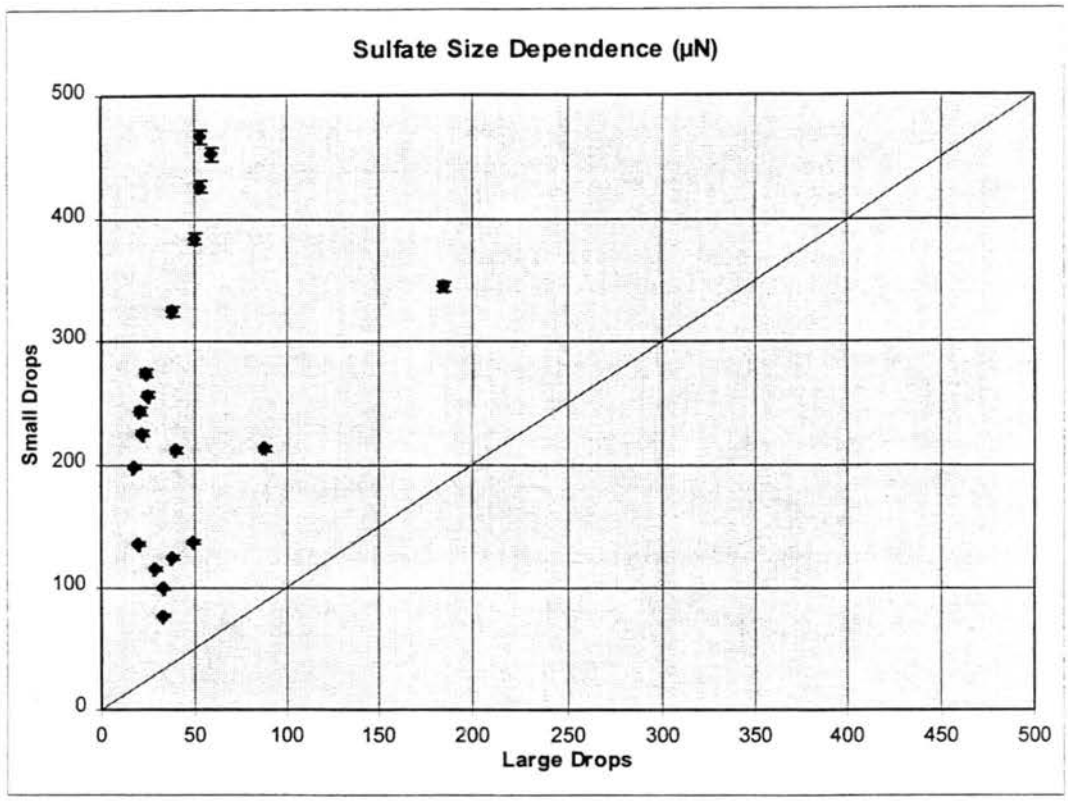
Sulfate Size Dependence (µN)
Small Drops
Large Drops
0
100
200
300
400
500
0
50
100
150
200
250
300
350
400
450
500

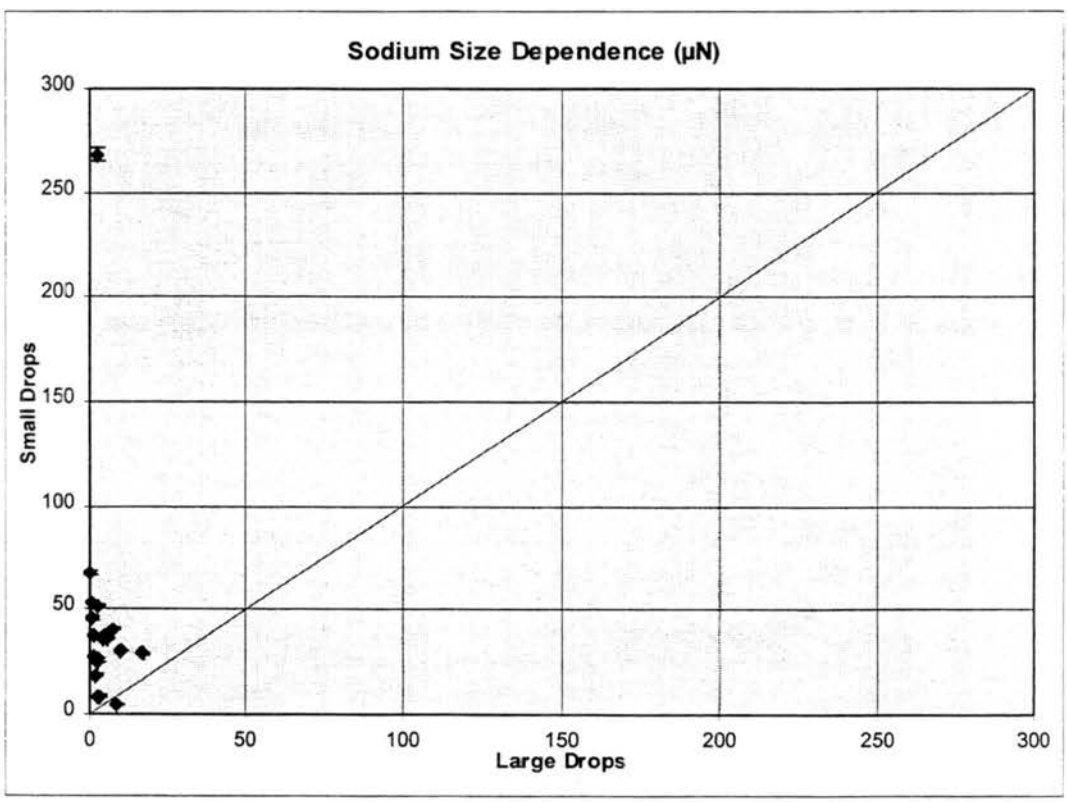
Sodium Size Dependence (µN)
Small Drops
Large Drops
0
50
100
150
200
250
300
0
50
100
150
200
250
300

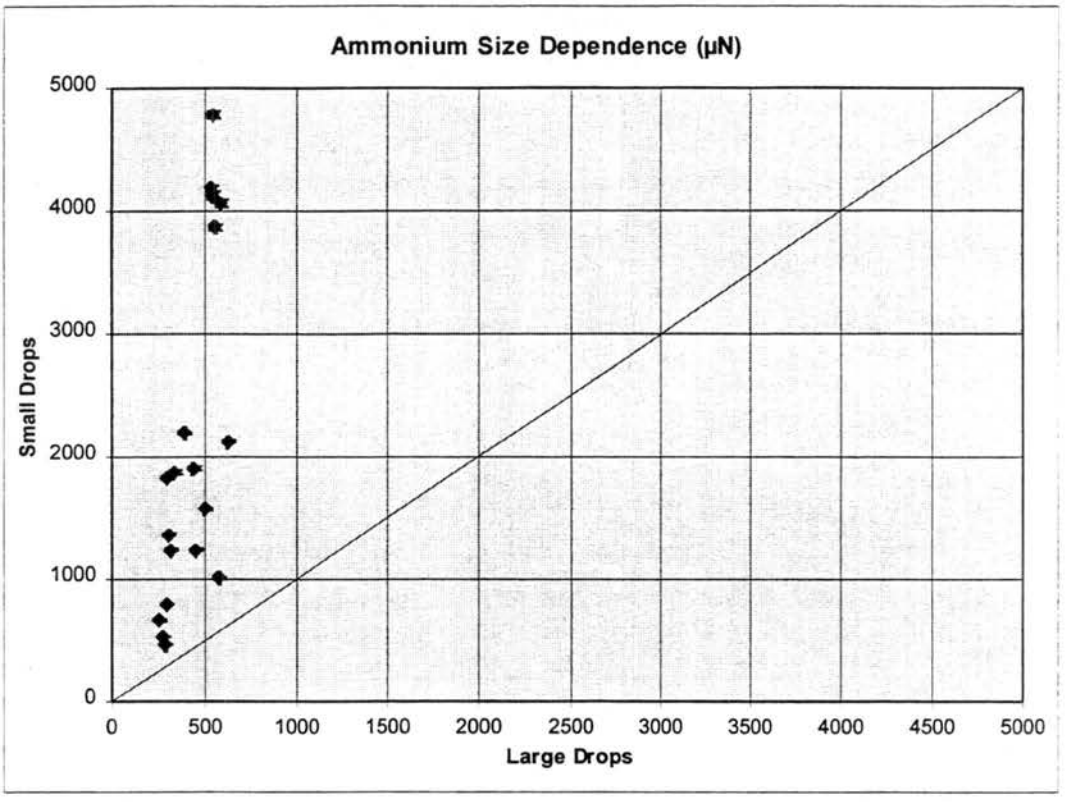
Ammonium Size Dependence (µN)
Small Drops
Large Drops
0
1000
2000
3000
4000
5000
0
500
1000
1500
2000
2500
3000
3500
4000
4500
5000

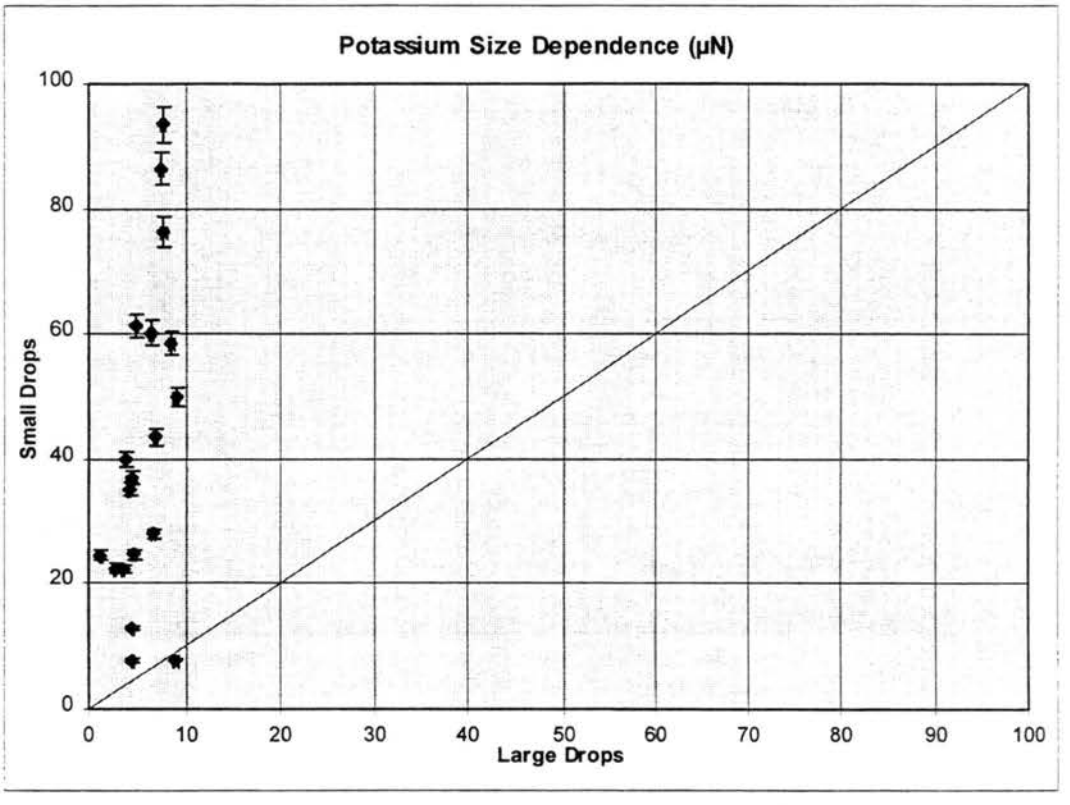
Potassium Size Dependence (µN)
Small Drops
Large Drops
0
20
40
60
80
100
0
10
20
30
40
50
60
70
80
90
100

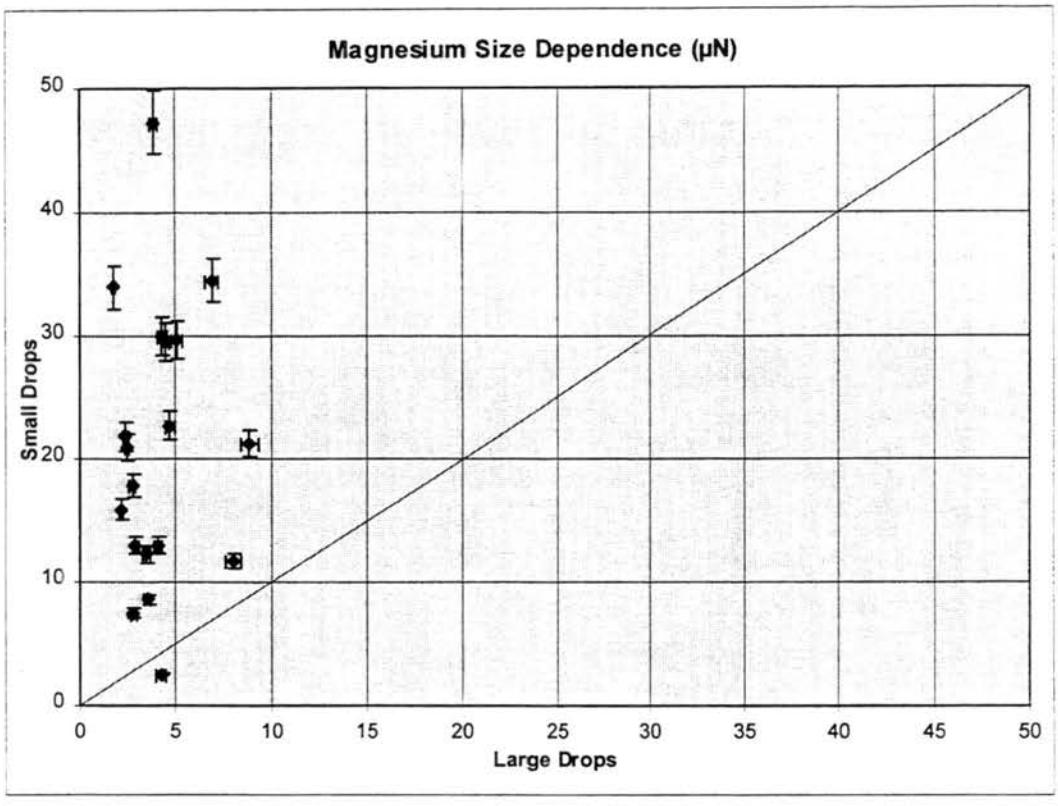
Magnesium Size Dependence (μN)
Small Drops
Large Drops
0
10
20
30
40
50
0
5
10
15
20
25
30
35
40
45
50

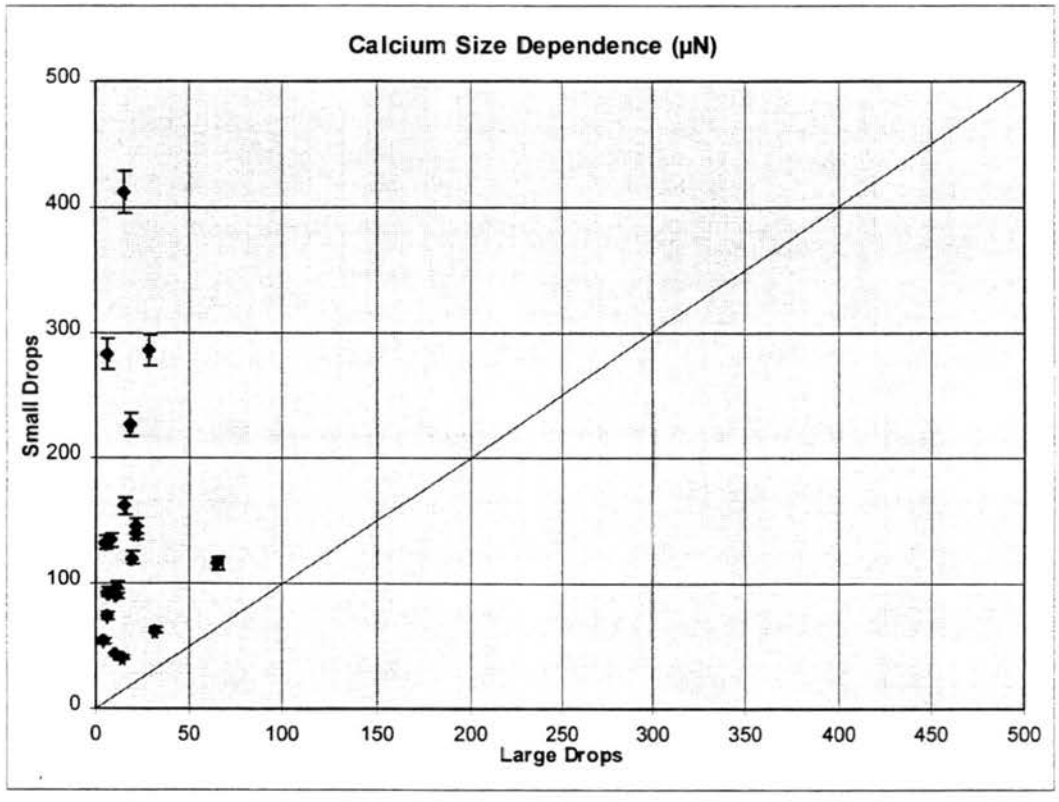
Calcium Size Dependence (μN)
Small Drops
Large Drops
0
100
200
300
400
500
0
50
100
150
200
250
300
350
400
450
500

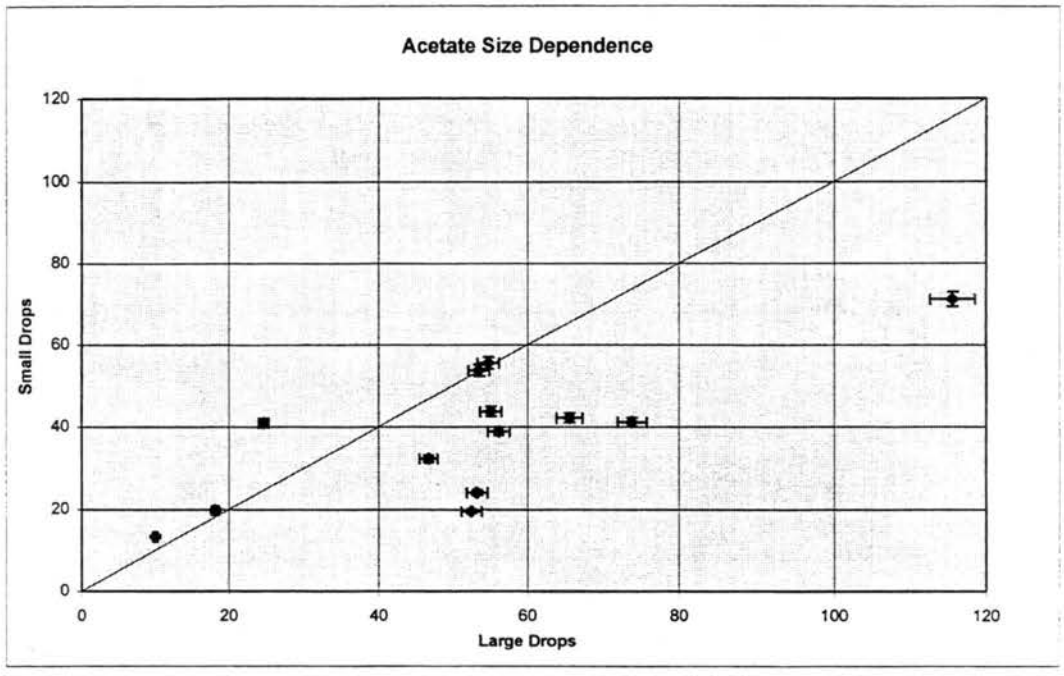

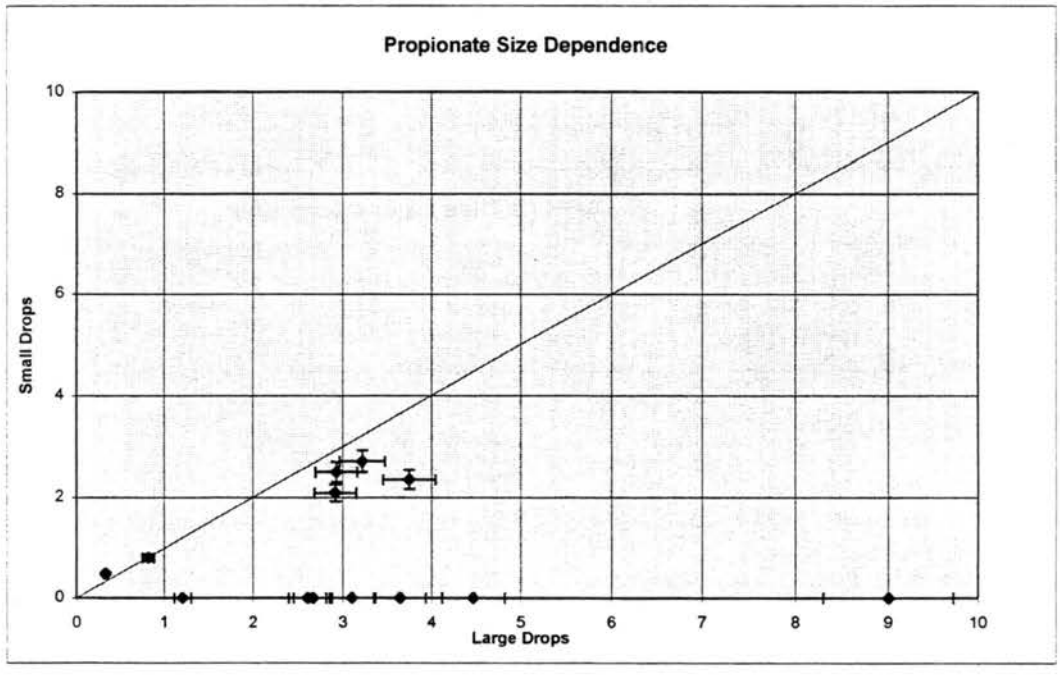

Concentrations are given in μN.

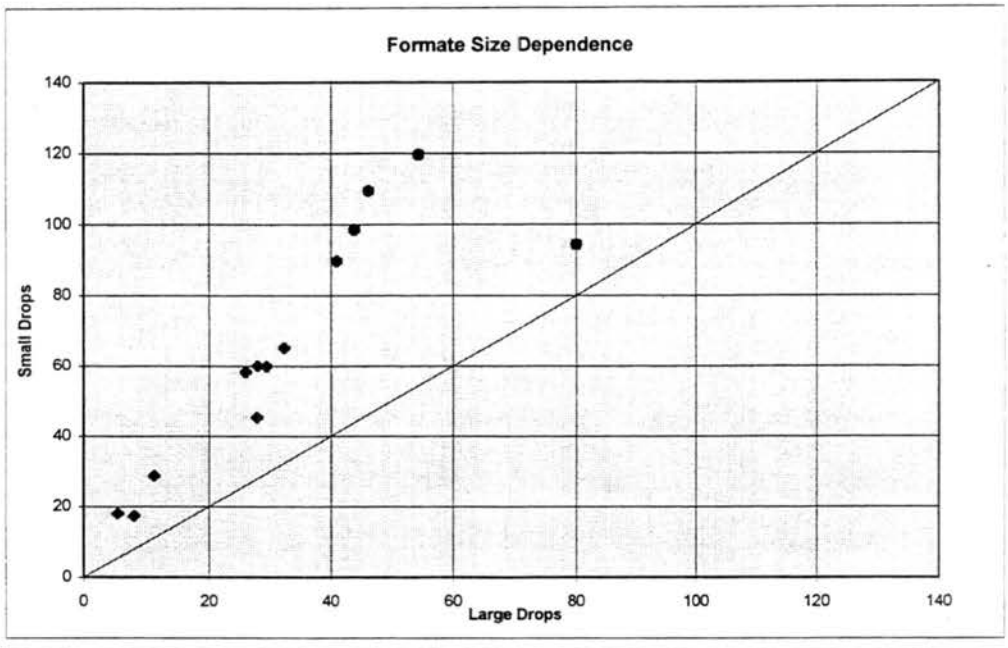

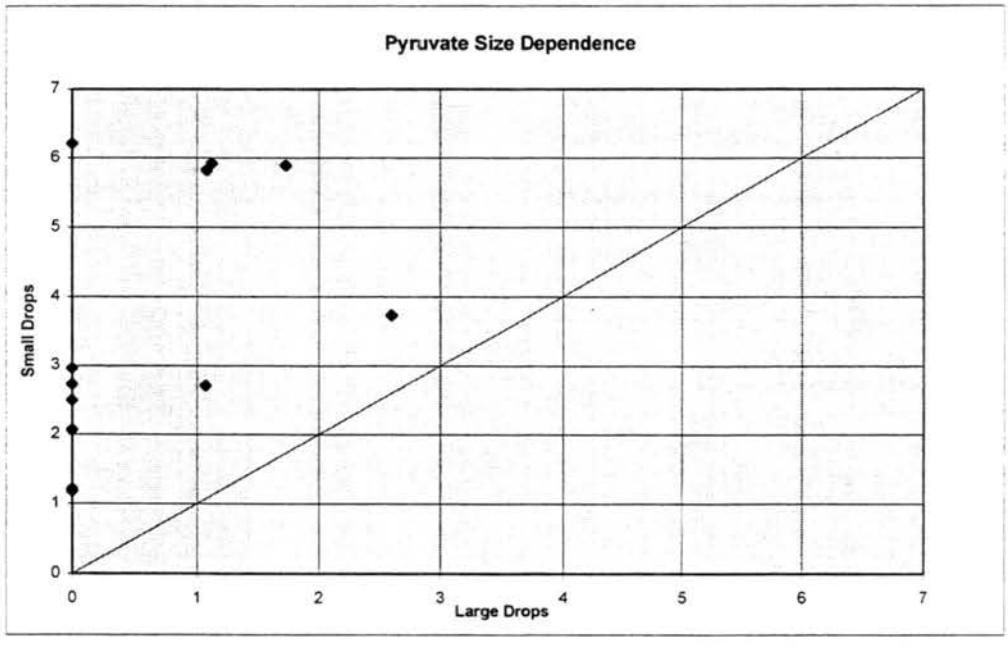

Concentrations are given in μN.

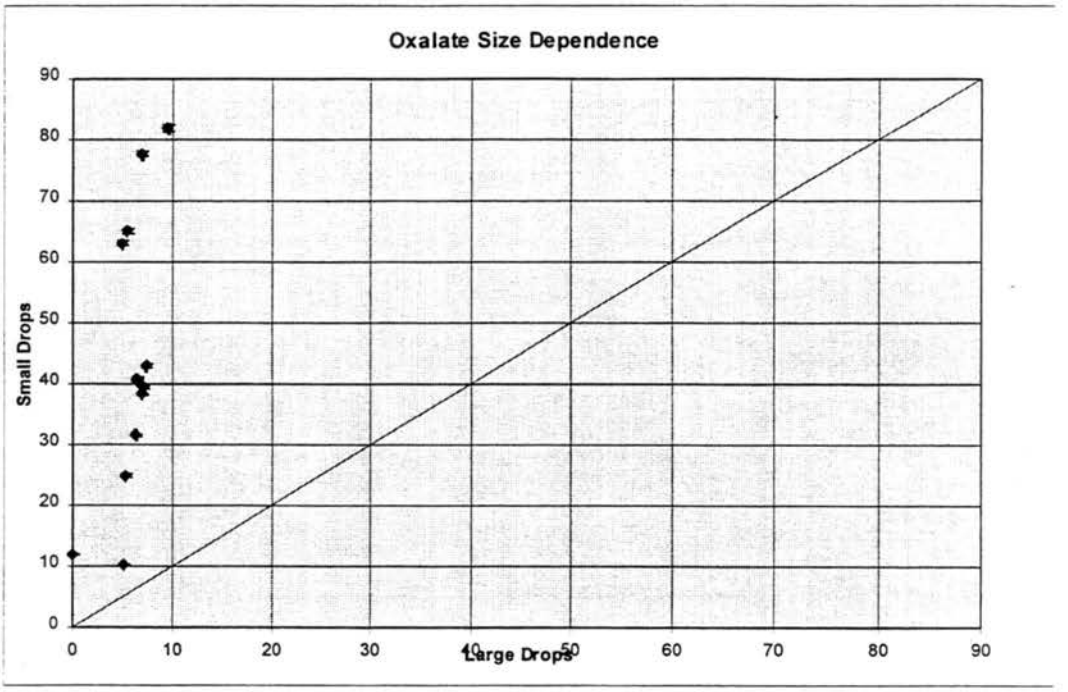

Concentrations are given in μN.

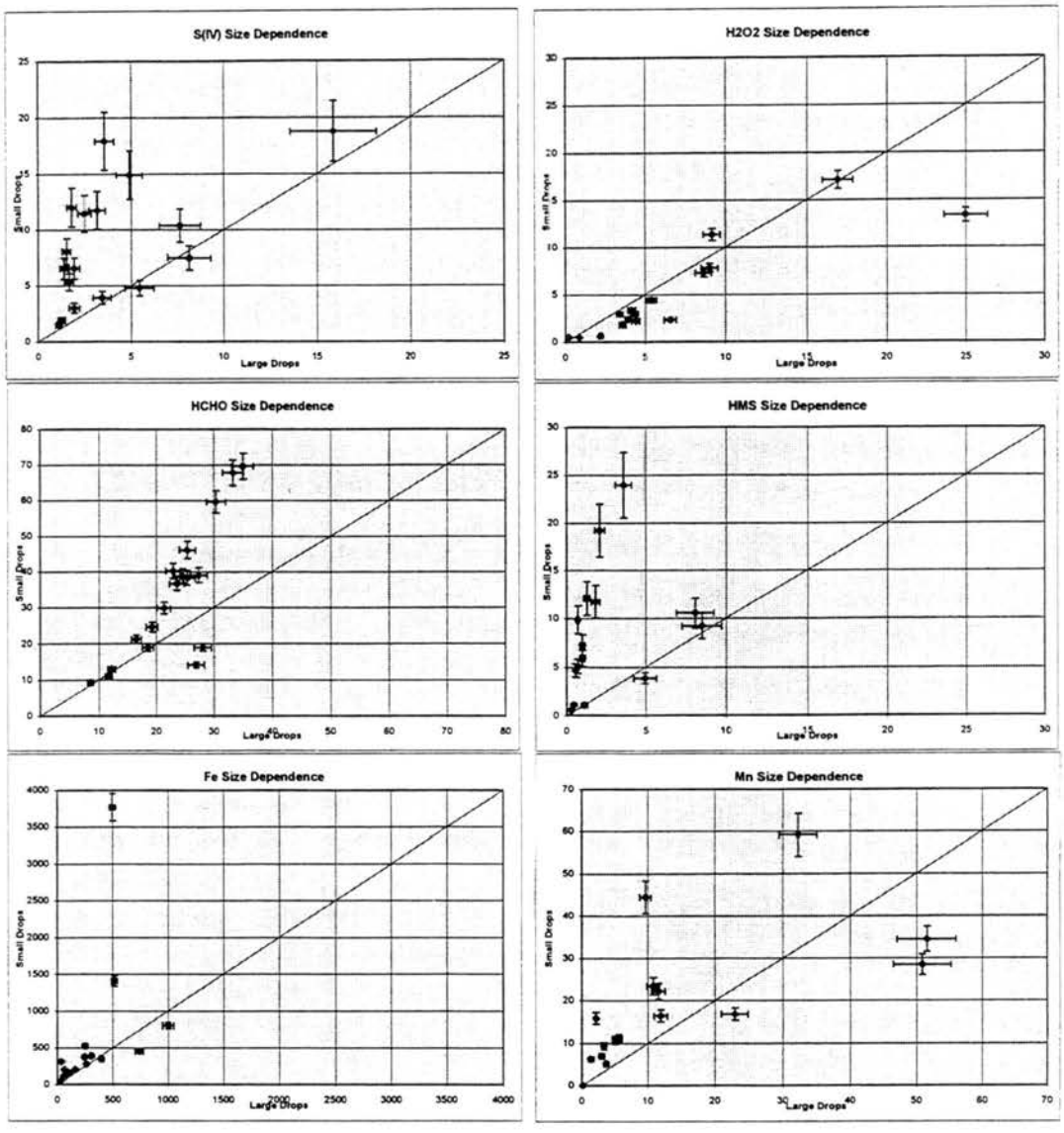

Concentrations of S(IV), H_2O_2, HCHO, and HMS are given in μM.

Concentrations of Fe and Mn are given in μg L^{-1}.

Timelines of measured concentrations in bulk fogwater throughout IMS95 at the three southern core sites.

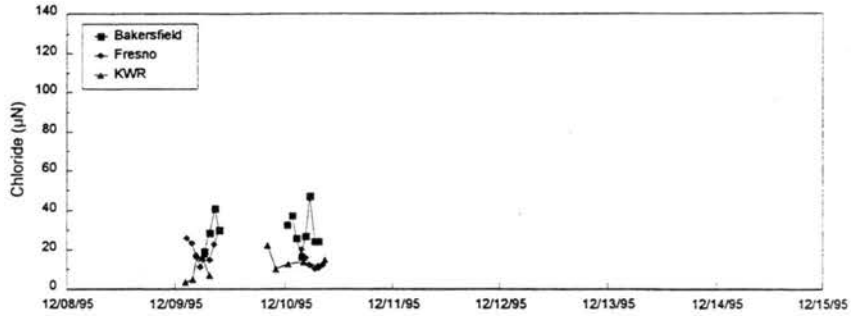

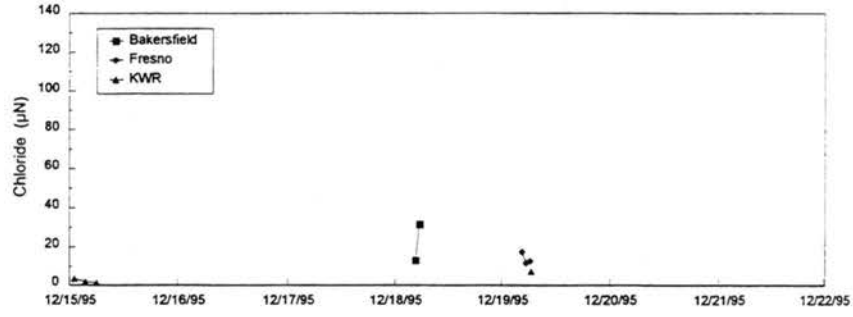

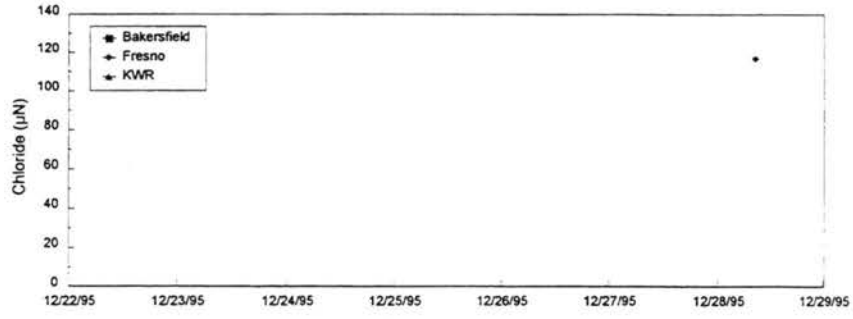

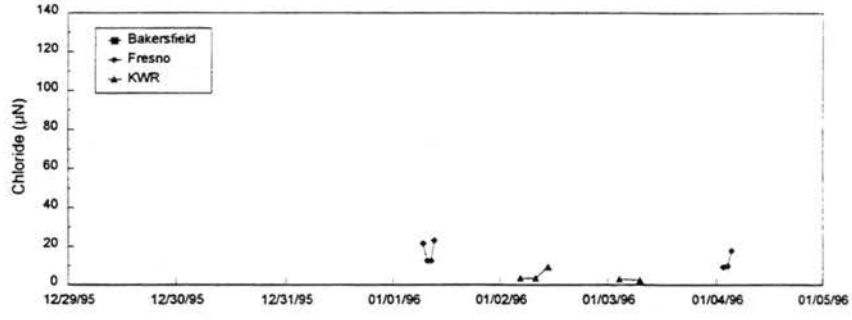

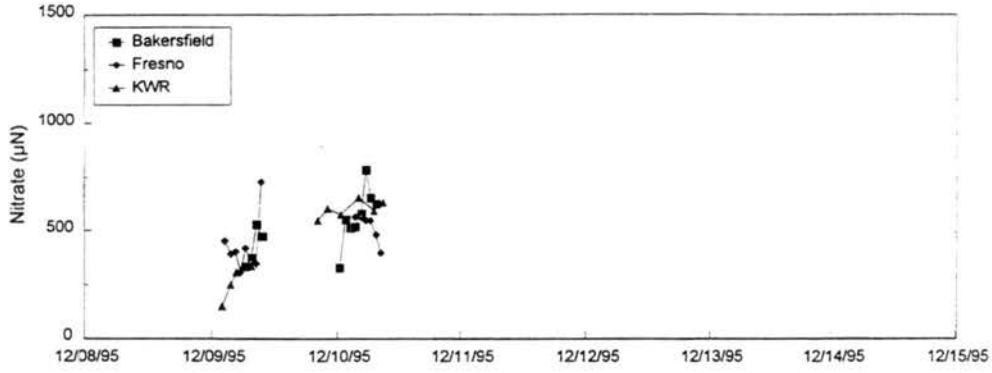
Bakersfield
Fresno
KWR
Nitrate (µN)
1500
1000
500
0
12/08/95
12/09/95
12/10/95
12/11/95
12/12/95
12/13/95
12/14/95
12/15/95

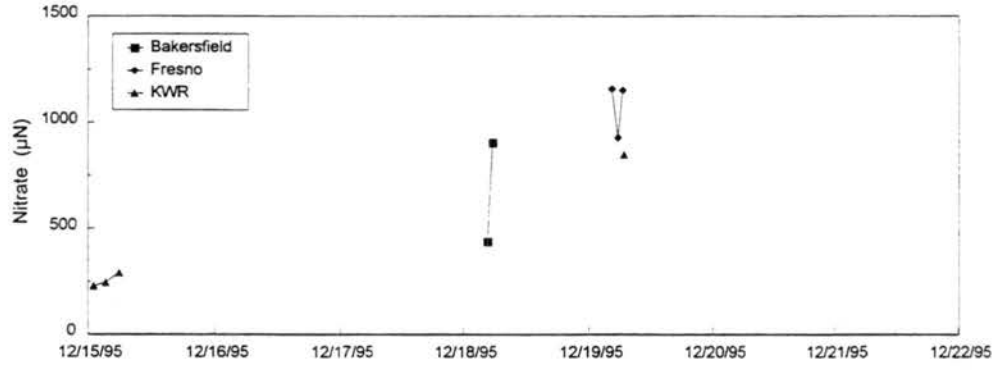
Bakersfield
Fresno
KWR
Nitrate (µN)
1500
1000
500
0
12/15/95
12/16/95
12/17/95
12/18/95
12/19/95
12/20/95
12/21/95
12/22/95

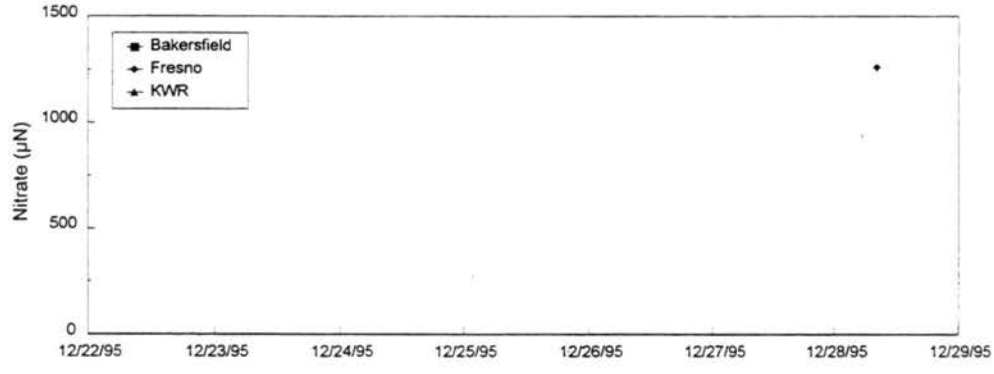
Bakersfield
Fresno
KWR
Nitrate (µN)
1500
1000
500
0
12/22/95
12/23/95
12/24/95
12/25/95
12/26/95
12/27/95
12/28/95
12/29/95

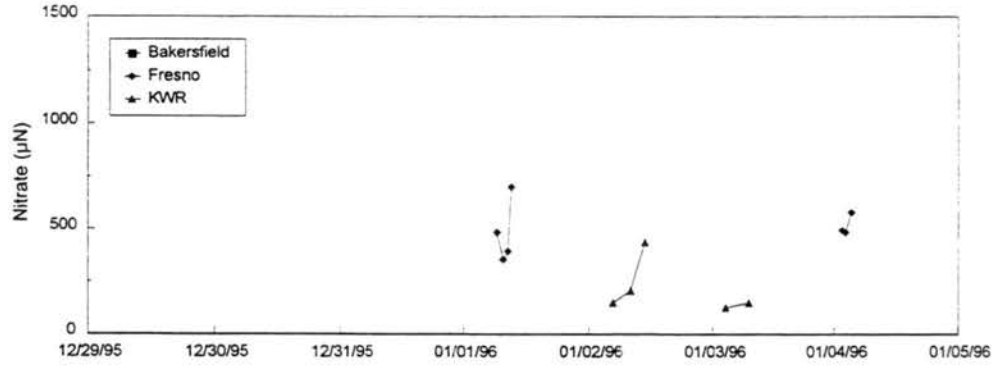
Bakersfield
Fresno
KWR
Nitrate (µN)
1500
1000
500
0
12/29/95
12/30/95
12/31/95
01/01/96
01/02/96
01/03/96
01/04/96
01/05/96

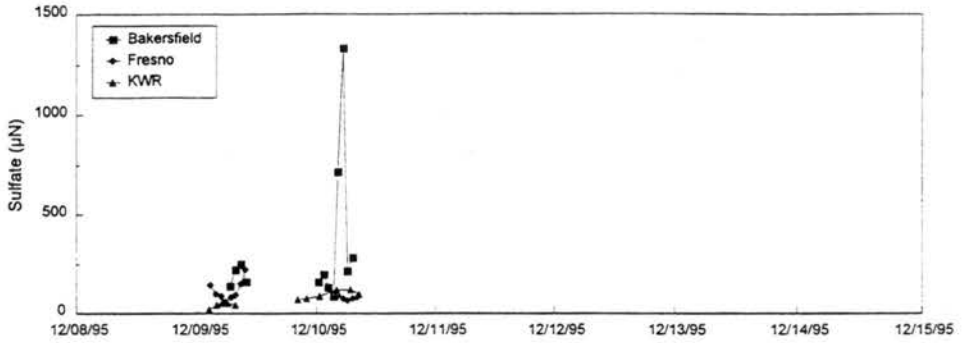
Bakersfield
Fresno
KWR
Sulfate (µN)
1500
1000
500
0
12/08/95
12/09/95
12/10/95
12/11/95
12/12/95
12/13/95
12/14/95
12/15/95

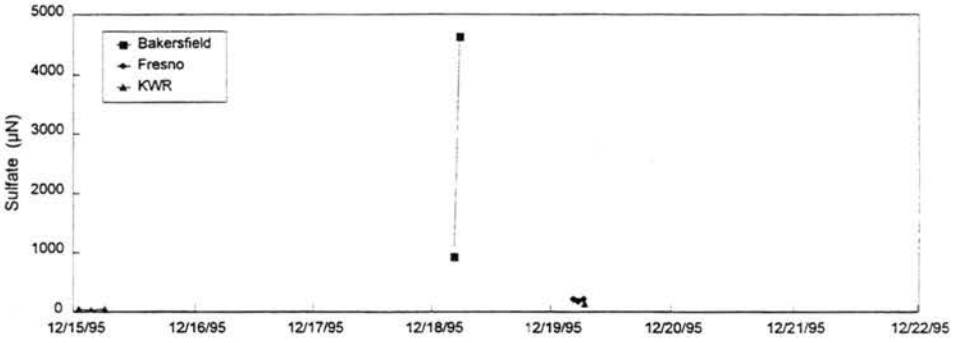
Bakersfield
Fresno
KWR
Sulfate (µN)
5000
4000
3000
2000
1000
0
12/15/95
12/16/95
12/17/95
12/18/95
12/19/95
12/20/95
12/21/95
12/22/95

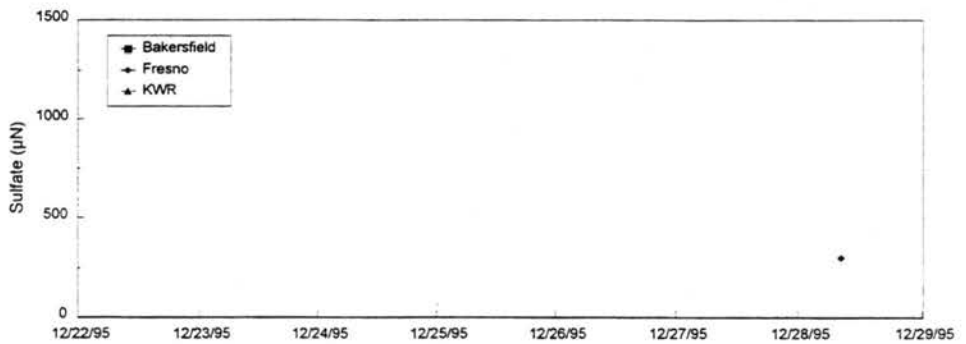
Bakersfield
Fresno
KWR
Sulfate (µN)
1500
1000
500
0
12/22/95
12/23/95
12/24/95
12/25/95
12/26/95
12/27/95
12/28/95
12/29/95

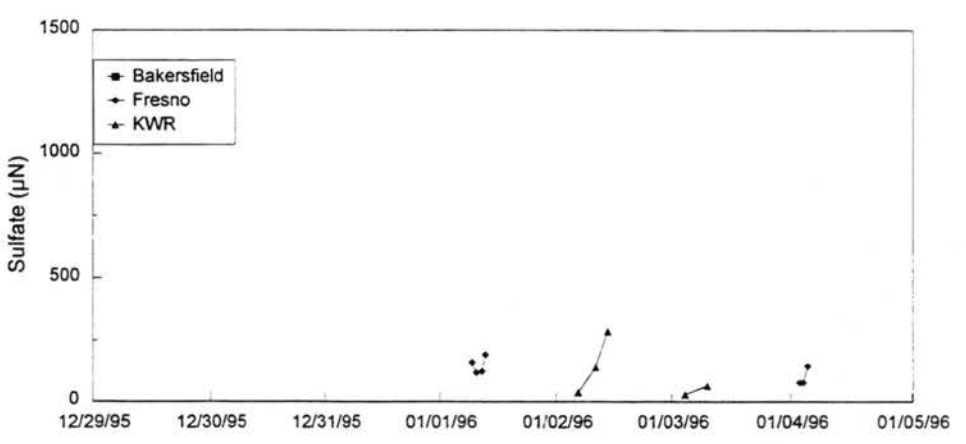
Bakersfield
Fresno
KWR
Sulfate (µN)
1500
1000
500
0
12/29/95
12/30/95
12/31/95
01/01/96
01/02/96
01/03/96
01/04/96
01/05/96

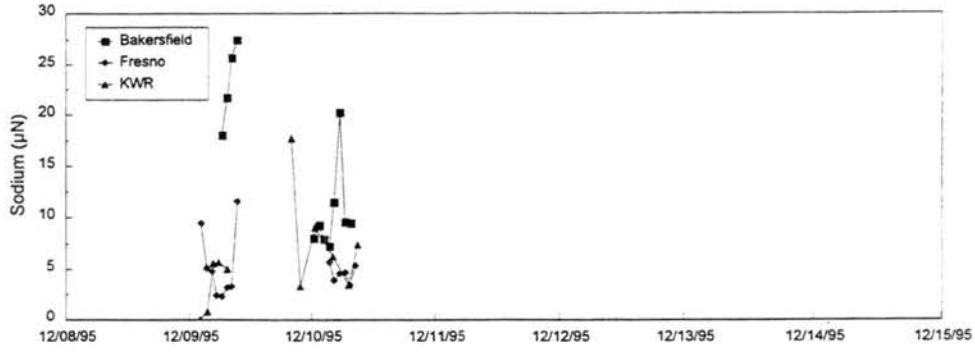
Bakersfield
Fresno
KWR
Sodium (µN)
0
5
10
15
20
25
30
12/08/95
12/09/95
12/10/95
12/11/95
12/12/95
12/13/95
12/14/95
12/15/95

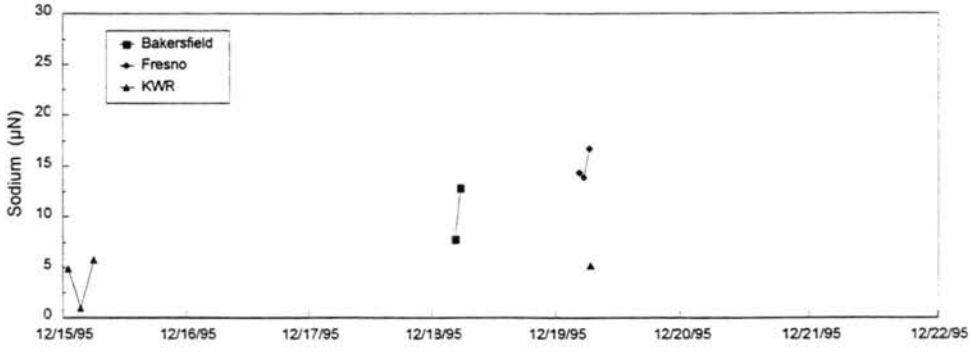
Bakersfield
Fresno
KWR
Sodium (µN)
0
5
10
15
20
25
30
12/15/95
12/16/95
12/17/95
12/18/95
12/19/95
12/20/95
12/21/95
12/22/95

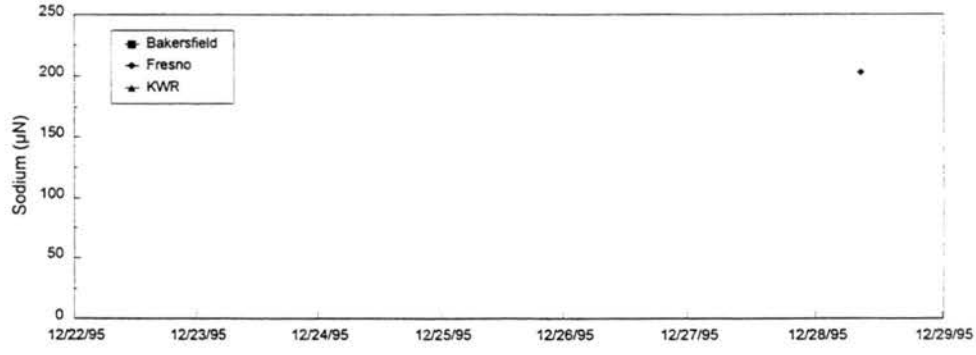
Bakersfield
Fresno
KWR
Sodium (µN)
0
50
100
150
200
250
12/22/95
12/23/95
12/24/95
12/25/95
12/26/95
12/27/95
12/28/95
12/29/95

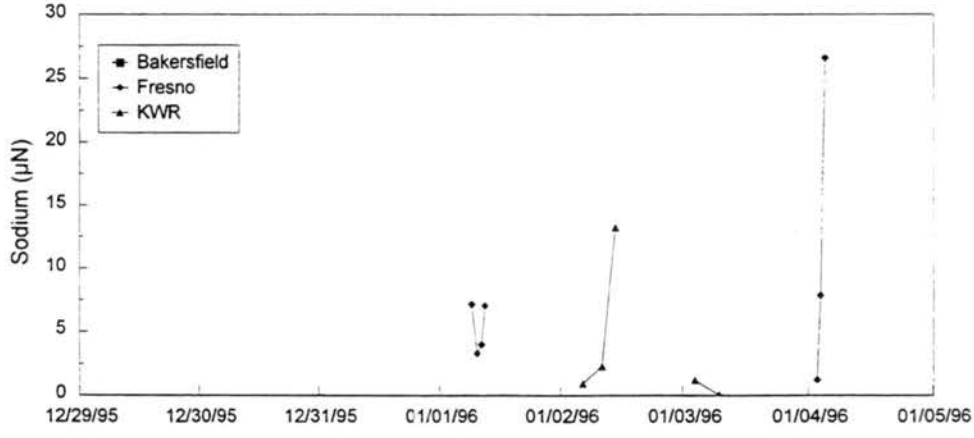
Bakersfield
Fresno
KWR
Sodium (µN)
0
5
10
15
20
25
30
12/29/95
12/30/95
12/31/95
01/01/96
01/02/96
01/03/96
01/04/96
01/05/96

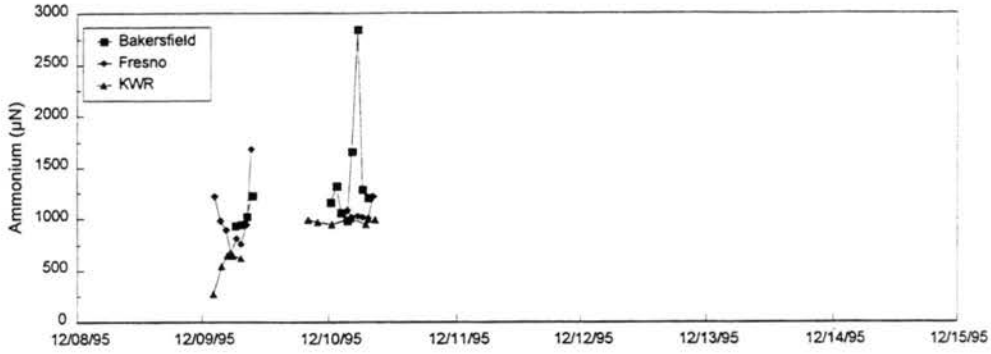
Bakersfield
Fresno
KWR
Ammonium (µN)
3000
2500
2000
1500
1000
500
0
12/08/95
12/09/95
12/10/95
12/11/95
12/12/95
12/13/95
12/14/95
12/15/95

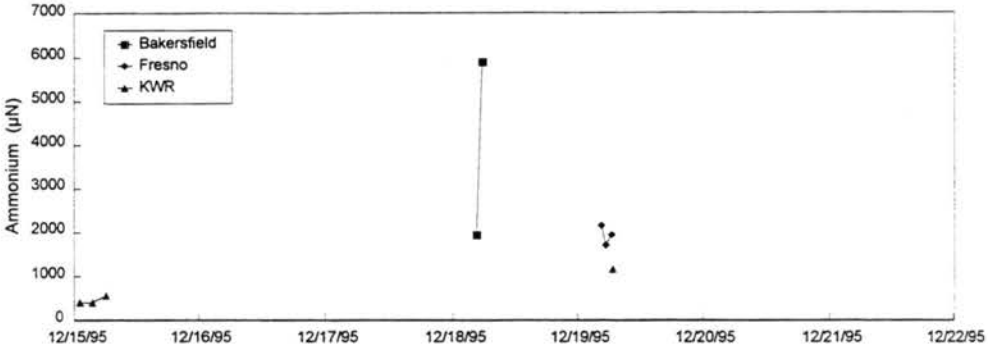
Bakersfield
Fresno
KWR
Ammonium (µN)
7000
6000
5000
4000
3000
2000
1000
0
12/15/95
12/16/95
12/17/95
12/18/95
12/19/95
12/20/95
12/21/95
12/22/95

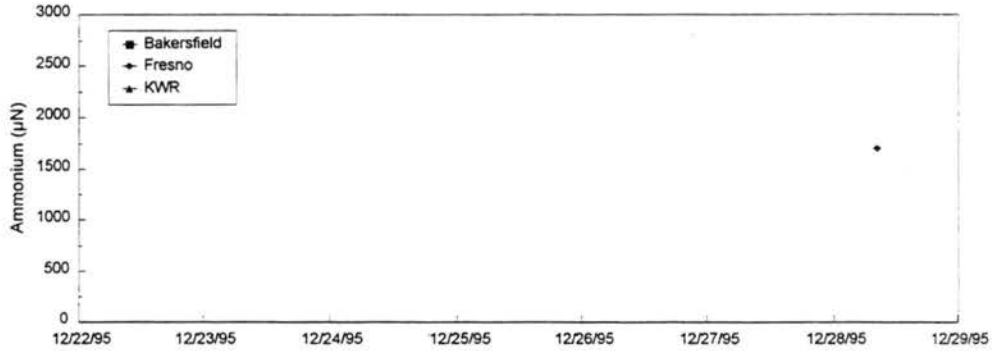
Bakersfield
Fresno
KWR
Ammonium (µN)
3000
2500
2000
1500
1000
500
0
12/22/95
12/23/95
12/24/95
12/25/95
12/26/95
12/27/95
12/28/95
12/29/95

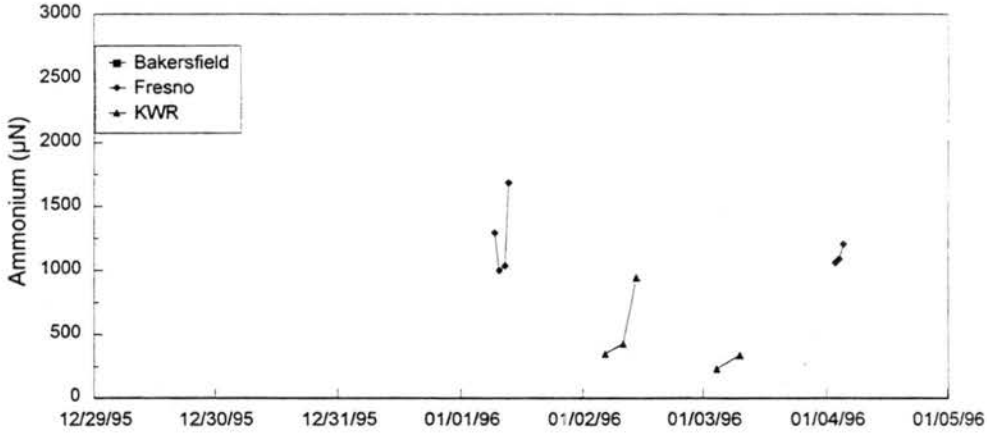
Bakersfield
Fresno
KWR
Ammonium (µN)
3000
2500
2000
1500
1000
500
0
12/29/95
12/30/95
12/31/95
01/01/96
01/02/96
01/03/96
01/04/96
01/05/96

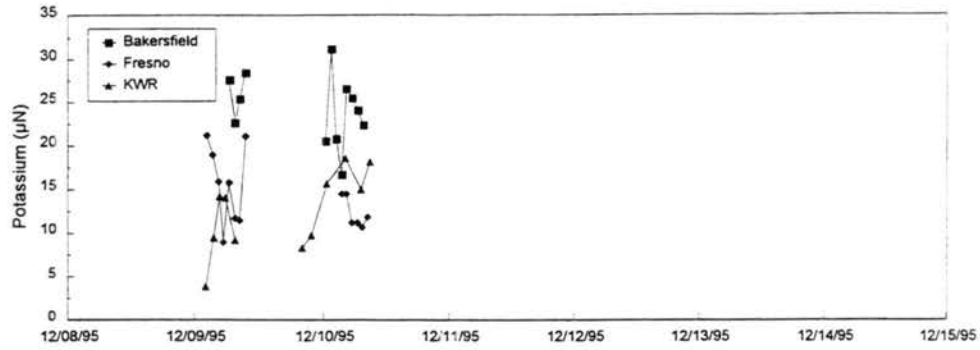
Bakersfield
Fresno
KWR
Potassium (µN)
0
5
10
15
20
25
30
35
12/08/95
12/09/95
12/10/95
12/11/95
12/12/95
12/13/95
12/14/95
12/15/95

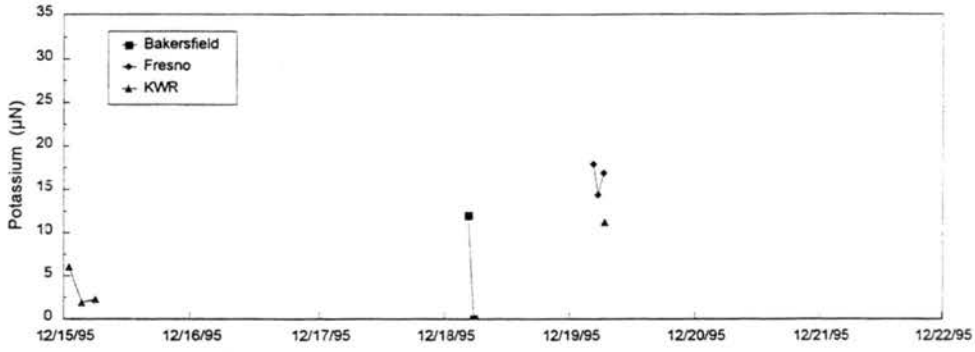
Bakersfield
Fresno
KWR
Potassium (µN)
0
5
10
15
20
25
30
35
12/15/95
12/16/95
12/17/95
12/18/95
12/19/95
12/20/95
12/21/95
12/22/95

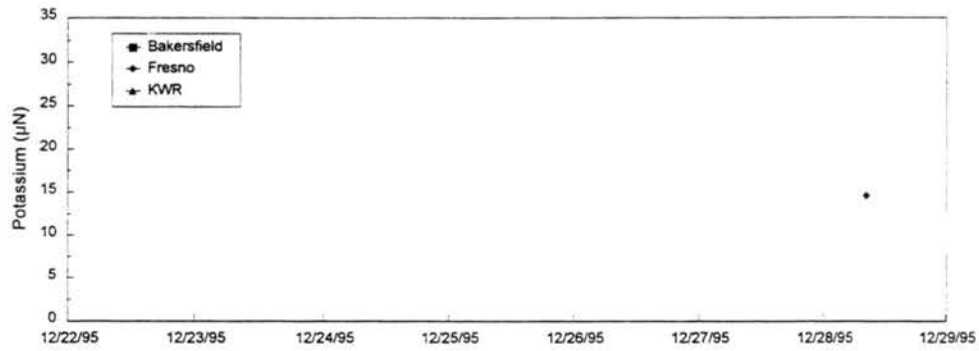
Bakersfield
Fresno
KWR
Potassium (µN)
0
5
10
15
20
25
30
35
12/22/95
12/23/95
12/24/95
12/25/95
12/26/95
12/27/95
12/28/95
12/29/95

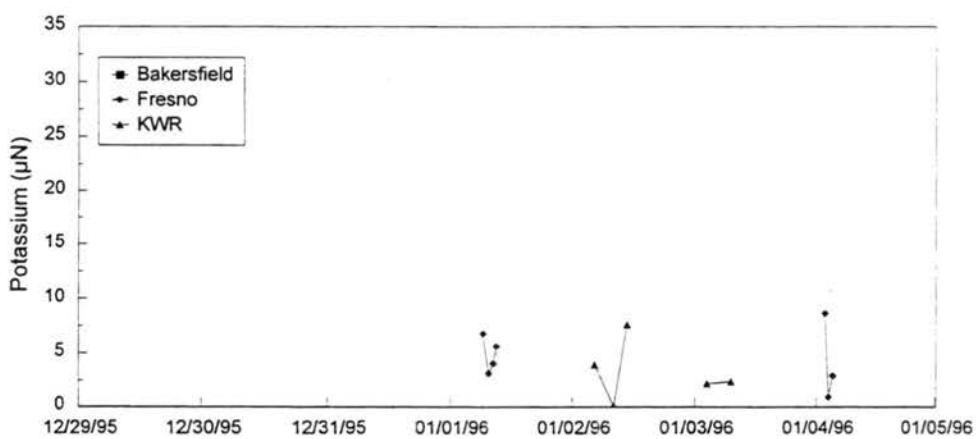
Bakersfield
Fresno
KWR
Potassium (µN)
0
5
10
15
20
25
30
35
12/29/95
12/30/95
12/31/95
01/01/96
01/02/96
01/03/96
01/04/96
01/05/96

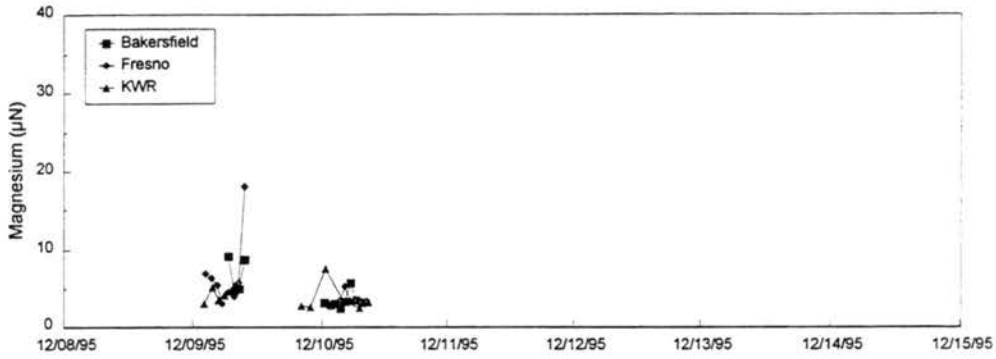
Bakersfield
Fresno
KWR
Magnesium (µN)
40
30
20
10
0
12/08/95
12/09/95
12/10/95
12/11/95
12/12/95
12/13/95
12/14/95
12/15/95

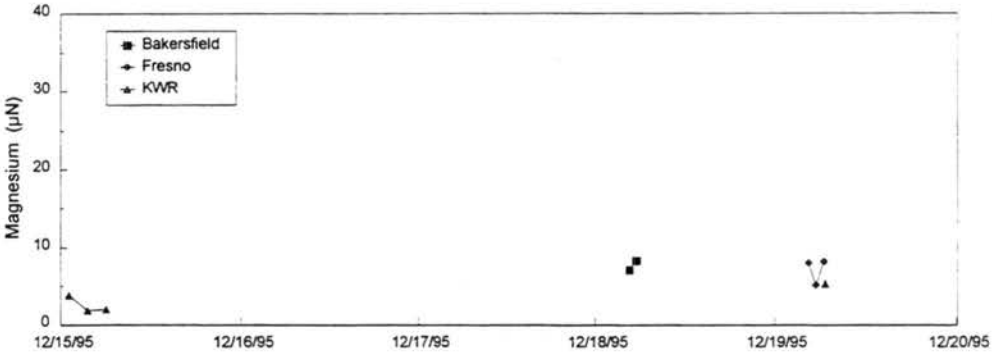
Bakersfield
Fresno
KWR
Magnesium (µN)
40
30
20
10
0
12/15/95
12/16/95
12/17/95
12/18/95
12/19/95
12/20/95

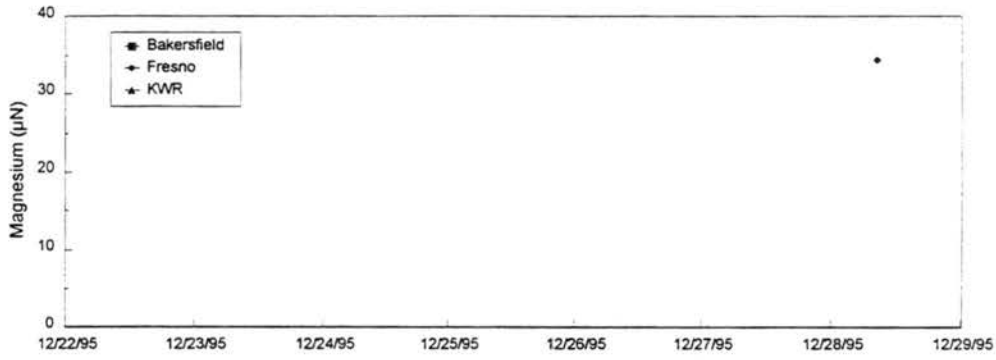
Bakersfield
Fresno
KWR
Magnesium (µN)
40
30
20
10
0
12/22/95
12/23/95
12/24/95
12/25/95
12/26/95
12/27/95
12/28/95
12/29/95

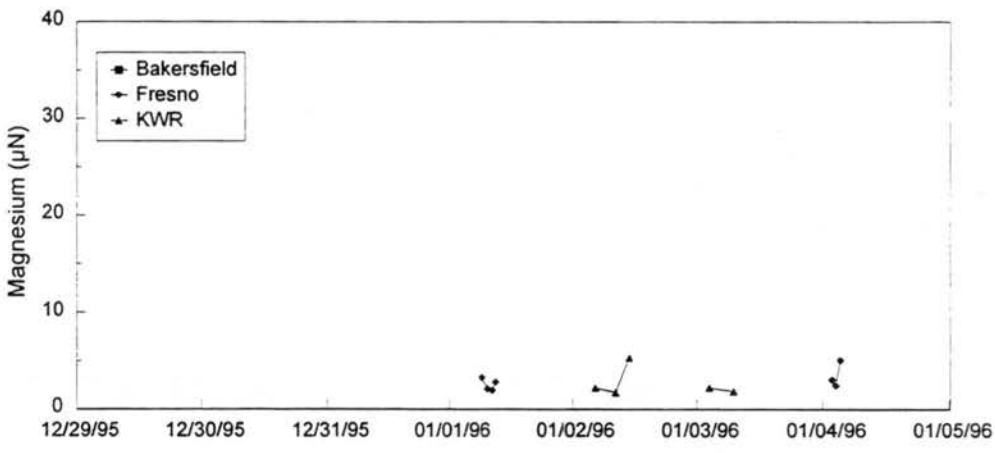
Bakersfield
Fresno
KWR
Magnesium (µN)
40
30
20
10
0
12/29/95
12/30/95
12/31/95
01/01/96
01/02/96
01/03/96
01/04/96
01/05/96

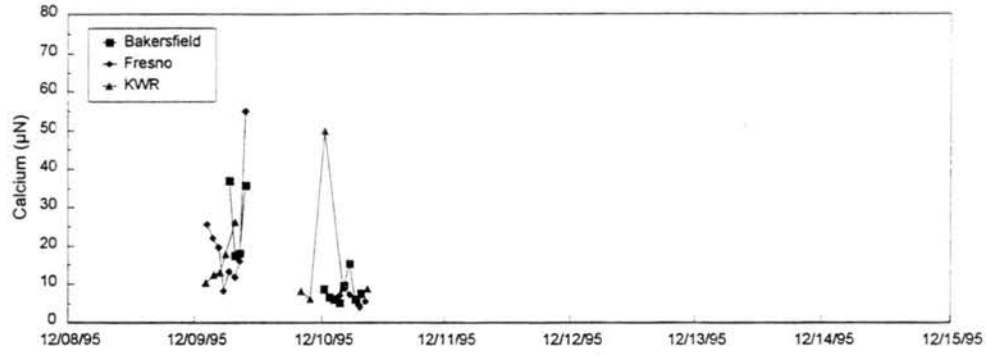
Bakersfield
Fresno
KWR
Calcium (µN)
0
10
20
30
40
50
60
70
80
12/08/95
12/09/95
12/10/95
12/11/95
12/12/95
12/13/95
12/14/95
12/15/95

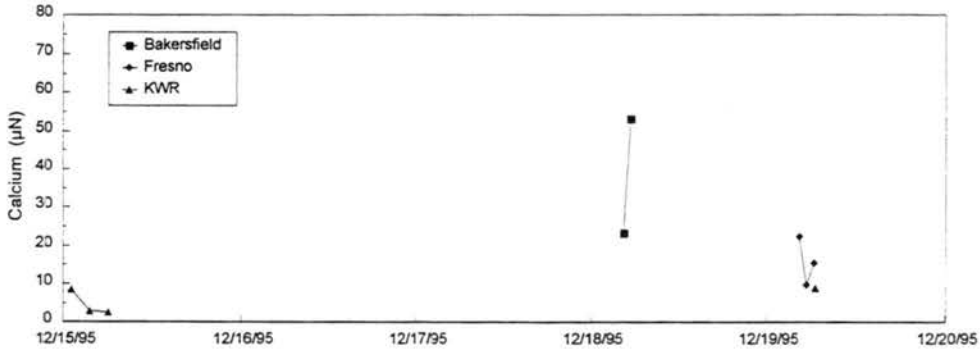
Bakersfield
Fresno
KWR
Calcium (µN)
0
10
20
30
40
50
60
70
80
12/15/95
12/16/95
12/17/95
12/18/95
12/19/95
12/20/95

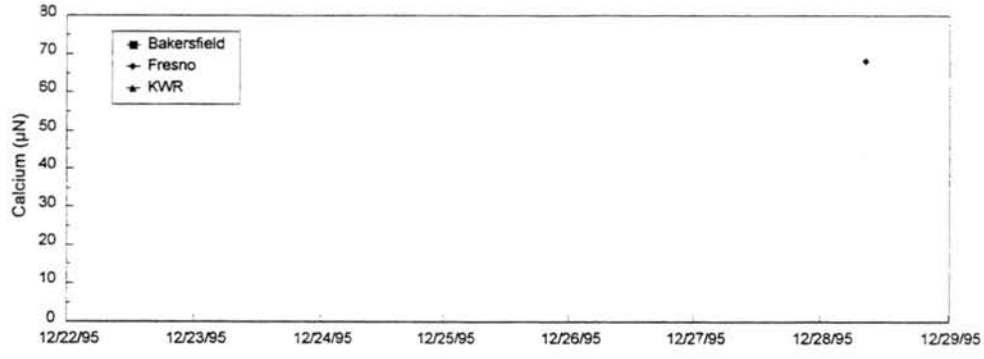
Bakersfield
Fresno
KWR
Calcium (µN)
0
10
20
30
40
50
60
70
80
12/22/95
12/23/95
12/24/95
12/25/95
12/26/95
12/27/95
12/28/95
12/29/95

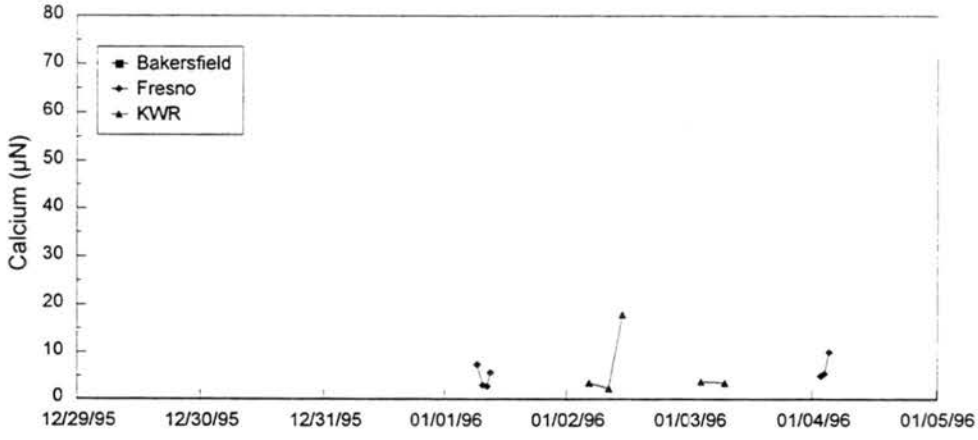
Bakersfield
Fresno
KWR
Calcium (µN)
0
10
20
30
40
50
60
70
80
12/29/95
12/30/95
12/31/95
01/01/96
01/02/96
01/03/96
01/04/96
01/05/96

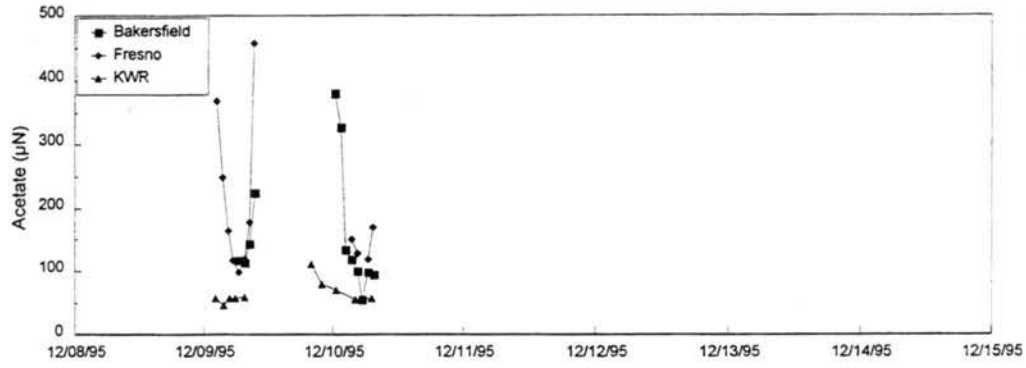
Bakersfield
Fresno
KWR
Acetate (µN)
500
400
300
200
100
0
12/08/95
12/09/95
12/10/95
12/11/95
12/12/95
12/13/95
12/14/95
12/15/95

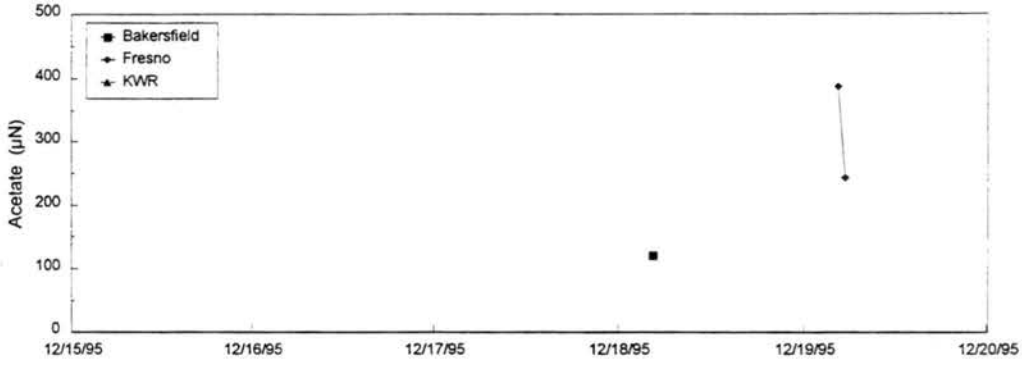
Bakersfield
Fresno
KWR
Acetate (µN)
500
400
300
200
100
0
12/15/95
12/16/95
12/17/95
12/18/95
12/19/95
12/20/95

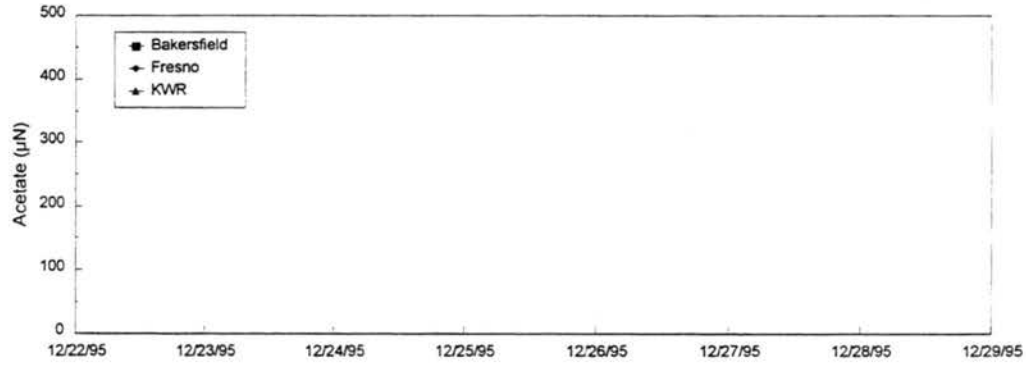
Bakersfield
Fresno
KWR
Acetate (µN)
500
400
300
200
100
0
12/22/95
12/23/95
12/24/95
12/25/95
12/26/95
12/27/95
12/28/95
12/29/95

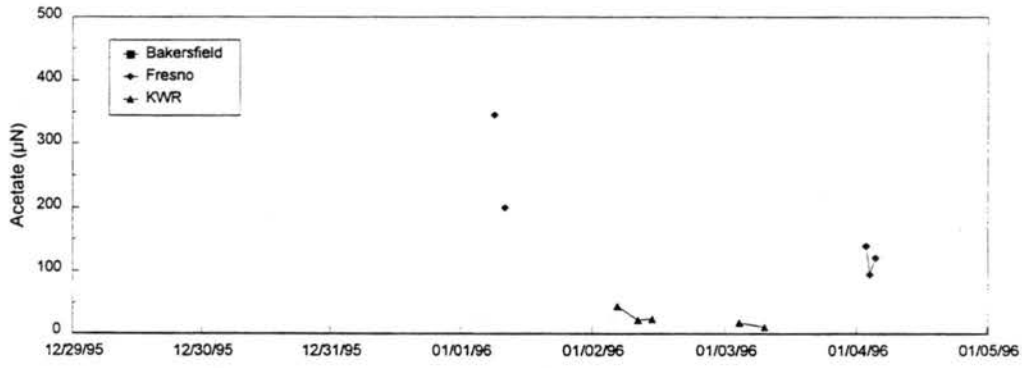
Bakersfield
Fresno
KWR
Acetate (µN)
500
400
300
200
100
0
12/29/95
12/30/95
12/31/95
01/01/96
01/02/96
01/03/96
01/04/96
01/05/96

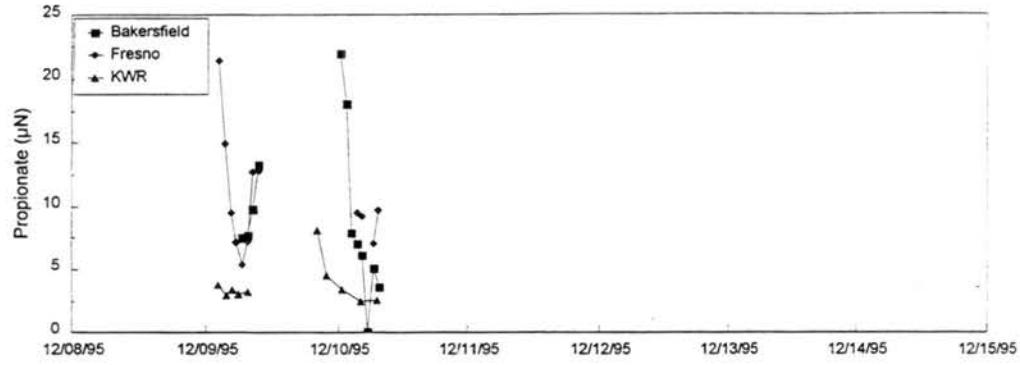
Bakersfield
Fresno
KWR
Propionate (µN)
25
20
15
10
5
0
12/08/95
12/09/95
12/10/95
12/11/95
12/12/95
12/13/95
12/14/95
12/15/95

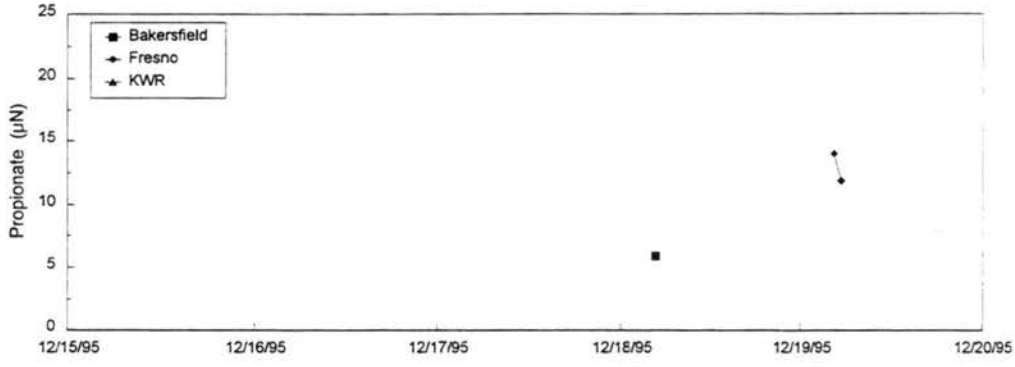
Bakersfield
Fresno
KWR
Propionate (µN)
25
20
15
10
5
0
12/15/95
12/16/95
12/17/95
12/18/95
12/19/95
12/20/95

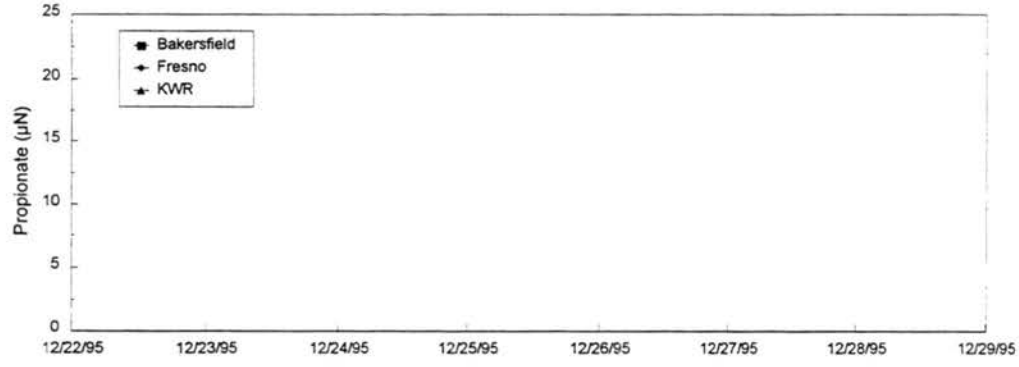
Bakersfield
Fresno
KWR
Propionate (µN)
25
20
15
10
5
0
12/22/95
12/23/95
12/24/95
12/25/95
12/26/95
12/27/95
12/28/95
12/29/95

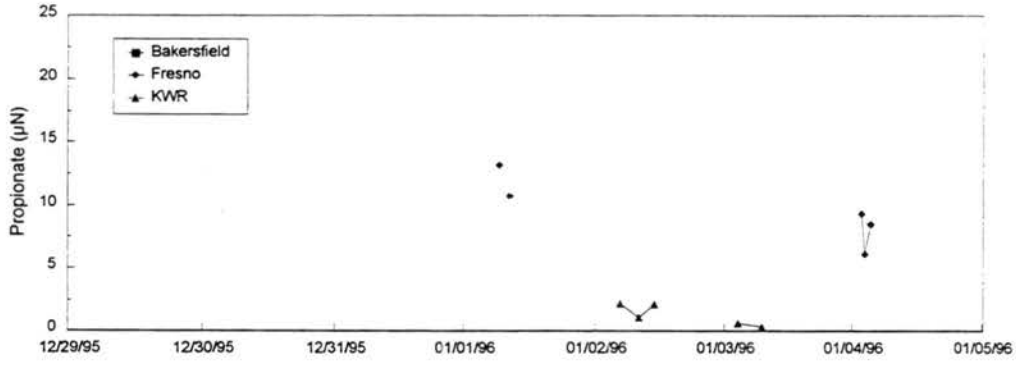
Bakersfield
Fresno
KWR
Propionate (µN)
25
20
15
10
5
0
12/29/95
12/30/95
12/31/95
01/01/96
01/02/96
01/03/96
01/04/96
01/05/96

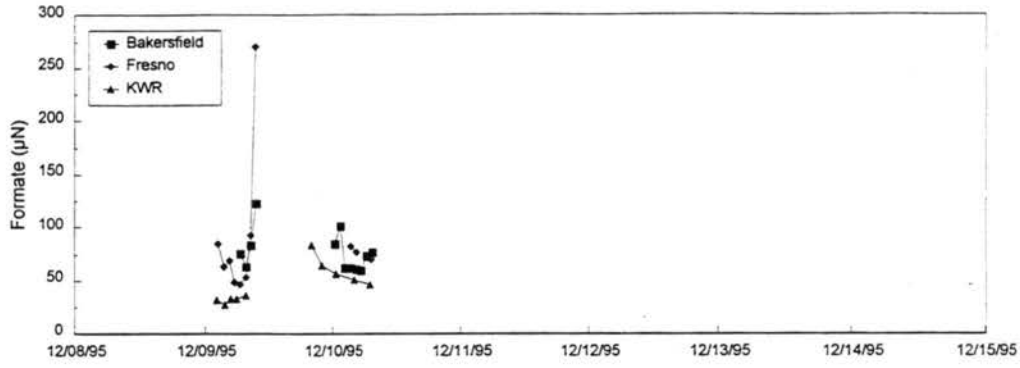
Bakersfield
Fresno
KWR
Formate (µN)
300
250
200
150
100
50
0
12/08/95
12/09/95
12/10/95
12/11/95
12/12/95
12/13/95
12/14/95
12/15/95

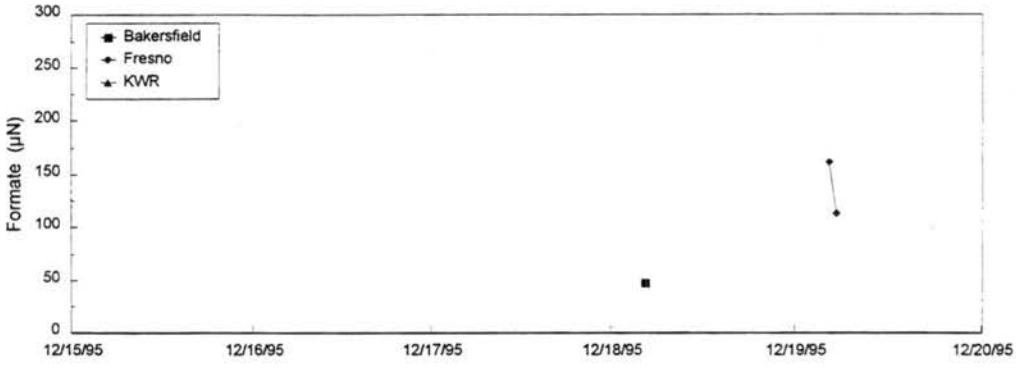
Bakersfield
Fresno
KWR
Formate (µN)
300
250
200
150
100
50
0
12/15/95
12/16/95
12/17/95
12/18/95
12/19/95
12/20/95

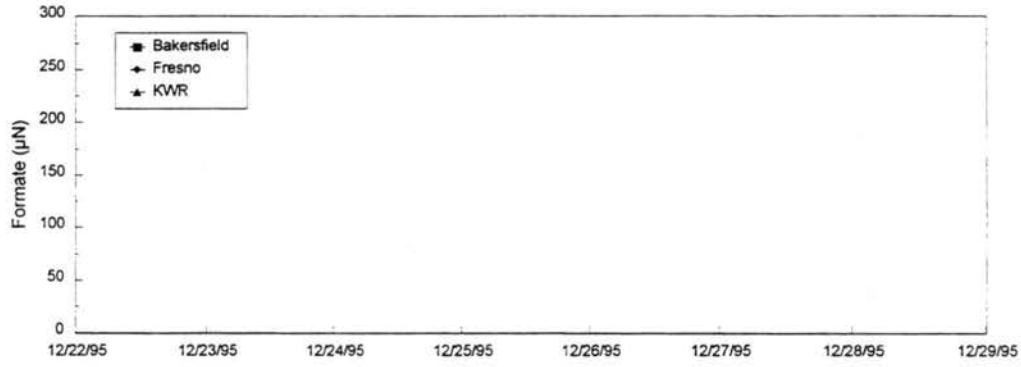
Bakersfield
Fresno
KWR
Formate (µN)
300
250
200
150
100
50
0
12/22/95
12/23/95
12/24/95
12/25/95
12/26/95
12/27/95
12/28/95
12/29/95

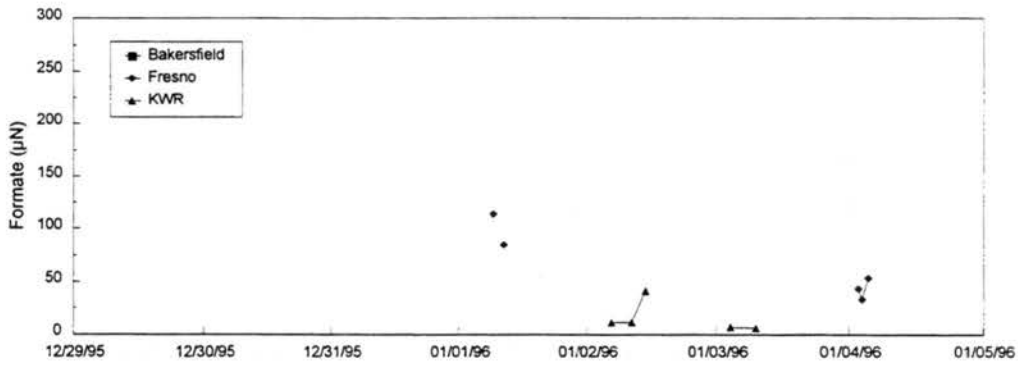
Bakersfield
Fresno
KWR
Formate (µN)
300
250
200
150
100
50
0
12/29/95
12/30/95
12/31/95
01/01/96
01/02/96
01/03/96
01/04/96
01/05/96

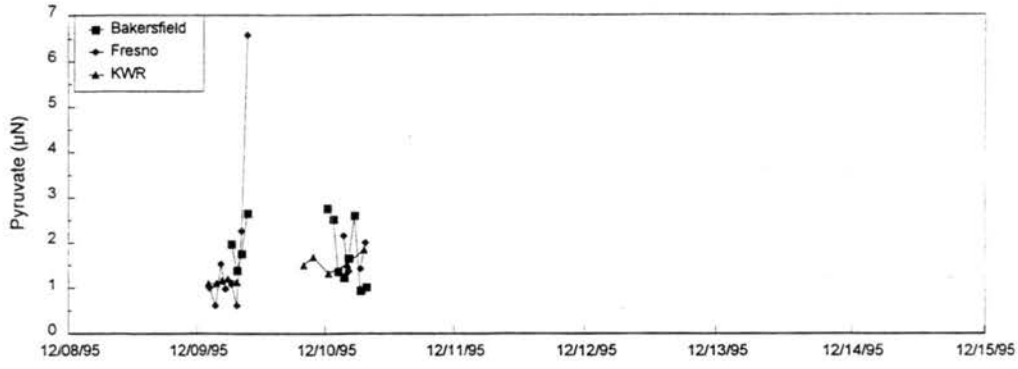
Bakersfield
Fresno
KWR
Pyruvate (µN)
0
1
2
3
4
5
6
7
12/08/95
12/09/95
12/10/95
12/11/95
12/12/95
12/13/95
12/14/95
12/15/95

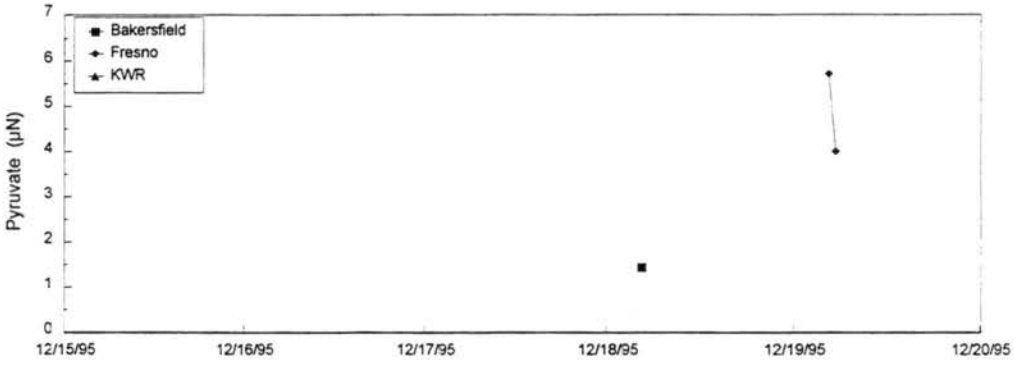
Bakersfield
Fresno
KWR
Pyruvate (µN)
0
1
2
3
4
5
6
7
12/15/95
12/16/95
12/17/95
12/18/95
12/19/95
12/20/95

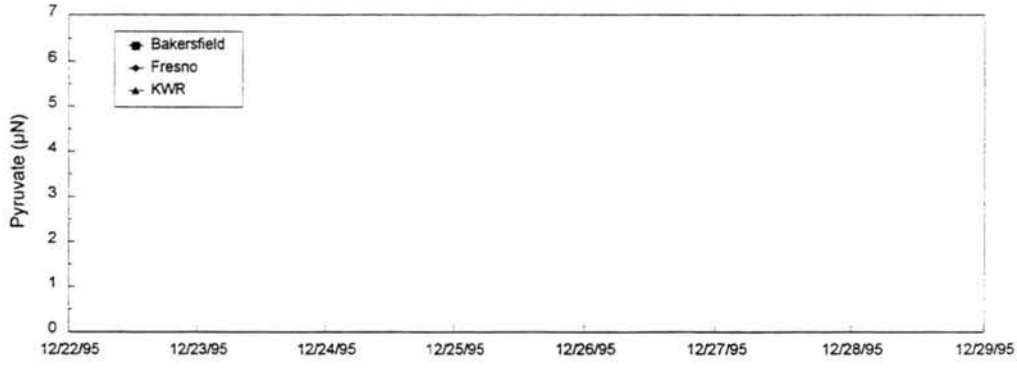
Bakersfield
Fresno
KWR
Pyruvate (µN)
0
1
2
3
4
5
6
7
12/22/95
12/23/95
12/24/95
12/25/95
12/26/95
12/27/95
12/28/95
12/29/95

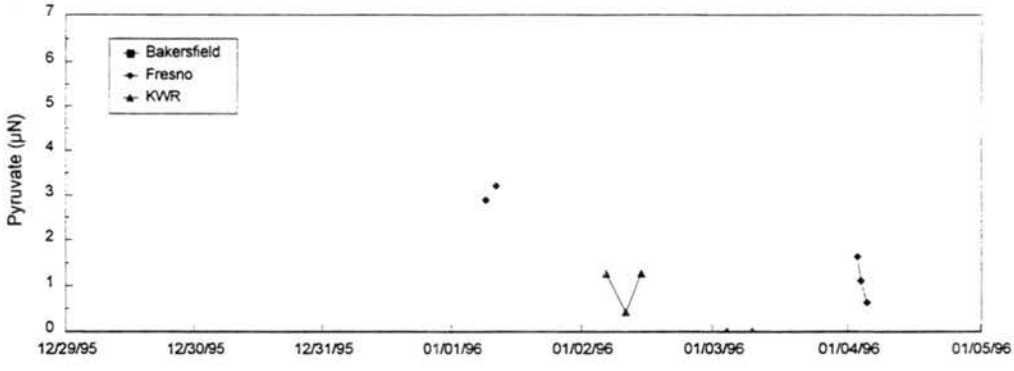
Bakersfield
Fresno
KWR
Pyruvate (µN)
0
1
2
3
4
5
6
7
12/29/95
12/30/95
12/31/95
01/01/96
01/02/96
01/03/96
01/04/96
01/05/96

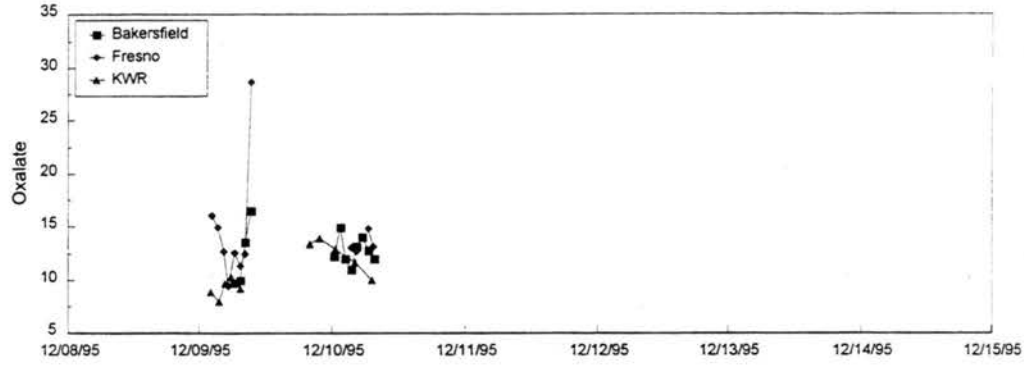
Bakersfield
Fresno
KWR
Oxalate
35
30
25
20
15
10
5
12/08/95
12/09/95
12/10/95
12/11/95
12/12/95
12/13/95
12/14/95
12/15/95

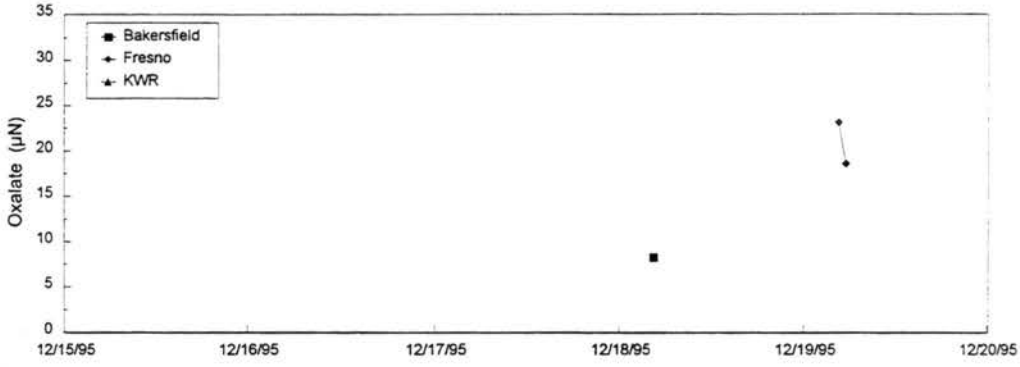
Bakersfield
Fresno
KWR
Oxalate (µN)
35
30
25
20
15
10
5
0
12/15/95
12/16/95
12/17/95
12/18/95
12/19/95
12/20/95

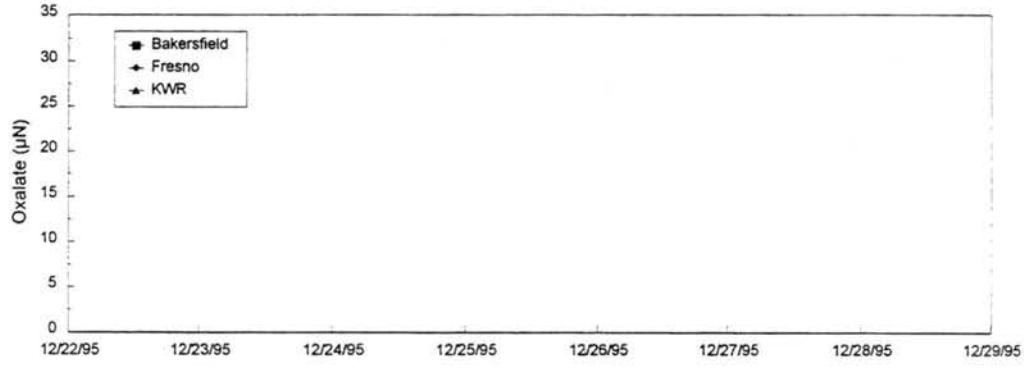
Bakersfield
Fresno
KWR
Oxalate (µN)
35
30
25
20
15
10
5
0
12/22/95
12/23/95
12/24/95
12/25/95
12/26/95
12/27/95
12/28/95
12/29/95

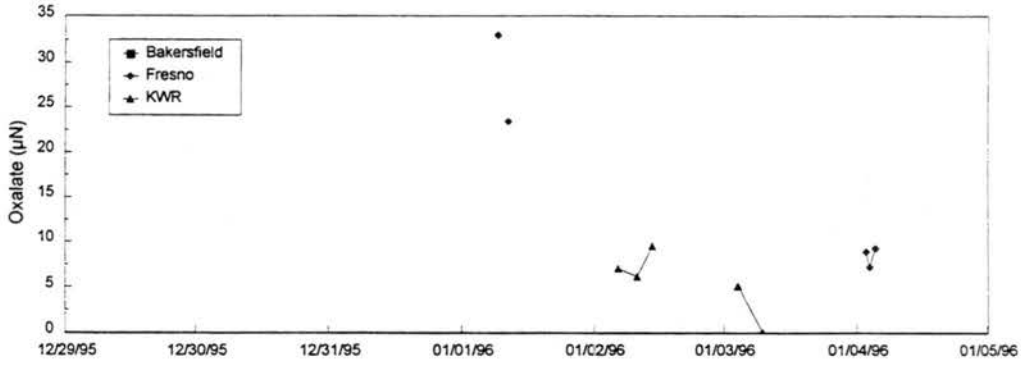
Bakersfield
Fresno
KWR
Oxalate (µN)
35
30
25
20
15
10
5
0
12/29/95
12/30/95
12/31/95
01/01/96
01/02/96
01/03/96
01/04/96
01/05/96

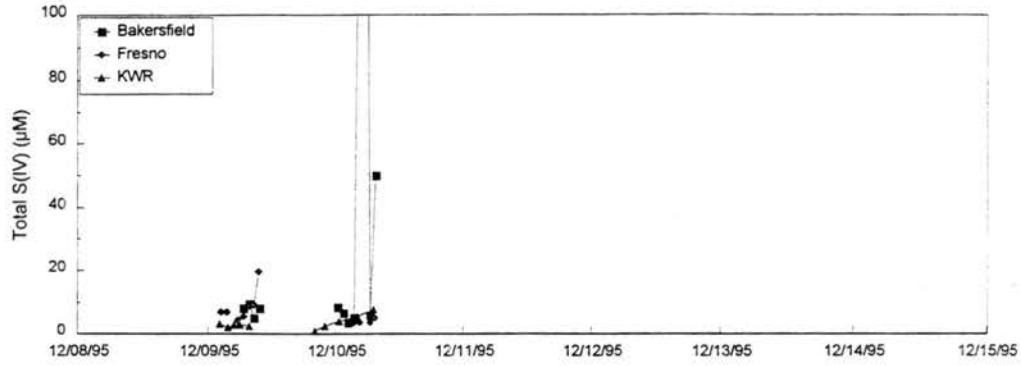
Bakersfield
Fresno
KWR
Total S(IV) (µM)
100
80
60
40
20
0
12/08/95
12/09/95
12/10/95
12/11/95
12/12/95
12/13/95
12/14/95
12/15/95

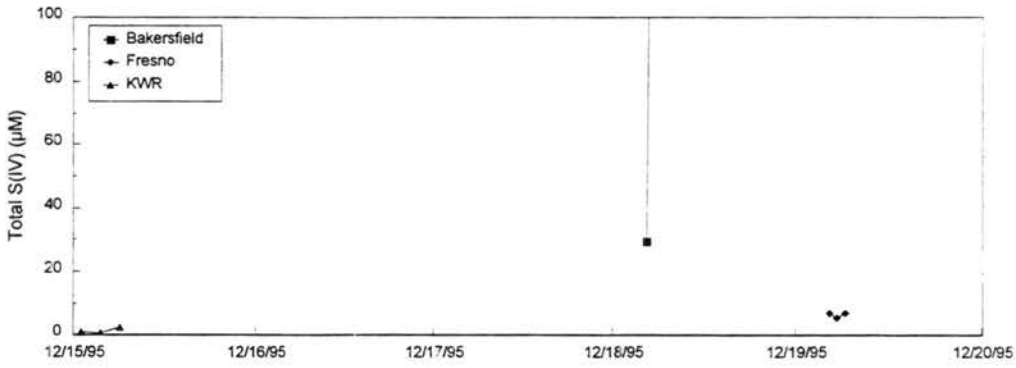
Bakersfield
Fresno
KWR
Total S(IV) (µM)
100
80
60
40
20
0
12/15/95
12/16/95
12/17/95
12/18/95
12/19/95
12/20/95

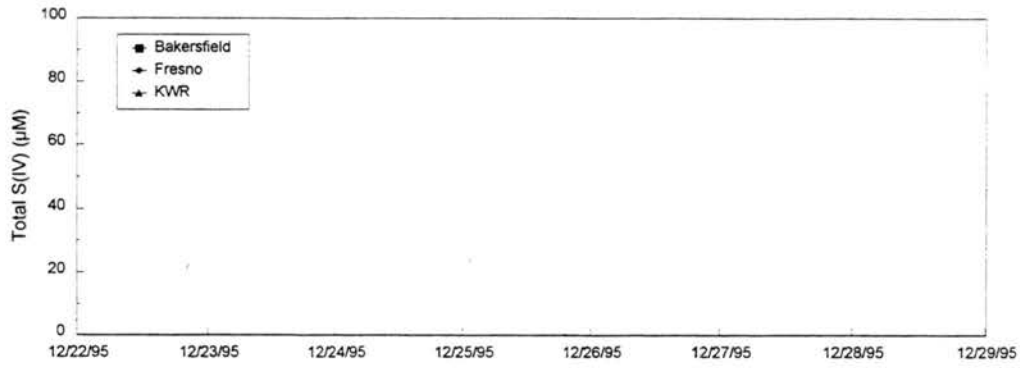
Bakersfield
Fresno
KWR
Total S(IV) (µM)
100
80
60
40
20
0
12/22/95
12/23/95
12/24/95
12/25/95
12/26/95
12/27/95
12/28/95
12/29/95

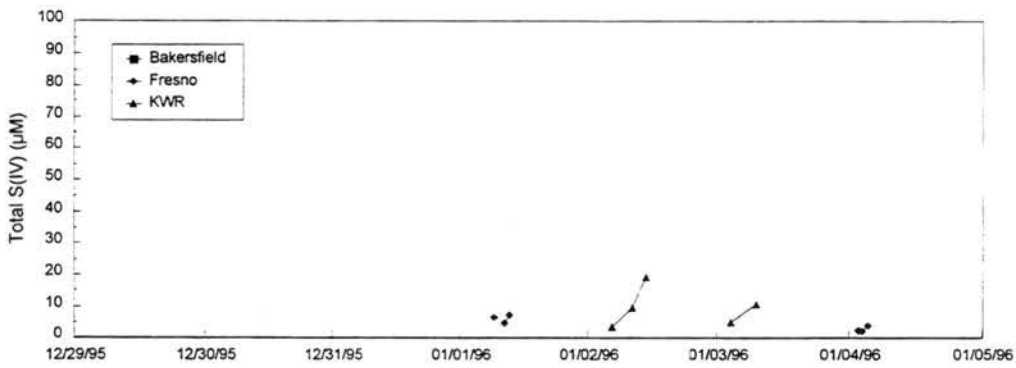
Bakersfield
Fresno
KWR
Total S(IV) (µM)
100
90
80
70
60
50
40
30
20
10
0
12/29/95
12/30/95
12/31/95
01/01/96
01/02/96
01/03/96
01/04/96
01/05/96

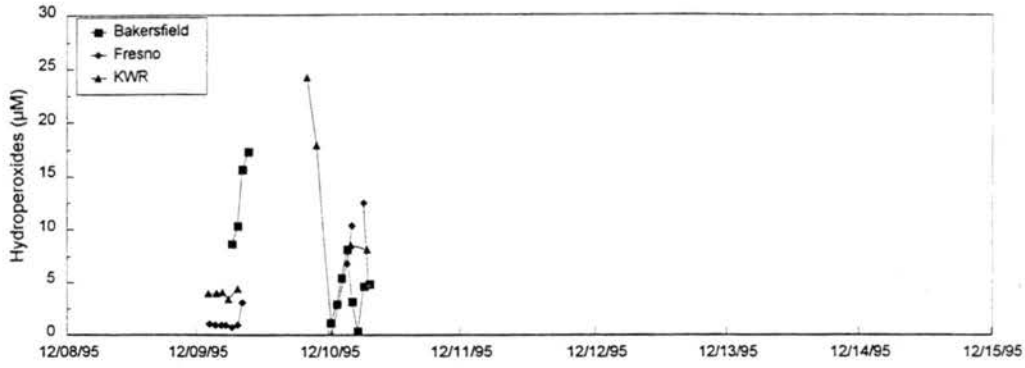
Bakersfield
Fresno
KWR
Hydroperoxides (µM)
0
5
10
15
20
25
30
12/08/95
12/09/95
12/10/95
12/11/95
12/12/95
12/13/95
12/14/95
12/15/95

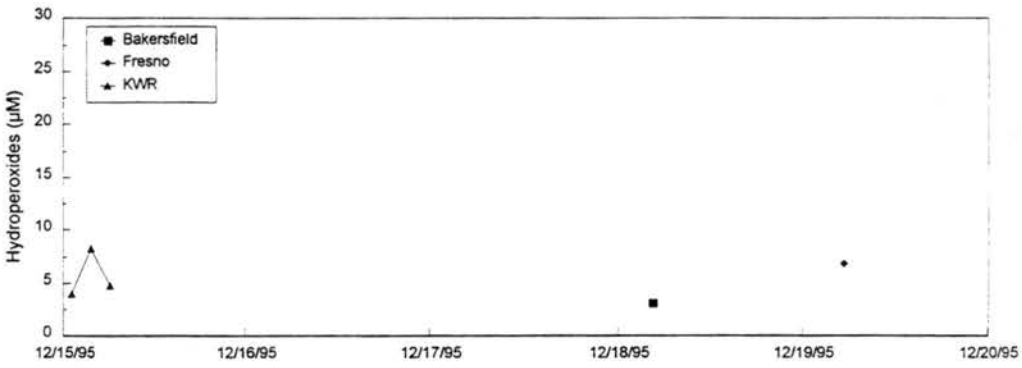
Bakersfield
Fresno
KWR
Hydroperoxides (µM)
0
5
10
15
20
25
30
12/15/95
12/16/95
12/17/95
12/18/95
12/19/95
12/20/95

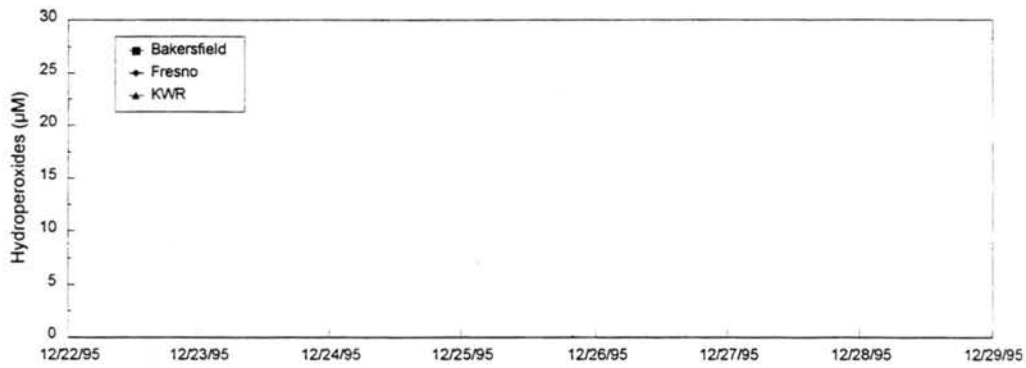
Bakersfield
Fresno
KWR
Hydroperoxides (µM)
0
5
10
15
20
25
30
12/22/95
12/23/95
12/24/95
12/25/95
12/26/95
12/27/95
12/28/95
12/29/95

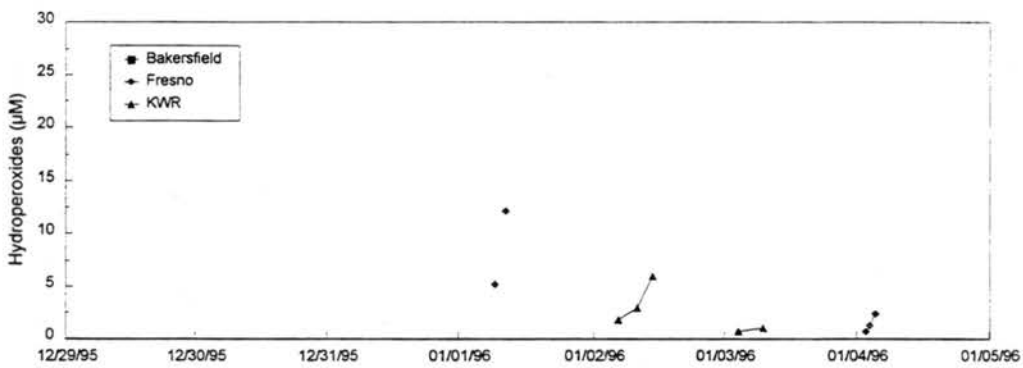
Bakersfield
Fresno
KWR
Hydroperoxides (µM)
0
5
10
15
20
25
30
12/29/95
12/30/95
12/31/95
01/01/96
01/02/96
01/03/96
01/04/96
01/05/96

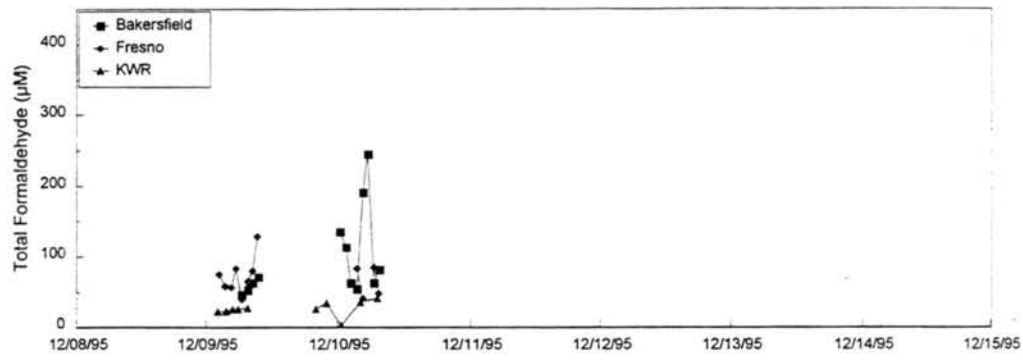
Bakersfield
Fresno
KWR
Total Formaldehyde (µM)
0
100
200
300
400
12/08/95
12/09/95
12/10/95
12/11/95
12/12/95
12/13/95
12/14/95
12/15/95

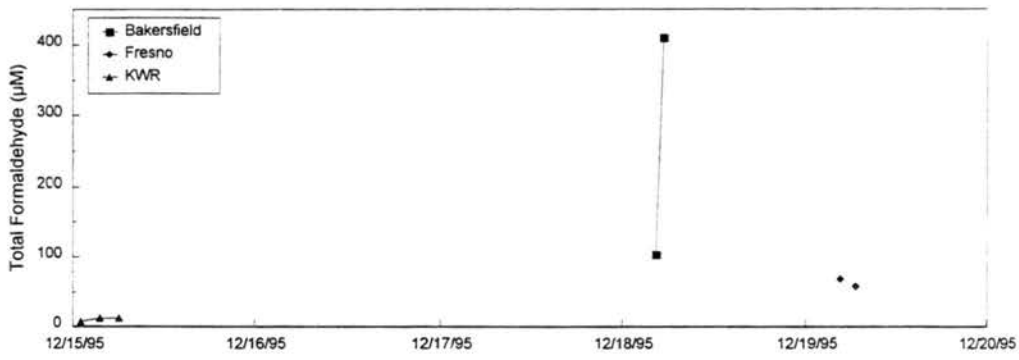
Bakersfield
Fresno
KWR
Total Formaldehyde (µM)
0
100
200
300
400
12/15/95
12/16/95
12/17/95
12/18/95
12/19/95
12/20/95

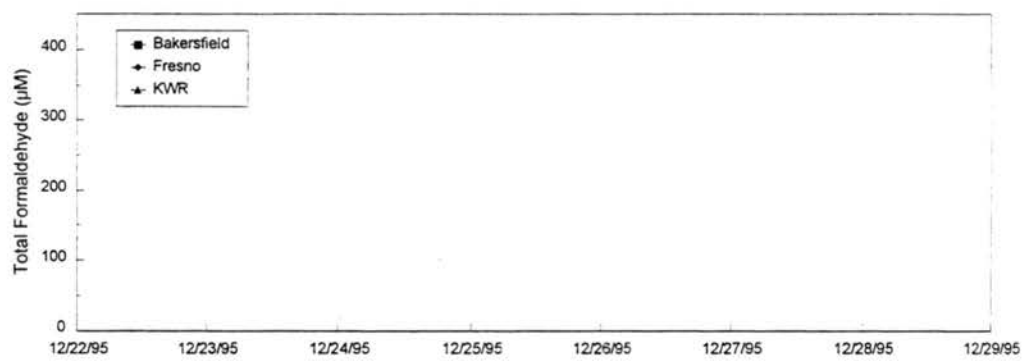
Bakersfield
Fresno
KWR
Total Formaldehyde (µM)
0
100
200
300
400
12/22/95
12/23/95
12/24/95
12/25/95
12/26/95
12/27/95
12/28/95
12/29/95

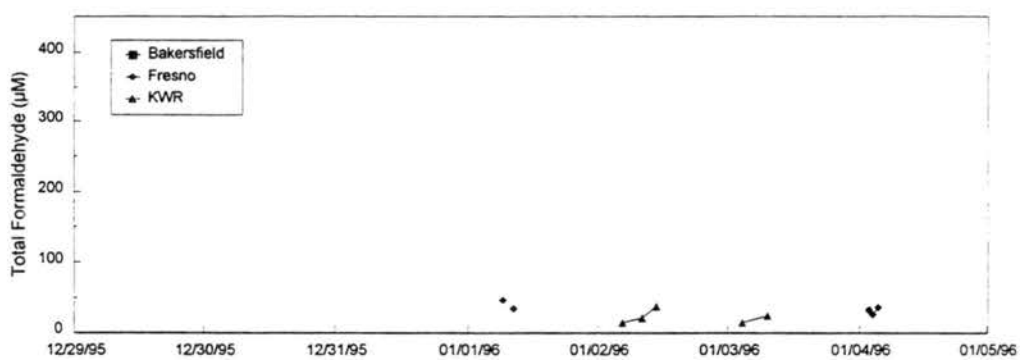
Bakersfield
Fresno
KWR
Total Formaldehyde (µM)
0
100
200
300
400
12/29/95
12/30/95
12/31/95
01/01/96
01/02/96
01/03/96
01/04/96
01/05/96

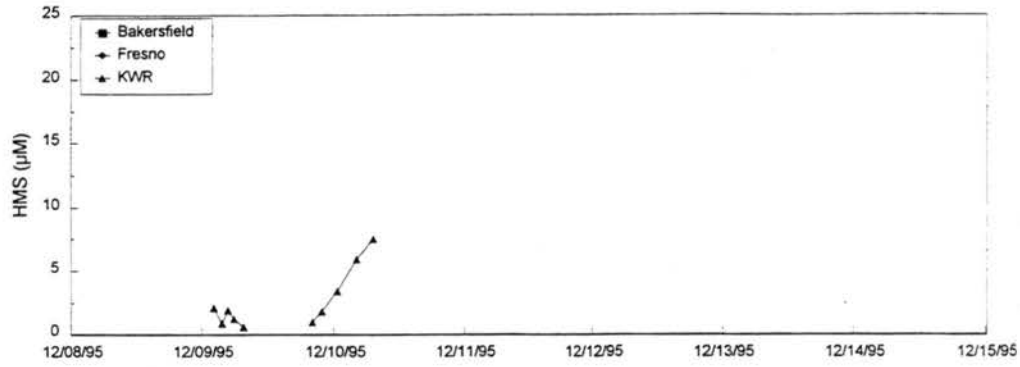
Bakersfield
Fresno
KWR
HMS (µM)
25
20
15
10
5
0
12/08/95
12/09/95
12/10/95
12/11/95
12/12/95
12/13/95
12/14/95
12/15/95

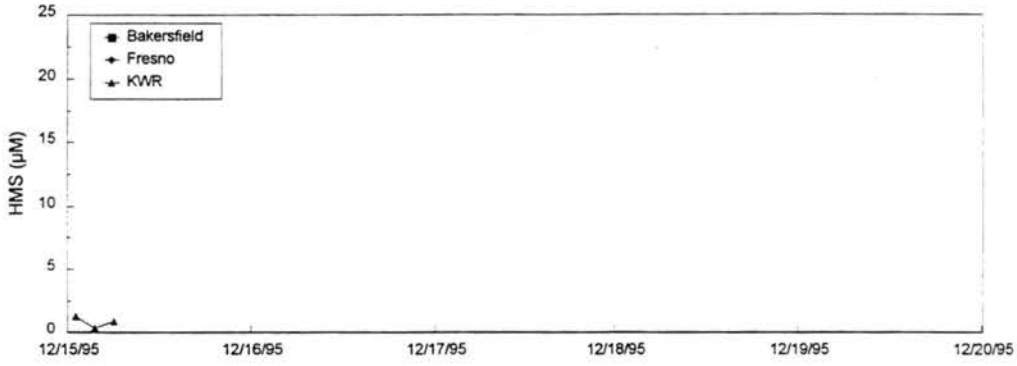
Bakersfield
Fresno
KWR
HMS (µM)
25
20
15
10
5
0
12/15/95
12/16/95
12/17/95
12/18/95
12/19/95
12/20/95

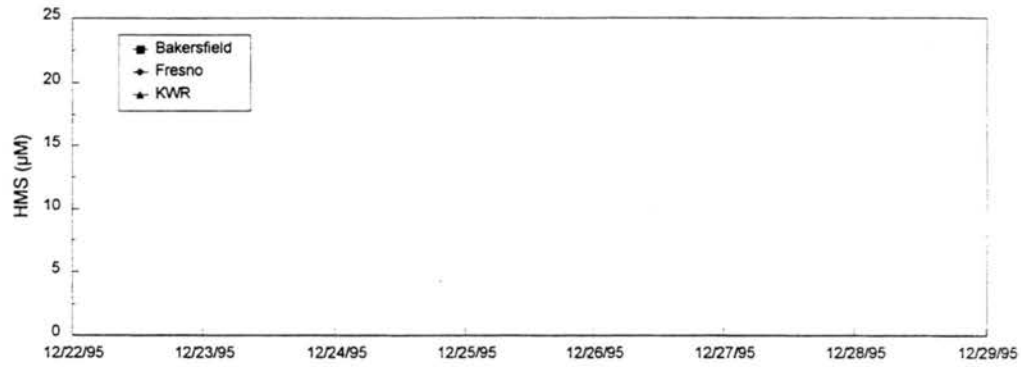
Bakersfield
Fresno
KWR
HMS (µM)
25
20
15
10
5
0
12/22/95
12/23/95
12/24/95
12/25/95
12/26/95
12/27/95
12/28/95
12/29/95

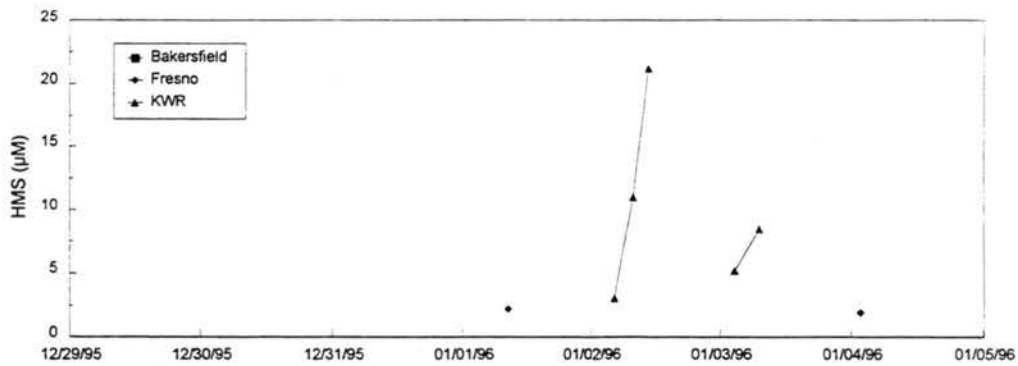
Bakersfield
Fresno
KWR
HMS (µM)
25
20
15
10
5
0
12/29/95
12/30/95
12/31/95
01/01/96
01/02/96
01/03/96
01/04/96
01/05/96

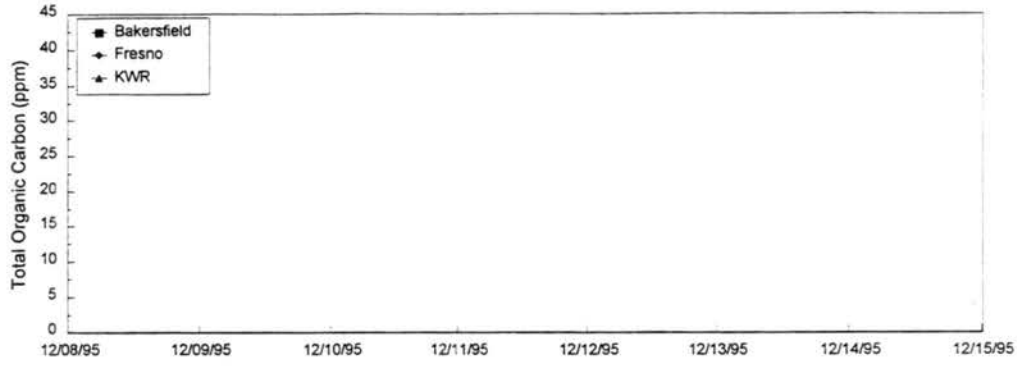
Bakersfield
Fresno
KWR
Total Organic Carbon (ppm)
0
5
10
15
20
25
30
35
40
45
12/08/95
12/09/95
12/10/95
12/11/95
12/12/95
12/13/95
12/14/95
12/15/95

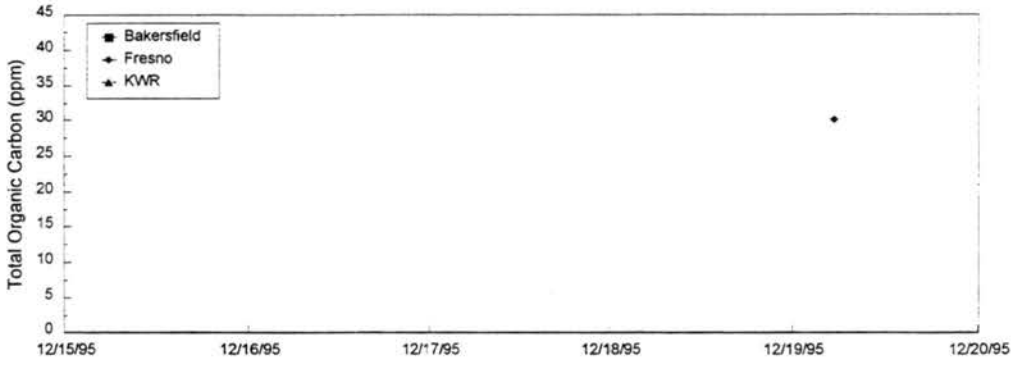
Bakersfield
Fresno
KWR
Total Organic Carbon (ppm)
0
5
10
15
20
25
30
35
40
45
12/15/95
12/16/95
12/17/95
12/18/95
12/19/95
12/20/95

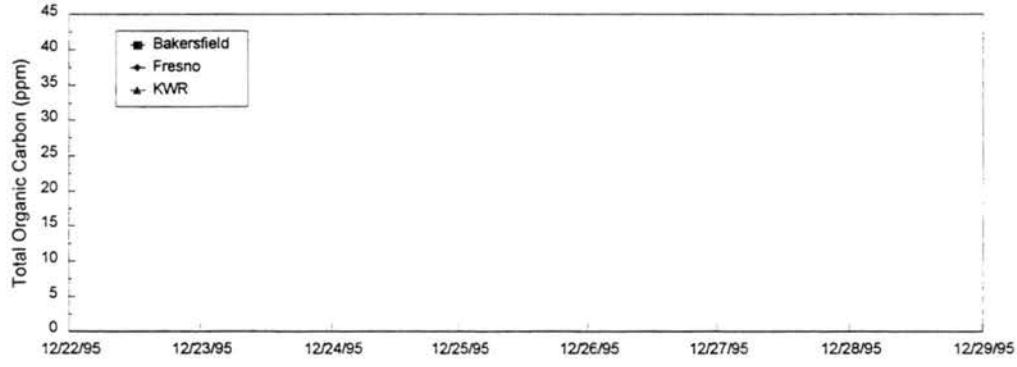
Bakersfield
Fresno
KWR
Total Organic Carbon (ppm)
0
5
10
15
20
25
30
35
40
45
12/22/95
12/23/95
12/24/95
12/25/95
12/26/95
12/27/95
12/28/95
12/29/95

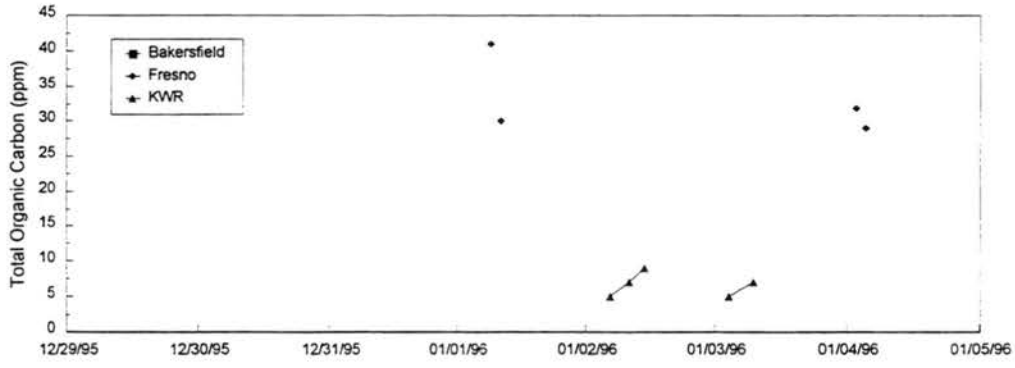
Bakersfield
Fresno
KWR
Total Organic Carbon (ppm)
0
5
10
15
20
25
30
35
40
45
12/29/95
12/30/95
12/31/95
01/01/96
01/02/96
01/03/96
01/04/96
01/05/96

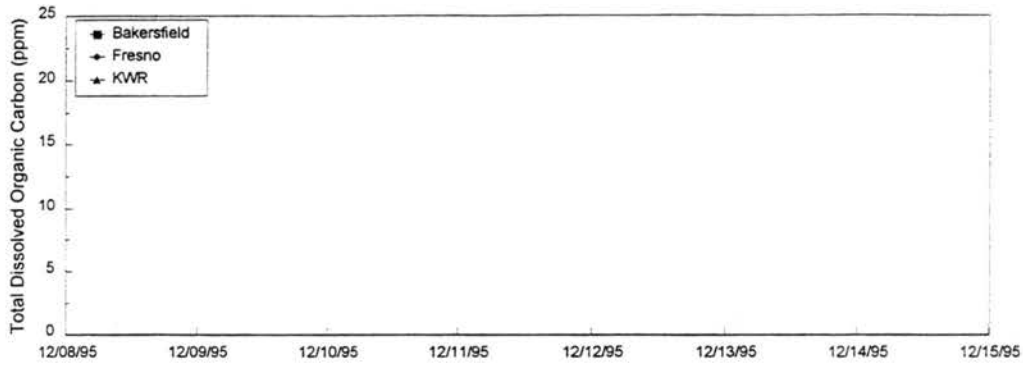
Bakersfield
Fresno
KWR
Total Dissolved Organic Carbon (ppm)
25
20
15
10
5
0
12/08/95
12/09/95
12/10/95
12/11/95
12/12/95
12/13/95
12/14/95
12/15/95

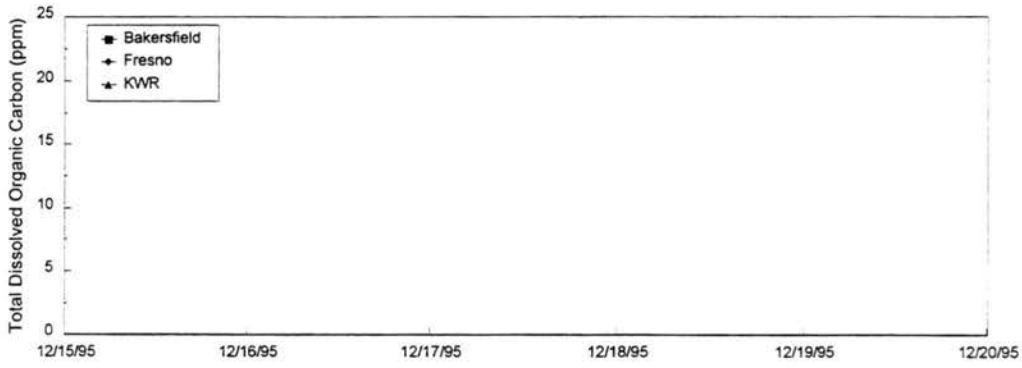
Bakersfield
Fresno
KWR
Total Dissolved Organic Carbon (ppm)
25
20
15
10
5
0
12/15/95
12/16/95
12/17/95
12/18/95
12/19/95
12/20/95

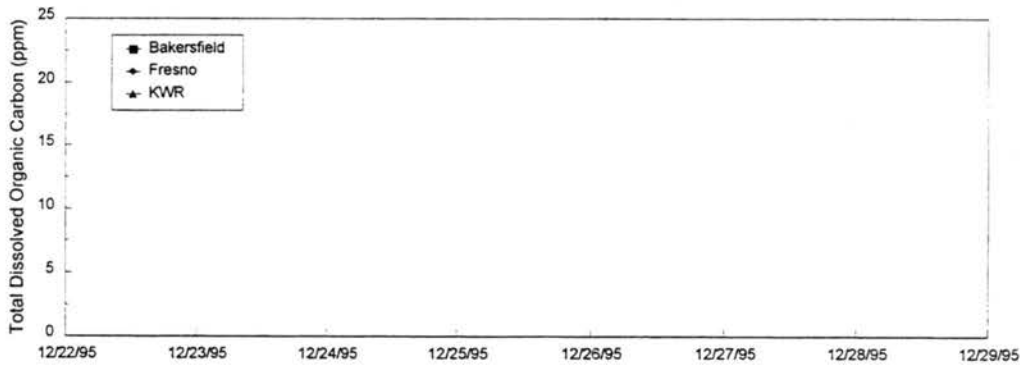
Bakersfield
Fresno
KWR
Total Dissolved Organic Carbon (ppm)
25
20
15
10
5
0
12/22/95
12/23/95
12/24/95
12/25/95
12/26/95
12/27/95
12/28/95
12/29/95

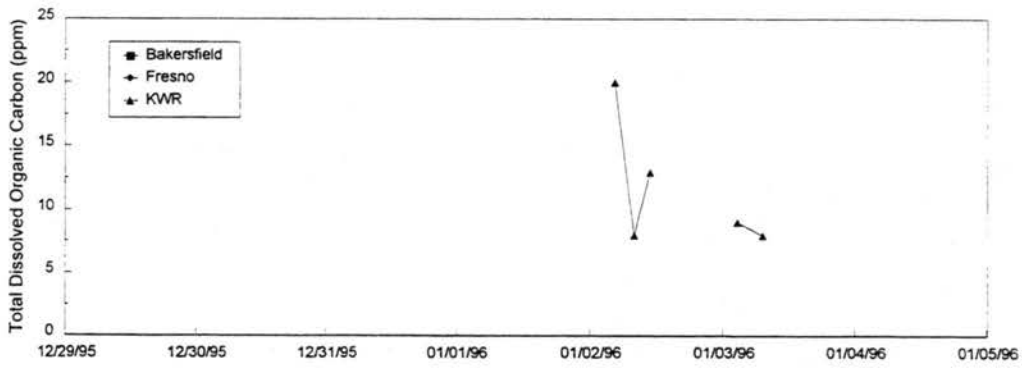
Bakersfield
Fresno
KWR
Total Dissolved Organic Carbon (ppm)
25
20
15
10
5
0
12/29/95
12/30/95
12/31/95
01/01/96
01/02/96
01/03/96
01/04/96
01/05/96

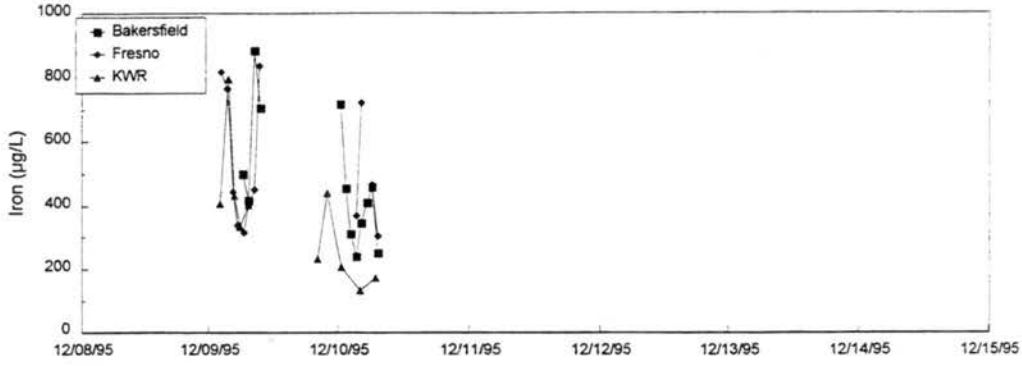
Bakersfield
Fresno
KWR
Iron (µg/L)
1000
800
600
400
200
0
12/08/95
12/09/95
12/10/95
12/11/95
12/12/95
12/13/95
12/14/95
12/15/95

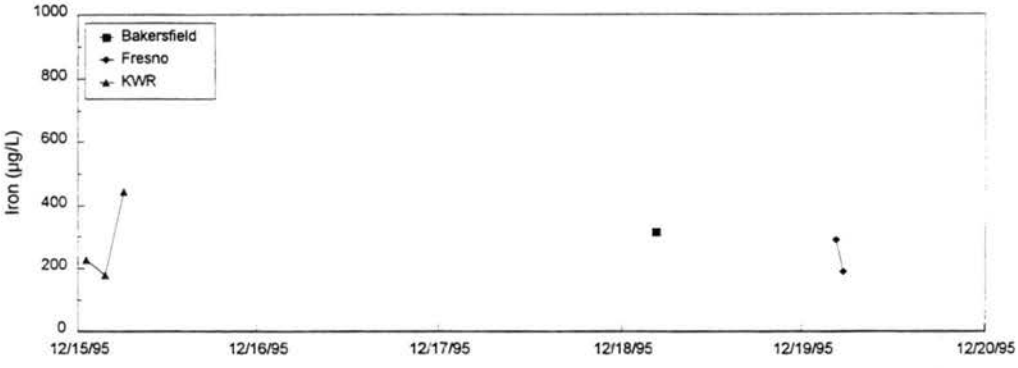
Bakersfield
Fresno
KWR
Iron (µg/L)
1000
800
600
400
200
0
12/15/95
12/16/95
12/17/95
12/18/95
12/19/95
12/20/95

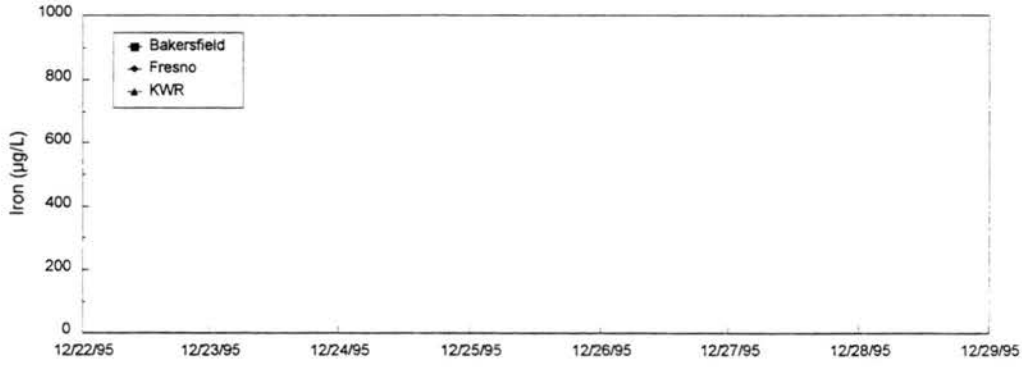
Bakersfield
Fresno
KWR
Iron (µg/L)
1000
800
600
400
200
0
12/22/95
12/23/95
12/24/95
12/25/95
12/26/95
12/27/95
12/28/95
12/29/95

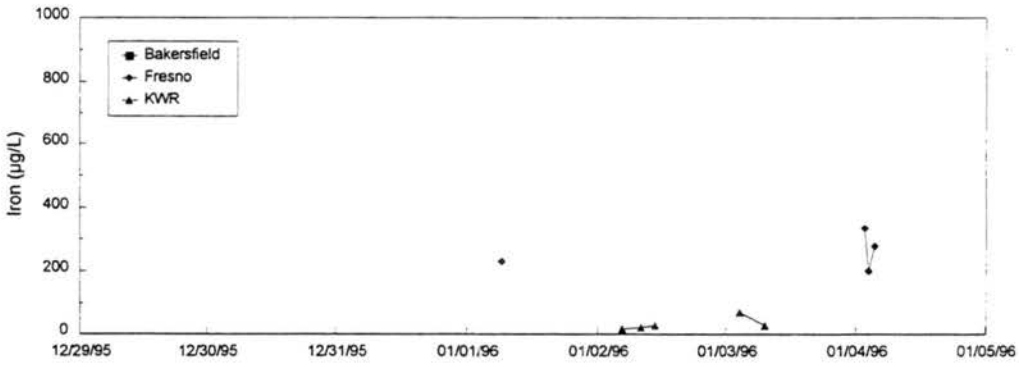
Bakersfield
Fresno
KWR
Iron (µg/L)
1000
800
600
400
200
0
12/29/95
12/30/95
12/31/95
01/01/96
01/02/96
01/03/96
01/04/96
01/05/96

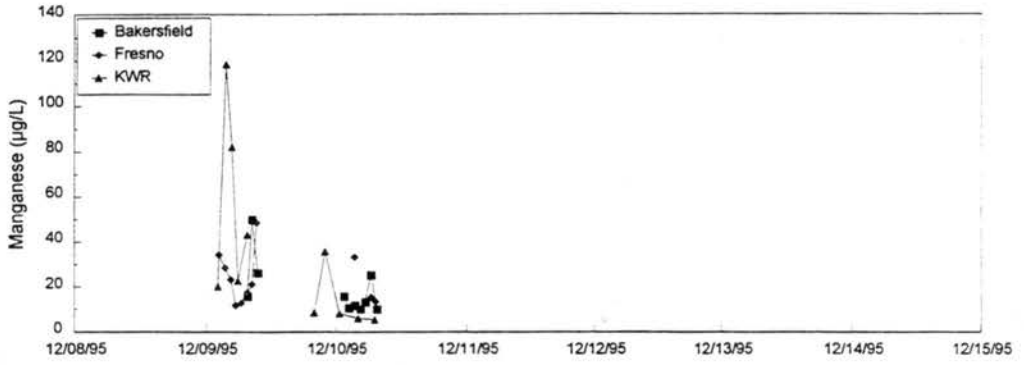
Bakersfield
Fresno
KWR
Manganese (µg/L)
140
120
100
80
60
40
20
0
12/08/95
12/09/95
12/10/95
12/11/95
12/12/95
12/13/95
12/14/95
12/15/95

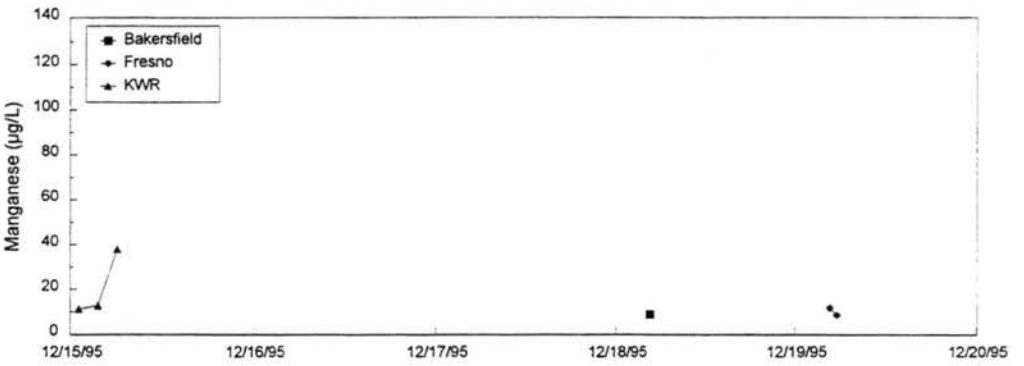
Bakersfield
Fresno
KWR
Manganese (µg/L)
140
120
100
80
60
40
20
0
12/15/95
12/16/95
12/17/95
12/18/95
12/19/95
12/20/95

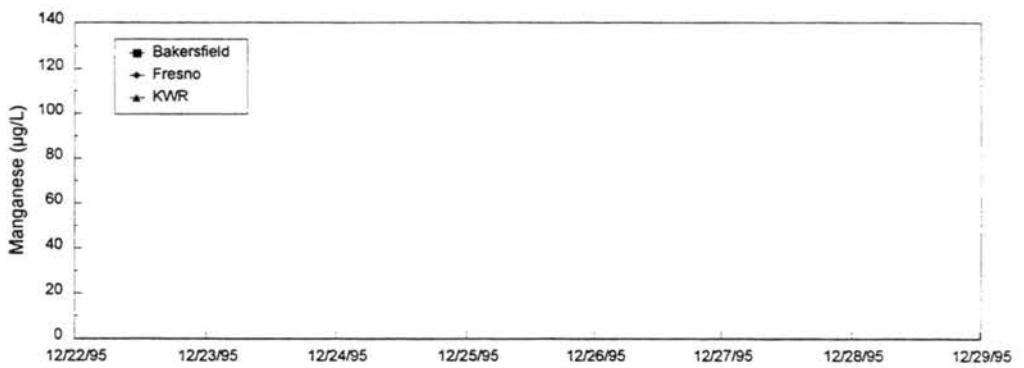
Bakersfield
Fresno
KWR
Manganese (µg/L)
140
120
100
80
60
40
20
0
12/22/95
12/23/95
12/24/95
12/25/95
12/26/95
12/27/95
12/28/95
12/29/95

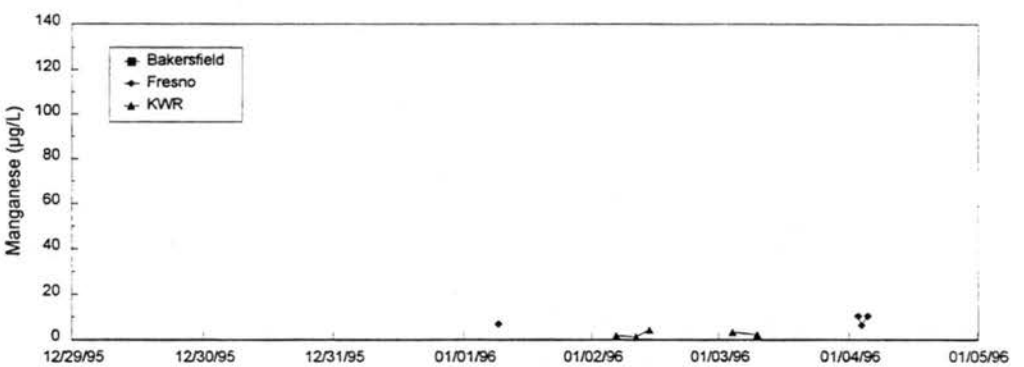
Bakersfield
Fresno
KWR
Manganese (µg/L)
140
120
100
80
60
40
20
0
12/29/95
12/30/95
12/31/95
01/01/96
01/02/96
01/03/96
01/04/96
01/05/96

Appendix C: Bulk S(IV) Oxidation Calculations

Timelines of S(IV) oxidation rates:

Plots show -d S(IV) / dt in M s^{-1} as functions of time for each oxidation pathway throughout fog events at each IMS95 fog sampling site.

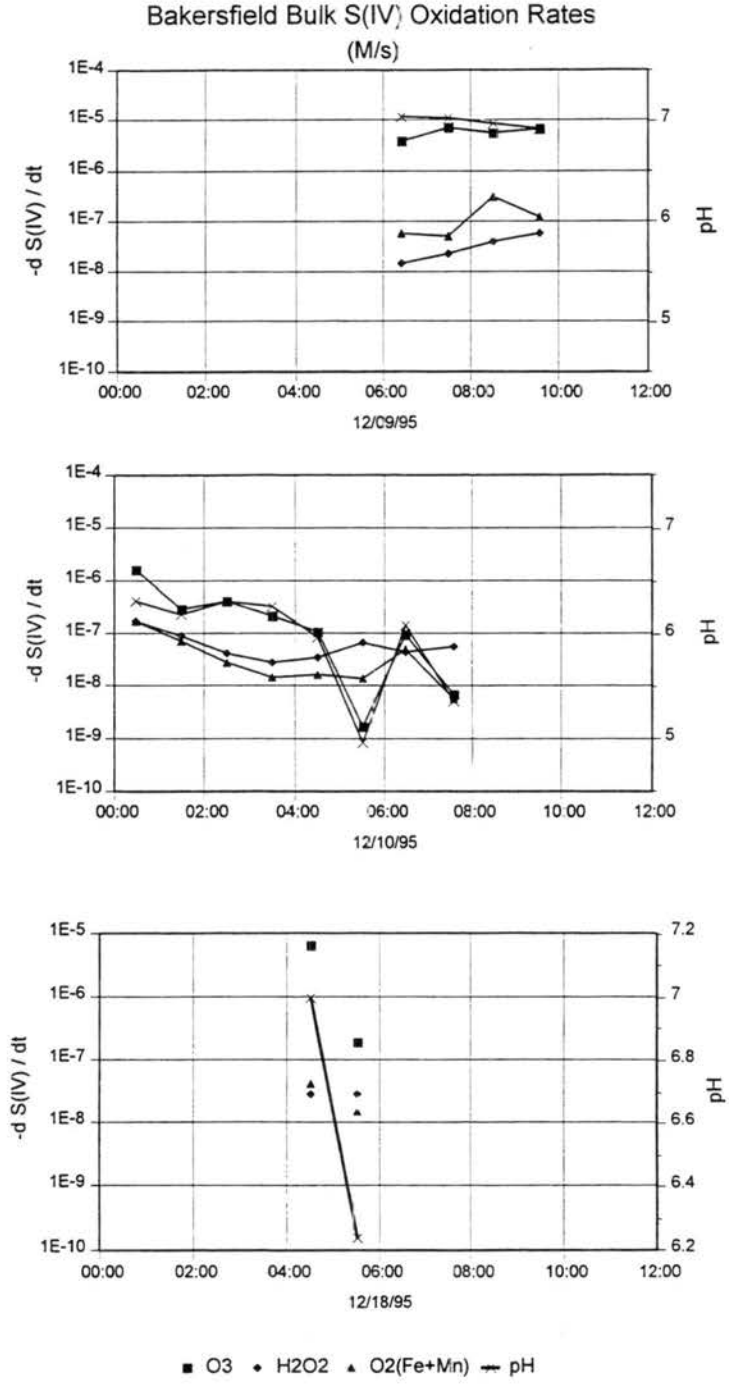

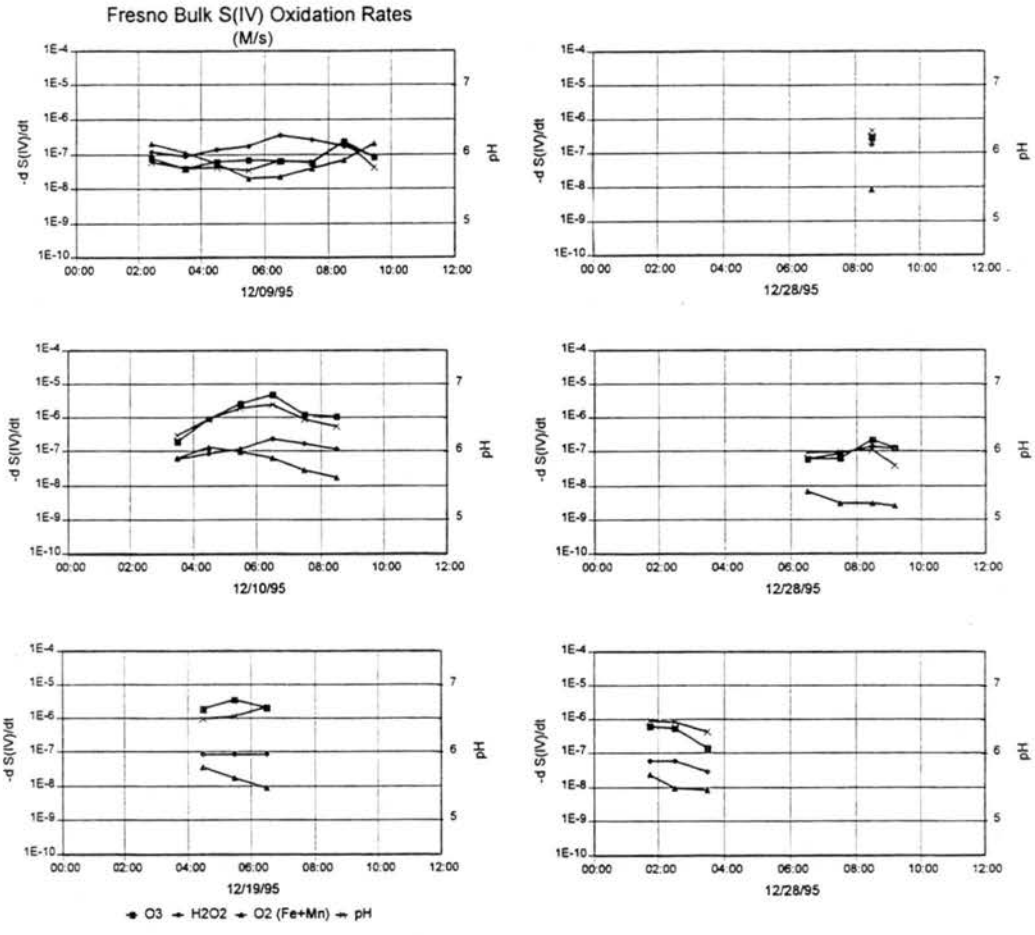
Fresno Bulk S(IV) Oxidation Rates
(M/s)
-d S(IV)/dt
pH
12/09/95
12/28/95
12/10/95
12/28/95
12/19/95
12/28/95
O3
H2O2
O2 (Fe+Mn)
pH

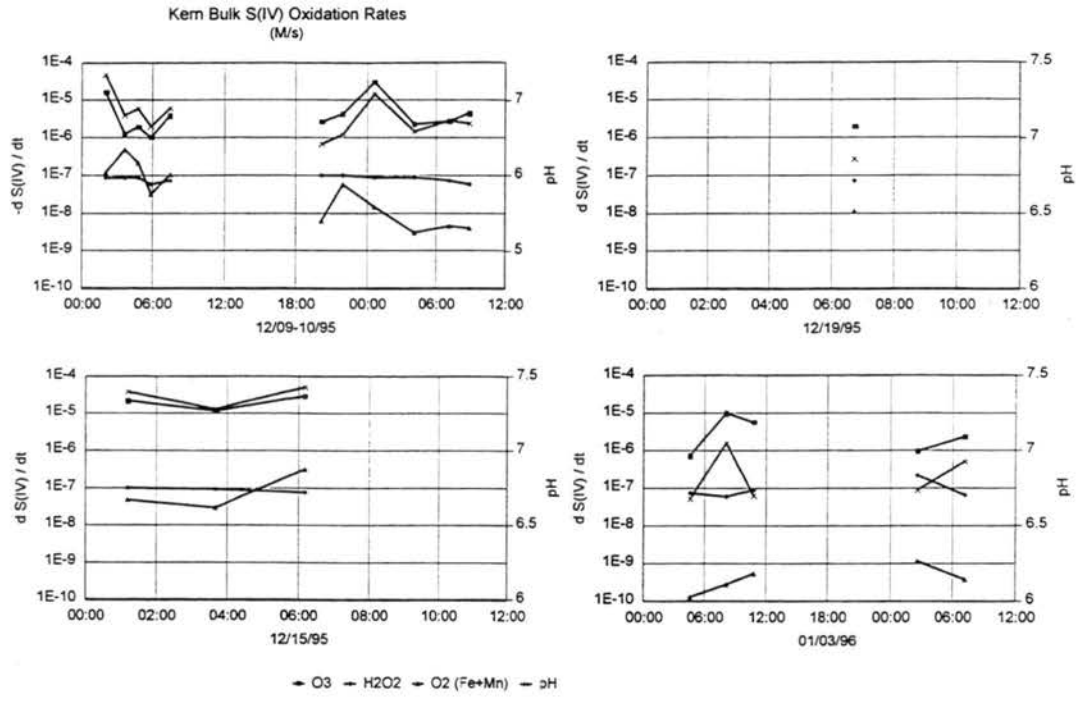
Kern Bulk S(IV) Oxidation Rates
(M/s)
-d S(IV) / dt
d S(IV) / dt
pH
1E-4
1E-5
1E-6
1E-7
1E-8
1E-9
1E-10
7.5
7
6.5
6
5
00:00
02:00
04:00
06:00
08:00
10:00
12:00
18:00
12/09-10/95
12/19/95
12/15/95
01/03/96
O3
H2O2
O2 (Fe+Mn)
pH

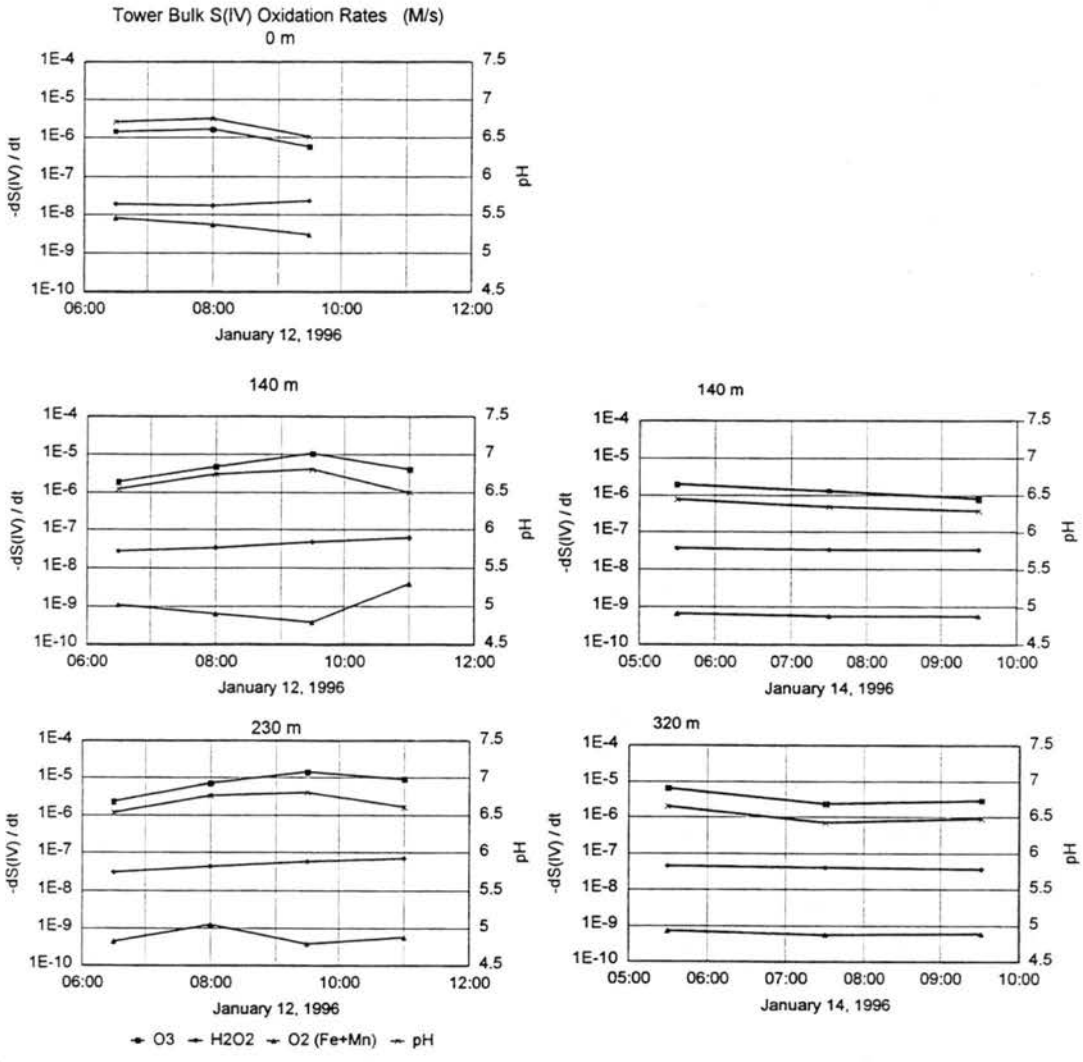
Tower Bulk S(IV) Oxidation Rates (M/s)
0 m
140 m
140 m
230 m
320 m
-dS(IV) / dt
pH
1E-4
1E-5
1E-6
1E-7
1E-8
1E-9
1E-10
7.5
7
6.5
6
5.5
5
4.5
06:00
08:00
10:00
12:00
05:00
07:00
09:00
January 12, 1996
January 14, 1996
O3
H2O2
O2 (Fe+Mn)
pH

The following plots show sulfate production in moles s^{-1} m^{-3} via the three S(IV) oxidation pathways as functions of time at each of the IMS95 southern SJV fog sampling sites.

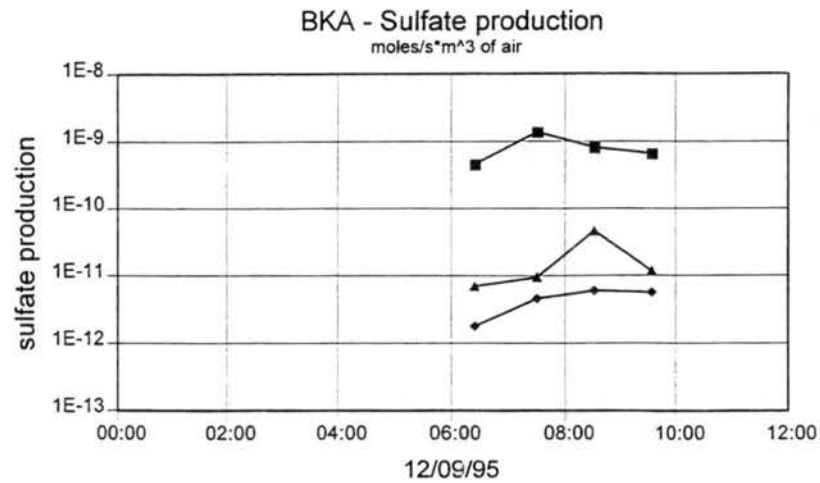

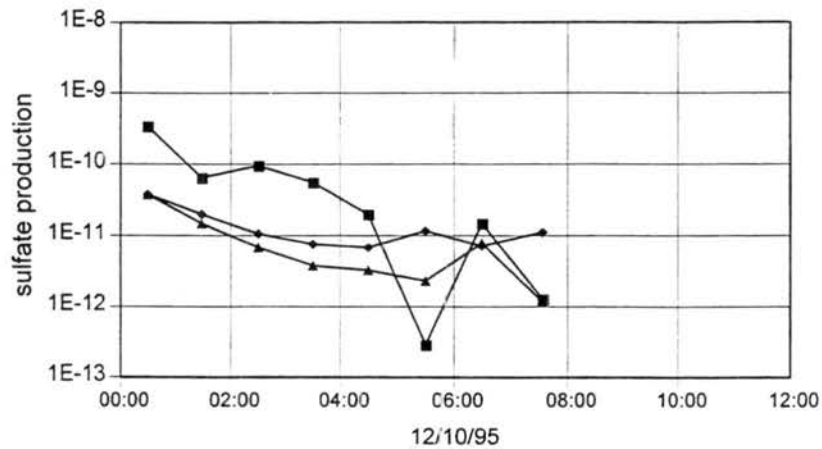

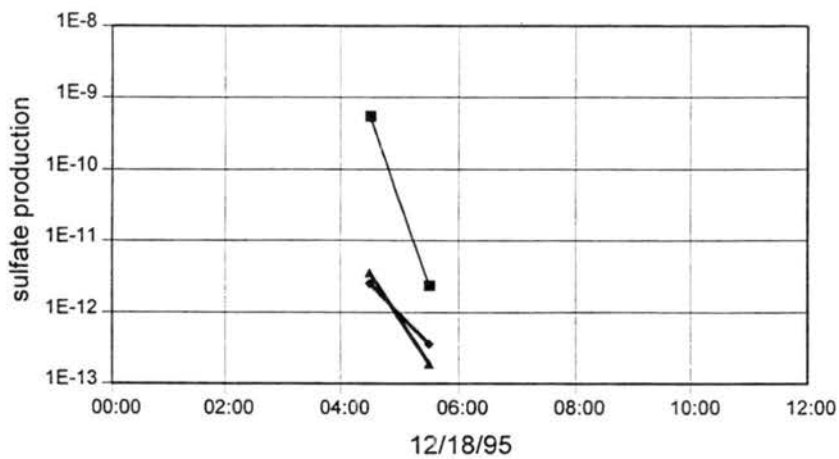

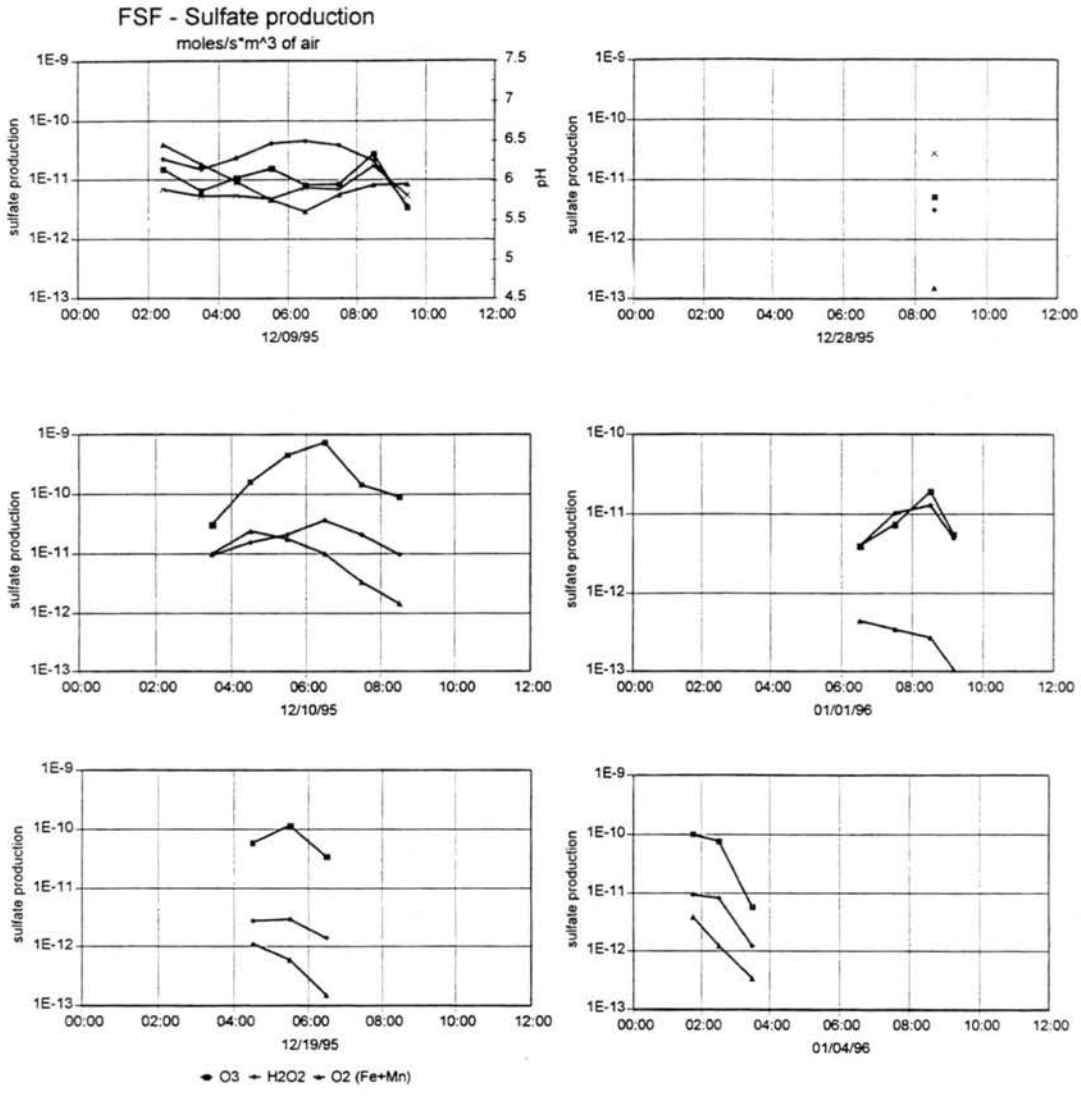
FSF - Sulfate production
moles/s*m^3 of air
sulfate production
pH
1E-9
1E-10
1E-11
1E-12
1E-13
7.5
7
6.5
6
5.5
5
4.5
00:00
02:00
04:00
06:00
08:00
10:00
12:00
12/09/95
12/28/95
12/10/95
01/01/96
12/19/95
01/04/96
O3
H2O2
O2 (Fe+Mn)

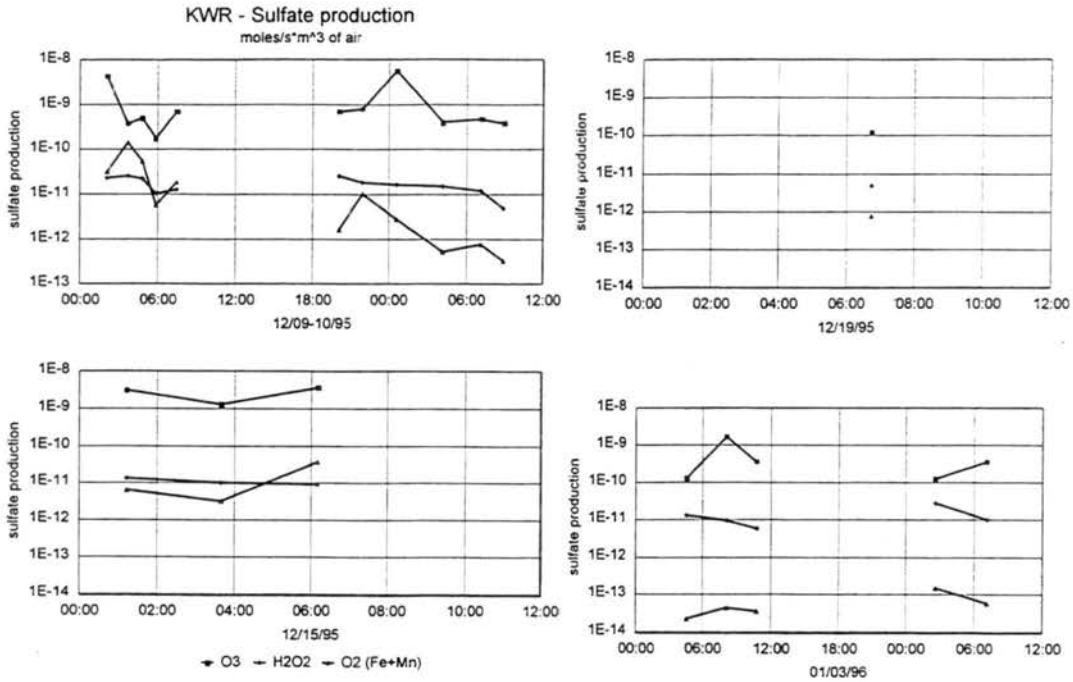
KWR - Sulfate production
moles/s*m^3 of air
sulfate production
1E-8
1E-9
1E-10
1E-11
1E-12
1E-13
1E-14
00:00
02:00
04:00
06:00
08:00
10:00
12:00
18:00
12/09-10/95
12/19/95
12/15/95
01/03/96
O3
H2O2
O2 (Fe+Mn)

The following tables show the following information for each bulk sample calculation presented in the previous plots:

Sample Name
Start Date - Month and day actual sample was collected
Start Time - Time sample was started
End Time - End time, when sample was removed from collector

Elevation (m) - Elevation of the sampler in meters (at Tower only)

MASS - mass of collected fog water in grams (values of -99 indicate missing data for that sample
PH - pH of collected fog water, measured on-site
LWC - Liquid water content from CASCC2 sample masses (in g m^{-3})

Fe(III) - Fe(III) used in S(IV) oxidation calculations (in M)
Mn(II) - Mn(II) used in S(IV) oxidation calculations (in M)

SO_2, O_3, and H_2O_2 values used in S(IV) oxidation calculations (in ppbv)

Calculated bulk S(IV) oxidation rates for each pathway (in M/s)

Bakersfield Bulk S(IV) Oxidation Calculations

SAMPLE_NAME	START_DATE	START_TIME	END_TIME	PH	Mass (g)	LWC (g/m^3)	Fe(III) (M)	Mn(II) (M)	SO2 (ppb)	O3 (ppb)	H2O2 (ppbv)	O3 rate -d S(IV)/dt Molar/s	H2O2 rate -d S(IV)/dt Molar/s	O2(Fe+Mn) rate -d S(IV)/dt Molar/s
BCC1209#1	12/09/95	05:51 AM	07:00 AM	7.04	39.1	0.1195	2.24E-006	2.73E-007	1	1	0.05	**3.92E-006**	**1.49E-008**	**5.99E-008**
BCC1209#2	12/09/95	07:00 AM	08:00 AM	7.02	56.5	0.1955	1.87E-006	2.89E-007	1	2	0.08	**7.15E-006**	**2.38E-008**	**5.10E-008**
BCC1209#3	12/09/95	08:00 AM	09:04 AM	6.97	45.4	0.1482	3.96E-006	9.15E-007	1	2	0.14	**5.68E-006**	**4.17E-008**	**3.13E-007**
BCC1209#4	12/09/95	09:04 AM	10:04 AM	6.92	27.6	0.0984	3.16E-006	4.84E-007	1	3	0.20	**6.77E-006**	**5.96E-008**	**1.21E-007**
BCC1210#1	12/10/95	12:00 AM	01:00 AM	6.32	61.1	0.2112	3.21E-006	2.73E-007	6	2	0.10	**1.71E-006**	**1.79E-007**	**1.83E-007**
BCC1210#2	12/10/95	01:00 AM	02:00 AM	6.19	60.9	0.2105	2.04E-006	2.95E-007	4	1	0.08	**3.13E-007**	**9.54E-008**	**7.27E-008**
BCC1210#3	12/10/95	02:00 AM	03:00 AM	6.32	68.4	0.2359	1.40E-006	1.97E-007	3	1	0.05	**4.27E-007**	**4.47E-008**	**2.88E-008**
BCC1210#4	12/10/95	03:00 AM	04:00 AM	6.27	73.1	0.2517	1.08E-006	2.13E-007	2	1	0.05	**2.26E-007**	**2.98E-008**	**1.51E-008**
BCC1210#5	12/10/95	04:00 AM	05:00 AM	5.98	53	0.1836	1.55E-006	1.83E-007	2.5	1.5	0.05	**1.12E-007**	**3.73E-008**	**1.76E-008**
BCC1210#6	12/10/95	05:00 AM	06:00 AM	4.97	47.7	0.1658	1.84E-006	2.39E-007	3	2	0.08	**1.76E-009**	**7.15E-008**	**1.41E-008**
BCC1210#7	12/10/95	06:00 AM	07:00 AM	6.09	44.2	0.1538	2.05E-006	4.63E-007	2	1	0.08	**9.89E-008**	**4.77E-008**	**5.21E-008**
BCC1210#8	12/10/95	07:00 AM	08:09 AM	5.36	62.5	0.1882	1.13E-006	1.84E-007	2	2	0.10	**6.93E-009**	**5.96E-008**	**6.08E-009**
BCC1218#1	12/18/95	04:00 AM	05:00 AM	7.00	23.8	0.0861	1.42E-006	1.69E-007	2	1	0.05	**6.52E-006**	**2.98E-008**	**4.34E-008**
BCC1218#2	12/18/95	05:00 AM	06:00 AM	6.24	2.55	0.0124	1.34E-006	1.82E-007	2	1	0.05	**1.97E-007**	**2.98E-008**	**1.56E-008**

Fresno Bulk S(IV) Oxidation Calculations

SAMPLE_NAME	START_DATE	START_TIME	END_TIME	PH	Mass (g)	LWC (g/m^3)	Fe(III) (M)	Mn(II) (M)	SO2 (ppb)	O3 (ppb)	H2O2 (ppbv)	O3 rate -d S(IV)/dt Molar/s	H2O2 rate -d S(IV)/dt Molar/s	O2(Fe+Mn) rate -d S(IV)/dt Molar/s
FCC1208#1	12/09/95	01:53 AM	03:00 AM	5.89	62.2	0.1928	3.67E-006	6.27E-007	4	1	0.10	**7.89E-008**	**1.19E-007**	**2.10E-007**
FCC1208#2	12/09/95	03:00 AM	04:00 AM	5.80	49.1	0.1707	3.44E-006	5.19E-007	3	1	0.10	**3.91E-008**	**8.94E-008**	**1.13E-007**
FCC1208#3	12/09/95	04:00 AM	05:00 AM	5.81	51.1	0.1771	1.99E-006	4.29E-007	3	1.5	0.15	**6.14E-008**	**1.34E-007**	**5.44E-008**
FCC1208#4	12/09/95	05:00 AM	06:00 AM	5.77	69.1	0.2382	1.52E-006	2.12E-007	3	2	0.20	**6.81E-008**	**1.79E-007**	**1.98E-008**
FCC1208#5	12/09/95	06:00 AM	07:00 AM	5.91	37.5	0.1312	1.42E-006	2.30E-007	3	1	0.40	**6.48E-008**	**3.58E-007**	**2.27E-008**
FCC1208#6	12/09/95	07:00 AM	08:00 AM	5.89	42	0.1463	1.81E-006	3.19E-007	3	1	0.30	**5.91E-008**	**2.68E-007**	**3.94E-008**
FCC1208#7	12/09/95	08:00 AM	09:00 AM	6.19	34.2	0.1201	2.02E-006	3.85E-007	3	1	0.20	**2.35E-007**	**1.79E-007**	**7.08E-008**
FCC1208#8	12/09/95	09:00 AM	09:55 AM	5.81	9.5	0.0423	3.75E-006	8.82E-007	3	2	0.10	**8.19E-008**	**8.94E-008**	**2.10E-007**
FCC1209#1	12/10/95	03:00 AM	04:00 AM	6.24	45.7	0.1589	1.64E-006	6.02E-007	2	1	0.10	**1.97E-007**	**5.96E-008**	**6.32E-008**
FCC1209#2	12/10/95	04:00 AM	05:00 AM	6.49	50	0.1739	3.23E-006	5.10E-007	2	1.5	0.15	**9.35E-007**	**8.94E-008**	**1.39E-007**
FCC1209#3	12/10/95	05:00 AM	06:00 AM	6.65	50	0.1739	2.69E-006	3.64E-007	2	2	0.20	**2.60E-006**	**1.19E-007**	**1.02E-007**
FCC1209#4	12/10/95	06:00 AM	07:00 AM	6.70	44.1	0.1535	2.10E-006	2.78E-007	2	3	0.40	**4.92E-006**	**2.38E-007**	**6.52E-008**
FCC1209#5	12/10/95	07:00 AM	08:00 AM	6.49	32.9	0.1158	1.37E-006	2.44E-007	2	2	0.30	**1.25E-006**	**1.79E-007**	**2.84E-008**
FCC1209#6	12/10/95	08:00 AM	09:00 AM	6.38	21.9	0.0800	1.12E-006	2.18E-007	2	3	0.20	**1.13E-006**	**1.19E-007**	**1.82E-008**
FCC1218#1	12/19/95	04:00 AM	05:00 AM	6.50	7.3	0.0313	1.30E-006	2.19E-007	3	2	0.10	**1.96E-006**	**8.94E-008**	**3.67E-008**
FCC1218#2	12/19/95	05:00 AM	06:00 AM	6.54	8	0.0339	8.41E-007	1.57E-007	3	3	0.10	**3.53E-006**	**8.94E-008**	**1.78E-008**
FCC1218#3	12/19/95	06:00 AM	07:00 AM	6.67	-99	0.0165	4.48E-007	1.27E-007	3	1	0.10	**2.14E-006**	**8.94E-008**	**9.19E-009**
FCC1227#1	12/28/95	08:15 AM	08:47 AM	6.33	2	0.0175	6.71E-007	1.82E-007	2	1	0.30	**2.98E-007**	**1.79E-007**	**8.60E-009**
FCC1231#1	01/01/96	06:02 AM	07:00 AM	5.98	17	0.0661	1.03E-006	1.33E-007	2	1	0.10	**5.96E-008**	**5.96E-008**	**6.79E-009**
FCC1231#2	01/01/96	07:00 AM	08:00 AM	6.00	32.3	0.1138	6.71E-007	9.10E-008	2	1	0.15	**6.54E-008**	**8.94E-008**	**3.08E-009**
FCC1231#3	01/01/96	08:00 AM	09:00 AM	6.03	23.7	0.0858	6.71E-007	9.10E-008	2	3	0.25	**2.25E-007**	**1.49E-007**	**3.17E-009**
FCC1231#4	01/01/96	09:00 AM	09:20 AM	5.80	3.4	0.0417	6.71E-007	9.10E-008	2	5	0.20	**1.30E-007**	**1.19E-007**	**2.57E-009**
FCC0103#1	01/04/96	01:30 AM	02:00 AM	6.49	23.3	0.1620	1.50E-006	1.91E-007	2	1	0.10	**6.23E-007**	**5.96E-008**	**2.44E-008**
FCC0103#2	01/04/96	02:00 AM	03:00 AM	6.47	39.4	0.1375	8.99E-007	1.24E-007	2	1	0.10	**5.68E-007**	**5.96E-008**	**9.21E-009**
FCC0103#3	01/04/96	03:00 AM	04:00 AM	6.32	10.1	0.0414	1.24E-006	1.92E-007	1	1	0.10	**1.42E-007**	**2.98E-008**	**8.28E-009**

Kern Bulk S(IV) Oxidation Calculations

SAMPLE_NAME	START_DATE	START_TIME	END_TIME	PH	Mass (g)	LWC (g/m^3)	Fe(III) (M)	Mn(II) (M)	SO2 (ppb)	O3 (ppb)	H2O2 (ppbv)	O3 rate -d S(IV)/dt Molar/s	H2O2 rate -d S(IV)/dt Molar/s	O2(Fe+Mn) rate -d S(IV)/dt Molar/s
KCC1208#3	12/09/95	01:05 AM	03:08 AM	7.35	-99	0.2624	1.82E-006	3.65E-007	1.00	1	0.30	1.63E-005	8.94E-008	1.22E-007
KCC1208#4	12/09/95	03:08 AM	04:17 AM	6.80	97.8	0.2918	3.56E-006	2.15E-006	1.00	1	0.30	1.30E-006	8.94E-008	4.98E-007
KCC1208#5	12/09/95	04:17 AM	05:20 AM	6.89	77.3	0.2535	1.93E-006	1.49E-006	1.00	1	0.30	1.96E-006	8.94E-008	2.17E-007
KCC1208#6	12/09/95	05:20 AM	06:25 AM	6.66	54.8	0.1754	1.50E-006	4.16E-007	1.00	1.5	0.20	1.02E-006	5.96E-008	3.31E-008
KCC1208#7	12/09/95	06:25 AM	08:35 AM	6.90	105.8	0.1698	1.79E-006	7.84E-007	1.00	2	0.25	4.11E-006	7.45E-008	1.07E-007
KCC1209#1	12/09/95	07:20 PM	09:00 PM	6.42	123.1	0.2543	1.04E-006	1.61E-007	1.00	12.05	0.35	2.72E-006	1.04E-007	6.53E-009
KCC1209#2	12/09/95	09:00 PM	11:00 PM	6.55	103.8	0.1799	1.97E-006	6.49E-007	1.00	10.95	0.35	4.50E-006	1.04E-007	5.86E-008
KCC1209#3	12/09/95	11:00 PM	02:15 AM	7.09	171.4	0.1827	9.30E-007	1.52E-007	1.00	6.29	0.30	3.10E-005	8.94E-008	1.52E-008
KCC1209#4	12/10/95	02:15 AM	06:04 AM	6.59	188.4	0.1717	5.96E-007	1.08E-007	1.00	4.67	0.30	2.31E-006	8.94E-008	3.09E-009
KCC1209#5	12/10/95	06:04 AM	08:18 AM	6.74	106.4	0.1656	7.77E-007	9.90E-008	1.00	2.91	0.25	2.87E-006	7.45E-008	4.57E-009
KCC1209#6	12/10/95	08:18 AM	09:31 AM	6.70	27.8	0.0830	7.83E-007	9.10E-008	1.00	5.81	0.20	4.76E-006	5.96E-008	3.99E-009
KCC1214#2	12/15/95	12:00 AM	02:25 AM	7.40	92.2	0.1333	1.02E-006	2.01E-007	1.13	1.00	0.30	2.31E-005	1.01E-007	4.79E-008
KCC1214#3	12/15/95	02:35 AM	04:45 AM	7.28	69	0.1123	7.96E-007	2.32E-007	1.00	1.00	0.30	1.18E-005	8.94E-008	2.92E-008
KCC1214#4	12/15/95	04:45 AM	07:38 AM	7.43	104.8	0.1273	1.99E-006	6.93E-007	1.00	1.25	0.25	2.96E-005	7.45E-008	3.06E-007
KCC1218#1	12/19/95	02:55 AM	10:35 AM	6.86	-99	0.0650	8.95E-007	1.82E-007	1.00	1.13	0.25	1.93E-006	7.45E-008	1.17E-008
KCC0101#1	01/02/96	02:44 AM	06:24 AM	6.68	193.1	0.1825	7.20E-008	3.28E-008	1.00	1.00	0.25	7.47E-007	7.45E-008	1.28E-010
KCC0101#2	01/02/96	06:24 AM	09:53 AM	7.05	165.8	0.1655	9.90E-008	2.86E-008	1.00	2.50	0.20	1.03E-005	5.96E-008	2.82E-010
KCC0101#3	01/02/96	09:53 AM	11:44 AM	6.70	32.5	0.0661	1.26E-007	7.77E-008	1.00	6.95	0.30	5.69E-006	8.94E-008	5.48E-010
KCC0102#1	01/03/96	12:00 AM	05:12 AM	6.74	194.5	0.1308	3.07E-007	6.48E-008	1.00	1.00	0.74	9.85E-007	2.20E-007	1.18E-009
KCC0102#2	01/03/96	05:12 AM	09:10 AM	6.93	177.9	0.1560	1.21E-007	3.91E-008	1.00	1.00	0.22	2.36E-006	6.65E-008	3.81E-010

Candelabra Tower Bulk S(IV) Oxidation Calculations

SAMPLE_NAME	ELEVATION (m)	START_DATE	START_TIME	END_TIME	PH	MASS (g)	LWC (g/m^3)	Fe(iii) (M)	Mn(II) (M)	SO2 (ppb)	O3 (ppb)	H2O2 (ppb)	O3 rate -d S(IV)/dt Molar/s	H2O2 rate -d S(IV)/dt Molar/s	O2(Fe+Mn) rate -d S(IV)/dt Molar/s
GCC0112#1	0	01/12/96	06:00 AM	07:00 AM	6.72	16.67	0.0632	1.24E-006	1.42E-007	0.81	2.00	0.08	**1.46E-006**	**1.90E-008**	**8.21E-009**
GCC0112#2	0	01/12/96	07:30 AM	08:30 AM	6.76	12.35	0.0490	9.17E-007	1.25E-007	0.81	2.00	0.07	**1.75E-006**	**1.77E-008**	**5.66E-009**
GCC0112#3	0	01/12/96	09:00 AM	10:00 AM	6.52	5.32	0.0238	8.95E-007	9.10E-008	0.85	2.00	0.09	**6.08E-007**	**2.40E-008**	**3.05E-009**
MCC0112#1	140	01/12/96	06:00 AM	07:00 AM	6.54	82.26	0.2825	3.89E-007	8.83E-008	0.71	6.73	0.13	**1.87E-006**	**2.73E-008**	**1.10E-009**
MCC0112#2	140	01/12/96	07:30 AM	08:30 AM	6.74	60.58	0.2094	2.70E-007	5.44E-008	0.71	6.94	0.16	**4.85E-006**	**3.45E-008**	**6.19E-010**
MCC0112#3	140	01/12/96	09:00 AM	10:00 AM	6.8	52.46	0.1818	1.34E-007	6.01E-008	0.74	10.99	0.22	**1.05E-005**	**4.86E-008**	**3.85E-010**
MCC0112#4	140	01/12/96	10:30 AM	11:30 AM	6.5	26.65	0.0953	6.58E-007	1.90E-007	0.74	17.11	0.28	**4.11E-006**	**6.23E-008**	**3.94E-009**
MCC0114#1	140	01/14/96	05:00 AM	06:00 AM	6.45	32.29	0.1138	2.69E-007	9.10E-008	0.69	11.01	0.18	**1.97E-006**	**3.78E-008**	**6.80E-010**
MCC0114#2	140	01/14/96	07:00 AM	08:00 AM	6.35	34.51	0.1212	2.69E-007	9.10E-008	0.68	12.01	0.17	**1.33E-006**	**3.48E-008**	**5.94E-010**
MCC0114#3	140	01/14/96	09:00 AM	10:00 AM	6.29	29.14	0.1034	2.69E-007	9.10E-008	0.72	9.15	0.16	**8.13E-007**	**3.40E-008**	**5.90E-010**
TCC0112#1	230	01/12/96	06:00 AM	07:00 AM	6.53	87.01	0.2983	3.29E-007	4.68E-008	0.64	9.77	0.16	**2.36E-006**	**3.11E-008**	**4.42E-010**
TCC0112#2	230	01/12/96	07:30 AM	08:30 AM	6.77	85.89	0.2946	4.45E-007	6.79E-008	0.64	10.12	0.22	**7.37E-006**	**4.25E-008**	**1.21E-009**
TCC0112#3	230	01/12/96	09:00 AM	10:00 AM	6.81	78.22	0.2491	2.05E-007	4.22E-008	0.66	16.76	0.30	**1.51E-005**	**5.98E-008**	**3.79E-010**
TCC0112#4	230	01/12/96	10:30 AM	11:30 AM	6.61	69.85	0.2408	2.21E-007	7.90E-008	0.66	26.83	0.36	**9.62E-006**	**7.03E-008**	**5.72E-010**
TCC0114#1	320	01/14/96	05:00 AM	06:00 AM	6.65	90.05	0.3085	2.69E-007	9.10E-008	0.57	17.51	0.26	**6.51E-006**	**4.51E-008**	**7.30E-010**
TCC0114#2	320	01/14/96	07:00 AM	08:00 AM	6.43	98.79	0.3376	2.69E-007	9.10E-008	0.57	17.89	0.24	**2.40E-006**	**4.04E-008**	**5.46E-010**
TCC0114#3	320	01/14/96	09:03 AM	10:00 AM	6.48	84.17	0.3037	2.69E-007	9.10E-008	0.58	16.80	0.21	**2.91E-006**	**3.61E-008**	**5.96E-010**

Appendix D:

The following tables show the following information for each size fractionated sample calculation presented in the previous plots:

Sample Name - Name of large drop fraction sample
Start Date - Month and day actual sample was collected
Start Time - Time sample was started
End Time - End time, when sample was removed from collector

Each of the following are given for both the small and large drop fraction:

pH - pH of collected fog water, measured on-site
MASS - mass of collected fog water (in grams)

when measured:
Fe(III) - Fe(III) used in S(IV) oxidation calculations (in M)
Mn(II) - Mn(II) used in S(IV) oxidation calculations (in M)

Calculated S(IV) oxidation rates for each pathway (in M/s) corresponding to the large and small drop pH values.

Calculated S(IV) oxidation rates for each pathway (in M/s) corresponding to the LWC weighted average H+ concentration. (Avg. or Bulk Ox. Rate)

A LWC weighted average of the large and small drop S(IV) oxidation rates for each pathway (in M/s). (Wtd. Avg. of Ox. Rates)

Bakersfield Size Fractionated S(IV) Oxidation Calculations

SAMPLE_NAME	START_DATE	START_TIME	END_TIME	Lg drop pH	Sm drop pH	Lg Mass (g)	Sm Mass (g)								
BEL1210#2	12/10/95	02:00 AM	03:00 AM	6.24	5.26	0.9	0.2								
BEL1210#3	12/10/95	04:00 AM	06:00 AM	5.69	4.67	1.6	0.3								
BEL1218#1	12/18/95	03:40 AM	06:10 AM	6.26	5.45	0.58	0.16								
	OZONE	OZONE	OZONE	OZONE	OZONE	H2O2	H2O2	H2O2	H2O2	H2O2					
	Large Drop	Small Drop	Ox. Rate	Wtd Avg of	Sulf. Ox.	Large Drop	Small Drop	Ox. Rate	Wtd Avg of	Sulf. Ox.	Total rate	Total rate	Total rate	Total rate	Total rate
	Ox. Rate	Ox. Rate	avg	Ox. Rates	Enhancement	Ox. Rate	Ox. Rate	avg	Ox. Rates	Enhancement	large drop	Small drop	'Bulk' (avg)	Wtd Avg. of rates	Enhancement
SAMPLE_NAME	(M/S)	(M/S)	(M/S)	(M/S)	Ratio	(M/S)	(M/S)	(M/S)	(M/S)	Ratio					Ratio
BEL1210#2	2.96E-007	3.29E-009	4.54E-008	2.43E-007	5.34	1.49E-008	1.49E-008	1.49E-008	1.49E-008	1.00	3.11E-007	1.82E-008	6.03E-008	2.58E-007	4.27
BEL1210#3	3.78E-008	3.64E-010	6.13E-009	3.19E-008	5.21	3.39E-008	3.39E-008	3.39E-008	3.39E-008	1.00	7.18E-008	3.43E-008	4.00E-008	6.58E-008	1.64
BEL1218#1	2.16E-007	5.23E-009	4.56E-008	1.71E-007	3.74	1.49E-008	1.49E-008	1.49E-008	1.49E-008	1.00	2.31E-007	2.01E-008	6.05E-008	1.85E-007	3.07

Fresno Size Fractionated S(IV) Oxidation Calculations

SAMPLE_NAME	START_DATE	START_TIME	END_TIME	Lg drop pH	Sm drop pH	Lg Mass (g)	Sm Mass (g)								
FEL1208#1	12/09/95	03:00 AM	04:00 AM	5.8	4.8	0.7	0.1								
FEL1208#2	12/09/95	05:00 AM	06:00 AM	5.82	4.6	0.6	0.1								
FEL1208#3	12/09/95	07:00 AM	08:00 AM	5.91	5.01	0.4	0.1								
FEL1209#1	12/10/95	04:00 AM	06:00 AM	6.73	6.2	1.3	0.2								
FEL1231#1	01/01/96	06:02 AM	08:00 AM	6.1	5.05	0.8	0.1								
	OZONE	OZONE	OZONE	OZONE	OZONE	H2O2	H2O2	H2O2	H2O2	H2O2					
	Large Drop	Small Drop	Ox. Rate	Wtd Avg of	Sulf. Ox.	Large Drop	Small Drop	Ox. Rate	Wtd Avg of	Sulf. Ox.	Total rate	Total rate	Total rate	Total rate	Total rate
	Ox. Rate	Ox. Rate	avg	Ox. Rates	Enhancement	Ox. Rate	Ox. Rate	avg	Ox. Rates	Enhancement	large drop	Small drop	'Bulk' (avg)	Wtd Avg. of rates	Enhancement
SAMPLE_NAM	(M/S)	(M/S)	(M/S)	(M/S)	Ratio	(M/S)	(M/S)	(M/S)	(M/S)	Ratio					Ratio
FEL1208#1	3.91E-008	4.07E-010	8.70E-009	3.43E-008	3.94	8.94E-008	8.94E-008	8.94E-008	8.94E-008	1.00	1.29E-007	8.98E-008	9.81E-008	1.24E-007	1.26
FEL1208#2	8.57E-008	3.32E-010	8.31E-009	7.35E-008	8.85	1.79E-007	1.79E-007	1.79E-007	1.79E-007	1.00	2.65E-007	1.79E-007	1.87E-007	2.52E-007	1.35
FEL1208#3	6.48E-008	1.05E-009	1.14E-008	5.21E-008	4.56	2.68E-007	2.68E-007	2.68E-007	2.68E-007	1.00	3.33E-007	2.69E-007	2.80E-007	3.20E-007	1.15
FEL1209#1	3.29E-006	2.87E-007	1.89E-006	2.89E-006	1.53	1.04E-007	1.04E-007	1.04E-007	1.04E-007	1.00	3.40E-006	3.91E-007	2.00E-006	3.00E-006	1.50
FEL1231#1	1.04E-007	6.42E-010	2.28E-008	9.21E-008	4.05	7.45E-008	7.45E-008	7.45E-008	7.45E-008	1.00	1.78E-007	7.53E-008	9.73E-008	1.67E-007	1.71

Kern Size Fractionated S(IV) Oxidation Calculations

SAMPLE_NAM	START_DATE	START_T	END_TIM	Lg PH	Sm PH	Lg Mass	Sm Mass	Lg Fe(II) M	Sm Fe(II) M	Lg Mn(II) M	Sm Mn(II) M									
KCL120807	12/08/95	03 08 AM	04 17 AM	7 02	6 39	152 1	18 3	3 31E-006	2 01E-006	9 26E-007	5 18E-007									
KCL120809	12/08/95	04 17 AM	05 20 AM	8 95	6 43	99 3	11 7	1 11E-006	2 36E-006	1 75E-007	8 09E-007									
KCL120811	12/08/95	05 20 AM	06 25 AM	6 93	6 41	88 8	10 3	1 37E-006	1 76E-006	2 10E-007	4 04E-007									
KCL120813	12/08/95	06 25 AM	06 35 AM	6 87	6 52	137 1	29	1 77E-006	1 58E-006	4 17E-007	3 06E-007									
KCL120881	12/08/95	07 20 PM	09 00 PM	6 54	6 27	323 3	7 8	4 48E-006	3 59E-006	9 39E-007	8 28E-007									
KCL120882	12/08/95	09 00 PM	11 00 PM	6 83	5 86	270 5	21	7 06E-007	9 36E-007	1 02E-007	2 02E-007									
KCL120883	12/08/95	11 00 PM	02 15 AM	7 48	6 21	442 4	39 8	1 09E-006	1 88E-006	1 97E-007	4 26E-007									
KCL120885	12/10/95	06 04 AM	06 18 AM	7 28	5 87	248 4	21	2 79E-007	9 40E-007	8 04E-008	1 69E-007									
KCL120888	12/10/95	06 18 AM	09 31 AM	6 96	5 94	86 3	12 8													
KCL121482	12/15/95	12 00 AM	02 25 AM	7 35	7 18	282 9	10 5	1 17E-006	1 27E-006	2 17E-007	2 99E-007									
KCL121483	12/15/95	02 35 AM	04 45 AM	7 49	7 02	139 4	22 4	1 40E-006		1 58E-007										
KCL121484	12/15/95	04 45 AM	07 58 AM	7 52	7 14	175 7	20 8	2 23E-006	1 69E-005	2 73E-009	0 00E+000									
KCL010181	01/02/96	02 44 AM	06 24 AM	7 11	7 08	461	4 1	1 55E-007	1 41E-006	3 84E-008	2 89E-007									
KCL010182	01/02/96	06 24 AM	09 53 AM	7 05	6 82	360 8	18 3	1 12E-007	1 98E-007	2 46E-008	1 13E-007									
KCL010183	01/02/96	09 53 AM	11 44 AM	6 97	6 81	62 8	4 4	2 05E-007		7 72E-008										
KCL010281	01/03/96	12 00 AM	05 12 AM	6 86	6 8	172 3	25 3	2 56E-007	3 97E-007	8 64E-008	9 34E-008									
KCL010282	01/03/96	05 12 AM	09 10 AM	6 92	6 57	196 2	18 2	2 43E-007	5 22E-007	5 39E-008	1 27E-007									
	OZONE	OZONE	OZONE	OZONE	OZONE	H2O2	H2O2	H2O2	H2O2	H2O2		O2	O2	O2						
	Large Drop	Small Drop	Ox. Rate	Wtd Avg of	Suff. Ox.	Large Drop	Small Drop	Ox. Rate	Wtd Avg of	Suff. Ox.		Large Drop Ox. Rate	Small Drop Ox. Rate	avg Ox. Rate	Wtd Avg. of Ox Rates	Catalyzed S(IV) Ox. Enhance	Total rate	Total rate	Total rate	Total rate	Total rate
	Ox. Rate	Ox. Rate	avg	Ox. Rates	Enhancement	Ox. Rate	Ox. Rate	avg	Ox. Rates	Enhancement		Synergism	Synergism	Synergism	Synergism	Factor	large drop	Small drop	'Bulk' (avg)	Wtd Avg. of rates	Enhancement
SAMPLE_NAM	(M/S)	(M/S)	(M/S)	(M/S)	Ratio	(M/S)	(M/S)	(M/S)	(M/S)	Ratio		(M/s)	(M/s)	(M/s)	(M/S)	(with synergism)					Ratio
KCL120807	3 57E-006	1 97E-007	2 06E-006	3 25E-006	1 57	8 94E-006	8 94E-006	8 94E-006	8 94E-006	1 00		2 57E-007	3 51E-008	1 92E-007	2 36E-007	1 23	3 92E-006	3 21E-007	2 35E-006	3 57E-006	1 52
KCL120809	2 59E-006	2 36E-007	1 87E-006	2 34E-006	1 40	8 94E-006	6 94E-006	8 94E-006	8 94E-006	1 00		1 45E-006	6 73E-008	1 91E-008	2 00E-006	1 05	2 89E-006	3 93E-007	1 78E-006	2 45E-006	1 37
KCL120811	3 54E-006	3 23E-007	1 78E-006	2 97E-006	1 67	5 96E-006	5 96E-006	5 96E-006	5 96E-006	1 00		2 06E-006	2 45E-008	1 98E-008	2 13E-006	1 06	3 82E-006	4 07E-007	1 86E-006	3 05E-006	1 64
KCL120813	3 58E-006	7 15E-007	2 42E-006	3 08E-006	1 27	7 45E-006	7 45E-006	7 45E-006	7 45E-006	1 00		4 78E-006	1 90E-006	3 81E-006	4 28E-006	1 09	3 71E-006	8 09E-007	2 54E-006	3 30E-006	1 26
KCL120881	4 73E-006	1 38E-008	4 54E-006	4 65E-006	1 02	1 04E-007	1 04E-007	1 04E-007	1 04E-007	1 00		1 69E-007	8 62E-008	1 65E-007	1 67E-007	1 01	5 00E-006	1 53E-006	4 81E-006	4 92E-006	1 02
KCL120882	6 50E-006	2 06E-007	3 66E-006	6 05E-006	1 65	1 04E-007	1 04E-007	1 04E-007	1 04E-007	1 00		3 38E-006	3 82E-009	3 03E-009	3 30E-009	1 08	6 61E-006	3 14E-007	3 77E-006	6 15E-006	1 63
KCL120883	1 87E-004	5 40E-007	3 10E-005	1 73E-004	5 53	8 94E-006	8 94E-006	8 94E-006	8 94E-006	1 00		4 78E-006	1 99E-008	2 36E-008	4 56E-006	1 94	1 87E-004	8 50E-007	3 12E-005	1 72E-004	5 51
KCL120885	3 44E-005	5 23E-006	4 03E-006	3 18E-005	7 89	7 45E-006	7 45E-006	7 45E-006	7 45E-006	1 00		2 38E-009	3 18E-009	1 35E-009	2 45E-009	1 81	3 45E-005	1 30E-007	4 10E-006	3 18E-005	7 76
KCL120888	1 56E-005	1 44E-007	3 19E-006	1 37E-005	4 31	5 96E-006	5 96E-006	5 96E-006	5 96E-006	1 00							1 56E-005	2 04E-007	3 25E-006	1 38E-005	4 25
KCL121482	1 84E-005	8 40E-008	1 78E-006	1 80E-005	1 01	1 01E-007	1 01E-007	1 01E-007	1 01E-007	1 00		4 71E-008	4 68E-008	4 71E-008	4 72E-008	1 00	1 85E-005	8 55E-008	1 79E-005	1 82E-005	1 01
KCL121483	3 11E-005	3 57E-008	1 83E-005	2 73E-005	1 42	8 94E-006	8 94E-006	8 94E-006	8 94E-006	1 00		5 08E-008			4 37E-008		3 13E-005	3 86E-006	1 84E-005	2 74E-005	1 43
KCL121484	4 48E-005	7 79E-006	3 40E-005	4 09E-005	1 20	7 45E-006	7 45E-006	7 45E-006	7 45E-006	1 00		1 50E-008	0 00E+000	1 98E-008	1 34E-008	0 68	4 49E-005	7 86E-006	3 41E-005	4 10E-005	1 20
KCL010181	5 41E-006	4 93E-008	5 41E-006	5 41E-006	1 00	7 45E-006	7 45E-006	7 45E-006	7 45E-006	1 00		5 93E-010	3 89E-006	6 71E-010	9 30E-010	1 39	5 49E-006	5 05E-006	5 48E-006	5 48E-006	1 00
KCL010182	1 03E-005	3 56E-006	9 61E-006	9 95E-006	1 03	5 96E-006	5 96E-006	5 96E-006	5 96E-006	1 00		2 45E-010	1 33E-009	2 90E-010	2 98E-010	1 03	1 03E-005	3 62E-006	9 67E-006	1 00E-005	1 03
KCL010183	1 97E-005	9 44E-006	1 86E-005	1 90E-005	1 02	8 94E-006	8 94E-006	8 94E-006	8 94E-006	1 00		1 22E-009			1 14E-009		1 96E-005	8 53E-006	1 87E-005	1 91E-005	1 02
KCL010281	1 71E-006	1 30E-006	1 65E-006	1 66E-006	1 01	2 20E-007	2 20E-007	2 20E-007	2 20E-007	1 00		1 09E-009	2 15E-009	1 21E-009	1 22E-009	1 01	1 93E-006	1 52E-006	1 67E-006	1 88E-006	1 01
KCL010282	2 26E-006	4 50E-007	1 85E-006	2 10E-006	1 14	6 65E-006	6 65E-006	6 65E-006	6 65E-006	1 00		9 24E-010	2 77E-009	1 05E-009	1 08E-009	1 03	2 32E-006	5 20E-007	1 91E-006	2 17E-006	1 13

Appendix E:

Table E-1: Dates for various titrations of 1994 Bakersfield and IMS95 fog samples.

SITE	Sample Name	In Field Titrations	------- Manual titrations -------			Manual/Auto Comp	Standard Acid titrations	Filtered	Same day as CO3/HCO3 rxns	Base titrations
BAK 1/15/94	SM C ASCC 1		6/5/96	06/06/96	06/07/96			8/18/97(A)	08/27/97 (A)	9/3/97 (A)
	SM CASCC 1B		6/5/96	06/06/96						
	SM CASCC 2		6/5/96	06/06/96	06/07/96			8/18/97(A)	08/27/97 (A)	
	Sm CA SCC 3									
	LG LG 1		05/08/95	06/07/96	07/31/97	8/7/97 (A)			08/27/97 (A)	
	Lg Lg 1b									
	LG LG 2		05/08/95	06/07/96					08/27/97 (A)	
	Lg Lg 2B									
	Lg Lg 3									
	LG SM 1		06/07/96							
	LG SM 2		05/08/95	06/06/96					08/27/97 (A)	
BKA 1995	BCC1209#1						8/12/97 (A)	8/15/97 (A)	8/27/97(A)	9/3/97 (A)
	BCC1209#2						8/12/97 (A)	8/15/97 (A)		
	BCC1209#3						8/12/97 (A)			
	BCC1209#4						8/12/97 (A)	8/15/97 (A)		
	BCC1210#1		06/01/97			8/7/97 (A)	8/12/97 (A)	8/15/97 (A)		
	BCC1210#2	12/22/95					8/12/97 (A)			
	BCC1210#3	12/22/95					8/12/97 (A)			
	BCC1210#4	12/22/95	06/01/97			8/7/97 (A)	8/12/97 (A)			
	BCC1210#5	12/22/95					8/12/97 (A)			
	BCC1210#6	12/22/95					8/12/97 (A)			
	BCC1210#7	12/22/95					8/12/97 (A)			
	BCC1210#8	12/22/95					8/12/97 (A)			
	BCC1218#1	12/22/95					8/12/97 (A)			
KERN 1995	KCC1208#2						8/13/97 (A)	8/18/97 (A)	8/27/97 (A)	
	KCC1208#3						8/13/97 (A)			
	KCC1208#4						8/13/97 (A)	8/18/97 (A)		9/3/97 (A)
	KCC1208#5						8/13/97 (A)			
	KCC1208#6						8/13/97 (A)			
	KCC1208#7						8/13/97 (A)			
	KCC1209#1						8/13/97 (A)			
	KCC1209#2						8/13/97 (A)			
	KCC1209#3						8/13/97 (A)			
	KCC1209#4						8/13/97 (A)			
	KCC1209#5						8/13/97 (A)			
	KCC1209#6						8/13/97 (A)			
	KCC1214#2						8/13/97 (A)			
	KCC1214#3						8/13/97 (A)			
	KCC1214#4						8/13/97 (A)	8/18/97 (A)		
	KCC1218#1						8/13/97 (A)			
	KCC0101#1	01/02/96					8/13/97 (A)			
	KCC0101#2						8/13/97 (A)			
	KCC0101#3						8/13/97 (A)			
	KCC0102#1						8/13/97 (A)			
	KCC0102#2						8/13/97 (A)			
	KCL1208#3						8/13/97 (A)			
	KCL1208#5						8/13/97 (A)			
	KCL1208#7						8/13/97 (A)			
	KCL1208#9						8/13/97 (A)			
	KCL1208#11						8/13/97 (A)			
	KCL1208#13						8/13/97 (A)			
	KCS1208#2						8/13/97 (A)			
	KCS1208#4						8/13/97 (A)			
	KCS1208#6						8/13/97 (A)			
	KCS1208#10						8/13/97 (A)			
	KCS1208#12						8/13/97 (A)			
	KCL1209#1		06/06/96	06/01/97		8/7/97 (A)	8/14/97 (A)			
	KCL1209#2		06/06/96				8/14/97 (A)			
	KCL1209#3		06/06/96				8/14/97 (A)			
	KCL1209#4		06/06/96	06/01/97	06/07/97	8/7/97 (A)	8/14/97 (A)			
	KCL1209#5		06/06/96				8/14/97 (A)			
	KCL1209#6						8/14/97 (A)			
	KCS1209#1		06/06/96							
	KCS1209#2		06/06/96				8/14/97 (A)			
	KCS1209#3		06/06/96				8/14/97 (A)			
	KCS1209#4		06/06/96				8/14/97 (A)			
	KCS1209#5		06/06/96				8/14/97 (A)			
	KCS1209#6						8/14/97 (A)			
	KCL1214#2						8/14/97 (A)			
	KCL1214#3						8/14/97 (A)			
	KCL1214#4						8/14/97 (A)			
	KCS1214#3						8/14/97 (A)			
	KCS1214#4						8/14/97 (A)			
	KCL0101#1						8/14/97 (A)			
	KCL0101#2	01/02/96					8/14/97 (A)			
	KCL0101#3						8/14/97 (A)			
	KCS0101#1						8/14/97 (A)			
	KCS0101#2	01/02/96					8/14/97 (A)			
	KCL0102#1						8/14/97 (A)			
	KCL0102#2						8/14/97 (A)			
	KCS0102#1						8/14/97 (A)			
	KCS0102#2						8/14/97 (A)			
	KIL1208#3						8/13/97 (A)			
	KIM1208#3						8/13/97 (A)			
	KIS1208#3						8/13/97 (A)			

Table D-1 continued.

SITE	Sample Name	In Field Titrations	---------- Manual titrations ----------		Man/Auto Comp	Standard Acid titrations	Filtering study	With carbonate mvmts	Base titrations
FSF 1995	FCC1206#1					8/11/97 (A)	08/15/97 (A)		9/3/97 (A)
	FCC1206#2					8/11/97 (A)			
	FCC1206#3					8/11/97 (A)			
	FCC1206#4					8/11/97 (A)			
	FCC1206#5					8/11/97 (A)			
	FCC1206#6					8/11/97 (A)			
	FCC1206#7					8/11/97 (A)			
	FCC1206#8					8/11/97 (A)			
	FCC1209#1					8/11/97 (A)			
	FCC1209#2					8/11/97 (A)			
	FCC1209#3					8/11/97 (A)			
	FCC1209#4					8/11/97 (A)			
	FCC1209#5					8/11/97 (A)			
	FCC1209#6					8/11/97 (A)	08/15/97 (A)	8/27/97 (A)	
	FCC1231#1	01/01/96	08/01/97		8/7/97 (A)				
	FCC1231#2					8/11/97 (A)	08/15/97 (A)		
	FCC1231#3	01/01/96	08/11/97			8/11/97 (A)			
	FCC1231#4					8/11/97 (A)			
	FCC0103#1					8/11/97 (A)			
	FCC0103#2	01/04/96	08/07/97	08/11/97	8/7/97 (A)	8/11/97 (A)			
	FCC0103#3					8/11/97 (A)			
TOWER 96	GCC0112#1					8/12/97 (A)			
	MCC0112#1					8/12/97 (A)			
	MCC0112#2					8/12/97 (A)			
	MCC0112#3					8/12/97 (A)			
	MCC0112#4					8/12/97 (A)			
	TCC0112#1					8/12/97 (A)			
	TCC0112#2					8/12/97 (A)			
	TCC0112#3					8/12/97 (A)			
	TCC0112#4					8/12/97 (A)			
	MCC0114#1					8/13/97 (A)			
	MCC0114#2					8/13/97 (A)			
	MCC0114#3					8/13/97 (A)			
	TCC0114#1					8/13/97 (A)			
	TCC0114#2					8/13/97 (A)			
	TCC0114#3					8/13/97 (A)			